# Controls on Anthropogenic Radionuclide Behaviour in the Sellafield-Impacted Eastern Irish Sea, UK

A thesis submitted to the University of Manchester for the degree of Doctor of Philosophy in the Faculty of Science and Engineering

**Daisy Ray**

**School of Chemistry**

**2018**

# Contents

**List of Figures**

**List of Tables**

**List of Abbreviations**

| | |
|---|---|
| AGR | Advanced Gas Cooled Reactor |
| AMS | Accelerator Mass Spectrometry |
| ATP | Adenosine Triphosphate |
| Bq | Becquerel |
| BEIS | Department for Business, Energy, and Industrial Strategy |
| BNFL | British Nuclear Fuels Ltd |
| CTBT | Comprehensive Test Ban Treaty |
| Cefas | Centre for Environment, Fisheries, and Aquaculture Science |
| CRR | Centre for Radiochemistry Research |
| CoRWM | Committee for Radioactive Waste Management |
| DEFRA | Department for the Environment, Food, and Rural Affairs |
| DNA | Deoxyribonucleic Acid |
| EPA | Environment Protection Agency |
| EARP | Enhanced Actinide Reprocessing Plant |
| EDTA | Ethylenediaminetetracetic acid |
| EPSRC | Engineering Physical Science Research Council |
| EXAFS | Extended X-Ray Absorption Fine structure |
| FDNPP | Fukushima Daiichi Nuclear Power Plant |
| FGMSP | First Generation Magnox Storage Pond |
| FSA | Food Standards Agency |
| GDF | Geological Disposal Facility |
| HLW | High Level Waste |
| HR-MC-ICPAES | High Resolution-Multi Collector-Inductively Coupled Plasma Atomic Emission Spectroscopy |
| IAEA | International Atomic Energy Authority |
| ICPAES | Inductively Coupled Plasma Atomic Emission Spectroscopy |
| ICPMS | Inductively Coupled Plasma Mass Spectroscopy |
| ILW | Intermediate Level Waste |
| LLW | Low-Level Waste |
| LLWR | Low-Level Waste Repository |
| LSC | Liquid Scintillation Counting |
| MOX | Mixed Oxide Fuel |
| NDA | National Decommissioning Authority |
| nMDS | Non-metric Multidimensional Scaling |
| OM | Organic Matter |
| ONU | Office for Nuclear Regulation |
| OTU | Operational Taxonomic Unit |
| PCR | Polymerase Chain Reaction |
| PBq | Picobequerel |
| PED | Primary Electron Donor |
| ppb | Parts per billion |
| ppm | Parts per million |
| PWR | Pressurised Water Reactor |
| rRNA | Ribosomal Ribonucleic Acid |

| | |
|---|---|
| SEES | School of Earth, and Environmental Sciences |
| SIMS | Secondary Ion Mass Spectrometry |
| SIXEP | Secondary Ion Exchange Process |
| SRB | Sulfate Reducing Bacteria |
| TBq | Terrabequerel |
| TEA | Terminal Electron Acceptor |
| TEAP | Terminal Electron Accepting Process |
| THORP | Thermal Oxide Reprocessing Plant |
| UKAEA | United Kingdom Atomic Energy Authority |
| VLLW | Very Low Level Waste |
| WHO | World Health Organisation |
| WIPP | Waste Isolation Pilot plant |
| XANES | X-Ray Absorption Near Edge Spectroscopy |
| XRD | X-Ray Diffraction |
| XRF | X-Ray Fluorescence |

**Abstract**

The University of Manchester

**Daisy Ray**

Doctor of Philosophy

Controls on Anthropogenic Radionuclide Behaviour in the Sellafield-Impacted Eastern Irish Sea

2018

Radioactive effluent has been discharged from the UK Sellafield nuclear reprocessing facility to the Eastern Irish Sea since 1952. Waste storage ponds and process liquors from spent fuel reprocessing activities are the main source of this effluent, and contain actinides and fission products (Am, Pu, Np, U, Tc, Cs). These radionuclides accumulate in finely-grained sediments in the Irish Sea and the onset of various biological and physical processes results in the resuspension of radionuclide-labelled sediments. Tidal and bottom currents then transport these radionuclides to neighbouring estuarine regions e.g. Ravenglass saltmarsh. The examination of radionuclide biogeochemistry in this environment provides a long-term (+65 years) assessment of radionuclide behaviour. To date, the majority of studies conducted with Sellafield-contaminated materials have focused on ascertaining radionuclide distribution profiles and matching these to discharge histories, where available. The importance of potential biogeochemical controls on actinide transport and eventual fate has not been studied in great detail.

Here, we have used ion-exchange separation techniques coupled with radiometric analysis, HR-MC-ICP-MS, and AMS to determine contemporary actinide ($^{241}$Am, $^{236}$U, $^{237}$Np, $^{238,239,240}$Pu, $^{241}$Pu) and fission product ($^{137}$Cs and $^{99}$Tc) distribution at two marine sites impacted by the Sellafield discharges (the Irish Sea mud-patch and Ravenglass saltmarsh). Elemental analysis of the sediments was also completed *via* ICP-AES and XRF techniques. The results suggest that the distribution and long-term fate of $^{137}$Cs, $^{241}$Am, and the Pu isotopes at the Ravenglass saltmarsh is largely independent of the ambient redox-related processes, and is instead controlled by the physical transport and burial of the time-integrated Sellafield discharge history. Plutonium in the laboratory has previously been shown to be influenced by trace metal cycling, however this was not observed here. The radionuclides, $^{99}$Tc, $^{236}$U, and $^{237}$Np at the Ravenglass saltmarsh did not reflect their discharge histories, and instead it is suggested that the redox-cycling of these radionuclides likely occurs, driven by the favourable sub-oxic conditions of the sediments, leading to post-depositional remobilisation. This is consistent with traditionally held views garnered from constrained laboratory studies, suggesting similarity between the real world and the laboratory. Sequential extraction experiments show Am and Pu to be primarily associated with the refractory sediment phases, and thus are not environmentally available, with a fraction of Cs present in the easily exchangeable fraction, consistent with the known preferential association of Cs with surfaces of clay minerals.

**Declaration**

No proportion of the work referred to in this thesis has been submitted in support of an application for another degree or qualification of this or any other university or other institute of learning.

**Copyright Statement**

i. The author of this thesis (including any appendices and/or schedules to this thesis) owns certain copyright or related rights in it (the "Copyright") and s/he has given The University of Manchester certain rights to use such Copyright, including for administrative purposes.

ii. Copies of this thesis, either in full or in extracts and whether in hard or electronic copy, may be made only in accordance with the Copyright, Designs and Patents Act 1988 (as amended) and regulations issued under it or, where appropriate, in accordance with licensing agreements which the University has from time to time. This page must form part of any such copies made.

iii. The ownership of certain Copyright, patents, designs, trade marks and other intellectual property (the "Intellectual Property") and any reproductions of copyright works in the thesis, for example graphs and tables ("Reproductions"), which may be described in this thesis, may not be owned by the author and may be owned by third parties. Such Intellectual Property and Reproductions cannot and must not be made available for use without the prior written permission of the owner(s) of the relevant Intellectual Property and/or Reproductions.

iv. Further information on the conditions under which disclosure, publication and commercialisation of this thesis, the Copyright and any Intellectual Property and/or Reproductions described in it may take place is available in the University IP Policy (see http://documents.manchester.ac.uk/display.aspx?DocID=24420), in any relevant Thesis restriction declarations deposited in the University Library, The University Library's regulations (see http://www.library.manchester.ac.uk/about/regulations/) and in The University's policy on Presentation of Theses

**Acknowledgements**

Here goes. Special thanks are directed to my co-supervisor, and general fountain of knowledge, Francis; thank you for being approachable, kind and for answering all my 'quick question' emails whether career, budget, or Pu-error related, it has been much appreciated. Kath, for your knowledge re: all things Ravenglass. My supervisor of many years, Gareth; thank you for your support, and guidance during this process, I am grateful for the opportunities and oversight you have provided. Aside from the 2 am columns, I hope it has been equally enjoyable for you. Peter and Graham, two consortia colleagues whose hard work (and high quality data) has added depth to this project. Heartfelt thanks also stretch many miles to those who made my time at Lawrence Livermore enjoyable; Claudia, I am forever indebted to you for your innate ability to keep us on track in the Seaborg Lab, and James for your 'banter' (and for fulfilling mentor duties relatively well).

There are those past and present who have made the CRR a pleasant place. The halcyon days of when there were just two…Nick MW (and your blue radio). Will and Connaugh for great face-mask time in the particle dungeon; Adam L for frequent origin assistance; NJ for neighbourly Ancoats time; Rosie for making sure we always spoke of going for a run; Adam F for driving the field trip van and keeping us alive during - and for numerous proof reads, and Hamza and Goti, two great sound boards during those early analysis days. Thanks also go to the Dalton Nuclear Institute for filling my evenings with Lego, and providing an outlet for me to dabble in public engagement. The EPSRC Nuclear First for far too many opportunities, NERC Lo-RISE consortium for the collaboration with other RATE consortia, and Terry and Chris for making our outreach dreams always come true, I think you are due cake.

The ladies who lunch contingent; Aruna (we need to stop synchronising our graduations); Helena for endless hours of chat across cohort, consortia, and coffee events; and Hollie for being desk/life/gym partner extraordinaire. To my friends outside the confines of the main campus who I see less often; Sham, Sadia, Kathy, Sinikka, and Walter, your kind words have been very much appreciated. Steve for listening to me ramble over a cup of coffee or two; Billy for the cooked

dinners after long evenings writing, and to his Molly for priceless cat-time. Hamid and Shafi, two great pillars of support, thank you for accommodating dinner plans around lab-time, the ride has been much easier by having you both around!

My flat-mate and special friend for this journey, Josh, I can recall many memories of our great times but most importantly thanks for making our flat(s) a great home. Clèment for filling uncountable weekends with Netflix and laughter, your support has been invaluable; Tu es un keeper! Mom and dad, so we might finally have a Dr in the family! Thank you for not getting too grumpy when visits lessened, and still keeping me fed and watered, you're the best. Bro, for looking after me (paying for dinners and otherwise) and generally helping me get through life. Didz and Jeej, for keeping your door wide-open whenever I needed to escape, and my Radha– hey look Maashi has a new book for you to read!

## Author

The Author attended The University of Manchester graduating with a BSc (Hons) Chemistry degree in 2012. This was followed by a Masters in Environmental Radiochemistry (MSc by research) in 2013 at the University of Manchester Centre for Radiochemistry Research (CRR). Thereafter, she remained at the CRR where she has been, to date, conducting the PhD research presented in this thesis.

# 1. Introduction

## 1.1. Thesis Content

**Chapter 1** details the rationale for the thesis and highlights the impact of the global nuclear industry on the marine and wider environment, focusing on the UK's nuclear legacy. Additionally, it provides an overview of the biogeochemistry of radionuclides relevant to the thesis ($^{99}$Tc, $^{137}$Cs, $^{236}$U, $^{237}$Np, $^{238}$Pu, $^{239,240}$Pu, $^{241}$Pu, and $^{241}$Am) and details the fundamental reaction pathways that govern their environmental behaviour. Chapter 1 ends with a section that details the project aims, and hypotheses.

In **Chapter 2** a detailed discussion of the laboratory methods is presented, including detail on fieldwork, and a short background to the analytical techniques used for geochemical and radionuclide measurement.

**Chapter 3** is a manuscript draft that has been submitted for publication to the Journal of Environmental Radioactivity titled: "Controls on Anthropogenic Radionuclide Distribution in Sellafield-Impacted Irish Sea Sediments". Here, contemporary radionuclide distribution profiles were measured for $^{137}$Cs, $^{241}$Am, and Pu isotopes, and the relative importance of biogeochemical vs. physical controls on radionuclide distribution were investigated. The author roles for this manuscript are as follows: Ray carried out the experimental and analytical work and lead writing of the manuscript; Law, Livens, and Morris provided scientific guidance and editorial guidance; Leary and Gray assisted with microbial ecology analysis and data interpretation; Muir provided additional Pu data; Abrahamsen and Bryan assisted with modelling work.

**Chapter 4** is a manuscript draft that will be submitted to the Journal of Environmental Radioactivity titled: "Sellafield Derived Technetium, Uranium, and Neptunium Distribution in the Ravenglass Saltmarsh, UK". This work utilises trace-level analytical techniques to determine the contemporary distribution of redox-active radionuclides ($^{99}$Tc, $^{236}$U, $^{237}$Np) in the Ravenglass saltmarsh, and explores the role of the ambient biogeochemistry on their fate. The author roles for this manuscript are as follows: Ray carried out the experimental and analytical work and lead writing of the manuscript; Law and Morris provided

scientific guidance and editorial guidance; Fuller and Fifield helped with $^{236}U$ analysis, Joseph, Zavarin, Begg, Zhao and Kersting assisted with $^{237}Np$ measurements.

**Chapter 5** is a manuscript draft that will be submitted to the Journal of Environmental Radioactivity titled: "Sequential Extraction of $^{137}Cs$, $^{241}Am$, and $^{239,240}Pu$ from Eastern Irish Sea Sediments, UK". Here, the partitioning of $^{137}Cs$, $^{241}Am$, and $^{239,240}Pu$ in geochemical phases at the Irish Sea mud-patch and Ravenglass saltmarsh are examined using a series of sequential extractions. The author roles for this manuscript are as follows: Ray and Katsouris carried out the experimental and analytical work; Law and Livens provided scientific guidance, with Law also providing editorial guidance.

**Chapter 6** is a summary of the results and conclusions, and suggestions for future areas of research.

### 1.2. Thesis Rationale

Effluent discharge from the Sellafield site has resulted in the contamination of nearby marine sediments. Present day discharges of radioactive low-level effluent into the Eastern Irish Sea have reduced significantly. However as they still continue, there lies an importance to understand the fate and behaviour of the Sellafield-derived radionuclides in affected areas, namely public locations. Further, this examination into contaminated sediments is particularly pertinent at present as construction of the proposed Moorside Nuclear Reactor near Sellafield may disturb areas of the local seabed during site investigation/construction. In addition, predicted sea-level rise would make low lying coastal nuclear sites e.g. Sellafield and the Low- Level Waste repository (LLWR) vulnerable to tidal inundation with oxygenated seawater. Further, understanding the marine biogeochemistry of contaminant radionuclides may also benefit contingency plans for incidents such as Fukushima, whereby multiple reactor meltdowns resulted in the discharge of ~ 27 PBq (1 PBq = $10^{15}$ Bq) of radioactivity into the Pacific Ocean (Bailly et al., 2012). This discharge and others associated with the nuclear fuel cycle have directly affected marine ecosystems and coastal economies (MacDonald and Bewers, 1996; Buesseler et al., 2012; Tierney at al., 2016; Sanial et al., 2017). Despite the importance of these impacts on local

communities (human health, biota, and food) we know surprising little about the behaviour of anthropogenic radionuclides in the marine environment. Indeed, as nuclear reactors are often located near coastal locations, understanding the long-term fate of radioactive contaminants will prove central to safeguarding the global oceans. This can better help with informed decision making for future planned and unplanned discharges from coastal nuclear sites.

This research builds on a legacy of work led by University of Manchester alumni concerning Sellafield-derived radionuclides (Livens, 1985; Morris, 1996; Morris et al., 2000; Keith-Roach et al., 2000; Marsden, 2003; Kimber et al. 2012; Al-Qasmi et al., 2016). To date, the majority of these and other studies conducted with materials from the Irish Sea have focussed on ascertaining radionuclide distribution at locations acting as a radionuclide sink. Uniquely, this work investigates radionuclide behaviour at both the hypothesised source and sink sites, within the same year. In recent years, the importance of biogeochemical controls on radionuclide stability and mobility in the natural environment has been recognised (Livens et al., 2010; Renshaw et al., 2011; Lloyd and Gadd, 2011; Brookshaw et al., 2012; Newsome et al., 2014). Accordingly, this PhD project examines potential biogeochemical, physical and microbial controls on anthropogenic radionuclide distribution in the Irish Sea mud-patch and Ravenglass saltmarsh, and investigates any potential teleconnections that may exist between these sites. The majority of the Sellafield-derived radionuclides have long half-lives, and this provides further interest in characterising their long-term behaviour in the environment. Further, the Eastern Irish Sea is one of a few public locations that has received inputs of radioactive effluent over a period of 65 years, and as such, insights gained on long-term radionuclide biogeochemistry can be used to inform issues in radioactive waste disposal (e.g. geodisposal safety cases) and contaminated site management (e.g. harbour and coastal areas surrounding the Fukushima Daiichi nuclear power plant).

### 1.3. Nuclear Power

Hahn, Strassman, and Meitner discovered in 1938 that the irradiation of uranium (U) with neutrons yielded not only transuranic metals, but elements whose relative atomic masses were close to half that of U (Hahn and Strassman, 1939).

Meitner went on to collaborate with fellow Austrian, Frisch, and together they rationalised their initial findings as nuclear fission (Meitner and Frisch, 1939), a chain reaction whose spontaneity and high energy density is 2 to 3 million times greater than the same mass from coal or oil (European Nuclear Society, 2017). This heat output is used to generate steam, which drives turbines, and is responsible for generating electricity in commercial nuclear reactors worldwide (Choppin et al., 2002).

Nuclear power now generates ~ 11 % of the world's electricity (World Nuclear Association, 2017a). Currently, there are 449 operational commercial reactors in 31 countries, with the major nuclear electricity producers based in Europe and North America (IAEA, 2017). France is particularly reliant on nuclear power, as the source currently supplies 75 % of the country's total electricity (World Nuclear Association, 2017). In addition, less affluent, developing countries have recognised the potential of nuclear power to supply for their rapid growth of living standards (Joyce and Port, 1999). The recent Paris climate conference agreement in 2015 has driven world leaders to keep the global temperature rise this century well below 2 °C above pre-industrial levels (United Nations, 2017a). Nuclear energy is widely viewed as a low-carbon emitting, green, energy source; however its large stockpile of waste from the nuclear fuel cycle presents itself as a potentially less attractive option to conventional renewable sources. Additionally, nuclear accidents including Three Mile Island (1979), Chernobyl (1986), and Fukushima Daiichi (2011) have asked questions regarding the safety of civil nuclear power production, and this has accentuated negative public perception.

### 1.4. The UK Nuclear Legacy

The legacy of over half a century's nuclear power and weapons production has left the UK with the burden of a complex nuclear challenge. This started in 1947 with the construction of two graphite moderated reactors known as the Windscale Piles. These reactors were designed to produce plutonium (Pu) for nuclear weapons, to support the UK's defence programme following the Second World War. However, a few years after Windscale Pile 1 became operational in 1950, a build-up of Wigner energy caused a fire in the reactor releasing radioactive

plumes out of the plant chimney across UK and Western Europe. Thereafter, as global tensions subsided, the UK government recognised the potential of a civil nuclear power program. Subsequently, the UK pioneered civil nuclear power in 1956, with the commissioning of Calder Hall (at the Sellafield site), the first nuclear reactor to supply commercial energy to the national grid (Sellafield, 2016). This was the first of a fleet of Magnox reactors built between 1956–1971, and included units at Sizewell, Oldbury, and Hinkley Point (World Nuclear Association, 2016). Thereafter, there was a transition to Advanced Cooled Reactors (AGR) with seven twin-unit AGRs starting up between 1976–1989 (World Nuclear Association, 2016). The next phase of the UK nuclear program was influenced by a change in government in mid-1979, with Margaret Thatcher's Conservative government supporting the Pressurised Water Reactor (PWR). Sizewell B followed becoming operational in 1983. Thereafter, there was a period of little growth for the UK nuclear industry; with the government enforcing no new nuclear build between 1989–1993, and a year later announcing that new nuclear would not receive public funding.

Currently, there are 15 operational nuclear reactors, generating 20.4 % of the UK's total electricity (IAEA, 2017a). An aging fleet of Magnox reactors in the process of decommissioning will likely reduce almost half of this capacity by 2025 (World Nuclear Association, 2017a). More recently, the importance of nuclear power to the energy mix has been recognised by the UK government, and the country is currently undergoing a period of new nuclear build, with Hinkley Point C scheduled for operation in 2025 (BEIS, 2017). If new build is to be successful, the UK government has a social responsibility to manage current legacy wastes and contaminated sites, by reducing the burden for future generations. This process may be supported by a deeper scientific understanding of radionuclide behaviour

### 1.5. The UK Nuclear Waste Inventory

A substantial legacy of radioactive waste from pioneering civil and defence-related nuclear programmes has accumulated in the UK. Some of this waste is currently in storage, however the majority remains part of existing facilities, and can only become waste once plants are shut-down, and decommissioning and

clean-up operations completed (NDA and BEIS, 2017). The UK has a sizeable waste inventory, with the total packaged volume for all radioactive waste up to 2125 comprising 1500 $m^3$ of High Level Waste (HLW), 449,000 $m^3$ of Intermediate Level Waste (ILW), and 1,600,000 $m^3$ of Low Level Waste (LLW) (NDA and BEIS, 2017)

The volume of HLW is relatively small, however it is important as it is heat generating and represents over 95 % of the radioactivity in all radioactive wastes (NDA and BEIS, 2017). Radioactive wastes which contain > 4 GBq/tonne alpha and 12 GBq/tonne beta/gamma activity and does not produce significant heat is termed ILW, and this fraction contains less than 5 % of the total radioactivity. Any radionuclide bearing materials that fall below the ILW threshold are termed as LLW and Very Low Level Waste (VLLW), and the large volume of this type of waste (90.6 %) corresponds to less than 0.01 % of the total radioactivity (NDA and BEIS, 2017). LLW is stored at the near-surface facility known as the Low Level Waste Repository (LLWR) near Drigg in Cumbria. The discharge of aqueous LLW, under authorisation, has taken place from the Sellafield nuclear reprocessing site to the Irish Sea since 1952 (Kershaw et al., 1992; Gray et al., 1995). As the LLWR is based close to the Cumbrian coastline, the predicted sea-level rise may result in tidal inundation, and this may affect the stability of LLW held at the site.

### 1.6. The Nuclear Fuel Cycle

Radioactive wastes are produced at each stage of the nuclear fuel cycle and key processes such as U mining and milling, and spent fuel reprocessing are the largest producers of radioactive waste (Abdelouas, 2006). Mining and milling of U ore is the first step of the nuclear fuel cycle (Figure 1.1). Canada, Australia, Kazakhstan, Russia, Namibia, and Niger are the leading global suppliers of U ore, collectively producing over 50,000 tonnes annually (Sharrad et al., 2011). Here, mined U ore undergoes a series of chemical reactions; this involves roasting and leaching the ore with acid, and several crushing stages (Wilson, 1996). Uranium undergoes a number of oxidation state changes during processing to reach the final milled product $U_3O_8$ (known as yellowcake), which contains 65–70 % U

(Choppin at al., 2002). Solid waste from this process is known as ‘mill tailings’ and contains high levels of residual U and radium (Ra).

A large percentage of the ‘waste’ radionuclides (e.g. Th and Ra) are separated from U during milling, and impurities such as boron (B), cadmium (Cd) and molybdenum (Mo) are removed *via* purification steps (Wilson, 1996). Natural U consists of three isotopes ($^{234}U$, $^{235}U$, and $^{238}U$) and these contribute to 0.055 %, 0.711 %, and 99.28 % of the natural abundance, respectively (Choppin et al., 2002). The concentration of $^{235}U$ is increased to 3–5 atom % for use in modern reactors, and this process requires converting $U_3O_8$ to $UF_6$ (Sharrad et al., 2011). Two fundamental chemical processes are used in commercial enrichment: (i) centrifugation, and (ii) gaseous diffusion (for further information see Wilson, 1996). In turn, the process produces a depleted U waste stream (0.2 atom %) and this contributes to the increasing global depleted U inventory. Early reactors such as the UK Magnox reactor were specifically designed to use natural U, thus allowing the use of fuel having a natural isotopic composition (Ewing, 1999).

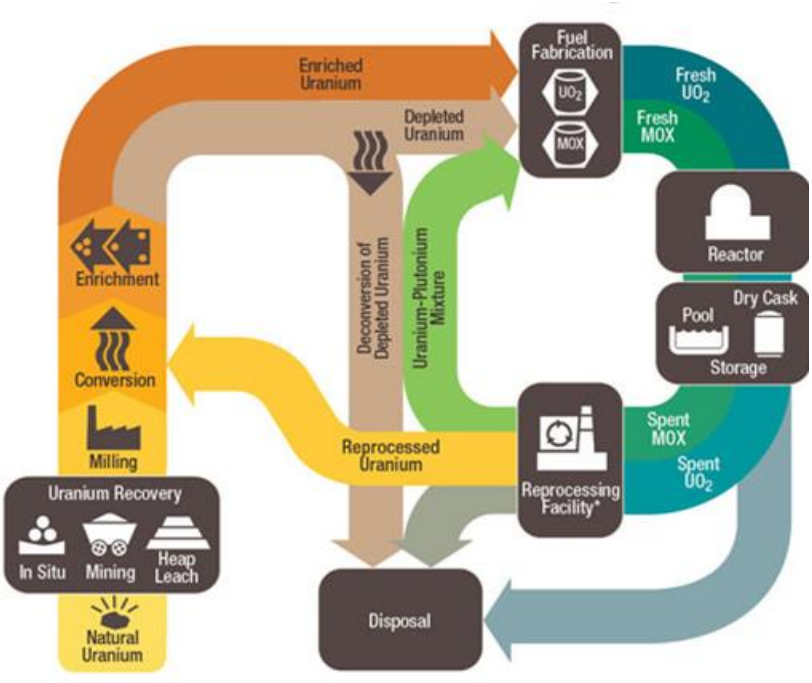


**Figure 1.1.** The Nuclear Fuel Cycle (taken from NRC, 2017).

Once enriched, U-bearing fuel is then fabricated. Here, $UF_6$ is converted to $UO_3$, reduced to ceramic $UO_2$, and pressed into pellets (Sharrad et al., 2011). These pellets are then loaded into zirconium-alloy or stainless steel rods which form a fuel assembly, a structure used to introduce fuel into a nuclear reactor. Currently 14 out of the UK's 15 operational nuclear power reactor units are Advanced Gas Reactors (AGR) (World Nuclear Association, 2017a), and these use enriched U and stainless steel cladding. Further, these reactors use $CO_2$ to remove heat from the reactor core. The remaining UK nuclear reactor, Sizewell B, is a Pressurised Water Reactor (PWR). The cooling mechanism for PWRs is *via* pressurised $H_2O$ and not $CO_2$ gas. Regardless, both absorb and then subsequently release heat to produce steam from water; and this drives turbine generating electricity.

Fuel which has been irradiated in a nuclear reactor and no longer has the ability to sustain a nuclear reaction is known as spent fuel. The ingrowth of contaminants, results in spent fuel being removed from a nuclear reactor after 3–4 years. As a result of the high radioactivity of the U fission products, the fuel is stored underwater in cooling ponds to allow: (i) decay heat to decrease, (ii) short-lived isotopes to decay, and (iii) to contain radiation that is emitted from the fission products (Chapman and McKinley, 1987). Solvent extraction forms the basis of spent fuel reprocessing, and utilises the differing chemical affinities of the actinides with ligands. The Plutonium Uranium Extraction (PUREX) method is employed by the UK, and this extracts Pu and U into the aqueous phase, separating them from fission products and from each other. However, it is important to note that additional waste streams are produced during this reprocessing step. Once reprocessed, both Pu and U can be used to produce Mixed Oxide (MOX) fuel. Of note, this is not the case in the UK, where instead they are stock-piled as a zero value asset.

There are two types of nuclear fuel cycles in current operation: (i) an open fuel cycle which includes the direct disposal of spent fuel; and (ii) a closed fuel cycle which creates an intricate array of waste streams through reprocessing operations (Sharrad et al., 2011). The open fuel cycle involves the storage of fuel in ponds to allow the decay of fission products and heat dissipation, followed by complete disposal as waste (Ewing, 1999). This is the method currently favoured by the

USA and Sweden. In contrast, the closed cycle provides options for waste management, reducing radiotoxicity and removing fissile material from spent fuel; the UK currently operates a closed fuel cycle. However, this may change in the future in the UK as both the Thermal Oxide Reprocessing Plant (THORP) and the Magnox reprocessing plant at Sellafield are scheduled to close in 2018 and 2020, respectively (Leafe, 2017).

Geological disposal has been chosen as the long-term management for Higher Activity Wastes (HLW and ILW) in England and Wales (CoRWM, 2006). This involves both the placement and segregation of waste in a Geological Disposal Facility (GDF) that is built within a suitable rock formation, to limit high doses of radioactivity from reaching the surface environment (NDA, 2011). The UK defines geological disposal as 'burial underground (200–1000 m) of radioactive waste in a purpose built facility with no intention to retrieve' (DEFRA, 2008). Currently the USA operates the world's only GDF (The Waste Isolation Pilot Plant, (WIPP)). In Europe, the Finnish and Swedish GDF programmes are well advanced, with disposal of waste scheduled in Onkalo, Finland during the 2020s (Posiva, 2017), and construction of the Swedish Nuclear Fuel and Waste Management Company (SKB) Spent Fuel Repository in Forsmark due to commence in the 2020s, with the facility scheduled to become operational 10 years later (SKB, 2016). The UK GDF programme remains in its infancy, and its implementation will require several decades of planning and construction, coupled with scientific understanding of the behaviour of radionuclides in geomedia. A consultation has recently been announced by the UK government which aims to seek views on engaging host communities for the GDF siting process (BEIS, 2018).

### 1.7. Major Sources of Anthropogenic Radionuclides to the Marine Environment

Decades of worldwide weapons production and testing, accidents, electricity generation, and spent fuel reprocessing has resulted in the radioactive contamination of the environment. In some instances, these unwanted radionuclides have been transferred on a large scale in the atmosphere, and

locally by surface waters, or groundwater plumes. Renshaw et al. (2011) have summarised key transfer processes that have been suggested to accelerate the migration of these radionuclides once they enter the environment (Figure 1.2). Globally, the biggest contributor to the environment is nuclear fallout, however this varies on a local scale; in the Irish Sea, the input of radionuclides from Sellafield reprocessing facility to the Irish Sea is the dominant contributor (IAEA, 2005) (see section 1.8). The marine environment in the vicinity of Sellafield is regularly monitored, and in 2015 this was conducted by the UK Environment Agency and the Food Standards Agency (FSA). This annual survey includes the effective dose rates, and radionuclide measurement of biota, water, and environmental materials (Cefas, 2017). Further, the radionuclides $^{241}$Am, $^{137}$Cs, $^{239,240}$Pu, and $^{60}$Co were monitored at the Ravenglass saltmarsh as part of this work, and highlight a temporal decrease in radionuclide activity over time (Cefas, 2017).

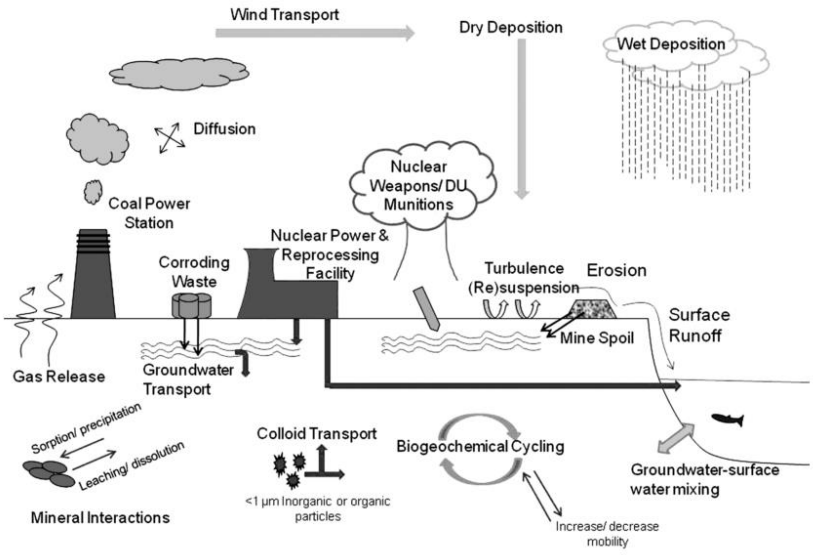


**Figure 1.2.** Schematic showing the primary sources of radionuclides in the environment, and the key processes that control their mobility in the environment (taken from Renshaw et al., 2011).

### 1.7.1. Nuclear Weapons Testing

Approximately 2000 nuclear weapons were tested between 1945 and the signing of the Comprehensive Nuclear-Test-Ban-Treaty (CTBT) in 1996 (United Nations,

2017b). Since the signing, there have been nuclear tests by India, Pakistan (Livingston and Povines, 2000), and more recently by the Democratic People's Republic of Korea, who have tested five nuclear missiles between 2006 and 2016 (World Nuclear Association, 2017). Global fallout from historical atmospheric nuclear tests are the dominant input of radionuclides from the stratosphere to the Earth's surface (including the surface waters of the global oceans) (Livingston and Povines, 2000). In addition, surface and underground nuclear tests were carried out historically at the Mururoa and Fangataufa Atolls in French Polynesia (Livingston and Povines, 2000), as the French detonated their first nuclear weapon test in 1966. This was followed thereafter with 210 nuclear tests until 1996 (IAEA, 1998). Here, the major source of contamination to the marine environment was by Pu buried in lagoon sediments released from the tests (Livingston and Povines, 2000). The total $^{239,240}$Pu inventory is ~ 30 TBq at both these sites (IAEA, 1999).

### 1.7.2. Nuclear Accidents

The Chernobyl (UNSCEAR, 2008) and, more recently the Fukushima Daichii (UNSCEAR, 2012) disasters are two nuclear accidents that have resulted in the contamination of the marine environment. Radionuclides released from the Chernobyl accident include $^{137}$Cs, $^{90}$Sr, and Pu, with the total activity of these radionuclides released into the environment reported as 85 PBq, 10 PBq, and 0.055 PBq, respectively (WHO, 1989). Radio-caesium from Chernobyl caused widespread contamination; however this was largely restricted to the Baltic Sea (IAEA, 2004). The Tohuku earthquake, and resulting tsunami, resulted in the loss of power and overheating at the Fukushima Daiichi Nuclear Power Plant (FDNPP) in 2012. This subsequently led to the release of contaminant radionuclides from the nuclear site into the Pacific Ocean by site operators. The magnitude of total $^{137}$Cs releases were considerably smaller than those from Chernobyl, and have been suggested to be similar in magnitude to $^{137}$Cs discharge from the Sellafield nuclear reprocessing facility (~ 15–16 PBq) (Buesseler et al., 2017). As a result of the Fukushima incident, there has been a renewed focus on understanding the impact of the discharged radioactive effluent on terrestrial and marine populations (Buesseler et al., 2011; Kinoshita et al., 2011; Buesseler et al., 2012; Castrillejo et al., 2016).

### 1.7.3. Authorised Releases from Nuclear Sites

The principal sources of radionuclide discharge to the sea have occurred from two nuclear sites; Cap la Hague in France, and Sellafield, UK (Salbu et al., 1993; Livingston and Povines, 2000). Low-level waste has been routinely discharged from Cap la Hague to the English Channel since 1966 (Schneider and Marignac, 2008), with ~ 8 PBq of activity being released up to 1985; and this included $9 \times 10^{14}$ Bq of $^{137}Cs$, and $3 \times 10^{12}$ of $^{238}Pu$ + $^{239,240}Pu$ (Salbu et al., 2003). The authorised discharge of Sellafield-derived effluent has taken place from 1952, and is the major source of radioactive contaminants in the Eastern Irish Sea area. This is discussed in more detail in section 1.8.1.

## 1.8. Sellafield

Sellafield Ltd. is the Site Licence Company (SLC) tasked with safely delivering decommissioning, reprocessing, nuclear waste management and fuel manufacturing activities at the Sellafield site, on behalf of the Nuclear Decommissioning Authority (NDA); a non-departmental public body sponsored by the UK government. Sellafield is located on the West Cumbrian coastline close to the village of Seascale, and was formerly owned by British Nuclear Fuels Ltd (BNFL), a government owned subsidiary until 2005. The site was constructed in 1947, and was designed to support the UK nuclear weapons programme. Since then, Sellafield has transitioned from a nuclear facility generating military-grade Pu, to one that focuses on the back end of the nuclear fuel cycle. As spent fuel reprocessing at the THORP and Magnox reprocessing plants near the end of their lifetime, the emphasis has shifted to remediation, and decommissioning of the ageing Windscale and Calder Hall reactors (Sellafield, 2016). This also includes the clean-up of legacy spent fuel storage ponds (e.g. First Generation Magnox Storage Pond (FGSMP)).

### 1.8.1. Authorised Sellafield LLW discharge

The authorised discharge of aqueous LLW from the Sellafield nuclear reprocessing facility has taken place since 1952, and resulted in the radioactive contamination of the nearby Eastern Irish Sea (MacKenzie and Scott, 1993; MacKenzie et al., 1994; McCartney et al., 1994; Morris et al., 2000; Lucey et al.,

2004; Marsden et al., 2006; Lindahl et al., 2011; Ray et al., 2018). This contamination has also been reported in locations further afield, including Dulas Bay, North Wales and Loch Etive, Scotland (Al-Qasmi et al., 2015, 2017); the North Sea, Scandinavian waters and sediments (Keith-Roach et al., 2003; Keith-Roach and Roos, 2004); the Norwegian Sea and the Barents Sea (Salbu et al., 1993); and the Arctic Ocean (Dahlgaard, 1995). The focus of this thesis is on the distribution of Sellafield-derived radionuclides in the Eastern Irish Sea, specifically in the offshore Irish Sea mud-patch and Ravenglass saltmarsh.

To provide validation for the effluent discharge from the Sellafield pipeline, tracer experiments were conducted in the late 1940s, which saw the release of fluorescent dye into the Irish Sea. Further, tidal movement and radionuclide uptake studies were also carried out (Kershaw et al., 1992). Thereafter, in 1952 low-level liquid effluent was discharged into the Irish Sea *via* pipelines extending seawards 2.5 km from the high water mark and ending 20 m below the surface of the water (Gray et al., 1995). On-site reprocessing activities and water used to purge storage ponds have been the major source of LLW released into the Eastern Irish Sea (Assinder et al., 1991; Gray et al., 1995). The discharge histories of the radionuclides examined in this thesis are shown in Figure 1.3. The majority of these radionuclides have been monitored by site operators since 1952.

Spent fuel reprocessing operations stopped temporarily in 1974, and this increased the residence time of Magnox fuel in storage ponds (Kershaw et al., 1992). As a result, there was an enhanced concentration of soluble radionuclides in the cooling pond waters, and this caused the activity of the majority of the Sellafield-derived radionuclides to increase between 1974–1978 (Figure 1.3). Thereafter, there was a gradual decline in activity for the majority of radionuclides in the 1980s, as stricter discharge limits were imposed and new effluent treatment methods were introduced. Here, the discharge of medium-active concentrate was terminated and fuel storage pond water was purified and treated by passing through several sand filters and clinoptilolite ion exchangers; a

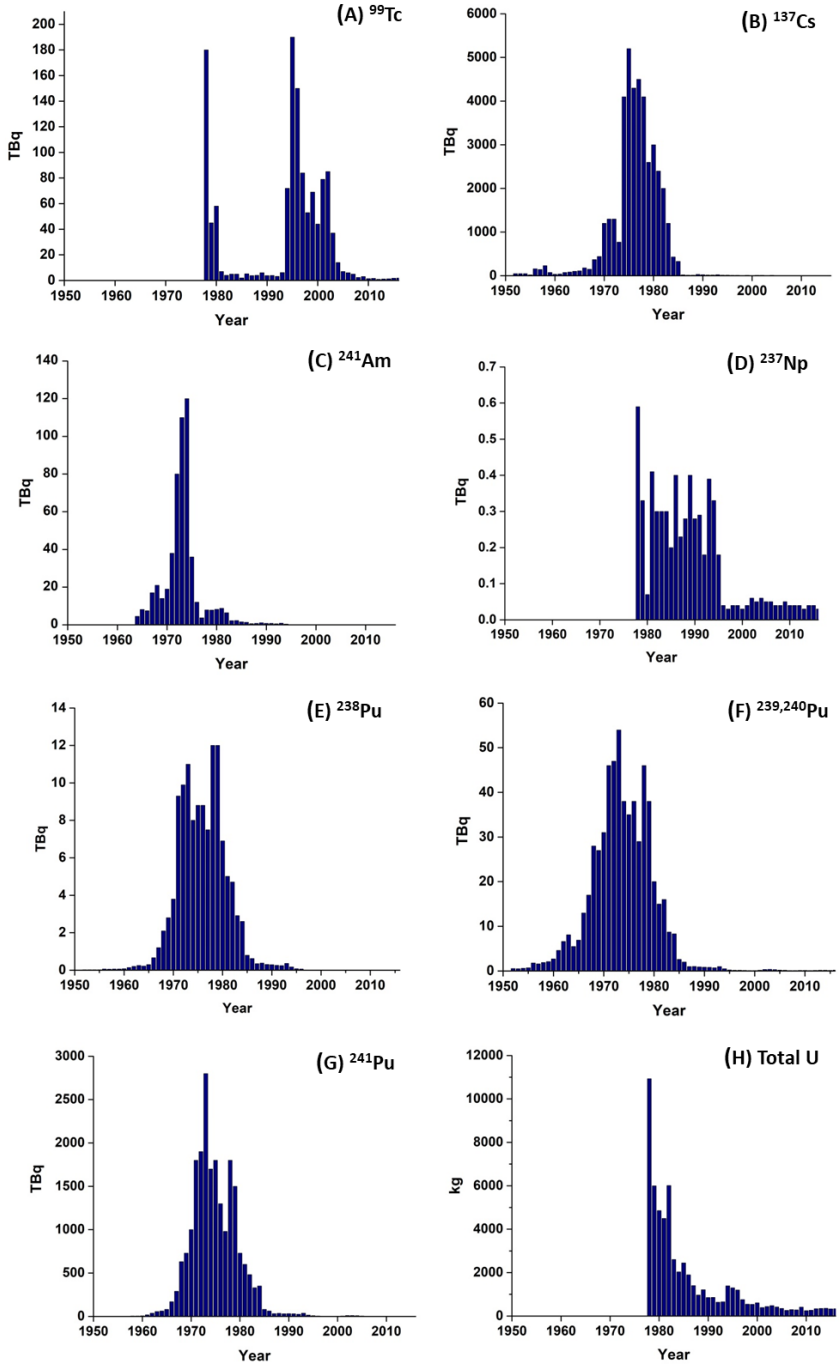


**Figure 1.3.** Discharge of (A) $^{99}$Tc; (B) $^{137}$Cs; (C) $^{241}$Am; (D) $^{237}$Np; (E) $^{238}$Pu; (F) $^{239,240}$Pu; (G) $^{241}$Pu, and (H) Total U in liquid effluent from Sellafield between 1952–2015 (adapted from Gray et al., 1992; BNFL 1993–2005; Sellafield Ltd, 2015).

process which took place at the Secondary Ion Exchange Effluent Plant (SIXEP). This plant was commissioned in 1986, followed by the Enhanced Actinide Reprocessing Plant EARP treatment (Gray et al., 1995) plant in 1994. However, these treatments were successful in reducing the activity of actinides in the effluent, but as they were used to process a backlog of wastes in the mid-1990s, this caused $^{99}$Tc concentrations to increase in discharges from 1994 onwards (BNFL, 1999) (Figure 1.3).

The chemical form of the discharged effluent will provide an insight into the speciation of the radionuclides. There are, however, limits to the extent of information available on Sellafield releases. Previously, Kershaw et al (1992) has reported that ammonia solution is added to Sellafield sea-tank effluent prior to pipeline discharge, and thus the pH of the effluent is suggested to be ~pH 8-9. The aqueous effluent may also contain iron; this may result in the precipitation of ferric hydroxide or iron floccs when the effluent enters the Irish Sea. At the point of discharge, the slightly basic effluent will interact with the saline environment of the Eastern Irish Sea. The pH of this environment (pH 7.6; Malcom et al., 1990) is slightly lower than the effluent (see above). The Eastern Irish Sea will have a higher ionic strength and this may influence the binding behaviour. In addition, the marine environment will host both dissolved/colloidal organics, alongside suspended sediment; these can all interact with the radionuclides present in the effluent (see section 1.9 for further info).

Sediment surfaces are typically negatively charged, and the radionuclides present in the effluent are commonly positively charged (Am(III); Cs(I); Pu(IV); Pu(V); $Np(V)O_2^+$). This coulombic attraction will likely result in the association of the radionuclide with any suspended sediment in the Eastern Irish Sea including any dissolved/colloidal organic material. Conversely, pertechnatate ($TcO_4^-$) is the common anionic species formed by Tc(VII),. Due to the anionic charge this species has a high solubility as it is repelled from sediment surfaces.

## 1.9. Biogeochemistry of the Subsurface

Once released into the marine environment, the mobility of the majority of the radionuclides discharged from the Sellafield pipeline will be dominated by their interactions with minerals in the subsurface (Koch-Steindl and Prohl, 2001; Renshaw et al., 2011). The actinides particularly will be sequestered from solution by minerals *via* sorption, complexation, co-precipitation or incorporation. Other processes that will occur in the marine environment and effect radionuclide behaviour are: hydrolysis and microbially-mediated reactions. Some of these processes are shown in Figure 1.4 and are briefly discussed below.

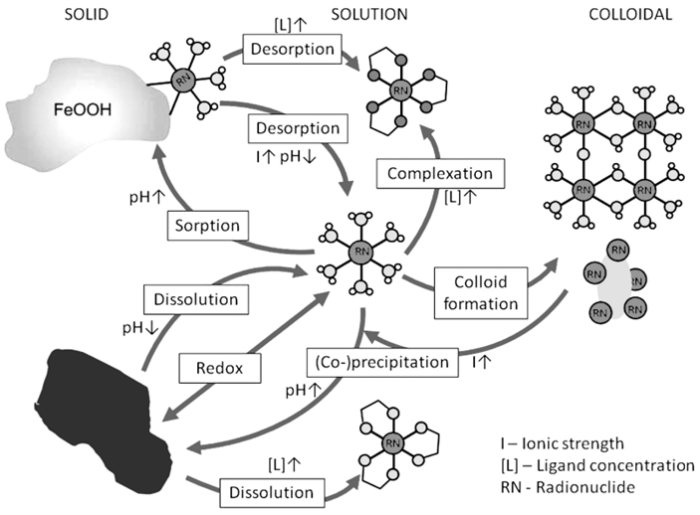


**Figure 1.4.** Key geochemical processes that may influence radionuclide behaviour in the environment (taken from Renshaw et al., 2011).

### 1.9.1. Sorption

The adsorption of metal ions on minerals is able to regulate their mobility in open waters. This mechanism involves O-donor atoms on hydroxyl groups (ubiquitous on mineral oxide/hydroxide surfaces) interacting with protons (to form water), and the metal of the oxide acting as a Lewis acid, thereby exchanging the OH group for other ligands to form a surface complex. There are three types of interaction between a surface and a free ion: chemisorption, physisorption, and ion exchange. Chemisorption involves the radionuclide forming a strong covalent

bond with the mineral surface, producing an inner sphere complex. Weak Van der Waals forces can associate a radionuclide to the surface of a mineral, known as physisorption, and this can form an outer sphere complex. Physisorption interactions are weak, and this increases the likelihood of radionuclide desorption from the mineral surface. The mechanism for ion-exchange involves the substitution of a radionuclide with a species from a mineral structure. For example, Cs has been shown to adsorb by simple ion exchange on clay basal planes (Fuller et al., 2014).

The sorption of radionuclides to the majority of environmentally relevant minerals can occur at near-neutral pH, with fluctuations in pH, and ligand concentration able to reduce the interaction or electrostatic attractions between the radionuclide and mineral. Adsorption-desorption reactions which take place under equilibrium conditions, at a solid boundary are estimated by a radionuclide's distribution coefficient ($K_d$) (Equation 1.1) (IAEA, 2004).

$$K_d = \frac{radionuclide\ concentration\ in\ solid\ phase\ (Bq/kg)}{radionuclide\ concentration\ in\ dissolved\ phase\ (Bq/L)}$$

(Equation 1.1)

$K_d$ is often used to estimate the approximate partitioning of a radionuclide between the dissolved and particulate phases (Assinder et al., 1984; EPA, 1999; Siegel and Bryan, 2003; Li and Kaplan, 2012). There is an assumption that the exchange of radionuclides between solid particulate matter and water is largely reversible when using the $K_d$ approximation, and as a result $K_d$ values are regularly used to determine the extent of radionuclide sorption. $K_d$ values for a range of radionuclides have been determined from both laboratory experiments and field observations. However, a limitation of $K_d$ approximation is that values are site-specific and are relevant only to the aqueous or geological system they were determined in (Vejsada, 2006), and as such real understanding of the processes between the solution and solid-phase is needed.

### 1.9.2. Incorporation/Precipitation Reactions

The effective adsorption of radionuclides to mineral surfaces can in certain cases lead to its incorporation (Cornell and Schwertmann, 2003a). This generally takes place when a mineral phase has formed with radionuclides in the vicinity, causing the radionuclide to be substituted into the structure of a mineral (NDA, 2010). The likelihood of this substitution is dependent on the valency of the radionuclide and the similarity of the ionic radii and valency of the cation being substituted in the mineral lattice (Goldschmidt, 1937). For example, Fe oxides are widespread in nature, and the mineral magnetite ($Fe_3O_4$) is able to incorporate other metal ions (including $Cu^{2+}$, $Mn^{2+}$, $Cd^{2+}$) into its lattice sites (Sidhu et al., 1978). It can accommodate these ions, and others, by expansion and contraction of its structure (Cornell and Schwertmann, 2003b). Once the radionuclide is incorporated into the mineral it is irreversibly bound, and can only be released back into solution by the dissolution of the host phase. However, it is generally regarded that structurally incorporated radionuclides will be difficult to access, and as such their migration will be significantly reduced.

### 1.9.3. Hydrolysis

Hydrolysis will affect radionuclides in solution. The interaction of water ligands with radionuclides can form soluble hydroxides, and oxide complexes, alongside precipitates of hydroxides, oxides, and basic salts (Clark et al.,1995). Reduced actinide (IV) ions (e.g. Pu(IV), Np(IV), and U(IV)) have a high charge density and as such can form hydrolysis products, even in extremely acidic solutions (as low as pH 0.73). For example, Pu(IV) has been recognised to form the hydroxide precipitate [$Pu(OH)_4$] in solution (Ewing, 1999). (Equation 1.2). Actinides in their pentavalent state (e.g. $Pu(V)O_2^+$ and $Np(V)O_2^+$) are not hydrolysed until pH> 9, with trivalent (Am(III)) and hexavalent species ($UO_2^{2+}$) not being readily hydrolysed below pH 4 at 25 °C (Clark, 1995). In solution the general trend in complex formation/stability is: $An^{4+} > An^{3+} \sim AnO_2^{2+} > AnO_2^+$ (Katz et al., 1986).

$$An^{4+} + H_2O \rightleftharpoons An(OH)^{3+} + H^+$$

(Equation 1.2)

### 1.9.4. Indigenous Microbial Activity

Microbes in the sub-surface can influence the fate of contaminant radionuclides in the environment by facilitating (bio)sorption, changing radionuclide speciation directly (if the radionuclide is redox active), and/or by indirectly producing chelating ligands. In the geosphere, microorganisms will aim to metabolise available substrates, and this can often influence the ambient redox conditions of the sediment system. Microorganisms tend to couple electron donors and acceptors that generate the highest yield (standard Gibbs free energy). Further, the yield generated is dependent on the Primary Electron Donor (PED) and the Terminal Electron Acceptor (TEA) (Konhauser, 2007). Microorganisms are specialised to utilise organic and inorganic substrates as PEDs (e.g. glucose, acetate, and $H_2$), and various chemical species as TEAs for energy production.

Microbial metabolism can drive a number of redox transformations within the sub-surface, resulting in a natural redox cascade as TEAs are progressively utilised by microbial communities. There is a typical sequence of TEAs exploited by microorganisms in order of decreasing free energy yield ($O_2 > NO_3^- > NO_2^-$, Mn(IV/III) > Fe(III) > $SO_4^{2-}$) after which methanogenesis may take place (if conditions are favourable) (Stumm and Morgan, 1995; Konhauser et al., 2002; Konhauser, 2007). This is a simplified analysis, and more often the boundaries between these zones may be less well-defined in a natural sediment system. This could be due to spatial changes in microbial community, physical mixing, the lack of electron donor, or a combination of these. Sediment redox zonation is discussed further in sections 1.10–1.11. The oxidation state transitions for redox-active radionuclides discussed in this thesis, and their corresponding Eh values are shown in Figure 1.5, alongside the common TEA processes in the environment. This highlights the overlap of these two redox-related processes, as the conditions relevant to the study sites discussed in this work may be favourable for both of these processes to take place.

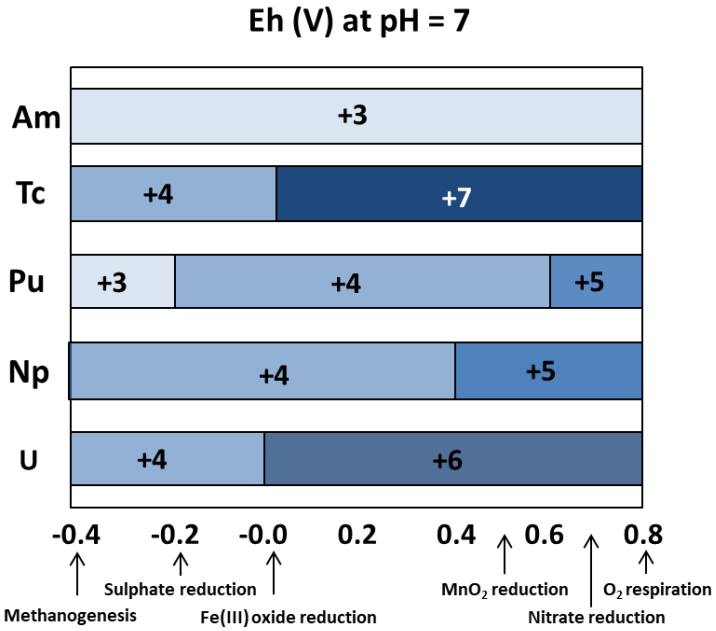


**Figure 1.5.** Oxidation state transitions of redox-active radionuclides across an Eh range of -0.4 to 0.8 V at pH 7 and corresponding Eh values for important microbial redox processes (adapted from Lloyd, 2003).

### 1.10. Oxic sediments and Aerobes

Bottom waters in oceans can supply surficial sediment with $O_2$ and as such diagenesis in this zone (the oxic zone) proceeds *via* aerobic metabolism. Here, aerobes use $O_2$ as an electron acceptor (due to the associated maximum Gibbs free energy gain; Equation 1.3). Aerobes are equipped with enzymes capable of breaking down complex organic molecules into smaller, more usable substances (Konhauser 2007); however in this thesis all respiratory reactions are expressed with acetate in order to provide easy comparison. Aerobes do not tend to influence radionuclide speciation.

$$CH_3COO^- + 2O_2 \rightarrow H_2O + 2CO_2 + OH^-$$

$$\Delta G° = -854\ kJ\ mol^{-1}\ acetate$$

(Equation 1.3)

### 1.11. Suboxic/Anoxic Sediments and Facultative and Obligate Anaerobes

The depletion of $O_2$ with depth in sediments leads to the formation of sub-oxic conditions, often within a few mm of the sediment-water interface (see Figure 1.6). Here, facultative anaerobes can switch TEAs from $O_2$ to other substrates, starting with the most energetically favourable (most negative $\Delta G°$): $NO_3^-$ > $NO_3^{2-}$ > $Mn^{4+}$ > $Fe^{3+}$ (see Figure 1.6). Eventually, a range of facultative and obligate anaerobes then switch to respire with $SO_4^{2-}$ and $CO_2$ in the anoxic sediment zone. The respiratory processes in these sediment zones are discussed further below. It is also noteworthy that a range of facultative and obligate anaerobes can directly and/or indirectly influence radionuclide speciation and hence solubility. These are highlighted in the relevant radionuclide section (1.12–1.13).

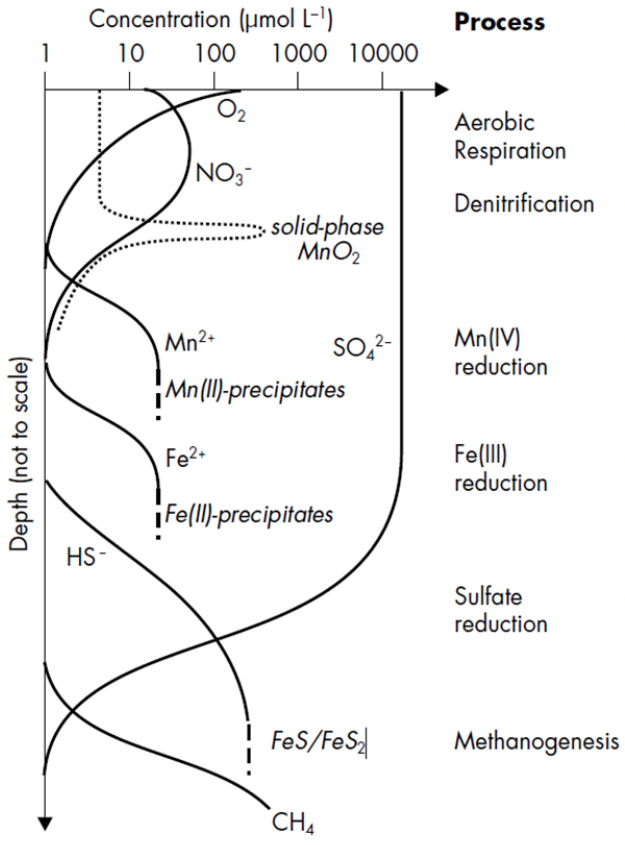


**Figure 1.6.** Porewater and solid-phase profiles based on the sequential utilisation of electron acceptors during the decomposition of organic matter (taken from Konhauser, 2007).

### 1.11.1. Nitrate Cycling

In suboxic sediments, the distribution of aqueous N species is largely controlled by nitrification and dissimilatory nitrate reduction (Konhauser et al., 2002; Konhauser, 2007). As the former is chemoautotrophic and not a terminal electron accepting process it is not discussed in this thesis. Microorganisms that utilise $NO_3^-$ as a TEA will gain a smaller Gibbs free energy ($\Delta G°$) than aerobic respiration, to fulfil their energy demands. Dissimilatory nitrate reduction includes the reduction of $NO_3^-$ to $NH_4^+$ by nitrate-reducing bacteria with denitrifying bacteria reducing $NO_3^-$ to $N_2$ (Equation 1.4; Figure 1.6). Denitrifiers can also completely degrade organic matter to carbon dioxide, similar to aerobic bacteria (Konhauser, 2007).

$$CH_3COO^- + 8NO_3 \rightarrow 4N_2 + +13OH^- + H_2O + 10CO_2$$

$$\Delta G° = -801\ kJ\ mol^{-1}\ acetate$$

(Equation 1.4)

Fermentative microorganisms have a similar role in this region of the sediment system, as they metabolise complex organic matter to more accessible organic substrates for the anaerobes. This happens once hydrolysis of the complex material by aerobes or denitrifiers has taken place.

### 1.11.2. Manganese Cycling

The oxidised form of Mn is generally found in nature as solid oxides and oxy(hydr)oxides (Stumm and Morgan, 1981). Manganese enters the ocean as oxide coatings on particulate matter transported by diffusion, wind and riverine processes (Calvert and Pedersen, 1993). Additionally, Mn oxides/hydroxide minerals exist in the ocean as poorly crystalline nodules; the dominant phases include mixed valence minerals such as hausmannite ($Mn_3O_4$), and the stable form of MnOOH, manganite Post, 1999). These oxy(hydr)oxides are thermodynamically stable in oxic seawater, however on burial into the sub-oxic and anoxic zones of the sediment, they enter reducing conditions where they become unstable (Konhauser, 2007). This instability, without the presence of $O_2$, and following denitrification results in the next energy efficient process:

microbial dissimilatory reduction of solid phase $MnO_2$ to dissolved Mn(II). Here, the reduction of oxidised Mn(IV) species to Mn(II) is coupled to organic matter oxidation (Equation 1.5) (Konhauser, 2007).

$$CH_3COO^- + 4MnO_2 + 3_2O \rightarrow 4Mn_2 + +2HCO_3 - +7OH^-$$

$$\Delta G° = -558\ kJ\ mol^{-1}\ acetate$$

(Equation 1.5)

For typical sediments, the concentration of reduced Mn species in porewater is negligible at the surface and increases in concentration after the maximum $NO_3^-$ concentration (see Figure 1.6). The solubility of Mn(II) species results in its cycling within sedimentary redox boundaries. Here, the onset of mixing and diffusion results in the upwards transport of Mn(II) to the surface, followed by re-oxidation to $MnO_2$, and further microbial reduction (if applicable). The potential importance of Mn in actinide biogeochemistry has been recognised for Pu, Np, and U (Powell et al., 2006; Wang et al., 2013). Further discussion on the specific connections between Mn and Pu/Np/U bio-cycling are discussed in sections 1.12–1.13.

### 1.11.3. Iron Cycling

The dissimilatory reduction of Fe(III) is able to influence the biogeochemical cycles of other metals in the environment. The microorganisms capable of this reduction possess hydrolytic enzymes that allow them to facilitate dissimilatory Fe(III) reduction for cell growth. The TEA in this process is Fe(III) and is transformed to Fe(II) *via* a $1e^-$ transfer, coupled to the oxidation of buried organic matter to $CO_2$ (Equation 1.6):

$$CH_3COO^- + 8Fe(OH)_3 \rightarrow 8Fe_2 + 2HCO_3 + 15OH^- + 5H_2O$$

$$\Delta G° = -337\ kJ\ mol^{-1}\ acetate$$

(Equation 1.6)

In aquatic sediments, hydrated Fe-oxide minerals will provide the dominant source of Fe(III). The presence of crystalline minerals including hematite ($Fe_2O_3$),

goethite (FeO(OH)), and magnetite ($Fe_3O_4$) in the sediment act as a source of reducible Fe (Konhauser, 2007). This process normally occurs below the zone of dissimilatory Mn(IV) reduction, and above the $SO_4^{2-}$ reducing zone (see Figure 1.6).

Ferric Fe inventories are replenished by the upwards diffusion of Fe(II) forming Fe oxides *via* the abiotic reaction with $NO_3^-$, and/or $O_2$. Further, the onset of microbially-mediated Fe(III)-reducing conditions have been shown to favour the abiotic electron transfer from biogenic Fe(II) to Tc(VII) (Lloyd et al., 2000; Begg et al., 2007; Plymale et al., 2011). However, this association is not limited to Tc, as reactive Fe(II) in the subsurface can also influence the cycling and mobility of Pu, Np, and U. This can reduce the contaminant radionuclide to a less soluble form, and result in the subsequent incorporation in, or adsorption onto the oxidised product, commonly an Fe(III) oxy(hydr)oxide or a mixed Fe(II/III) solid such as magnetite (see sections 1.12–1.13 for further discussion, specific to each radionuclide).

### 1.11.4. Sulfur Cycling

Sulfate Reducing Bacteria (SRBs) couple the reduction of $SO_4^{2-}$ to simple organic compounds creating $H_2S$ and/or other sulphide compounds e.g. $HS^-$ (Equation 1.7; Figure 1.6).

$$CH_3COO^- + SO_4^{2-} + H_2O \rightarrow H_2S + 2HCO_3 + OH^-$$

$$\Delta G° = -48\ kJ\ mol^{-1}\ acetate$$

(Equation 1.7)

In sediments supporting sulfate reduction, Fe monosulphide minerals such as mackinawite (FeS) may form leading to mineralisation (Konhauser, 2007). These minerals and free sulfide in solution, can react with redox-active radionuclides (e.g. U, Np, Pu) lessening their solubility (for further detail see Moyes et al. (2002), Hua and Deng, (2009), and Carpenter et al. (2015)).

## 1.12. Radionuclide Biogeochemistry

The solubility of a radionuclide and its speciation (the chemical form of the species in aqueous solution) has an effect on its mobility in the environment. It has been suggested that the aquatic chemistry of certain radionuclides (e.g. Pu, U, Np, Tc) in aqueous solution depend on three factors: (i) redox processes, which can result in the presence of a principal oxidation state in solution (discussed in section 1.9.4); (ii) solid phases that are able to act as surface for radionuclide immobilisation (see section 1.19.1 for discussion on sorption), and (iii) complexation reactions with ligands ubiquitous in aqueous systems (e.g. hydroxide ions). The $OH^-$ species is ubiquitous in the marine environment, with the hydration of a radionuclide with water molecules able to increase its solubility, whereas the formation of hydroxides or hydrolysed complexes will tend to decrease the solubility of a radionuclide (see section 1.9.3 for detail on hydrolysis) (Altmaier and Vercouter, 2012a). This will determine how radionuclides are transported in oxic and anoxic conditions, and this is particularly important for examining the long-term fate of contaminants in the marine system.

The following sections (1.12.1–1.12.6) provide an overview of the environmental behaviour of the radionuclides that are the focus of this thesis, and reviews previous, relevant work carried out in the Irish Sea.

### 1.12.1 Americium

Americium ($^{241}$Am; $t_{1/2}$ = 432.2 years) is formed by successive neutron capture of $^{239}$Pu, followed by the eventual $\beta^-$ decay of $^{241}$Pu. Unstable $^{241}$Am predominantly decays *via* α-emission, with a weak γ by-product; this low-energy γ-emission at 59.5 keV is most readily used to characterise $^{241}$Am in the environment (see Equation 1.8).

$$^{241}Am \rightarrow {}^{237}Np + \alpha + \gamma\ 59.54\ keV$$

(Equation 1.8)

Americium is commonly found in the environment as Am(III) (Lovett, 1978; Lehto and Hou, 2010; McDonald, 2011) and as a result of its high charge density,

Am normally undergoes hydrolysis and precipitates as a solid or sorbs to surfaces (Lehto and Hou, 2010). As a result of the strong sorption characteristics of the hydroxide produced, Am is generally found associated with colloids, sediment, and humic materials, and it has previously been suggested that $Am(CO)_3(OH)$ is the limiting species for the solubility of Am in sea water (MacKenzie et al., 1994). The high affinity of $^{241}Am$ for solid surfaces is further highlighted by its measured $K_d$ value of $10^6$ (IAEA, 2004; McDonald et al., 2001). Americium only has access to the III oxidation state under ambient Eh and pH conditions, and thus redox reactions do not impact its solubility.

A number of studies have investigated the fate of Am in the Irish Sea (Aston and Stanners, 1981; Aston and Stanners, 1982; Kershaw, 1984; Kershaw et al., 1999), and have concluded that the majority of the $^{241}Am$ inventory has rapidly and effectively been removed from seawater to sediments. Thus, in the Irish Sea, the dominant reaction mechanism for Sellafield derived $^{241}Am$ is likely rapid association to suspended particulates followed by deposition in nearby sediment followed by gradual transport elsewhere in the Irish Sea. For example, Aston and Stanners (1982) found that Am from Sellafield was transported from the Irish Sea mud-patch to the Cumbrian coast ~ 2.5 years after authorised discharge into the Irish Sea. This implies transport of Am bearing particulates in currents rather that rapid transport of a solvated Am cation. Additionally, the contemporary ingrowth of $^{241}Am$ can occur driven by the β-decay of discharged $^{241}Pu$. Sellafield discharge records have shown that~ 27 % of the total $^{241}Am$ content in the Irish Sea originated from the decay of $^{241}Pu$ (Day and Cross, 1981).

The distribution of $^{241}Am$ has been investigated at the Ravenglass saltmarsh previously; with the most recent study showing a maximum activity of ~130 kBq/kg, in sediment cores collected in 2002 (Lucey et al., 2003). Elevated $^{241}Am$ was observed at the bottom of the sediment core highlighted by a shallow peak. Further, a range of sites were examined in the Eastern Irish Sea, including the Irish Sea mud-patch which showed an $^{241}Am$ activity of ~625 Bq/kg (MacKenzie et al., 1999) in a surface sediment sample collected in 1992.

### 1.12.2. Caesium

There are two caesium isotopes produced by nuclear reactors: $^{134}$Cs ($t_{1/2}$ = 2.06 years), and $^{137}$Cs ($t_{1/2}$ = 30.2 years). The short-lived $^{134}$Cs is an activation product that has been used as an isotopic signature in the aftermath of the Fukushima accident to monitor the dispersion of the contamination in the Pacific Ocean (Buesseler et al., 2011; Kameník et al., 2013). Due to its short half-life $^{134}$Cs is of little environmental concern in the long-term. Instead, the longer lived $^{137}$Cs isotope is examined in this thesis. It is a high energy γ-emitter and fission product and is present in the marine environment, due to both nuclear fallout and effluent discharge. The reprocessing plant at Sellafield has released a total $^{137}$Cs activity of 41 PBq to the Irish Sea between 1952–1998 (Smith, 2011) and as such this is the major source of $^{137}$Cs present in the Irish Sea. In addition, a significant amount of $^{137}$Cs was released into the northern hemisphere as a result of the Chernobyl accident (Ilyin et al., 1990). However, it is likely that this signal will be masked in Irish Sea sediments by the enhanced Sellafield discharge. $^{137}$Cs decays predominantly *via* β-emission to $^{137m}$Ba (an unstable isomer of Ba), and subsequently decays to ground state $^{137}$Ba within a few minutes, releasing a characteristic photon (Equation 1.9):

$$^{137}Cs \rightarrow {}^{137m}Ba \rightarrow {}^{137}Ba + \gamma\ 662keV$$

(Equation 1.9)

Caesium is highly soluble and is present as the 'conservative' monovalent cation ($Cs^+$) under all conditions of pH and Eh. The measured $K_d$ value for Cs is $10^3$–$10^4$ (Hunt and Kershaw, 1990) reflecting its high solubility in aqueous media. As a result, its concentration in seawater (and its mobility) is controlled by its association on the surface of soil minerals, commonly *via* cation exchange (Sawhney, 1972; Cornell, 1992). Caesium forms compounds *via* electrostatic interactions, and interestingly, its behaviour has been recognised to differ between open water and that of sediments (Aston and Stanners, 1981). Caesium is not readily adsorbed onto Fe-oxide minerals (Wang et al., 2000) and is instead principally adsorbed to clay mineral surfaces (Grütter et al., 1990; Chibowski and

Zygmunt, 2002). The mechanism of Cs adsorption to clay minerals occurs *via* several pathways. This includes outer-sphere adsorption which is the electrostatic bonding of a hydrated ion to a surface; inner sphere adsorption of the dehydrated ion to the surface reactive site; and incorporation into the clay structure (Fuller et al., 2015).

The majority of discharged $^{137}$Cs present in the Irish Sea has been shown to remain in the solution phase, and as a result has been transported out of the basin. Baxter et al. (1979) highlighted a transit time of 6 months for radio-caesium to reach the North Channel. However ~ 10 % of the Cs inventory has been recognised to associate with finely grained sediment, offshore from Sellafield (Miller et al., 1982; Kershaw et al., 1983). Caesium hydroxide (CsOH) has been shown to be formed sparingly at high pH (Lehto and Hou, 2010; Renshaw et al., 2011), however this is not observed in seawater which has a pH between 7.5–8.4. Thus, the environmental mobility and transport of Cs in the marine environment will be predominantly by solution transport in open waters, and this will be controlled by tidal circulation. However, for the sediment systems investigated in this thesis the transport of Cs is likely moderated by the transport of Cs associated to particulates.

The most recent study into $^{137}$Cs distribution at the Ravenglass saltmarsh, collected sediment cores in 2002 and highlighted an activity of ~ 7 kBq/kg, with elevated concentrations observed between 25–30 cm in depth (Lucey et al., 2003). Further, as Cs is a conservative radionuclide it has been examined in Irish Sea waters previously (Jefferies, 1973; Cook et al., 1997) with higher $^{137}$Cs activities typically associated with surface waters. Earlier work by MacKenzie et al. (1999) showed the presence of ~475 Bq/kg $^{137}$Cs for a surface sediment sample in the offshore Irish Sea mud-patch, collected in 1992.

### 1.12.3. Plutonium

Plutonium is present in the environment principally due to historical nuclear weapons tests and effluent release from nuclear sites. Plutonium-238 ($t_{1/2}$ = 87.7 years) is a fissile isotope and is produced in nuclear reactors from the decay of $^{238}$Np. The long-lived Pu isotope, $^{239}$Pu ($t_{1/2}$ = 2.4 x $10^4$ years) is the primary radionuclide used for nuclear weapons, and the fission of this isotope generates

heat in a nuclear reactor (alongside $^{235}$U) (Choppin et al., 2002). The capture of a slow neutron in a nuclear reactor transforms $^{239}$Pu to $^{240}$Pu ($t_{1/2}$ = 6560 years). Fuel is removed from the reactor and stored to cool down. Of note, the longer the residence time of spent fuel in storage ponds prior to reprocessing, the greater the ingrowth of $^{240}$Pu. Additionally, $^{241}$Pu ($t_{1/2}$ = 14.4 years) is a fissile isotope and is significant to environmental analysis as it decays to the short-lived, α-emitting $^{241}$Am. As a result of their long-half-lives and toxicity, the isotopes $^{239}$Pu and $^{240}$Pu will be one of the main contributors to the total hazardous inventory in a geological disposal scenario. The dominant decay pathways for these radionuclides and their γ and β emissions commonly measured are shown in Equation 1.10 a–d):

$$(a)\ {}^{238}Pu \rightarrow {}^{234}U + \alpha\ 5.593\ MeV$$
$$(b)\ {}^{239}Pu \rightarrow {}^{235}U + \alpha\ 5.245\ MeV$$
$$(c)\ {}^{240}Pu \rightarrow {}^{236}U + \alpha\ 5.256\ MeV$$
$$(d)\ {}^{241}Pu \rightarrow {}^{241}Am + \beta\ 20.8\ keV$$

(Equation 1.10)

It is now well accepted that the oxidation state of Pu significantly affects its geochemical behaviour, and wider mobility. Plutonium is capable of simultaneously existing in four oxidation states: Pu(III), Pu(IV), Pu(V), and Pu(VI), with Pu(V) and Pu(IV) being the most dominant forms in seawater (Choppin, 2006). Plutonium is highly sensitive to oxidation state transformations, and potentially susceptible to biogeochemical changes, and as such it can display complex chemistry in solution. The reduced Pu(IV) species is sparingly soluble, and relatively immobile, and is scavenged by suspended matter and colloids, reducing its mobility in aqueous solution (Nelson and Lovett, 1978). Pu(IV) will also likely undergo hydrolysis forming an aqueous Pu species e.g. [$Pu(OH)_4$], and this has been shown by Ewing (1999) to dominate in oxidised natural waters. In contrast, Pu(V) is more soluble and mobile than Pu(IV) and does not form strong complexes with solid surfaces, instead forming actinyl ions ($PuO_2^+$) in solution (Kersting, 2013), and this has been suggested to dominate in waters close to the coastline or surface (Choppin and Wong, 1998). The measured $K_d$ value for Pu is

between $10^4$–$10^6$ (McDonald et al., 2001), and this reflects its affinity for solid surfaces in the marine environment.

A number of authors have investigated the interaction of Pu with mineral surfaces in laboratory experiments. Shaughnessy et al. (2003) recently highlighted the effective sorption of Pu(VI) to manganite (MnOOH) and hausmannite ($Mn_3O_4$), which showed 100 % sorption at pH 8. This work also showed that the reduction of Pu(VI) to Pu(IV) occurred after complexation with the Mn mineral surface. Duff et al. (1999) showed the preferential sorption of Pu to Mn oxides in heterogeneous mineral systems, with the sorbed Pu showing an average Pu oxidation state between that of Pu(V) and Pu(VI). Other studies have also discussed the oxidation state transformation of Pu *via* interactions with Fe-bearing minerals. Keeney-Kennicutt and Morse (1985) have demonstrated the reduction of Pu(V) adsorbed to goethite (α-FeOOH) with this reduction driving further adsorption of aqueous Pu(V). More recent work has shown the effective adsorption and reduction of $Pu(V)O_2$ with magnetite ($Fe_3O_4$) (Powell et al., 2004), and hematite ($\alpha$-$Fe_2O_3$) (Powell et al., 2005). The direct abiotic reduction of Pu(VI) has been shown by *Bacillus subtilis* (Ohnuki et al., 2007). In addition, Renshaw et al. (2009) demonstrated the reduction of Pu(V) by *Geobacter sulfurreducens,* with the same author highlighting that certain strains of bacteria (*Shewanella oneidensis, Geobacter sulfureducens and Geobactersulfureducens*) can further reduce Pu(IV) to Pu(III).

Focusing on the Irish Sea, it has been estimated that ~ 90 % of the Pu inventory is incorporated into the narrow belt of fine-grained sediments as insoluble Pu(IV) (Mitchell et al., 1995; McDonald et al., 2001). The remaining 10 % has been suggested to exist as the soluble Pu(V) species and as a result has been transported out of the Irish Sea over time (Jefferies et al., 1973; Lovett, 1978; Baxter et al., 1979). Field studies in the Irish and Mediterranean Seas have shown that Pu(V) is the dominant species in the dissolved phase, with particulate Pu present almost entirely in the reduced Pu(IV) form (Mitchell et al., 1995). The highly insoluble $Pu(OH)_4$ complex has been found by Aston and Stanners (1981) to be associated with the non-detrital Fe/Mn oxide phases in Irish Sea sediments. Further, large organic rich-particles have been found in the Esk estuary (Hamilton, 1989), and here, Sellafield-derived Pu and Am species have been

suggested to associate with an Fe and Mn rich layer shown to surround the agglomerate.

The most recent work examining $^{239,240}$Pu distribution at the Ravenglass saltmarsh collected sediment cores in 2002 and highlighted an activity of 7 kBq/kg (Lucey et al., 2003; Lindahl et al., 2011). Further, Marsden et al. (2006) collected sediment cores in 2000 and showed a maximum $^{239,240}$Pu activity of ~16 kBq/kg, with a peak observed in the mid-region of the core. At the Irish Sea mud-patch, $^{239,240}$Pu was shown to have an activity of ~350 Bq/kg (MacKenzie et al., 1999) in a surface sediment sample collected in 1992. However, the majority of the studies concerning the Irish Sea mud-patch are either historical or have focused on surface sediments and not a sediment core.

### 1.13.5. Technetium

The fission product $^{99}$Tc is present in the environment as a result of authorised and accidental releases, and is of particular importance due to its long half-life ($t_{1/2}$ = 2.1 x $10^5$ years) and high mobility. The majority of Tc in effluent has been produced as a result of neutron irradiation of $^{235}$U and $^{239}$Pu, and subsequent fission in the reactor core (Lindahl et al., 2003). Unstable $^{99}$Tc decays *via* low-energy β-emission to form stable $^{99}$Ru (Equation 1.11).

$$^{99}Tc \rightarrow {}^{99}Ru + \beta\ 294\ keV$$

(Equation 1.11)

The redox chemistry of Tc is a major control on it environmental mobility. Under oxidising conditions Tc dominates as the highly soluble pertechnatate anion: $Tc(VII)O_4^-$ (11 mol/L) (Boyd, 1978) reacting weakly to mineral surfaces (e.g. Burke et al., 2005; Lear et al., 2010) as these are often negatively charged. As a result Tc(VII) is considered one of the most mobile radionuclide species in the environment (Bondietti and Francis, 1979; Lloyd et al., 2000).

The direct reduction of soluble $Tc(VII)_{(aq)}$ to poorly soluble $Tc(IV)_{(s)}$ has been shown to occur biotically *via* reaction with hydrogenase enzymes on certain Fe(III) and sulphate-reducing bacteria (Lloyd et al., 2000; Wildung et al., 2000;

Marshall et al., 2008). It is important to note, that at environmental concentrations of Tc(VII) and Fe, the indirect, abiotically-mediated reduction of Tc(VII) with biogenic Fe(II)-bearing minerals and sorbed Fe(II) is widely accepted as the dominant reduction pathway (Lloyd et al., 2000; Begg et al., 2007; Zachara et al., 2007; Marshall et al., 2008; Plymale et al., 2011; Brookshaw et al., 2016). This reduction has shown the formation of poorly soluble, hydrous $TcO_2$-like phases (e.g. Fredrickson et al., 2004; Wildung et al., 2004; Burke et al., 2005; McBeth et al., 2007; Masters-Waage et al., 2017) with this reduced counterpart exhibiting a much lower solubility than Tc(VII) ($\sim 10^{-9}$ mol/L; Bondietti and Francis, 1979). As a result, these Tc(IV) phases have been shown to form discrete precipitates, readily sorb to clays, or associate with mineral surfaces, organic matter, sulphides and carbonates (Begg et al., 2007; Morris et al., 2008; Peretyazhko et al., 2009). Further, the biogenic production of Fe sulphides can also lead to its co-precipitation with Tc(IV) (Lee et al., 2014). It is now well established that Tc is cycled between the solution and solid phase under suboxic conditions, with recent work highlighting the recalcitrance of Tc during multiple redox iterations (Masters-Waage et al., 2017). However, little is known of whether Tc behaves in a similar way in the field, where it will be present at lower concentrations than those used in laboratory experiments.

The bioreduction of Tc (i.e. the addition of an electron donor to $^{99}$Tc contaminated sediments and groundwater to promote microbially-mediated metal-reducing conditions) has been shown to effectively reduce $TcO_4^-$ to sparingly soluble Tc(IV) concurrent with Fe(III) reduction (Lloyd et al., 2000; McBeth et al., 2007; Law et al., 2010; Prakash et al., 2013; Newsome et al., 2014, 2017; Thorpe et al., 2016). The stimulation of these biogeochemical processes can be used to clean-up nuclear legacy contaminated land, and as such bioremediation has been proposed as a viable decontamination technique (see Newsome et al., 2014). This would be relevant in sites where Tc has been found in surface and ground water where nuclear waste has been processed or stored (Morris et al., 2000; Standrig et al., 2002; Lloyd et al., 2005). At Sellafield, its varying industrial history has led to a number of leaks from the site, causing contamination of the underlying soils and groundwater (Sellafield Ltd, 2014). Here, $^{99}$Tc was detected in wells outside the site perimeter. Maximum $^{99}$Tc was

detected near the separation area within the site boundary and included maximum activities of 50–60 Bq/L in 2014 (Sellafield Ltd, 2016).

As Tc exists as the highly soluble, conservative $TcO_4^-$ in oxygenated waters, the majority of studies in the Eastern Irish Sea have focused on determining $^{99}$Tc concentrations in seawater and its accumulation in biota to ascertain the impact of modern post-EARP discharges. (Leonard et al., 1997, 2004, 2008; McDonald et al., 1998; Kershaw et al., 1999; Smith et al., 2001; McCubbin et al., 2002; Lindahl et al., 2003). Other authors have examined the accumulation of Tc in Irish Sea sub-tidal (McCubbin et al., 2006; Finegan et al., 2009; Jenkinson et al., 2014) and coastal sediments (Morris et al., 2000; Keith-Roach et al., 2003; Lucy et al., 2004; Finegan et al., 2009). The most recent work into $^{99}$Tc at the Ravenglass saltmarsh used sediments collected in 2002 (Lucey et al., 2004; Finegan et al., 2009) and showed a sub-surface enrichment of $^{99}$Tc, similar to Morris et al. (2000).

### 1.13.6. Uranium

Uranium exists in the Earth's crust as the primordial isotopes: $^{238}$U (~99.3 %), $^{235}$U (~0.72 %), and $^{234}$U (0.005 %). The U isotope, $^{236}$U ($t_{1/2}$ = 2.4 x $10^7$ years) also exists naturally albeit at very low concentrations ($^{236}$U:$^{238}$U ratio of ~$10^{-10}$–$10^{-11}$) (Zhao et al., 1997; Marsden et al., 2001). On release to the environment, the concentration of $^{235}$U and $^{238}$U present in radioactive effluent are readily diluted by the natural U baseline present in seawaters and sediments. However, as $^{236}$U is produced in nuclear reactors at a higher concentration than produced in nature, it is also present in effluent and can be used as a fingerprint to determine the presence of civil reactor-derived U in the environment (e.g. Marsden et al., 2001; De Cesare et al., 2013; Al-Qasmi et al., 2016; Froehlich et al., 2016; Tims et al., 2016). The principal decay chain for $^{236}$U is *via* α-emission, generating stable $^{232}$Th (Equation 1.12). As the environmental concentrations of $^{236}$U are in the order of ~$10^{-9}$ Bq/kg, the limitation of $^{236}$U analysis is that sensitive, expensive mass spectrometry techniques are required (Marsden et al., 2001).

$$^{236}U \rightarrow {}^{232}Th + \alpha\ 4.494\ MeV$$

(Equation 1.12)

Uranium is predominantly present as U(VI) under oxic conditions, forming the largely soluble uranyl species ($U(VI)O_2^{2+}$) (Waite et al., 1994; Gorman-Lewis et al., 2008). However, in the presence of carbonate, at circumneutral pH U(VI)-carbonato complexes ($UO_2(CO_3)_3^{4-}$) will likely dominate (Clark et al., 1995), whereas hydroxyl complexes ($UO_2$-OH) will tend to exist when carbonate concentrations are low (Choppin et al, 2002).

Further, oxidised U(VI) species have been shown to sorb to organic matter and mineral surfaces, including clays and Fe oxy(hydr)oxides (Ortiz-bernad et al., 2004; Scott et al., 2005; Kaplan et al., 2016) and this is often reversible at pH > 7 (Cumberland et al., 2016). As a result, U may be removed from mineral surfaces in a natural system leading to its removal into solution. The biotic reduction of U(VI) to crystalline $UO_{2(s)}$ (solubility ca. $10^{-17}$ mol/L at pH > 4) was shown in early work, mediated by Fe(II)-reducing bacteria (Langmuir, 1978; Lovley et al., 1991). This $UO_2$ species is generally acknowledged as a desirable product of bioreduction due to its low solubility under reducing conditions (Ulrich et al., 2008). However, more recent work has shown that the bioreduction of U(VI) can produce alternative U(IV) products, termed non-crystalline or monomeric U(IV) (Bernier-Latmani et al., 2010; Campbell et al., 2011; Alessi et al., 2014).

The indirect, abiotic reduction of U(VI) to U(IV) has been shown to proceed under Fe reducing conditions, whereby an abiotic electron transfer takes place from the reactive Fe(II)-bearing mineral to U(VI) (Latta et al., 2012). The simultaneous enzymatic reduction of Fe(III) and U(VI) has been observed (Behrends and Cappellen, 2005) with the abiotic reduction of U(VI) to U(IV) also being shown to take place with Fe(II)-bearing minerals. A number of authors have also observed the incorporation of U into the lattice of Fe oxy(hydr)oxides (Duff et al., 2002; Marshall et al., 2014; Roberts et al., 2017).

Focusing on Sellafield-contaminated materials, the tracer $^{236}U$ has been used to determine U input to Ravenglass and other UK coastal sediments (Marsden et al., 2001; Al Qasmi et al., 2017). Here, Marsden et al. (2001) showed $^{236}U$:$^{238}U$ activity ratios at the Ravenglass saltmarsh that were well above the natural baseline, highlighting a distinct enrichment of $^{236}U$ in middle of the sediment core (~ 18 cm). Similarly to Tc, there are large volumes of U contaminated

groundwater at many nuclear sites, including Sellafield. Here, *in situ* immobilisation of U, *via* the microbially mediated reduction of U(VI) to U(IV) has been proposed as a strategy (Lovley et al., 1991; Ortiz-Bernad et al. 2004; Lloyd et al., 2002; Finneran et al. 2002). It is important to note that the legacy discharge of waste from the Albright and Son Marchon Phosphoric acid in Whitehaven, Cumbria has released phosphogympsum waste containing 30 tonnes of U into the Irish Sea (Howe et al., 1999). However, as this was natural U, it is not thought that this will influence the anthropogenic $^{236}$U signal in coastal and offshore Irish Sea sediments.

### 1.13.4. Neptunium

Neptunium is a transuranic element, and its most dominant isotope in the environment, $^{237}$Np, has a long half-life ($t_{1/2}$ = 2.1 x $10^6$ years) and high radiotoxicity. The radionuclide is formed as a by-product in thermal reactors *via* successive neutron captures of fissile $^{235}$U. It is also a long-lived decay product of $^{241}$Pu and $^{241}$Am, and is expected to become the major transuranic in radioactive waste between $10^4$ and $10^7$ years (Kaszuba and Runde, 1999; Lloyd and Renshaw, 2005). $^{237}$Np decays to $^{233}$Pa *via* α-emission (Equation 1.13).

$$^{237}Np \rightarrow {}^{233}Pa + \alpha\ 4.959\ MeV$$

(Equation 1.13)

Neptunium can exhibit a wide range of oxidation states, ranging from Np(III) to Np(VI) (Patil et al., 1978; Degueldre, 1995; Kaszuba and Runde, 1999), with its chemistry in the environment dominated by its speciation. Under oxidising conditions Np exists mainly as the soluble, neptunyl species ($Np(V)O_2^+$) (Keeney-Kennicutt and Morse, 1984; Yamamoto et al., 1991; Kaszuba and Runde, 1999) at pH < 10 (Schmeide and Bernhard, 2010), with a solubility of up to $10^{-4}$ mol/L (Choppin, 2007). However, when carbonate concentrations are high, soluble Np-carbonato complexes are likely to dominate (e.g. $NpO_2CO_3$) (Schmeide and Bernhard, 2010).

The sorption of Np(V) to Fe oxy(hydr)oxides has been examined previously. Combes et al. (1992) showed the effective sorption of Np(V) to goethite (α–

FeOOH), and this association led to ~95 % uptake onto the surface of goethite. However, from an environmental perspective, the desorption of Np(V) has also been observed from metal minerals that are common and reactive; Mn oxy(hydr)oxides (Zhao et al., 2005) and Fe oxy(hydr)oxides (Keeney-Kennicutt and Morse, 1984; Nakata et al., 2000; Tinnacher et al., 2011). This observed reversibility of Np may result in its remobilisation in the environment after a period of adsorption to mineral surfaces. Previous work has also shown the immobilisation of Np by bio-sorption (Gorman-Lewis et al., 2013). Similarly to Tc, Np(V) reduction can also occur *via* biotic and abiotic pathways. The direct or biotic reduction of Np(V) and Np(V) citrate by microorganisms has been observed (Icopini et al., 2007). In turn, the biological reduction and removal of Np(V) by two microorganisms (*S.putrefaciens* and *Citrobacter sp)* was shown by Lloyd et al. (2000).

Further, the indirect reduction of Np(V) to Np(IV) in sterile Fe(II)-bearing microcosm systems has been shown to take place *via* the abiotic electron transfer from reactive Fe(II) minerals to Np(V) (Law et al., 2010). A number of mineral surfaces have been successful in the reduction of Np(V), occurring on several reactive Fe(II) surfaces e.g. mackinawite (FeS) (Moyes et al., 2002), green rust (an Fe(II), Fe(III) layered double hydroxide) (Christiansen et al., 2011) and on phyllosilicates (Brookshaw et al., 2015). The latter two studies observed the precipitation of nanoparticulate Np(IV) phases, with Brookshaw et al. (2015) using EXAFS techniques to characterise the reduced Np(IV) phase. Further, the microbially-mediated Mn reduction conditions in sediment microcosms were successful in the reduction of Np(V) (Thorpe et al., 2015).

Studies at the Esk estuary have used varying analytical techniques to examine $^{237}$Np, however in most cases these were limited to surface sediment samples (Pentreath and Harvey, 1981; Assinder et al., 1991; Hursthouse et al., 1991; Yamamoto et al., 1991; Kuwabara et al., 1996; Assinder, 1999). The most recent study of $^{237}$Np distribution at Ravenglass showed an activity of 0.6–13 Bq/kg between 0–20 cm in depth with an enhanced concentration at the near-surface of the sediment core (Morris et al., 2000). This was considered by Morris et al. (2000) to be due caused by post-depositional effects. There is a limited body of literature on the environmental behaviour of $^{237}$Np, in comparison to other

Sellafield-derived radionuclides due primarily to the difficulty in obtaining accurate field $^{237}$Np data. Our understanding of Np biogeochemistry predominantly comes from laboratory experiments conducted at relatively high concentrations (micromolar and above) under constrained laboratory systems.

### 1.14. The Irish Sea

The Irish Sea is a semi-enclosed basin, with water entering *via* St George's Channel in the South, and leaving through the North Channel. The circulation within the Irish Sea is typically driven by tidal activity (up to 10 m in the Solway Firth) and high winds. The Western Irish Sea is a relatively deep channel with maximum depths exceeding 100 m (McDonald, 2011). In contrast, the Eastern Irish Sea, which is the focus of this thesis brings water to Cumbria and Lancashire, North West England, and is much shallower in depth (< 50 m).

#### 1.14.1. Tides and Currents

The Irish Sea has a semi-diurnal tidal cycle which varies in range (Hanley et al., 2013). The Lancastrian and Cumbrian coasts experience spring tides reaching 8m with the lowest tidal rangeing less than 2m in the North Channel and along the Irish coast south of Arklow (Kennington and Hisscott, 2013).

Residual currents in the Irish Sea are complex; surface and bottom currents can often flow in opposing directions (Figure 1.7; Kennington and Hisscot, 2013). The net long term flow in the Irish Sea is from south to north with residence times estimated to be approximately one year for waters to pass through the Irish Sea. However, these times can be longer for the Eastern Irish Sea and Liverpool Bay area where eddy systems can interrupt flow (Kennington and Hisscott, 2013). Additionally, research into sea-bed sediments for hydrocarbons by the Department of Trade and Industry found a strong finding between annual mean tidal peak currents and annual mean seabed stress; this highlights that any stress placed on the seabed by tidal currents is a major influence on sediment composition (Holmes and Tappin, 2005).

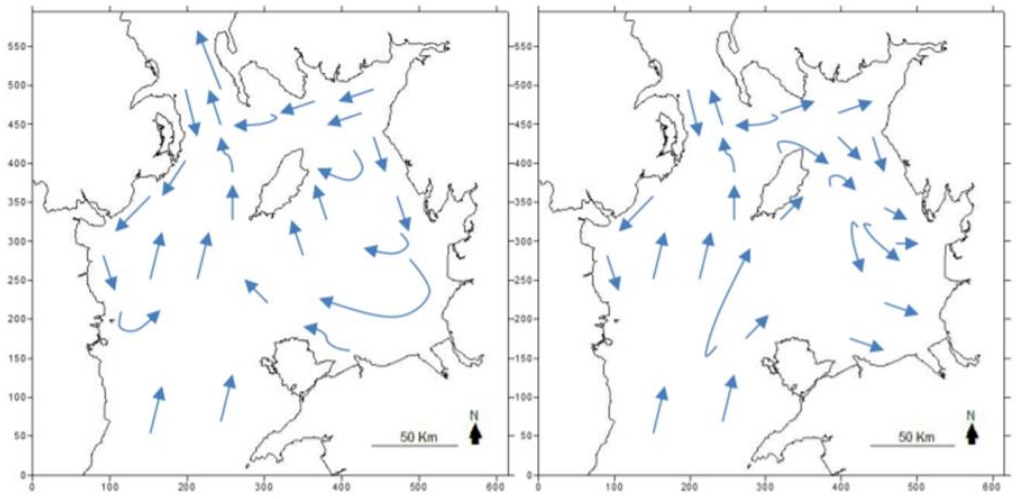


**Figure 1.7.** Residual current patterns in surface (left) and bottom (right) waters of the Irish Sea (taken from Kennington and Hisscott, 2013).

### 1.14.2. Sediments

The sediment types in the Eastern Irish Sea range from sandy to muddy. In the vicinity of the Sellafield pipeline, the dominant sediment type consists of a belt of fine-grained, mud-like particulates. Further, muddy sediments are located in two main areas: a belt of muddy sands and muds parallel to the Cumbrian coast extending into Liverpool Bay, and across the mouth of the Solway Firth to Wigtown Bay (Kershaw et al., 1992). Radionuclides that are deposited here may tend to strongly associate with the fine-grained sediment. Storms in the Irish Sea in the winter months can result in the displacement of sea-bed sediment. Remote storms can generate swell waves which are longer wavelength, longer period, waves and can travel large distances (Hanley et al., 2013). These may be capable of distributing surface-layers of sea bed sediment. Alongside storms, sediment disturbance will also likely occur in the Eastern Irish Sea by bottom trawling.

### 1.14.3. The Irish Sea Mud-Patch

The Irish Sea mud-patch is a belt of fine-grained sediment located parallel to the Cumbrian coast, ~ 10 km NW from the Sellafield pipeline (Figure 1.8), and a proportion of the legacy releases over time has associated with this offshore stretch of finely grained seabed sediments. The mud-patch (15 km x 2.5 km) has

been suggested to act as a major repository for Sellafield-derived radionuclides (Lovett, 1978; McCartney et al., 1994; Cook et al., 1997; MacKenzie et al., 1999; Kershaw et al., 1999). Hydrological and sedimentological data suggest that the mud-patch is an area of active sedimentation, albeit low (~1 mm) (Kershaw et al., 1988). The sediment composition of the mud-patch has been shown to be comprised of fine sand (46 %), silt (37 %) and clay (13 %) (McDonald et al., 1990). Early work at the site has shown the accumulation rate at the mud-patch to be low (maximum of 0.08 cm/yr) with the sediment being mixed to a depth of 1.5 m (Kershaw et al., 1983; Kershaw, 1984). At the mud-patch Eh was shown to decrease from 300–500mV to 50–250 mV between the overlying water and 5–10 cm depth, with the pH ~7.6 in this region (Malcolm et al., 1990).


**Figure 1.8.** Map of the United Kingdom with inset showing the location of the Irish Sea mud-patch and Ravenglass saltmarsh.

Previous studies have recognised the role of bioturbation in physically mixing the radionuclide inventory that have deposited at the mud-patch over time, causing redissolution or resuspension of Sellafield derived radionuclides back into the water column (Kershaw et al., 1983; Kershaw, 1984; MacKenzie et al., 1987. The distribution of radionuclides in sediment/soil systems can be altered by faunal

mixing of the subsurface (Aller and Aller, 1992; Forster et al., 1995). Bioturbation encompasses two types of activities, namely particle reworking (direct movement of particles by animals), and burrow ventilation (direct movement of water) (Kristensen et al., 2012). Bioturbation is important in understanding the fate and transport of radionuclides in the Irish Sea basin. For example, Forster et al. (1995) found that for certain radionuclides (e.g. Cs) that have been deposited in the Irish Sea mud patch, the burrowing motion of polycheates caused significant mixing and particle re-working of the sediments, causing radionuclides to be re-suspended back into the water column and augmenting offshore transport. Further, this bioturbative mixing has been shown to cause redistribution of radionuclides to a depth of 1.5 m in sediment samples taken from Irish Sea sediments (Kershaw et al., 1984).

The Eastern Irish Sea basin area is shallow, aerobic and relatively biologically rich. As a result, it may be assumed that there is a constant flux of organic matter falling to the sediments. However, the majority of this does not reach the sediments of the sea-floor due to the large number of benthic organisms which inhabit the Irish Sea that are detrivores (eat detritus). Further, the work of Tierney et al., 2016 showed a rapid uptake of $^{14}C$ enriched organic material in the benthic food web at the Irish Sea mud-patch. Here, high biological activity was also evident through lower sediment bulk activities vs benthic organism activities. In addition the complex benthic community inhabiting the mud-patch and the Eastern Irish Sea are likely consuming the carcasses and organic particles in the overlying water, and this may result in a low organic matter content at the mud-patch. Dominant benthic species include: heart urchins (also known as sea potatoes) and spoon worms which consume organic particles. It has also been suggested that the Irish Sea basin retains planktonic larvae of the commercially valuable *Nephrops norvegicus* (Norway lobster) (McCubbin et al., 2006). These species may also consume any detrital matter that reaches the sea floor, further highlighting the biologically active character of the Eastern Irish Sea. The nephrops communities have also accumulated $^{99}Tc$ during the heighted release in the early 1990s (McCubbin et al., 2006)

### 1.15. Ravenglass Saltmarsh

The Ravenglass saltmarsh is part of the Esk estuary situated 15 km south from the Sellafield nuclear reprocessing facility (Carr and Blackley, 1986). The estuary is macro-tidal and has a mean spring tidal range of over 7m (Halcrow Group, 2013). Littoral sediment transport (on the open coast towards the south of the estuary) is northerly, while on the northern side of the estuary it is southerly; the estuary entrance is therefore a zone of sediment convergence (Halcrow Group, 2013). The estuary experiences relatively high tidal discharges and velocities relative to its size, however the rivers (Mite, Irt and Esk) that feed into it have relatively small discharges.

Previous measurements at Ravenglass show a decrease in Eh with depth (+45 mV at 1 cm to -350mV at 24 cm) and a pH between 7.3 at 1 cm to 6.7 at 15 cm) (Lucey et al., 2004). Salinity values at Ravenglass vary from an upper limit of 31‰ at high tide (Hamilton and Clarke, 1984), to a lower limit of 0.2 ‰ (Carr and Blackley, 1986) during low water inundation, highlighting the dynamic nature of the estuary. In turn, previous measurements at Ravenglass show a decrease in Eh with depth (+45 mV at 1 cm to -350mV at 24 cm) and a pH between 7.3 at 1 cm to 6.7 at 15 cm) (Lucey et al., 2004). There is also an interesting tide-driven "upward-percolation" at the Ravenglass estuary and this potentially exposes sediments of the estuary to changing salinity and unknown oxygen levels. It is important to note that this variability will have potential implication on any metal/contaminant/radionuclide behaviour.

There is also a gradual transition from sandy sediments at the mouth of the estuary to muds near the limits of tidal influence. Specifically, the sediments of the estuary have been shown to be predominantly silt (~75 %; >2–63 μm) with lower quantities present as clay (~19%; <0.2 μm) and sand (7 %; >63 μm) (Morris et al., 2000). The majority of the clay in the estuary is illite (Kelly and Emptage, 1992). Previous work has highlighted that this site is an area of active accretion with sedimentation rates observed between 0.2–6.8 cm/yr (Aston and Stanners, 1981; Clifton and Hamilton, 1982; Morris et al., 2000; Marsden et al., 2006; Ray et al., 2018; Chapter 3).

The estuary has also been suggested to have increased in area as a result of the railway viaducts constructed in the mid-nineteenth century (Carr and Blackley, 1986). Authors who have studied the site previously have suggested that biological mixing is minor in the estuary (Hetherington and Harvey, 1978), however small species such as *Corophium Voltutator* are present in the summer season, and re-work the upper few cm of the muddy-silt deposits (Hamilton and Clarke, 1984). The tidal range also varies across the saltmarsh, with high-tide at times not reaching the lower marshes, whereas the higher marshes are submerged during equinoctial springs. At low-water the majority of the estuarine sediment is exposed.

At the present time there are localised areas of marsh edge erosion and accretion which reflect patterns of change in the low water channels. The estuary at present is close to a state of dynamic equilibrium. Its future evolution will depend upon the balance between sea level rise and sediment availability (Halcrow Group, 2013). An acceleration in the rate of erosion in future years would be likely to provide sufficient sediment to allow the estuary to keep pace with sea level rise.

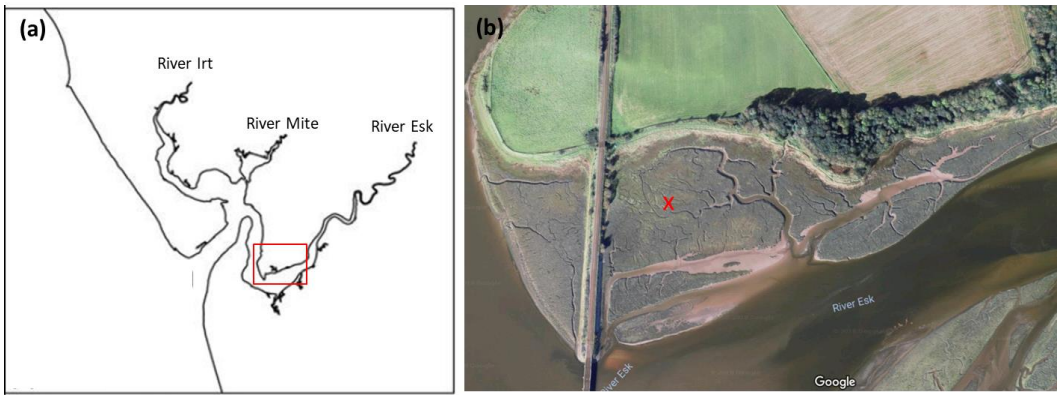


**Figure 1.9**. (a) Map of Eastern Cumbria focusing in on the Ravenglass saltmarsh (b) Inset: aerial view of the Ravenglass saltmarsh (taken from Google Maps) including the sample site (X).

### 1.16. Sediment Transport Mechanisms

A unique mechanism has been hypothesised to take place in the Irish Sea which results in the potential accumulation and distribution of radionuclides from off-shore areas of the Eastern Irish Sea to coastal locations in Cumbria. Previous authors have suggested that this transfer of radionuclides is a step-wise process and is a result of many factors which occur in the natural, diverse eastern Irish Sea.

Specifically, it is thought that a proportion of the radionuclides on release to the Eastern Irish Sea precipitate or associate with suspended sediment surfaces and/or colloidal organics that are present in the marine environment. In turn, there is offshore transport of sediment-bearing radionuclides to a finely grained mud-patch that is situated a few km from the effluent outfall. The radionuclides associate with the surface of the mud-patch. The mud-patch has been recognised to be biologically active, and it has been suggested that the feeding habits of the *Maximuelleria lankestri* cause the re-working of the mud-patch sediment down to 1.5 m, in some cases. This prevents any distinct stratification of the sediment, instead resulting in the redissolution of the sediment-bearing radionuclides from the surface, causing them to be suspended in the eastern Irish Sea. A combination of long and off-shore currents has then been hypothesised to transport the radionuclides (either *via* solid or solution transport depending on the speciation of the radionuclide) to low-energy locations e.g. Ravenglass saltmarsh. As shown in Figure 1.7, the circulation of both the residual and particularly the bottom currents likely favour the transport of some of the contaminated sediment from the mud-patch to coastal locations in Cumbria. It has been hypothesised that the deposited radionuclides accumulate at sites like the saltmarsh and are slowly buried with time; this has been attributed to the minimal (bio) resuspension at the site. However, an alternative that should also be considered is the direct southward, nearshore transport from the pipeline to Ravenglass.

Sediments in the low energy, intertidal region of the Ravenglass saltmarsh have been suggested to receive an input of the legacy Sellafield-derived radionuclides from the mud-patch (Lovett, 1978; Hamilton and Clarke, 1984; McCartney et al., 1994). As a result the low energy, intertidal region has been studied in the past

(Aston et al., 1985; Carr and Blackley, 1986; Morris et al., 2000; Keith-Roach et al., 2000; Keith-Roach et al., 2002; Marsden et al., 2006) with the majority of these studies focussing on the distribution of anthropogenic radionuclides in sediments in this area. These authors found that there is largely a preservation of the enhanced Sellafield discharge signal in Cumbrian intertidal sediments, with levels of activity still being observed at the surface of the sediment core. It is important to note that there has been no substantial investigation on understanding the role of the sediment biogeochemistry when considering the behaviour of the redox-active radionuclides.

### 1.17. Thesis Aims and hypotheses

The overarching aim of this project is to *determine the contemporary distribution of environmentally-relevant Sellafield-derived radionuclides in the Eastern Irish Sea, and understand the relative importance of ambient biogeochemistry vs. physical processes in determining their distribution.* Reflecting this, the focus of this work is to relate the anthropogenic radionuclide inventory at both the Ravenglass saltmarsh and Irish Sea mud-patch sites with the complex geochemistry, mineralogy and microbiology of each site. Further, this examination into contaminated sediments is particularly pertinent at present as construction of the proposed Moorside Nuclear Reactor near Sellafield may disturb areas of the local seabed during site investigation/construction. In addition, predicted sea-level rise would make low lying coastal nuclear sites e.g. Sellafield and the LLWR vulnerable to tidal inundation with oxygenated seawater, and this may compromise the stability of the LLW stored at the facility. Finally the study sites are public locations and are not within the Sellafield grounds, and thus it is vital to monitor, and understand the behaviour of radionuclides that have accumulated over time.

Specifically, the work aims to;

(a) Determine the contemporary activity and distribution of key anthropogenic radionuclides in the Irish Sea mud-patch and Ravenglass saltmarsh, and compare to radionuclide discharge histories;

(b) Assess whether the ambient biogeochemistry of the Irish Sea mud-patch and Ravenglass saltmarsh impact radionuclide distribution and hence understand the long-term stability of radionuclide deposition in these locations;

(c) Understand whether radionuclide processes observed in the laboratory are present in the field, and explore the extent of post-depositional remobilisation for Sellafield-derived radionuclides at the Irish Sea mud-patch and Ravenglass saltmarsh;

(d) Investigate the bioavailability of Sellafield-derived radionuclides across four geochemical phases at the Ravenglass saltmarsh.

Reflecting this, the following hypotheses are tested in this thesis:

1. Post-depositional remobilisation of Sellafield-derived $^{137}$Cs and $^{241}$Am at the Ravenglass saltmarsh, will be negligible.
2. Plutonium ($^{238}$Pu, $^{239,240}$Pu, $^{241}$Pu) at the Ravenglass saltmarsh will be influenced by the ambient site biogeochemistry, leading to significant post-depositional remobilisation.
3. The activity of $^{137}$Cs, $^{241}$Am, and the Pu isotopes ($^{238}$Pu, $^{239,240}$Pu, $^{241}$Pu) at the surface of the Irish Sea mud-patch will be negligible, due to low modern discharge rates from the Sellafield Ltd. site.
4. The distribution of $^{99}$Tc and $^{236}$U in Ravenglass saltmarsh sediments will be influenced by the biogeochemistry of the site.
5. Sellafield-derived plutonium ($^{239,240}$Pu) will be dominantly hosted in the reducible oxide fraction in Irish Sea mud-patch and Ravenglass sediments.
6. Sellafield-derived $^{137}$Cs and $^{241}$Am will be dominantly hosted in the exchangeable and organic fractions respectively, in Irish Sea mud-patch and Ravenglass sediments.

## References


Abdelouas, A., 2006. Uranium mill tailings: geochemistry, mineralogy, and environmental impact. Elements. 2, 335–341.

Al-Qasmi, H., Law, G.T.W., Bryan, N.D., Livens, F.R., 2015. Transport and accumulation of stable metals and radonuclides in Dulas Bay, North Wales, in: Environmental Radiochemical Analysis V. 50–60.

Al-Qasmi, H., Law, G.T.W., Fifield, L.K., Livens, F.R., 2016. Origin of artificial radionuclides in soil and sediment from North Wales. J. Environ. Radioactiv. 151, 244–249.

Al-Qasmi, H., Law, G.T.W., Fifield, K.L., Howe, J., Brand, T., Cowie, G.L., Law, Kathleen, A., Livens, F.R., 2017. Deposition of artificial radionuclides in sediments of Loch Etive, Scotland. J. Environ. Radioactiv (In press).

Alessi, D.S., Lezama-Pacheco, J.S., Stubbs, J.E., Janousch, M., Bargar, J.R., Persson, P., Bernier-Latmani, R., 2014. The product of microbial uranium reduction includes multiple species with U(IV) phosphate coordination. Geochim. Cosmochim. Ac. 131, 115–127.

Aller, R.C., Aller, J.Y., 1992. Meiofauna and solute transport in marine muds. Limnol. Oceanogr. 37, 1018–1033.

Altmaier, M., Vercouter, T., 2012. Aquatic chemistry of the actinides: aspects relevant to their environmental behavior in: Radionuclide behaviour in the natural environment: Science, implications and lessons for the nuclear industry. Woodhead Publishing. 44–69.

Assinder, D.J., Kelly, M., Aston, S.R., 1984. Conservative and non-conservative behaviour of radionuclides in an estuarine environment, with particular respect to the behaviour of plutonium isotopes. Environ. Technol. Lett. 5, 23–30.

Assinder, D.J., Yamamoto, M., Kim, C.K., 1991. Neptunium in intertidal coastal and estuarine sediments in the Irish Sea. 14, 135–145.

Assinder, D.J., 1993. Radioisotopes of thirteen elements in interidal sediments. 170, 333–346.

Assinder, D.J., 1999. A review of the occurrence and behaviour of neptunium in the Irish Sea. J. Environ. Radioactiv. 44, 335–347.

Aston, S.R., Stanners, D.A., 1981. Americium in intertidal sediments from the coastal environs of Windscale. Mar. Pollut. Bull. 12, 149–153.

Aston, S.R., Stanners, D.A., 1981. Plutonium transport to and deposition and immobility in Irish Sea intertidal sediments. Nature. 289, 581–582.

Aston, S.R., Stanners, D.A., 1982. The transport to and deposition of americium in intertidal sediments of the ravenglass estuary and its relationship to plutonium. Environ. Pollut. Ser. B. 3, 1–9.

Aston, S.R., Assinder, D.J., Kelly, M., 1985. Plutonium in intertidal coastal and

estuarine sediments in the Northern Irish Sea. Estuar. Coast. Shelf S. 20, 761–771.

Bailly, P., Laguionie, P., Boust, D., Korsakissok, I., Didier, D., Fiévet, B., 2012. Estimation of marine source-term following Fukushima Daiichi accident. J. Environ. Radioactiv. 114, 2–9.

Baxter, M.S., McKinley, I., MacKenzie, A., Jack, W., 1979. Windscale Radiocaesium in the Clyde Sea area. Mar. Pollut. Bull. 10, 116–120.

Begg, J.D.C., Burke, I.T., Morris, K., 2007. The behaviour of technetium during microbial reduction in amended soils from Dounreay, UK. Sci. Total. Environ. 373, 297–304.

Behrends, T., Van Cappellen, P., 2005. Competition between enzymatic and abiotic reduction of uranium(VI) under iron reducing conditions. Chem. Geol. 220, 315–327.

BEIS, 2017. Hinkley Point C. London.

BEIS., 2018. Consultation: working with communities: implementing geological disposal. Department for Business, Energy, and Industrial Strategy, Department of Agriculture, Environment, and Rural affairs. London

Bernier-Latmani, R., Veeramani, H., Vecchia, A., Junier, P., Lezama-Pacheco, J., Suvorova, E., Sharp, J., Wigginton, N., Bargar, J., 2010. Non-uraninite products of microbial U(VI) reduction. Environ. Sci. Technol. 44, 9456–9462.

BNFL, 1993–2005 Annual report on radioactive discharges and monitoring of the environment. Bristish Nuclear Fuels plc. Risley.

BNFL, 1999. Annual report on radioactive discharges and monitoring of the environment. Bristish Nuclear Fuels plc. Risley

Bondietti, E., Francis, C., 1979. Geologic migration potentials of technetium-99 and neptunium-237. Science. 203, 1337–1340.

Boyd, G., 1978. Osmotic and activity coefficients of aqueous $NaTcO_4$ and $NaReO_4$ solutions at 25 $^{o}$C. J. Sol. Chem. 7, 229–238.

Brookshaw, D., Patrick, A., Lloyd, J., Vaughan, D., 2012. Microbial effects on mineral–radionuclide interactions and radionuclide solid-phase capture processes. Min. Mag. 76, 777–806.

Brookshaw, D.R., Pattrick, R.A.D., Bots, P., Law, G.T.W., Lloyd, J.R., Mosselmans, F.J.W., Vaughan, D.J., Dardenne, K., Morris, K., 2015. Redox interactions of Tc(VII), U(VI), and Np(V) with microbially reduced biotite and chlorite. Environ. Sci. Technol. 49, 13139–13148.

Brookshaw, D.R., Lloyd, J.R., Vaughan, D.J., Pattrick, R.A.D., 2016. Effects of microbial Fe(III) reduction on the sorption of Cs and Sr on biotite and chlorite. Geomicrobiol. J. 33, 206–215.

Buesseler, K., Aoyama, M., Fukasawa, M., 2011. Impacts of the Fukushima

nuclear power plants on marine radioactivity. Environ. Sci. Technol. 45, 9931–9935.

Buesseler, K., Dai, M., Aoyama, M., Benitez-Nelson, C., Charmasson, S., Higley, K., Maderich, V., Morris, P.J., Oughton, D., Smith, J.N., 2017. Fukushima Daiichi–derived radionuclides in the ocean: transport, fate, and impacts. Annu. Rev. Mar. Sci. 9, 173–203.

Buesseler, K.O., Jayne, S.R., Fisher, N.S., Rypina, I.I., Baumann, H., Baumann, Z., Breier, C.F., Douglass, E.M., George, J., MacDonald, A.M., Miyamoto, H., Nishikawa, J., Pike, S.M., Yoshida, S., 2012. Fukushima-derived radionuclides in the ocean and biota off Japan. Proc. Natl. Acad. Sci. 109, 5984–5988.

Burke, I.T., Boothman, C., Lloyd, J.R., Mortimer, R.J.G., Livens, F.R., Morris, K., 2005. Effects of progressive anoxia on the solubility of technetium in sediments. Environ. Sci. Technol. 39, 4109–4116.

Burns, R., Burns, V.M., 1977. Marine manganese nodules in: marine manganese Nodules. Amsterdam. 185–248.

Byrne, A.R., 1986. Determination of $^{237}$Np in Cumbrian (UK) sediments by neutron activation analysis: preliminary results .J. Environ. Radioactiv. 4, 133–144.

Calvert, S., Pedersen, T., 1993. Geochemistry of recent oxic and anoxic marine sediments: implications for the geological record. Mar. Geol. 113, 67–88.

Campbell, K.M., Davis, J.A., Bargar, J., Giammar, D., Bernier-Latmani, R., Kukkadapu, R., Williams, K.H., Veramani, H., Ulrich, K.-U., Stubbs, J., Yabusaki, S., Figueroa, L., Lesher, E., Wilkins, M.J., Peacock, A., Long, P.E., 2011. Composition, stability, and measurement of reduced uranium phases for groundwater bioremediation at Old Rifle, CO. Appl. Geochem. 26, S167–S169.

Carpenter, J., Bi, Y., Hayes, K.F., 2015. Influence of iron sulfides on abiotic oxidation of $UO_2$ by nitrite and dissolved oxygen in natural sediments. Environ. Sci. Technol. 49, 1078–1085.

Carr, A., Blackley, M.W.L., 1986. Implications of sedimentological and hydrological processes on the distribution of radionuclides : the example of a salt marsh near Ravenglass. 529–543.

Carr, A., Blackley, M., 1986. Seasonal changes in surface level of a saltmarsh. Earth. Surf. Process. Landforms. 11, 427–439.

Castrillejo, M., Casacuberta, N., Breier, C.F., Pike, S.M., Masque, P., Buesseler, K.O., 2016. Cs in the coast off Japan derived from the Fukushima Dai-ichi nuclear accident. Environ. Sci. Technol. 50, 173–180.

Cefas, 2017. Radioactivity in food and the environment. 2016.

Chapman, N.A., McKinley, I., 1987. The geological disposal of nuclear waste. JohnWiley & Sons.

Chibowski, S., Zygmunt, J., 2002. The influence of the sorptive properties of

organic soils on the migration rate of $^{137}$Cs. J. Environ. Radioactiv. 61, 213–223.

Choppin, G.R., Wong, P.J., 1998. The Chemistry of Actinide Behavior in Marine Systems. Aquat. Geochemistry 4, 77–101.

Choppin, G., 2006. Environmental behavior of actinides. Czechoslov. J. Phys. 56, 13–21.

Choppin, G.R., 2007. Actinide speciation in the environment. J. Radioanal. Nucl. Chem. 273, 695–703.

Choppin, G.R., Liljenzin, J., Rydberg, J., 2002. Radiochemistry and Nuclear Chemistry. Heinemann and Butterworth, Oxford.

Christiansen, B.C., Geckeis, H., Marquardt, C.M., Bauer, A., Römer, J., Wiss, T., Schild, D., Stipp, S.L.S., 2011. Neptunyl ($NpO_2$) interaction with green rust, GR $NaSO_4$. Geochim. Cosmochim. Ac. 75, 1216–1226.

Clark, D.L., David Hobart, I.E., Neu, M.P., 1995. Actinide carbonate complexes and their importance in actinide environmental chemistry. Chem. Rev. 95, 25–48.

Cook, G.T., MacKenzie, A.B., McDonald, P., Jones, S.R., 1997. Remobilization of Sellafield-derived radionuclides and transport from the North-East Irish Sea. J. Environ. Radioactiv. 35, 227–241.

Cornell, R.M., 1992. Adsorption behaviour of cesium on marl. Clay. Miner. 27, 363–371.

Cornell, R.M., Schwertmann, U., 2003a. Adsorption of ions and molecules in: The iron oxides: structure, properties, reactions, occurrences and uses. Wiley-VCH.

Cornell, R.M., Schwertmann, U., 2003b. Introduction to the iron oxides in: The iron oxides: structure, properties, reactions, occurences and uses. Wiley-VCH.

CoRWM, 2006. Managing our Radioactive Waste Safely.

Cumberland, S.A., Douglas, G., Grice, K., Moreau, J.W., 2016. Uranium mobility in organic matter-rich sediments: a review of geological and geochemical processes. Earth. Sci. Rev. 159, 160–185.

Dahlgaard, H., 1995. Transfer of european coastal pollution to the Arctic: radioactive Tracers. Mar. Pollut. Bull. 31, 3–7.

Day, J.P., Cross, J.E., 1981. $^{241}$Am from the decay of $^{241}$Pu in the Irish Sea. Nature. 292, 43–45.

De Cesare, M., Fifield, L.K., Sabbarese, C., Tims, S.G., De Cesare, N., D'onofrio, A., D'arco, A., Esposito, A.M., Petraglia, A., Roca, V., Terrasi, F., 2013. Actinides AMS at CIRCE and 236 U and Pu measurements of structural and environmental samples from in and around a mothballed nuclear power plant. Nucl. Instrum. Meth. B. 294, 152–159.

DEFRA, 2008. Managing radioactive waste safely: a Framework for

implementing geological disposal.

Degueldre, C., 1995. Retention of redox sensitive elements the case of neptunium. J. Environ. Radioactiv. 29, 75–87.

Duff, M.C., Hunter, D., Triay, I., Bertsch, P., Reed, D., Sutton, S., Shea-McCarthy, G., Kitten, J., Eng, P., Chipera, S., Vaniman, D., 1999. Mineral associations and average oxidation states of sorbed Pu on Tuff. Environ. Sci. Technol. 33, 2163–2169.

Duff, M.C., Coughlin, J.U., Hunter, D.B., 2002. Uranium co-precipitation with iron oxide minerals.Westinghouse Savannah River Company (WSRC-MS-2002-00322).

EPA, 1999. Understanding variation in partition coefficient, Kd values. The Kd model methods of measurment, and application of chemical reaction codes. Washington.

European Nuclear Society, 2017. Fuel comparison (accessed October 2017).

Ewing, R.C., 1999. Nuclear waste forms for actinides. 96, 3432–3439.

Finegan, P., León Vintró, L., Mitchell, P.I., Boust, D., Lien Gouzy, A., Kershaw, P.J., Lucey, J.A., 2009. Accumulation, solid partitioning and remobilisation of $^{99}$Tc in subtidal and intertidal sediments in the Irish Sea. Cont. Shelf. Res. 29, 1995–2010.

Finneran, K.T., Anderson, R.T., Nevin, K.P., Lovley, D.R., 2002. Potential for bioremediation of uranium-contaminated aquifers with microbial U(VI) reduction. Soil. Sediment. Contam. 11, 339–357.

Forster, S., Graf, G., Kitlar, J., Powilleit, M., 1995. Effects of bioturbation in oxic and hypoxic conditions: a microcosm experiment with a North Sea sediment community. Mar. Ecol. Prog. Ser. 116, 153–161.

Fowler, S.W., Warnau, M., Teyssie, J.-L., 1996. Biokinetics of selected heavy metals and radionuclides in the common Mediterranean echinoid *Paracentrotus lividus*: sea water and food exposures. Mar. Ecol. Prog. Ser. 141, 83–94.

Fredrickson, J.K., Zachara, J.M., Kennedy, D.W., Kukkadapu, R.K., McKinley, J.P., Fredrickson, L., James Fredrickson, A.K., Heald, S.M., Liu, C., Plymale, A.E., 2004. Reduction of $TcO_4$-by sediment-associated biogenic Fe(II). Geochim. Cosmochim. Ac. 68 (15), 3171–3187.

Froehlich, M.B., Chan, W.Y., Tims, S.G., Fallon, S.J., Fifield, L.K., 2016. Time-resolved record of $^{236}$U and $^{239,240}$Pu isotopes from a coral growing during the nuclear testing program at Enewetak Atoll (Marshall Islands). J. Environ. Radioactiv. 165, 197–205.

Fuller, A.J., Shaw, S., Peacock, C.L., Trivedi, D., Small, J.S., Abrahamsen, L.G., Burke, I.T., 2014. Ionic strength and pH dependent multi-site sorption of Cs onto a micaceous aquifer sediment. Appl. Geochem. 40, 32–42.

Fuller, A.J., Shaw, S., Ward, M.B., Haigh, S.J., Frederick, J., Mosselmans, W.,

Holmes, R, and Tappin, D. R, 2005. DTI Strategic Environmental Assessment Area 6, Irish Sea, Seabed and Surficial Geology and Processes. British Geological Survey Commissioned Report, CR/05/057.

Peacock, C.L., Stackhouse, S., Dent, A.J., Trivedi, D., Burke, I.T., 2015. Caesium incorporation and retention in illite interlayers. Appl. Clay. Sci. 108, 128–134.

Goldschmidt V.M, 1937. The principles of distribution of chemical elements in minerals and rocks. J. Chem. Soc. 655–673.

Gorman-Lewis, D., Fein, J.B., Burns, P.C., Szymanowski, J.E.S., Converse, J., 2008. Solubility measurements of the uranyl oxide hydrate phases metaschoepite, compreignacite, Na–compreignacite, becquerelite, and clarkeite. J. Chem. Thermodyn. 40, 980–990.

Gorman-Lewis, D., Jensen, M.P., Harrold, Z.R., Hertel, M.R., 2013. Complexation of neptunium(V) with *Bacillus subtilis* endospore surfaces and their exudates. Chem. Geol. 341, 75–83.

Gray, J., Jones, S.R., Smith, A.D., 1995. Discharges to the environment from the Sellafield site, 1951-1992. J. Radiol. Prot. 15, 99–131.

Grütter, A., Von Gunten, H.R., Kohler, M., Rössler, E., 1990. Sorption, desorption and exchange of cesium on glaciofluvial deposits. Radiochim. Acta. 50, 177–184.

Hahn, O., Strassman, F., 1939. Concerning the existence of alkaline earth metals resulting from neutron irradiation of uranium. Nature. 27, 11.

Hamilton, E.I., Clarke, K.R., 1984. The recent sedimentation history of the Esk estuary, Cumbria, U.K: the application of radiochronology. Sci. Total. Environ. 35, 325–386.

Hamilton, E.I., 1989. Radionuclides and large particles in estuarine sediments. 2, 603–607.

Hetherington, J., Harvey, B., 1978. Uptake of radioactivity by marine sediments and implications for monitoring metal pollutants. Mar. Pollut. Bull. 9, 102–106.

Howe, S.E., Davidson, C.M., Mccartney, M., 1999. Operational speciation of uranium in intertidal sediments from the vicinity of a phosphoric acid plant by means of the BCR sequential extraction procedure and ICP-MS. J. Anal. Atom. Spectrom. 14, 163–168.

Hua, B., Deng, B., 2009. Reductive immobilization of uranium (VI ) by amorphous iron sulfide . Environ. Sci. Technol. 43, 1237–1238.

Hunt, G.J., Kershaw, P., 1990. Remobilisation of artificial radionuclides from the sediment of the Irish Sea. J. Radiol. Prot. 10, 147–151.

Hursthouse, A.S., Baxter, M.S., Livens, F.R., Duncan, H.J., 1991. Transfer of Sellafield-derived $^{237}$Np to and within the terrestrial environment. J. Environ. Radioact. 14, 147–174.

IAEA, 2005. Radionuclide Levels in Oceans and seas. Vienna (accessed June 2017).

IAEA, 2004. Sediment distribution coefficients and concentration factors for biota in the marine environment. (accessed Feb 2017).

IAEA, 1999. The radiological situation at the Atolls of Mururoa and Fangataufa. J. Radiol. Prot. 19, 194–195.

IAEA, 2017a. PRIS: Reactor status reports: operational long-term shutdown. Vienna (accessed May 2017).

IAEA, 2017b. Nuclear Power Reactors in the World. Vienna (accessed May 2017).

Icopini, G.A., Boukhalfa, H., Neu, M.P., 2007. Biological reduction of Np(V) and Np(V) citrate by metal-reducing bacteria. Environ. Sci. Technol. 41, 2764–2769.

Ilyin, L., Balonov, M., Buldakov, L., Bur'yak, V., Gordeev, K., Dement'ev, S., Zhakov, I., Zubovsky, G., Kondrusev, A., Konstantinov, Y., Linge, I., Likhtarev, I., Lyaginskaya, A., Matyuhin, V., Pavlovsky, O., Potapov, A., Prysyazhnyuk, A., Ramsaev, P., Romanenko, A., Savkin, M., Starkova, N., Tron'ko, N., Tsyb, A., 1990. Radiocontamination patterns and possible health consequences of the accident at the Chernobyl nuclear power station. J. Radiol. Prot. 10, 3–29.

Jefferies, D., Preston, A., Steele, A., 1973. Distribution of Caesium-137 in British coastal waters. Mar. Pollut. Bull. 4, 118–122.

Jenkinson, S., McCubbin, D., Kennedy, P.H., Dewar, A., Bonfield, R., Leonard, K., 2014. An estimate of the inventory of $^{99}$Tc in the sub-tidal sediments of the Irish Sea. J. Environ. Radioactiv. 133, 40–47.

Joyce, M.J., Port, S.N., 1999. Environmental impact of the nuclear fuel cycle, in: Environmental impact of nuclear power. Royal society of chemistry. 73–96.

Kameník, J., Dulaiova, H., Buesseler, K.O., Pike, S.M., Štastná, K., 2013. Cesium-134 and 137 activities in the central North Pacific Ocean after the Fukushima Dai-ichi nuclear power plant accident. Biogeosciences. 10, 6045–6052.

Kaplan, D.I., Kukkadapu, R., Seaman, J.C., Arey, B.W., Dohnalkova, A.C., Buettner, S., Li, D., Varga, T., Scheckel, K.G., Jaffé, P.R., 2016. Iron mineralogy and uranium-binding environment in the rhizosphere of a wetland soil. Sci. Total Environ. 569570, 53–64.

Kaszuba, J.P., Runde, W.H., 1999. The aqueous geochemistry of neptunium: dynamic control of soluble concentrations with applications to nuclear waste Disposal. Environ. Sci. Technol. 33, 4427–4433.

Katz, J., Seaborg, G., Morss, L., 1986. The chemistry of the actinide elements. 2nd ed. Chapman and Hall. London, UK.

Keeney-Kennicutt, W.L., Morse, J.W., 1984. The interaction of $Np(V)O_2^+$ with common mineral surfaces in dilute aqueous solutions and seawater. Mar. Chem.

15, 133–150.

Keith-Roach, M.J., Day, J.P., Fifield, L.K., Bryan, N.D., Livens, F.R., 2000. Seasonal variations in interstitial water transuranium element concentrations. Environ. Sci. Technol. 34, 4273–4277.

Keith-Roach, M.J., Livens, F.R., Bryan, N.D., Bardgett, R.D., 2002. Seasonal changes in the microbial community of a saltmarsh, measured by phospholipid fatty acid analysis. Biogeochemistry. 60, 77–96.

Keith-Roach, M.J., Morris, K., Dahlgaard, H., 2003. An investigation into technetium binding in sediments. Mar. Chem. 81, 149–162.

Keith-Roach, M.J., Roos, P., 2004. Redox-dependent behaviour of technetium-99 entering a permanently stratified anoxic fjord (Framvaren fjord, Norway). Estuar. Coast. Shelf Sci. 60, 151–161.

Kennington, K. and Hisscott, A., 2013. Hydrology, Weather and Climate, Climatology. In Hanley et al., (eds.), Manx Marine Environmental Assessment. Isle of Man Marine Plan. Isle of Man Government, 45

Kershaw, P.J., Swift, D.J., Pentreath, R.J., Lovett, M.B., 1983. Plutonium redistribution by biological activity in Irish Sea sediments. Nature. 306, 774–775.

Kershaw, P.J., Swift, D., Pentreath, R., Lovett, M., 1984. The incorporation of plutonium, americium and curium into the Irish Sea seabed by biological activity. Sci. Total Environ. 40, 61–81.

Kershaw, P.J., Swift, D.J., Denoon, D.C., 1988. Evidence of recent sedimentation in the Eastern Irish Sea. Mar. Geol. 85.

Kershaw, P.J., Pentreath, R.J., Woodhead, D.S., Hunt, G.J., 1992. A review of radioactivity in the Irish Sea: Aquatic environment monitoring group. MAFF. Lowestoft.

Kershaw, P.J., Denoon, D.C., Woodhead, D.S., 1999. Observations on the redistribution of plutonium and americium in the Irish Sea sediments, 1978 to 1996: concentrations and inventories. J. Environ. Radioactiv. 44, 191–221.

Kershaw, P.J., Mccubbin, D., Leonard, K.S., 1999. Continuing contamination of North Atlantic and Arctic waters by Sellafield radionuclides. Sci. Total Environ. 237/238, 119–132.

Kersting, A.B., 2013. Plutonium transport in the environment. Inorg. Chem. 52, 3533–3546.

Kimber, R.L., Boothman, C., Purdie, P., Livens, F.R., Lloyd, J.R., 2012. Biogeochemical behaviour of plutonium during anoxic biostimulation of contaminated sediments. Min. Mag. 76, 567–578.

Kinoshita, N., Sueki, K., Sasa, K., Kitagawa, J.-I., Ikarashi, S., Nishimura, T., Wong, Y.-S., Satou, Y., Handa, K., Takahashi, T., Sato, M., Yamagata, T., 2011. Assessment of individual radionuclide distributions from the Fukushima nuclear accident covering central-east Japan. Proc. Natl. Acad. Sci. 108, 19526–19529.

Koch-Steindl, H., Prohl, G., 2001. Considerations on the behaviour of long-lived radionuclides in the soil. Radiat. Environ. Biophys. 40, 93–104.

Konhauser, K., 2007. Introduction to Geomicrobiology. Blackwell Publishing Ltd, Oxford.

Konhauser, K., Mortimer, R.J.G., Morris, K., Dunn, V., 2002. The role of microorganisms during sediment diagenesis: implications for radionuclide mobility, in: interactions of microorganisms with the environment. Elsevier.

Kristensen, E., Penha-Lopes, G., Delefosse, M., Valdemarsen, T., Quintana, C., Banta, G., 2012. What is bioturbation? The need for a precise definition for fauna in aquatic sciences. Mar. Ecol. Prog. Ser. 446, 285–302.

Kuwabara, J., Yamamoto, M., Assinder, D.J., Komura, K., Ueno, K., 1996. Sediment profile of $^{237}$Np in the Irish Sea: estimation of the total amount of $^{237}$Np discharged from Sellafield. Radiochim. Acta 73, 73–81.

Langmuir, D., 1978. Uranium solution-mineral equilibria at low temperatures with applications to sedimentary or deposits. Geochim. Cosmochim. Ac. 42, 547–569.

Latta, D.E., Boyanov, M.I., Kemner, K.M., O'loughlin, E.J., Scherer, M.M., 2012. Abiotic reduction of uranium by Fe(II) in soil. Appl. Geochem. 27, 1512–1524.

Law, G.T.W., Geissler, A., Boothman, C., Burke, I.T., Livens, F., Lloyd, J.R., Morris, K., 2010a. Role of nitrate in conditioning aquifer sediments for technetium bioreduction. Environ. Sci. Technol. 44, 150–155.

Law, G.T.W., Geissler, A., Lloyd, J.R., Livens, F.R., Boothman, C., Begg, J.D.C., Denecke, M.A., Rothe, J., Dardenne, K., Burke, I.T., Charnock, J.M., Morris, K., 2010b. Geomicrobiological redox cycling of the transuranic element neptunium. Environ. Sci. Technol. 44, 8924–8929.

Leafe, M., 2017. End in sight for reprocessing nuclear fuel at Sellafield. NDA.

Lear, G., McBeth, J.M., Boothman, C., Gunning, D.J., Ellis, B.L., Lawson, R.S., Morris, K., Burke, I.T., Bryan, N.D., Brown, A.P., Livens, F.R., Lloyd, J.R., 2010. Probing the biogeochemical behavior of technetium using a novel nuclear imaging approach. Environ. Sci. Technol. 44, 156–162.

Lee, J.-H., Zachara, J.M., Fredrickson, J.K., Heald, S.M., Mckinley, J.P., Plymale, A.E., Resch, C.T., Moore, D.A., 2014. Fe(II)- and sulfide-facilitated reduction of $^{99}Tc(VII)O_4$ in microbially reduced hyporheic zone sediments. Geochim. Cosmochim. Ac. 136, 247–264.

Lehto, J., Hou, X., 2010. Chemistry and Analysis of Radionuclides: Laboratory Techniques and Methodology. Wiley-Vch.

Leonard, K.S., McCubbin, D., Brown, J., Bonfield, R., Brooks, T., 1997. Distribution of technetium-99 in UK coastal waters. Mar. Pollut. Bull. 34, 628–636.

Leonard, K., McCubbin, D., Jenkinson, S., Bonfield, R., McMeekan, I., 2008. An assessment of the availability of Tc-99 to marine foodstuffs from contaminated sediments. Lowestoft.

Leonard, K.S., McCubbin, D., McDonald, P., Service, M., Bonfield, R., Conney, S., 2004. Accumulation of technetium-99 in the Irish Sea? Sci. Total Environ. 322, 255–270.

Li, D., Kaplan, D.I., 2012. Sorption coefficients and molecular mechanisms of Pu, U, Np, Am and Tc to Fe (hydr)oxides: a review. J. Hazard. Mater. 243, 1–18.

Lindahl, P., Ellmark, C., Gäfvert, T., Mattsson, S., Roos, P., Holm, E., Erlandsson, B., 2003. Tc in the marine environment on the Swedish west coast. J. Environ. Radioactiv. 67, 145–156.

Lindahl, P., Worsfold, P., Keith-Roach, M., Andersen, M.B., Kershaw, P., Leonard, K., Choi, M.-S., Boust, D., Lesueur, P., 2011. Temporal record of Pu isotopes in intertidal sediments from the northeastern Irish Sea. Sci. Total Environ. 409, 5020–5025.

Liu, D.J., Fan, X.H., 2005. Adsorption behavior of $^{99}Tc$ on Fe, $Fe_2O_3$ and $Fe_3O_4$. J. Radioanal. Nucl. Chem. 264, 691–698.

Livens, F.R., 1985. Geochemistry of plutonium and artificial radionuclides in Cumbrian soils. University of Manchester.

Livens, F.R., Al-Bokari, M., Fomina, M., Gadd, G.M., Geissler, A., Lloyd, J.R., Renshaw, J.C., Vaughan, D.J., 2010. Microbial transformations of actinides in the environment. IOP Conference. Series: Materials Science and Engineering. 9, 1–11.

Livingston, H., Povines, P., 2000. Anthropogenic marine radioactivity. Ocean. Coast. Manag. 43, 689–712.

Lloyd, J.R., Sole, V.A., Van Praagh, C. V., Lovley, D.R., 2000. Direct and Fe(II)-mediated reduction of technetium by Fe(III)-reducing bacteria. Appl. Environ. Microbiol. 66, 3743–9.

Lloyd, J.R., Yong, P., Macaskie, L., 2000. Biological reduction and removal of Np(V) by two microorganisms. Environ. Sci. Technol. 34, 1297–1301.

Lloyd, J.R., Chesnes, J., Glasauer, S., Bunker, D.J., Livens, F.R., Lovley, D.R., 2002. Reduction of Actinides and Fission Products by Fe(III)-Reducing Bacteria. Geomicrobiol. J. 19, 103–120.

Lloyd, J.R., 2003. Microbial reduction of metals and radionuclides. FEMS Microbiol. Rev. 27, 411–425.

Lloyd, J.R., Renshaw, J.C., 2005. Microbial transformations of radionuclides : Fundamental mechanisms and biogeochemical implications interactions in laboratory and field-scale studies. Current opinion in biotechnology. 16, 254–260.

Lovett, M., Nelson, N.D., 1978. Oxidation state of Pu in the Irish Sea. Nature 276, 599–601.

Lovley, D.R., Phillips, E.J., Gorby, Y.A., Landa, E.R., 1991. Microbial reduction of uranium. Nature 350, 413–416.

Lucey, J.A., Gouzy, A., Boust, D., Leon Vintro, L., Kershaw, P.J., Mitchell, P.I., 2004b. Geochemical fractionation of plutonium in anoxic Irish Sea sediments using an optimised sequential extraction protocol. Appl. Radiat. Isotopes. 60, 379–385.

MacDonald, R.W., Bewers, J.M., 1996. Contaminants in the arctic marine environment: priorities for protection. ICES J. Mar. Sci. 53, 537–563.

MacKenzie, A.B., Scott, R.D., Williams, T.M., 1987. Mechanisms for northwards dispersal of Sellafield waste. Nature 329, 42–45.

MacKenzie, A.B., Scott, R.D., 1993. Sellafield waste radionuclides in Irish Sea intertidal and salt marsh sediments. Environ. Geochem. Hlth 15, 173–184.

MacKenzie, A., Scott, R., Allan, R.L., Ben Shaban, Y.A., Cook, G., Pulford, I.D., 1994. Sediment radionuclide profiles: implications for mechanisms of Sellafield waste dispersal in the Irish Sea. J. Environ. Radioactiv. 23, 39–69.

MacKenzie, A.B., Cook, G.T., McDonald, P., 1999. Radionuclide distributions and particle size associations in Irish Sea surface sediments: implications for actinide dispersion. J. Environ. Radioactiv. 44, 275–296.

Marsden, O.J., 2003. Determination of actinide distributions in intertidal sediments from West Cumbria. University of Manchester.

Marsden, O.J., Abrahamsen, L., Bryan, N.D., Philip Day, J., Keith Fifield, L., Gent, C., Goodall, P.S., Morris, K., Livens, F.R., 2006. Transport and accumulation of actinide elements in the near-shore environment: field and modelling studies. Sedimentology 53, 237–248.

Marsden, O.J., Livens, F.R., Day, J.P., Fifield, L.K., Goodall, P.S., 2001. Determination of $^{236}U$ in sediment samples by accelerator mass spectrometry. Analyst. 126, 633–636.

Marshall, M.J., Plymale, A., Kennedy, D.W., Shi, L., Wang, Z., Marshall, L., Matthew Marshall, A.J., Reed, S.B., Dohnalkova, A., Simonson, C., Liu, C., Saffarini, D.A., Romine, M.F., Zachara, J.M., Beliaev, A.S., Fredrickson, J.K., Plymale, A.E., Dohnalkova, A.C., Simonson, C.J., 2008. Hydrogenase-and outer membrane c-type cytochrome-facilitated reduction of technetium(VII) by *Shewanella oneidensis* MR-1. Environ. Microbiol. 10, 125–136.

Marshall, T.A., Morris, K., Law, G.T.W., Livens, F.R., Frederick, J., Mosselmans, W., Bots, P., Shaw, S., 2014. Incorporation of uranium into hematite during crystallization from ferrihydrite. Environ. Sci. Technol. 48, 3724–3731.

Masters-Waage, N.K., Morris, K., Lloyd, J.R., Shaw, S., Frederick, J., Mosselmans, W., Boothman, C., Bots, P., Rizoulis, A., Livens, F.R., Law, G.T.W., 2017. Impacts of repeated redox cycling on technetium mobility in the environment. Environ. Sci. Technol. 51, 14301–14310.

McBeth, J.M., Lear, G., Lloyd, J.R., Livens, F.R., Morris, K., Burke, I.T., 2007. Technetium reduction and reoxidation in aquifer sediments. Geomicrobiol. J. 24, 189–197.

McBeth, J.M., Lloyd, J.R., Law, G.T.W., Livens, F.R., Burke, I.T., Morris, A.K., 2011. Redox interactions of technetium with iron-bearing minerals. Min. Mag. 75, 2419–2430.

McCartney, M., Kershaw, P.J., Woodhead, D.S., Denoon, D.C., 1994. Artificial radionuclides in the surface sediments of the Irish Sea, 1968–1988. Sci. Total Environ. 141, 103–138.

McCubbin, D., Leonard, K.S., Brown, J., Kershaw, P.J., Bonfield, R., Peak, T., 2002. Further studies of the distribution of technetium-99 and caesium-137 in UK and European coastal waters. Cont. Shelf. Res. 22, 1417–1445.

McCubbin, D., Leonard, K.S., McDonald, P., Bonfield, R., Boust, D., 2006. Distribution of Technetium-99 in sub-tidal sediments of the Irish Sea. Cont. Shelf Res. 26, 458–473.

McDonald, P., Busby, R.., McCartney, M., 1998. Temporal and spatial responses of the bioindicator fucus to discharge of $^{99}$Tc in Eastern Irish Sea in: International Symposium on Marine Pollution. Monaco, 25–30.

McDonald, P., Vives I Batlle, J., Bousher, A., Whittall, A., Chambers, N., 2001. The availability of plutonium and americium in Irish Sea sediments for re-dissolution. Sci. Total. Environ. 267, 109–123.

McDonald, P., 2011. Radioactivity in the Irish Sea. RSC. Environ. Radiochem. Anal. IV. 2, 87–94.

Meitner, L., Frisch, O.R., 1939. Disintegration of uranium by neutrons: a new type of nuclear reaction. Nature 143, 239–240.

Miller, J.M., Thomas, B.W., Roberts, P.D., Creamer, S.C., 1982. Measurement of marine radionuclide distribution using a towed sea-bed spectrometer. Mar. Pollut. Bull. 13, 315–319.

Mitchell, P.I., Vives Batille, J., Downes, A.B., Condren, O.M., Leon Vintro, L., Sa, J.A., 1995. Recent observations on the physico-chemical speciation of plutonium in the Irish Sea and the Western Mediterranean. Appl. Radiat. Isotopes. 46, 1175–1190.

Morris, K., 1996. Geoochemical interactions of transuranic elements in intertidal areas from West Cumbria, UK. University of Manchester.

Morris, K., Butterworth, J.C., Livens, F.R., 2000. Evidence for the remobilization of Sellafield waste radionuclides in an intertidal saltmarsh, West Cumbria, U.K. Estuar. Coast. Shelf S. 51, 613–625.

Morris, K., Livens, F.R., Charnock, J.M., Burke, I.T., Mcbeth, J.M., Begg, J.D.C., Boothman, C., Lloyd, J.R., 2008. An X-ray absorption study of the fate of technetium in reduced and reoxidised sediments and mineral phases. Appl. Geochem. 23, 603–617.

Moyes, L.N., Jones, M.J., Pattrick, R.A.D., 2002. An X-ray absorption spectroscopy study of neptunium (V) reactions with mackinawite (FeS). Environ. Sci. Technol. 36, 179–183.

Nakata, K., Nagasaki, S., Tanaka, S., Sakamoto, Y., Tanaka, T., Ogawa, H., 2000. Sorption and desorption kinetics of Np(V) on magnetite and hematite. Radiochim. Acta 88, 453–457.

NDA, 2011. Radioactive wastes in the UK: a summary of the 2010 inventory. Harwell

NDA, 2010. Geological disposal: radionuclide behaviour status report. Harwell.

NDA, BEIS, 2017. Radioactive wastes in the UK: UK radioactive waste inventory report.

Newsome, L., Morris, K., Lloyd, J.R., 2014. The biogeochemistry and bioremediation of uranium and other priority radionuclides. Chem. Geol. 363, 164–184.

Newsome, L., Cleary, A., Morris, K., Lloyd, J.R., 2017. Long-term immobilization of technetium *via* bioremediation with slow-release substrates. Environ. Sci. Technol. 51, 1595–1604.

Ohnuki, T., Yoshida, T., Ozaki, T., Kozai, N., Sakamoto, F., Nankawa, T., Suzuki, Y., Francis, Arokiasamy, J., 2007. Chemical speciation and association of plutonium with bacteria, kaolinite clay, and their mixture. Environ. Sci. Technol. 41, 3134–3139.

Ortiz-bernad, I., Anderson, R.T., Vrionis, H.A., Lovley, D.R., 2004. Resistance of solid-phase U (VI ) to microbial reduction during in situ bioremediation of uranium-contaminated groundwater. Appl. Environ. Microbiol. 70, 7558–7560.

Patil, S.K., Ramakrishna, V. V., Ramaniah, M. V., 1978. Aqueous coordination complexes of neptunium. Coord. Chem. Rev. 25, 133–171.

Pentreath, R.J., Harvey, B.R., 1981. The presence of $^{237}$Np in the Irish Sea. Mar. Ecol. Prog. Ser. 6, 243–247.

Peretyazhko, T., Zachara, J.M., Heald, S., Jeon, B., Kukkadapu, R.K., Peretyazhko, L., Peretyazhko, A.T., Liu, C., Moore, D., Resch, C., Zachara, J., Kukkadapu, R., 2009. Heterogeneous reduction of Tc(VII) by Fe(II) at the solid–water interface. Geochim. Cosmochim. Ac. 72, 1521–1539.

Plymale, A.E., Frederickson, J.K., Zachara, J.M., Dohnalkova, A.C., Heald, S.M., Moore, D.A., Kennedy, D.W., Marshall, M.J., Wang, C., Resch, C.T., Nachimuthu, P., 2011. Competitive reduction of pertechnetate ($^{99}TcO_4^-$) by dissimilatory metal reducing bacteria and biogenic Fe(II). Environ. Sci. Technol. 45, 951–957.

Posiva, 2017. General time schedule for final disposal (accessed Dec 2017)

Post, J.E., 1999. Manganese oxide minerals: crystal structures and economic and environmental significance. Proc.Natl. Acad. Sci. 96, 3447–3454.

Powell, B.A., Fjeld, R.A., Kaplan, D.I., Coates, J. T., Serkiz, S.M., 2004. $Pu(V)O_2$ adsorption and reduction by synthetic magnetite ($Fe_3O_4$). Environ. Sci. Technol. 38, 6016–6024.

Powell, B.A, Duff, M., Kaplan, D., Fjeld, R., Newville, M., Hunter, D., Bertsch, P., Coates, J., Eng, P., Rivers, M., Serkiz, S., Sutton, S., Tiay, I.S., Vaniman, D., 2006. Plutonium oxidation and subsequent reduction by Mn(IV) minerals in Yucca Mountain tuff. Environ. Sci. Technol. 40, 3508–3514.

Powell, B.A., Fjeld, R.A., Kaplan, D.I., Coates, J. T., Serkiz, S.M., 2005. $Pu(V)O_2$ adsorption and reduction by synthetic hematite and goethite. Environ. Sci. Technol. 39, 2107–2114.

Prakash, D., Gabani, P., Chandel, A.K., Ronen, Z., Singh, O. V., 2013. Bioremediation: a genuine technology to remediate radionuclides from the environment. Microb. Biotechnol. 6, 349–360.

Ray, D., Livens, F.R., Leary, P., Gray, N., Abrahamsen-Mills, L., Muir, G.K.P., Law., K.A., Fuller, A.J., Bryan, N.D., Howe, J., Cook, G.T., Law, G.T.W., 2018. Controls on anthropogenic radionucldie distribution in the Sellafield-impacted eastern Irish Sea, UK. J. Environ. Radioactiv (Submitted).

Renshaw, J.C., Lloyd, J.R., Livens, F.R., 2007. Microbial interactions with actinides and long-lived fission products. CR.Chim. 10, 1067–1077.

Renshaw, J.C., Law, N., Geissler, A., Livens, F.R., Lloyd, J.R., 2009. Impact of the Fe(III)-reducing bacteria *Geobacter sulfurreducens* and *Shewanella oneidensis* on the speciation of plutonium. Biogeochemistry. 94, 191–196.

Renshaw, J.C., Handley-Sidhu, S., Brookshaw, D.R., Hester, R.E., Harrison, R.M., 2011. Pathways of radioactive substances in the environment, in: Nuclear power and the environment. 152–175.

Roberts, H., Morris, K., Law, G.T., Mosselmans, J.F., Bots, P., Kvashina, K., Shaw, S., 2017. Uranium(V) incorporation mechanisms and stability in Fe(II)/Fe(III) (oxyhydr)oxides. Environ. Sci. Technol. Lett. 4, 421-426.

Sajih, M., Livens, F.R., Alvarez, R., Morgan, M., 2010. Physicochemical characterisation of depleted uranium (DU) particles at a UK firing test range. Sci. Total Environ. 408, 5990–5996.

Salbu, B., Bjornstad, H.E., Svaren, I., Prosser, S.L., Bulman, R.A., Harvey, B.R., Lovett, M.B., 1993. Size distribution of radionuclides in nuclear fuel reprocessing liquids after mixing with seawater. Sci. Total Environ. 130/131, 51–63.

Salbu, B., Skipperud, L., Germain, P., Guegueniat, P., Strand, P., Lind, O.C., Christensen, G., 2003. Radionuclide speciation in effluent from La Hague reprocessing plant in France. Health. Phys. 85, 311–322.

Sanial, V., Buesseler, K.O., Charette, M.A., Nagao, S., 2017. Unexpected source of Fukushima-derived radiocesium to the coastal ocean of Japan. Proc. Natl. Acad. Sci. 114, 11092-11096.

Sawhney, B.., 1972. Selective sorption and fixation of cations by clay minerals: a

review. Clays. Clay. Miner. 20, 93–100.

Schmeide, K., Bernhard, G., 2010. Applied geochemistry sorption of Np(V) and Np(IV) onto kaolinite: effects of pH, ionic strength, carbonate and humic acid. Appl. Geochem. 25, 1238–1247.

Schneider, M., Marignac, Y., 2008. Spent nuclear fuel reprocessing in France.

Scott, T.B., Allen, G.C., Heard, P.J., Randell, M.G., 2005. Reduction of U(VI) to U(IV) on the surface of magnetite. Geochim. Cosmochim. Ac. 69, 5639–5646.

Sellafield, 2016. Sixty years since the day that changed the nuclear industry. Sellafield Ltd (accessed 2017).

Sellafield Ltd, 2015. Monitoring our Environment: annual report on discharges and monitoring in the UK

Sellafield Ltd, 2014. Groundwater monitoring report: Sellafield annual data review.

Sharrad, C.A., Harwood, L.M., Livens, F.R., 2011. Nuclear fuel cycles: interfaces with the environment, in Nuclear Power and the Environment. RSC publishing. 40–56.

Sherman, D.M., Peacock, C.L., Hubbard, C.G., 2008. Surface complexation of U (VI) on goethite (α-FeOOH ). Geochim. Cosmochim. Ac. 72, 298–310.

Sidhu, P.S., Gilkes, R.J., Posner, A.M., 1978. The synthesis and some properties of Co, Ni, Zn, Cu, Mn, and Cd substituted magnetites. J. Inorg. Nucl. Chem. 40, 429–435.

SKB, 2016. A repository for nuclear fuel that is placed in 1.9 billion years old rock (accessed August 2017).

Smith, V., Fegan, M., Pollard, D., Long, S., Hayden, E., Ryan, T.P., 2001. Technetium-99 in the Irish marine environment. J. Environ. Radioactiv. 56, 269–284.

Smith, J., 2011. Nuclear accidents, in: Nuclear power and the environment. RSC publishing. 57–81.

Standrig, W.J.F., Oughton, D.H., Salbu, B., 2002. Potential remobilization of $^{137}$Cs, $^{60}$Co, $^{99}$Tc, and $^{90}$Sr from contaminated mayak sediments in river and estuary environments. Environ. Sci. Technol. 36, 2330–2337.

Stumm, W., Morgan, J, J., 1981. Aquatic chemistry, in: Earth science reviews. Wiley-Interscience, New York. 780.

Stumm, W., Morgan, James, J., 1995. Aquatic chemistry: chemical equilibria and rates in natural waters. 1040

Thompson, R.C., 1982. Neptunium: the neglected actinide: a review of the biological and environmental neptunium-the neglected actinide: a review of the biological and environmental literature. Radiat. Res. 90, 1–32.

Thorpe, C.L., Morris, K., Lloyd, J.R., Denecke, M.A., Law, K.A., Dardenne, K., Boothman, C., Bots, P., Law, G.T. w., 2015. Neptunium and manganese biocycling in nuclear legacy sediment systems. Appl. Geochem. 63, 303–309

Thorpe, C.L., Lloyd, J.R., Law, G.T.W., Williams, H.A., Atherton, N., Cruickshank, J.H., Morris, K., 2016. Retention of $^{99m}$Tc at ultra-trace levels in flowing column experiments–insights into bioreduction and biomineralization for remediation at nuclear facilities. Geomicrobiol. J. 33, 199–205.

Tierney, K.M., Muir, G.K.P., Cook, G.T., MacKinnon, G., Howe, J.A., Heymans, J.J., Xu, S., 2016. Accumulation of Sellafield-derived radiocarbon ($^{14}$C) in Irish Sea and West of Scotland intertidal shells and sediments. J. Environ. Radioactiv. 151, 321–327.

Tims, S.G., Froehlich, M.B., Fifield, L.K., Wallner, A., De Cesare, M., 2016. $^{236}$U and $^{239,240}$Pu ratios from soils around an Australian nuclear weapons test site. J. Environ. Radioactiv. 151, 563–567.

Tinnacher, R.M., Zavarin, M., Powell, B.A., Kersting, A.B., 2011. Kinetics of neptunium(V) sorption and desorption on goethite: an experimental and modeling study. Geochim. Cosmochim. Ac. 75, 6584–6599.

U.S. NRC, 2017. NRC: Stages of the Nuclear Fuel Cycle (accessed July 2017).

Ulrich, K.-U., Singh, A., Schofield, E., Bargar, J., Veeramani, H., Sharp, J. O., Bernier-Latmani, R., Giammar, D., 2008. Dissolution of biogenic and synthetic $UO_2$ under varied reducing conditions. Environ. Sci. Technol. 42, 5600–5606.

United Nations, 2017a. The Paris Agreement (accessed May, 2017).

United Nations, 2017b. Ending Nuclear Testing (accessed May 2017).

UNSCEAR, 2008. Sources and Effects of Ionizing Radiation. Report to the general assembly with scientific annexes. New York.

UNSCEAR, 2012. Sources, effects and risks of ionizing radiation. Report to the general assembly with scientific annexes. New York.

Vejsada, J., 2006. The uncertainties associated with the application of batch technique for distribution coefficients determination-a case study of cesium adsorption on four different bentonites. Appl. Radiat. Isotopes. 64, 1538–1548.

Waite, T.D., Davis, J.A., Payne, T.E., Waychunas, G.A., Xi, N., 1994. Uranium(VI) adsorption to ferrihydrite: application of a surface complexation. Geochim. Cosmochim. Ac. 58, 5465–5478.

Wang, X., Dong, W., Li, Z., Du, J., Tao, Z., 2000. Sorption and desorption of radiocesium on red earth and its solid components: relative contribution and hysteresis. Appl. Radiat. Isotopes. 52, 813–819.

Wang, Z., Sung-Woo, L., Kapoor, P., Tebo, B., Giammar, D., 2013. Uraninite oxidation and dissolution induced by manganese oxide: a redox reaction between two insoluble minerals. Geochim. Cosmochim. Ac. 100, 24–40.

WHO, 1989. Health hazards from radiocaesium following the Chernobyl nuclear accident: report on a WHO working group. J. Environ. Radioact. 10, 257–295.

Wildung, R.E., Gorby, Y.A., Krupka, K.M., Hess, N.J., Li, S.W., Plymale, A.E., McKinley, J.P., Fredrickson, J.K., 2000. Effect of electron donor and solution chemistry on products of dissimilatory reduction of technetion by *Shewanella putrefaciens*. Appl. Environ. Microbiol. 66, 2451–2460.

Wildung, R.E., Li, S.W., Murray, C.J., Krupka, K.M., Xie, Y., Hess, N.J., Roden, E.E., 2004. Technetium reduction in sediments of a shallow aquifer exhibiting dissimilatory iron reduction potential. FEMS. Microbiol. Ecol. 49, 151–162.

Wilson, P., 1996. Nuclear Fuel Cycle: from ore to wastes. OUP.

World Nuclear Association, 2016. Nuclear Development in the United Kingdom (accessed October 2017).

World Nuclear Association, 2017. Nuclear power in France, French nuclear energy (accessed October 2017).

World Nuclear Association, 2017a. Nuclear power today, nuclear energy (accessed October 2017).

World Nuclear Association, 2017b. Nuclear power in the United Kingdom, UK Nuclear Energy (accessed October 2017).

World Nuclear Association, 2017. Nuclear proliferation case studies (accessed November 2017).

Yamamoto, M., Yamauchi, Y., Komura, K., Ueno, K., Assinder, D.J., 1991. Chemical leaching behaviour of $^{237}$Np from intertidal coastalsediment n the rish sea. J. Radioanal. Nucl. Chem. Lett. 154, 299–307.

Yamamura, T., Kitamura, A., Fukui, A., Nishikawa, S., Yamamoto, T., Moriyama, H., 1998. Solubility of U(VI) in highly basic solutions. Radiochim. Acta. 83, 139–146.

Zachara, J.M., Heald, S.M., Jeon, B.-H., Kukkadapu, R.K., Liu, C., Mckinley, J.P., Dohnalkova, A.C., Moore, D.A., 2007. Reduction of pertechnetate [Tc(VII)] by aqueous Fe(II) and the nature of solid phase redox products. Geochim. Cosmochim. Ac. 71, 2137–2157.

Zavarin, M., Powell, B.A., Bourbin, M., Zhao, P., Kersting, A.B., 2012. Np(V) and Pu(V) ion exchange and surface-mediated reduction mechanisms on montmorillonite. Environ. Sci. Technol. 46, 2692–2698.

Zhao, P., Johnson, M.R., Roberts, S.K., Zavarin, M., 2005. Np and Pu sorption to manganese oxide minerals. Lawrence Livermore National Laboratory (UCRL-TR-241984).

Zhao, X.-L., Kilius, L.R., Litherland, A.E., Beasley, T., 1997. AMS measurement of environmental U-236 preliminary results and perspectives. Nucl. Instrum. Meth. Phys. Res. B. 126, 297–300.

## Chapter 2: Materials and Methods

This chapter includes a detailed discussion on the fieldwork and experimental techniques that have been used throughout this project. Subsequent research chapters (Chapters 3–5) also contain details of the methods used (as they are reproductions of manuscripts either submitted or in the process of submission).

## 2. Materials and Methods

All reagents used in the laboratory were of analytical grade or better. De-ionised water from a Barnstead Milli-Q De-ionised water (DI) system (resistivity: 18.2 MΩ) was used when preparing all solutions. Glassware was cleaned overnight in a 5 % $HNO_3$ bath, followed by rinsing with 18.2 MΩ DI water.

### 2.1. Field Sample Collection and Preparation

Two locations in the Eastern Irish Sea area were sampled for this thesis: the Irish Sea mud-patch and the Ravenglass saltmarsh. The sampling campaign began in June 2014, aboard the RV Prince Madog, with sediment cores being collected from the Irish Sea mud-patch. The Ravenglass saltmarsh was sampled in September 2014. These sites were chosen as they have previously been recognised to accumulate Sellafield-derived radionuclides (Kershaw et al., 1992; MacKenzie et al., 1994). Sediment cores were collected from one site at the Irish Sea mud-patch: 54’26.80 N, 03’42.89 W; and two sites at the Ravenglass saltmarsh: 54’20.24 N, 03’24.20 W, and: 54’20.24 N, 03’24.06 W (approximately 5 m apart) (Figure 2.1). A hydraulic mega-corer was used to collect undisturbed sediment cores from the Irish Sea mud-patch.


**Figure 2.1**. Locations of the sampling sites for this project (the Irish Sea mud-patch and Ravenglass saltmarsh).

The mega-corer was comprised of a rounded frame with a sampling head attached by a hydraulic damper (Figure 2.2A). Core tubes made of extruded acrylic, of length 50 cm and diameter 10 cm, were inserted into the sampling head prior to the device being lowered *via* winch onto the seabed. The core tubes were then driven into the sediment under gravity, using a lead weight on the sampling head. The motion was controlled by a hydraulic damper system to collect an undisturbed sediment core. Cores of ~ 36 cm length were retrieved from the mud-patch.

Several cores were collected from the same site on the mud-patch, some were sectioned under anaerobic conditions in a $N_2$ filled Aldrich Atmosbag (Figure 2.2B). These cores were sliced at 1 cm resolution from the sediment water interface to 10 cm depth, and at 2 cm resolution thereafter to 36 cm. A further long sediment core (~ 1.5 m) was taken using a gravity corer, and this was sectioned in 2 cm resolution to 1 m, and 5 cm thereafter on deck. The bottom 1 cm of the cores was disposed of, as they become disturbed by the trap mechanism that holds the cores in place during winching of the mega-corercorer back onto the ship. Further, gaseous $O_2$ can penetrate into the bottom of the core. Porewater was extracted from each core section by centrifugation (10 minutes at 4500 rpm; 1811 *g*). On collection the porewater was transferred to LDPE vials and fixed by addition of Aristar grade c$HNO_3$ (100 µL). These samples were then stored in the dark at 5 °C until further analysis. The remaining cores were sampled on deck in the open air at the same resolution (Figure 2.2C).

Sediment cores were collected from two sites (approximately 5 m apart) from the Ravenglass saltmarsh, a location on the Esk Estuary. Similar to the sampling carried out at the Irish Sea mud-patch, cores were collected in extruded acrylic tubes (50 cm in length and 10 cm in diameter). These tubes were manually inserted into the ground until they reached the desired depth. Thereafter, the core tops were sealed and the core tubes removed under vacuum. Two sediment cores were collected with one being sectioned under $N_2$ atmosphere, and the other being sectioned in the open atmosphere, as per the mud-patch sampling regime (see above). Sediment samples from both sites (Irish Sea mud-patch and Ravenglass saltmarsh) were sealed in PVC bags, labelled and then frozen at -20 °C. On return to the home laboratory, sediment cores that were sampled

aerobically were freeze-dried and thoroughly homogenised for further analysis using a Fritsch agate ball grinder (7 minutes at 350 rpm; 10.9 $g$). Sediment samples from the glove bag were frozen at -80 °C until analysis.


**Figure 2.2.** The Irish Sea mud-patch sampling campaign: (A) hydraulic mega-corer used to collect sediment cores from the mud-patch; (B) sampling of core in an $O_2$-free atmosbag; (C) aerobic sampling of cores on deck.

## 2.2. Elemental Analysis

### 2.2.1. Loss on Ignition (LOI)

Sediments were exposed to a sequential heating process to determine the percentage of water and carbon within the sample. Three stages of heating are required in order to calculate the LOI. Ground sediment (~5.5 g) from each sample was dried at 105 °C in an oven for 24 hours to remove water from the sediment. This was then placed in a desiccator to cool the sample to room temperature, and the mass was subsequently recorded. The sample was heated in a Carbolite 201 furnace at 375 °C for 19 hours using a ramp rate of 1 °C/min, to remove organic carbon from the sediment sample. This was placed in a desiccator to cool to room temperature, and the mass recorded. Then, the sample was ashed at 950 °C for 10 hours in the furnace at a ramp rate of 10 °C/min, to eliminate inorganic carbon from the sample. Then, samples were oven dried at 105 °C for 1 hour to remove any moisture. The sample was cooled in a desiccator, and the final mass recorded. The mass of the sample after each heating stage was used to calculate the total LOI.

### 2.2.2. X-Ray Fluorescence (XRF)

XRF is a non-destructive elemental analysis technique. Photons of sufficiently high energy are emitted from an X-ray source which subsequently interacts with analyte atoms, inducing ionisation of their inner-shell electrons by the photoelectric effect. This results in the transition of outer shell electrons to this vacancy (Janssens, 2014) and emission of characteristic fluorescence radiation. The emitted photon has a well-defined energy corresponding to the difference in energy between the atomic shells involved. The measurement of the emitted wavelength and the intensity of the characteristic photon allow the identification of elements in an environmental sample.

The bulk elemental composition of the Irish Sea mud-patch and Ravenglass saltmarsh was determined *via* XRF. Sediment pellets were made from ground sediment (12 g), and this was added to powdered wax binder (3 g) and further homogenised (7 minutes at 350 rpm; 10.9 *g*). The sediment/wax mixture was then transferred into a pellet pressing mould and a hydraulic press (pressure: 10 t) was used to create a pellet with a smooth analytical surface. The pellet was then analysed using an Axios Sequential X-Ray Fluorescence Spectrometer. The major elements were analysed using standardless analysis combined with an IQ+ software package. The IQ+ software is based on an advanced fundamental parameters algorithm that provides accurate analysis of a wide range of elements from atomic number 8 to 95, over a large concentration range, between 0.01–100 %. Trace elemental analysis was completed using Pro-Trace which provides accurate analysis with detection limits ranging from sub-ppm levels to 6 ppm depending on the element of interest. After analysis, the data was oxide and LOI normalised.

### 2.2.3. Inductively Coupled Plasma-Atomic Emission Spectroscopy (ICP-AES)

This is a multi-element technique, commonly used for trace metal analysis of aqueous samples. The sample of interest is delivered to the nebuliser by a peristaltic pump, where it forms a fine aerosol of droplet size ≤ 20 μm in diameter (De Laeter, 2001). This process is inefficient as only 1 % of the nebulised sample

is transferred to the argon (Ar) plasma torch. Here, a high temperature (10,000 K) is generated by the ionisation of Ar gas within a strong electromagnetic field (Hill, 2007). The electrons of an atom absorb energy generated by the plasma and reach higher energy levels. However, as the lifetime of the excited atom is short ($\sim 10^{-8}$ s) (Dean, 2005) the atom quickly returns to the ground state emitting a characteristic photon of energy at a specific wavelength and intensity. The photon of light is isolated and converted to an electrical signal used to characterise and quantify elemental abundance via calibration with reference samples. Typical limits of detection for ICP-AES are low parts per million (ppm).

In this project, porewater Fe and Mn concentrations were measured by ICP-AES, using a Perkin Elmer Optima 5300 Dual View ICP-AES. Porewater (200 μL) was diluted with 2 % $HNO_3$ (4.8 mL) to reduce matrix effects. Standards of known concentration (for the analyte in question) are required to calibrate the instrument. A range of standards (1–100 ppb; $R^2 \geq 0.99$) were matrix-matched to the samples using standard seawater. The limit of detection (LOD) for each analyte

### 2.2.4. Inductively Coupled Plasma-Mass Spectrometry (ICP-MS)

Inductively Coupled Plasma Mass Spectrometry is a technique used for trace metal analysis in environmental samples. An aqueous sample is introduced in the same manner as ICP-AES however the role of the plasma torch is to generate ions, which are then transferred to a high vacuum quadrupole mass analyser for separation and then subsequent detection. A quadrupole mass spectrometer consists of an ionizer, ion accelerator, and a mass filter consisting of four parallel metal rods. These rods utilise the variable ion trajectories in an oscillating electric field to separate ions independent on their mass to charge (*m/z*) ratio (Broekaert, 2014). The strength of the electric field is chosen so that ions of specific *m/z* ratio will pass through to the detector, whilst other competing ions are not transferred. The atoms of different elements of the periodic table have a different relative atomic mass, and this allows for identification of various elements. The signal produced by the detector is compared to a calibration line, composed of known concentrations of analyte. Additionally, quadrupole ICP-MS is able to scan the mass spectrum from 3-250 within a few seconds, and can move from mass to mass with a high degree of precision (Sneddon and Vincent, 2008).

In this project, ICP-MS was used for the detection of $^{99}$Tc in Ravenglass saltmarsh samples, and Fe and Mn in sequential extraction leachates at the Irish Sea mud-patch and Ravenglass saltmarsh, as it can achieve significantly lower limits of detection (low ppt to ppq). In this work, samples from the Tc extraction (10 μL) were diluted with 2 % $HNO_3$ (4.99 mL) and analysed on the Agilent 7500cx ICP-MS. A series of $^{99}$Tc standards (0–300 ppt; $R^2 = >0.99$) were used here to calibrate the instrument. The leachates from the sequential extraction experiments (2 mL) were diluted to 5 mL using 2 % $HNO_3$ (for certain samples a lower aliquot of samples was utilised to reduce the presence of total dissolved solids).

### 2.3. DNA Sequencing

DNA was extracted using a FastDNA Spin Kit for Soil (MP Biomedicals) as per manufacturer's instructions. DNA underwent Polymerase Chain Reaction, using universal primer pair F515 and R926 (positions 515 to 926 in the V4–V5 region; *Escherichia coli* numbering), which target both Bacteria and Archaea. Forward primers used 'golay_12' barcodes and Torrent adaptor A for identification. Initial denaturation was at 95 °C for 5 minutes; 30 cycles of 95 °C for 1 minute, 55 °C for 1 minute, 72 °C for 1 minute; and a final elongation step of 72 °C for 10 minutes. PCRs were performed on a Techne 512 thermocycler, and in triplicate to reduce bias. Amplicons were cleaned using Agencourt AMPure XP (Beckman Coulter), quantified *via* Qubit 3.0 fluorometer (Life Technologies) and pooled.

Sequencing was performed internally on an Ion Torrent Personal Genome Machine (Thermo Fisher Scientific) on a 316 chip. Sequencing produced reads with a modal length of 481 bases. The average number of reads in individual binned closed-reference libraries after filtering and operational taxonomic unit (OTU) phylogenetic assignment filtering was 4836.41 for the Irish Sea mud-patch ranging from 5808 to 23402 and 13271.68 for the Ravenglass sediment core, ranging from 6922 to 21972. Libraries were rarefied to 6900 sequences for the saltmarsh core and 5800 sequences for the mud-patch core to allow for comparative analysis of sequences. Sequences for both sediment cores were deposited in the NCBI's Sequence Read Archive (SRA), and are available under BioProject. Pipeline analysis was performed using QIIME 1.9.1, (Caporaso et al.,

2010) with OTU matching performed at 99 % similarity against the SILVA128 closed-reference database (Quast et al., 2012). OTU tables were standardised by total for each sample depth, and square root transformed, in PRIMER 6 (Clarke and Gorley, 2009). Bray Curtis similarity and non-metric-Multidimensional Scaling analysis was then performed. Taxonomy summary bar charts were chosen to represent trends in community change as a function of depth (based on assignments of OTUs to the genus level where possible). Dominant taxa and their abundance change with depth were related to other geochemical parameters based on geochemical functions inferred from the conserved phenotypic characteristics of close relatives. It is important to highlight that Ion Torrent does not delineate live vs dead, or active vs inactive bacteria.

### 2.4. Radionuclide Analysis

### 2.5. Gamma Spectrometry ($^{241}$Am and $^{137}$Cs)

The activity of γ-emitting radionuclides can be detected with a solid-state detector (Lehto and Hou, 2010) using γ-spectroscopy. The γ-rays emitted by the radionuclides interact with the intrinsic region of a semiconductor material. High purity Ge (HPGe) and Ge(Li) are materials commonly used for semi-conductors. The detection of γ-ray photons is dependent on their interaction with electrons of the semi-conductor material (Rittersdorf, 2007). The photon interacts with the medium in three ways: photoelectric absorption, Compton scattering, and pair production.

In brief, photoelectric absorption involves the loss of the incident γ-ray, with a photoelectron being generated from one of the electron shells of the absorbing material (Rittersdorf, 2007). Compton scattering includes the scattering of a γ-ray photon off an unbound electron, creating a scattered γ-ray photon, and a recoil electron, and pair production transforms the γ-ray into an electron-positron pair (Rittersdorf, 2007). The latter can only take place when the γ-ray is in close proximity to the electric field near the nuclei of the absorbing material. The photoelectric effect dominates for low energy photons and high *z* material; pair production for high energy photons and high *z* materials; and Compton scattering for moderate energies (Rittersdorf, 2007).

The emitted electrons have a maximum energy that is equal to the energy of the incident γ-photon. The energy associated with the three types of interaction is then deposited and converted into charge in the semi-conductor crystal. The crystal is cooled to 77 K with liquid nitrogen to prevent the leakage of the thermally-induced current, thereby increasing the resolution of the detector (Smith and Lucas, 1991). At very low temperatures, the valence electrons in the semi-conductor crystal are present in energy levels known as valence bands, with the higher energy level conduction band unoccupied. The deposition of energy results in an increasing temperature in the crystal, and this causes the promotion of valence electrons to the conduction band, leaving a hole in the valence band. This promotion is only possible if the energy difference between these two bands (the band gap) is less than 2 eV; germanium is well suited for this purpose as it has a band-gap of 0.6 eV (Fielder and Tench, 1971).

Appling a voltage to the detector causes the electrons to migrate to the cathode whilst the holes move to the anode, creating a current (Gilmore, 2008). The equipment amplifies and shapes the pulses to boost the signal, and shortens the duration of the pulse. The energy of the photon is determined from the number of promotions in the semi-detector, and thus, the magnitude of the signal from the detector is proportional to the energy of the γ-photon. This signal is then converted to a digital form and stored in a Multi-Channel Analyser 42 (MCA) to produce the spectrum.

Radiochemical separation is not normally required for the analysis of γ-emitting radionuclides, due primarily to the penetrative nature of the high-energy γ-rays. However, it is important to calibrate the counting system for energy, efficiency and geometry, as any fluctuations will introduce additional error into the system (Lehto and Hou, 2010). A HPGe detector was used in this work to detect $^{241}$Am and $^{137}$Cs. The detector was of coaxial geometry to maximise its surface area to absorb a high number of γ-rays As a result, the XRF pellets from section 2.2.2 were used here as they had a constant size and mass. In addition the Broad Ge γ-spectrometer was used for $^{237}$Np analysis (see section 2.9), and the Canberra HP(Ge) DSPEC-50 γ-spectrometer was used for $^{99m}$Tc analysis (see section 2.10).

The interaction of the γ-radiation with the detector generates a count rate (counts per unit time). This is used, along with the efficiency of the detector, to calculate the activity (Bq/g) of the radionuclides in the Irish Sea mud-patch and Ravenglass sediments, using Equations 2.1 and 2.2:

$$Count\ rate\ \left(\frac{counts}{s}\right) = \frac{No.of\ counts}{Detection\ time}$$

(Equation 2.1)

$$Activity_{(Unknown)}(Bq/g) = \frac{Count\ Rate\ _{(Unknown)} \times Activity_{(Tracer)}}{Mass\ of\ Sample\ (g) \times Count\ Rate_{(Tracer)}}$$

(Equation 2.2)

Due to the ease of sample preparation and the efficiency of the detector, γ-spectroscopy was chosen as the technique to quantify $^{241}$Am and $^{137}$Cs activities in the Irish Sea mud-patch and Ravenglass sediment samples. The pellets used for XRF analysis (see section 2.2.2) were sealed in PTFE plastic containers (30 mL) using PTFE gas sealant tape and Parafilm. These containers were then sealed for a minimum of 30 days prior to analysis in order for radioactive equilibrium to be obtained between $^{226}$Ra and $^{222}$Rn. All the samples were placed in the centre of the detector to prevent artefacts from being introduced due to changes in sample position. The samples were counted for 24 hours using a Canberra GC1019 HPGe detector housed in a 11 cm thick lead shield (20-1800 keV), and the characteristic γ-ray emission at 59.5 keV and 661.6 keV monitored for $^{241}$Am, and $^{137}$Cs, respectively.

A γ-standard was prepared (to determine the yield efficiency) by homogenising a low activity soil sample (~15 g), using a Fritsch agate ball grinder (7 minutes at 350 rpm; 10.9 *g*). The homogenised sample was mixed with copious amounts of ethanol (~250 mL) to form a slurry. This was allowed to settle and the top layer of ethanol was spiked with $^{241}$Am (100 Bq), $^{137}$Cs (100 Bq), $^{226}$Ra (100 Bq) and $^{210}$Pb (500 Bq) (Amersham International). The slurry was gently homogenised and warmed on a sand-bath until dry. Then, 12 g of the dried sample was mixed with powdered wax binder (3 g) and transferred into a pellet pressing mould.

Using a hydraulic press, pressure (10 t) was applied, and the standard was also counted for 24 hours using the same HPGe γ-detector to ensure that a sufficient count rate for each isotope was observed. The resulting spectra were also corrected for background noise. The yield obtained for the standards was used to correct the samples for detector efficiency.

### 2.6. Plutonium Analysis ($^{238}$Pu and $^{239,240}$Pu)

In this project the analysis of $^{238}$Pu, and $^{239,240}$Pu in Irish Sea sediments required three steps; (i) ion extraction chromatography, to separate Pu from the sediment matrix and other competing species, (ii) electrodeposition, to plate the extracted Pu as a thin layer, and (iii) alpha (α)-spectroscopy which allows the detection and quantification of the plated Pu fraction.

#### 2.6.1. Ion Extraction Chromatography

Several methods have been previously used to chemically separate actinides from the sediment matrix and other co-contaminants. These have focused on extraction chromatography, a technique that combines the selectivity of solvent extraction with the ease of column chromatography (Horwitz, 1996). In this project the extraction chromatographic resins TEVA® and UTEVA®, and the ion-exchange resin AG1®-X8 were used to extract environmentally relevant actinides from the sediment matrix.

There are three major components of an extraction chromatographic system: (i) inert support: this is comprised of porous silica or organic polymer framework (50 to 150 μm); (ii) stationary phase: this varies between resins and hosts the aqueous extractant; (iii) mobile phase: typically an acid solution e.g. nitric or hydrochloric acid. Ions with a high charge density are more effectively retained on the column, due to the increased Coulombic interaction with the functional group of the resin (Lehto and Hou, 2010). Aqueous samples are introduced into the column containing resin, causing ions of opposite charge to be retained onto the pores of the resin. Thus, ions of specific oxidation states are retained on the column and this is achieved by varying the pH of the solutions introduced into the column. A further change in pH of the resin will transform the coordination environment of the target ion, resulting in elution from the column.

The Triskem TEVA® exchange resin was used in this work to chemically extract Pu isotopes from the sediment matrix. The active component trialkylmethylammonium nitrate (Aliquat 336) acts as the stationary phase (Horwitz et al., 1995). Here, the TEVA® resin preferentially sorbs all tetravalent actinides (as their nitrato complexes) in 2–4 M $HNO_3$ solutions e.g. $[Pu(NO_3)_6]^{2-}$ (Horwitz, 1996). The functional groups of the TEVA® resin are in a liquid form (rather than fixed to polymer backbone) allowing for greater flexibility when forming complexes with the target ion. Other radionuclides, for example Am(III), Np(V), and U(VI) are not retained by the resin and pass through the column. The UTEVA® resin contains diamyl amylphosphonate (DA[AP]) as the stationary phase, and this compound is able to selectively extract U(VI) as a neutral nitrato complex, from other constituents e.g. Al, Fe (Horwitz, 1996). This approach was used in $^{236}U$ analysis (see section 2.8) and $^{237}Np$ analysis (see section 2.9).

The Bio-Rad AG1®-X8 anion exchange resin was used in this thesis to clean $^{237}Np$ during the chemical separation procedure (section 2.9). This resin contains quaternary amine functional groups held on styrene divinylbenzene polymeric beads (Biorad, 2000). The quaternary amine contains a chloride counter ion which is exchanged by the target ion e.g. $[Np(Cl)_6]^{2-}$. The target ion is then reduced by an appropriate reducing agent, resulting in Np being eluted from the column.

Homogenised sediment (~2.3 g) from each sample was ashed in a furnace at 550 °C for 8 hours in order to remove the organics present in the sediment matrix. The ashed sample (1.0 g) was leached in *aqua regia* (3:2 v/v cHCl:c$HNO_3$) for 3 hours to induce partial dissolution of the radionuclides (extract into solution). Solids were filtered (Whatman GF/A; 0.22 µm), and rinsed with 3 M $HNO_3$. The filtrate was made up to 50 mL to make a stock solution. In this thesis, a method based on Nygren et al. (2003) was used to extract Pu from Irish Sea sediments. An aliquot of the stock solution (25 mL) was spiked with a $^{242}Pu$ tracer (100 µL, 0.75 Bq/mL) and evaporated to incipient dryness. The residue was taken up in 3 M $HNO_3$ (15 mL). Then, 0.2 M $NaNO_2$ (0.21 g) was added and the solution heated at 90 °C for 20 minutes, and cooled to room temperature, to ensure Pu was in the tetravalent Pu(IV) state. This step ensures strong uptake of Pu, by the resin, under 3 M $HNO_3$ conditions (Horwitz, 1996). The column (Eichrom TEVA®

resin, 2 mL, 100–150 mesh; Figure 2.3A) was conditioned with 3 M $HNO_3$ (5 mL), and the sample loaded onto the column. The beaker containing the sample was rinsed with 3 M $HNO_3$ (5 mL) and these washings were also loaded onto the column. The resin was then rinsed with 3M $HNO_3$ (3 x 5 mL) to remove U(VI), Am(III), Np(V), and Fe alongside other trace metals. Once eluted, 9 M HCl (5 mL) was added to extract Th(IV) from the resin medium (Lehto and Hou, 2011). Then, Pu was eluted from the column using 0.1 M $NH_4I$ (0.216 g) in 9 M HCl (3 x 5 mL) resulting in desorption of the radionuclide from the resin as Pu(III). Then, 10 % $KHSO_4$ carrier solution (1 mL) was added to prevent retention of Pu on the glass beaker and 3 M $HNO_3$ (3 mL) was added to the beaker, and warmed gently (to oxidise $I^-$ to $I_2$). The solution was then evaporated to incipient dryness to decompose the eluent, and the residue taken up in 30 % vol $H_2O_2$ (1 mL) to further decompose the eluent on evaporation to incipient dryness. The residue was then taken up in cHCl (3 mL) to remove any residual $NO_2^-$, and evaporated to incipient dryness.

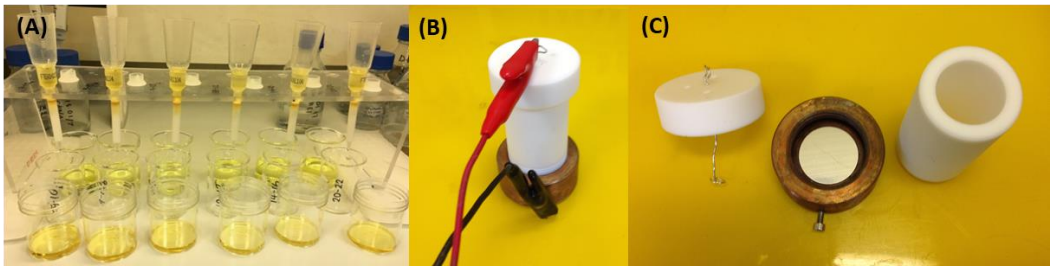


**Figure 2.3.** (A) TEVA® resin columns; (B) set-up of the electrochemical cell connected to the power source; (C) components of the electrochemical cell with exposed stainless steel planchette.

### 2.6.2. Electrodeposition

To detect $^{238}Pu$ and $^{239,240}Pu$ with α-spectroscopy, a thin, uniform deposit of Pu was necessary. To achieve this, Pu was plated onto a metal disc using an electro-deposition cell, in which a platinum wire acts as the anode and a stainless steel planchette (metal disk) the cathode (Lehto and Hou, 2010; Figure 2.3B and 2.3C). A power supply provides a direct current to the anode, oxidising the Pu atoms and

allowing them to dissolve in solution. At the stainless steel cathode, the dissolved Pu ions in the electrolyte solution are reduced, and plate out onto the cathode disc.

For electrodeposition, the final extract from the TEVA® column separation was taken up in electrolyte solution 4 % $(NH_4)_2C_2O_4$ in 0.3 M HCl (15 mL). The solution was added to the electrodeposition cell fixed with a stainless steel planchette at the base. The beaker containing the extract was rinsed with deionised water (10 mL, 18.2 MΩ) and added to the cell. Electrodeposition was completed over 2.5 hours (0.5 A, 20 V). The current ensures the metal ions were reduced and deposited as hydroxides or in metallic form, forming a thin layer on the surface of the planchette (Lehto and Hou, 2010). Ammonia solution (1 mL) was added to the cell one minute prior to the end of the deposition. The planchette was rinsed with deionised water (18.2 MΩ), followed by ethanol, and acetone and subsequently dried in air. The planchette was sealed in a PVC bag ready for analysis on a Canberra 7401 α-spectrometer.

### 2.6.3. Alpha Spectroscopy

Alpha spectroscopy is an analytical technique used to determine the activity of α-emitting radionuclides. Alpha particles arise from transitions between well-defined, discrete energy levels, and as a result are emitted with characteristic energies. Alpha spectrometers utilise a semiconductor detector made up of an *n*-type block of Si/Ge of which one surface is exposed to air to produce a thin *p*-type layer. As a reverse bias is applied an intrinsic layer is formed between the two semiconductor types. As α-particles hit the intrinsic region, a current is induced as the charge is detected.

As α-particles are easily absorbed, a vacuum is present between the *p*-type layer of the detector and the thin source of Pu on the planchette. This is to ensure that α-particles are not absorbed before reaching the Si detector. Also, the samples must be chemically pure, to prevent the presence of any foreign α-emitting radionuclides. Due to the resolution limitations of α-spectrometry, it can often prove difficult to resolve peaks of similar energy. For Pu, the isotopes $^{239}$Pu and $^{240}$Pu emit α-particles of similar energy, (5.16 MeV and 5.17 MeV, respectively)

resulting in a single peak being observed, and as a result, data is commonly reported as $^{239,240}$Pu.

A yield monitor is required (given the complexities of the extraction technique) and in this work a known activity of $^{242}$Pu tracer (~0.075 Bq/100 µL) was added to the sample at the start of the separation procedure to determine the percentage loss of the Pu isotopes during the extraction procedure. The counts obtained for a given sample is equal to the number of disintegrations. The error associated with the number of counts was also recorded. Thus, the activity of the Pu isotopes (Bq/g) of interest can be calculated using Equation 2.3. The percentage recovery of the $^{242}$Pu yield monitor was then calculated using Equation 2.4

$$Activity_{(Unknown)}\,(Bq/g) = \frac{Number\ of\ Counts_{(Unknown)} \times Activity_{(Tracer)}}{Mass\ of\ Sample\ (g) \times Counts}$$

(Equation 2.3)

$$\%\ Recovery = \frac{Number\ of\ counts_{(Tracer)}}{Time \times Detector\ efficiency \times Activity_{(Tracer)}} \times 100$$

(Equation 2.4)

The detector efficiency of the instrument is assumed to be moderate and is given a standard value of 25 %. In this work the stainless steel planchettes were counted for 24 hours on a Canberra 7401 α- spectrometer in order to obtain a sufficient count rate (as $^{238}$Pu exists in low concentrations).

### 2.7. Plutonium Analysis ($^{241}$Pu)

TEVA® resin (Eichrom, 2 mL, 100150 mesh) was also used in this project to extract $^{241}$Pu from the sediment matrix, similar to the procedure outline for the lower mass Pu isotopes ($^{238}$Pu, $^{239,240}$Pu) (section 2.6). Sediment (~1.3 g) from each sample from the Irish Sea mud-patch and Ravenglass saltmarsh was ashed in a Carbolite 201 furnace at 550 °C for 8 hours to remove any organics present in the sediment matrix. The ashed sample (1.0 g) was leached in *aqua regia*

(3:2 v/v cHCl; $cHNO_3$) for 3 hours to induce partial dissolution of the radionuclides from the sediment matrix. Solids were then filtered (Whatman GF/A; 0.22 μm) and rinsed with 3 M $HNO_3$. The filtrate was made up to 30 mL in 3 M $HNO_3$ ready to enter the column. An aliquot of $^{241}Pu$ (11.7 Bq/100μL) was added, as this was the yield monitor. Plutonium was then extracted from the sediment using the TEVA® separation as discussed in section 2.6.1. The extracted Pu fraction was then ready for liquid scintillation counting.

### 2.7.1. Liquid Scintillation Counting (LSC)

Liquid scintillation counting is commonly used to detect low energy radioisotopes, mostly α and β-emitting isotopes. The technique requires the radioactive sample to be dissolved in a scintillation cocktail which is comprised of a large majority of solvent (60–99 %), along with molecules of phosphor (National Diagnostics, 2004). The role of the solvent is to absorb energy, whilst the dissolved phosphor converts the absorbed energy into light. Alpha and beta (β) particles directly ionise phosphor atoms, adding or removing electrons, and photons are emitted as a result in the de-excitation process. These photons are consequently detected by a pair of photomultiplier tubes located on either side of the sample vial in the scintillation counter. The signals are passed through a pre-amplifier, an amplifier, and finally to a coincidence circuit (Horrocks, 1974). The coincidence circuit only allows the event to be registered when the pulses occur in both photomultiplier tubes simultaneously (the pulses are ~15 ns). This system reduces the background noise and allows a greater instrumental sensitivity. This allows a liquid scintillation counter to count the absolute number of decay events taking place within a sample, resulting in a high efficiency (~100 % for certain isotopes).

Certain instruments, such as the Quantulus ultra low background LSC are able to distinguish between α and β events using a Pulse Shape Analyser (PSA) circuit (Passo and Cook, 1994). The PSA is used to differentiate between α and β-scintillation events, as true β events have a short scintillation in comparison to a longer, delayed α- scintillation event. In this project, LSC was used to determine the activity of $^{241}Pu$ in sediment samples, and to monitor the activity of $^{239}Np$ leached from $^{243}Am$ (see section 2.9).

Two methods were hypothesised for the determination of β-emitting $^{241}$Pu; (i) stripping of the α-planchette used to detect $^{238}$Pu, $^{239,240}$Pu into solution, and count this on the LSC; or (ii) use TEVA® resin to separate Pu, and use the Pu-α: Pu-β ratio obtained from LSC to determine Pu-β. The second method was chosen to quantify $^{241}$Pu as there was uncertainty regarding the recovery of the first method. The actual Pu-α activity for each of the sediment samples was known (due to the addition of a $^{242}$Pu tracer during $^{238}$Pu, and $^{239,240}$Pu analysis (see section 2.6). Thus, as LSC can distinguish between Pu-α and Pu-β counts, this ratio was used in combination with the total Pu-α activity from α-spectroscopy to determine the $^{241}$Pu-activity.

The eluted Pu fraction was evaporated down with a heat lamp, and taken up in 2 % HCl (2 mL). This solution was then transferred to a plastic scintillation vial (20 mL), and Hi-safe Optiphase scintillation cocktail (10 mL) added to the vial. The samples were inverted twice to allow the cocktail and sample to mix and the samples were then stored in darkness for 24 hours to avoid chemiluminescence. Ravenglass saltmarsh samples were counted for 4 hours and Irish Sea mud-patch for 8 hours on a Quantulus 1220 (Wallac, Perkin-Elmer) to ensure collection of adequate counts. Thereafter, once data acquisition of the α and β peaks had taken place, the addition of a known activity of internal standard was used to determine the counting efficiency. Here, a $^{241}$Pu tracer (100 µL; 10 Bq) was added to each scintillation vial and inverted twice. The vial was then counted on the Quantulus 1220 (Wallac, Perkin-Elmer) for 1 hour. Errors for $^{241}$Pu activity were determined using an integrated errors approach (Equation 2.5).

$$\frac{[{\sigma_{eff}}^2 + {\sigma_{Pu-beta}}^2 + {\sigma_{Pu-alpha}}^2 + {\sigma_{Pu-alphaspec}}^2]}{2}$$

**(**Equation 2.5**)**

$\sigma_{eff}^2$ = error in counts of $^{241}$Pu before and after yield tracer addition

$\sigma_{Pu\text{-}\beta}$ = error associated with Pu- β counts

$\sigma_{Pu\text{-}\beta}$ = error associated with Pu- α counts

$\sigma_{Pu\text{-}alphaspec}$ = error associated with the total-α activity (from α-spectroscopy data)

An increasing inventory of $^{241}$Am is produced from $^{241}$Pu ($t_{1/2}$ = 14.7 years) ingrowth, due to its short half-life. As a result, the amount of $^{241}$Am produced from the decay of $^{241}$Pu was determined using Equation 2.6 (modified from Day and Cross (1981)). The concentration of $^{241}$Pu determined was decay corrected to the hypothesised date of deposition (using an average sediment accumulation rate of 0.68 cm/yr) prior to decay (Equation 2.6). Thereafter the decay corrected $[^{241}Pu]_t$ was used to determine the ingrowth of $[^{241}Am]_t$ (Equation 2.7)

$$[^{241}Pu]_0 = exp\left(ln\,(2)\,x\,\frac{t}{T_{Pu}}\right)$$

(Equation 2.6)

$$[^{241}Am]_t = [^{241}Am] \times \frac{T_{Pu}}{(T_{Am} - T_{Pu})}\,exp\left(\frac{t\,ln\,(2)}{T_{Am}}\right) - exp\left(\frac{t\,ln\,(2)}{T_{Pu}}\right)$$

(Equation 2.7)

$[^{241}Pu]_0/[^{241}Am]_0$ = Activity of $^{241}$Pu/$^{241}$Am prior to decay

$[^{241}Am]_t$ = Activity of $^{241}$Am from the decay of $^{241}$Pu

t = Time period between hypothesised deposition date to surface date (2014)

$T_{Pu}$ = half-life of $^{241}$Pu (14.6 years)

$T_{Am}$ = half-life of $^{241}$Am (432.2 years)

## 2.8. Uranium Analysis ($^{236}$U)

Extraction chromatography was used to determine the concentration of $^{236}$U in Ravenglass saltmarsh samples. Here, the resin UTEVA® was utilised to extract uranium from the dissolved sediment matrix. A discussion of the UTEVA® resin can be found in section 2.6.1.

The activity of ultra-trace $^{236}$U was determined *via* extraction chromatography (Eichrom Technologies, 2005), similar to the method utilised by (Al-Qasmi et al., 2016). Ravenglass saltmarsh sediment (2.0 g) was ashed at 500 °C for 5 hours and

spiked with $^{233}U$ yield tracer (300 µL; 4.8 mBq/mL). The sample was then boiled with *aqua regia*, (3:2, v/v cHCl:c$HNO_3$) for 2 hrs, and the resulting solution filtered (Whatman GF/A; 0.22 µm). The sediment residue was then rinsed with deionised water, and the filtrate evaporated to near-dryness. The dried residue was dissolved in 3 M $HNO_3$ (30 mL). Then, UTEVA® resin (Eichrom; 2 mL; 100–150 mesh) was preconditioned with 3 M $HNO_3$ (5 mL), and the sample (30 mL) passed through the column. The sample was washed through with 3 M $HNO_3$ (5 mL), 9 M HCl (20 mL), and 5 M HCl/0.05 M oxalic acid (20 mL). All these eluates were discarded, and thereafter U was eluted with 1 M HCl (15 mL), to a beaker containing carrier solution (10 % w/v $KHSO_4$; 1 mL).

The U samples were prepared for Accelerator Mass Spectrometry (AMS) based on the method by Marsden et al. (2001) and Al-Qasmi et al. (2006). The U fraction (15 mL) was reduced to (~3 mL), and Fe(III) nitrate nonahydrate in 0.1 M HCl (1 mL; 5 mg Fe/mL) added. This was evaporated to dryness, and the residue was dissolved in 1 M $HNO_3$ (15 ml) to remove any residual chlorides. This was evaporated to dryness and baked for ~1 hour at ~250 °C to convert the $Fe(NO)_3$ into $Fe_2O_3$.. The oxide residue was then placed in a Carbolite 201 furnace at 450 °C for 8 hr to ensure the conversion to Fe oxide. The U oxide (0.1 g) was mixed with Al powder (1 mg) and the mixture pressed into the small pit of an Al sample holder.

### 2.8.1. Accelerator Mass Spectrometry (AMS)

Accelerator Mass Spectrometry (AMS) is an ultra-sensitive technique capable of detecting atoms present at very low-levels of sensitivity in the environment. Here, the key difference between traditional Mass Spectrometry and AMS is the energy of the ions accelerated; in MS the energies are thousands of electron volts (1 keV = $1.6 \times 10^{-16}$ J) whilst these are amplified to millions of electron volts (MeV) in AMS (Tuniz et al., 1998). This high energy is achieved by using linear accelerators, designed for nuclear physics research, and results in the better detection of atomic and molecular ions with the same mass. AMS systems are now capable of detecting isotopic ratios for specific elements down to 1 in $10^{15}$ (~ parts per quadrillion level), with sample sizes of < 1 mg being used to achieve this selectivity (Tuniz et al., 1998).

At the Australian National University AMS facility, the sample of interest was firstly bombarded by a focused $Cs^+$ beam (~ 10 keV), which ejected secondary charged ions from the surface of the sample by a process known as sputtering. A series of focusing lens and magnets then guided the mass analysed beam into the accelerator (Fifield et al., 1994). A Heavy Ion accelerator (14UD) was then used to speed up the analyte ions to 10 % of the speed of light. Here, a Van De Graff accelerator is housed in a 40 m concrete and steel framework. Negative ions were injected into the top of the accelerator, and were drawn towards the positive terminal (half-way down the accelerator). These speeding ions passed through a thin carbon foil which removes electrons, resulting in a positively charged atom, which is quickly repelled to the bottom of the Van De Graff accelerator (Tuniz et al., 1998). The beam of ions that leave the accelerator are then steered by magnets into specific beamlines. Ions that are not of interest after scattering are identified and rejected by a detector (Tuniz et al., 1998); this improves the detection limit of many isotopes in comparison to conventional Secondary Ion Mass Spectroscopy (SIMS).

At the AMS facility, the U samples were loaded onto the 32-sample wheel, inserted into the ion source of the AMS, and sequentially sputtered and analysed. The $^{236}U$: $^{238}U$ ratio was determined using a 14UD pelletron accelerator at the Australian National University. The detection system is based on a combined high-resolution velocity measurement by time-of-flight and energy measurements (see Fifield, 2008; Fifield et al., 2013). In addition, $^{236}U$:$^{234}U$ and $^{234}U$:$^{238}U$ ratios were measured using AMS, and calibrated for yield errors from the $^{233}U$ peak.

### 2.9. Neptunium Analysis ($^{237}Np$)

The experimental procedure developed by Zhao et al. (2014) was adapted for use in this project to determine the activity of $^{237}Np$ in Ravenglass saltmarsh sediments. This was carried out at the Glenn T. Seaborg institute at the Lawrence Livermore National Laboratory. Perfluoroalkoxy (PFA) jars (Savillex) were thoroughly cleaned with boiling 5 % $HNO_3$ and 18.2 MΩ DI water.

A $^{239}Np$ ($t_{1/2}$ = 2.36 days; 50–100 Bq/mL) yield tracer solution was used to monitor the loss of $^{237}Np$ during the experimental procedure. The $^{243}Am$ ($t_{1/2}$ = 7370 years) stock solution used in this method was produced from the

transformation of five successive neutron captures of $^{238}U$ during the irradiation of nuclear fuel (Zhao et al., 2014), whilst the α-decay of $^{243}Am$ generates the desirable $^{239}Np$ tracer. Additionally, the stock solution contains $^{241}Am$ as a contaminant, the decay of which produces $^{237}Np$, the analyte of interest. The long half-life of $^{237}Np$ ($t_{1/2}$ = 2.14 million years) results in its accumulation in the stock solution, whilst $^{239}Np$ reaches a secular equilibrium with $^{243}Am$ after two weeks. As a result the $^{237}Np/^{239}Np$ ratio increases with time. The first stage of the experiment involved purifying the long-lived $^{243}Am$ parent to limit the presence of $^{237}Np$ in the $^{239}Np$ tracer.

### 2.9.1. Column 1 and 2: $^{243}$Am Purification

The $^{243}Am$ stock solution was purified by removing both Np isotopes using two cycles of AG®1-X8 ion exchange resin (Bio-Rad laboratory; 2 mL; 50–100 mesh). A few drops of c$HNO_3$ were added to the $^{243}Am$ stock (20–30 kBq), this was then taken down to almost dryness and re-dissolved in cHCl + HI (50:1 v/v) (~ 1 mL). The solution was warmed in a closed jar on the hotplate for 10–20 minutes to adjust the Np oxidation state to Np(IV), and placed aside to cool. A column was made from a 1 mL disposable pipette plugged with a porous frit, and packed with AG®1-X8 ion exchange resin (Bio rad laboratory; 2 mL; 50–100 mesh). This was preconditioned with deionised water 18.2 MΩ (1 mL) followed by cHCl + HI (50:1 v/v) (1 mL). The $^{243}Am$ stock was loaded onto the column, as well as two rinses of the vial with cHCl + HI (50:1 v/v) (2 x 0.5 mL) to collect any residual $^{243}Am$ stock solution. The Np(IV) was retained onto the column whilst $^{243}Am(III)$ was eluted from the column with 5 x 1 mL of cHCl + HI (50:1 v/v), followed by 2–3 mL of cHCl and collected in a pre-weighed 15 mL PFA vial. An aliquot (2 µL) of the $^{243}Am$ eluent was added to Ultima Gold™ scintillation cocktail (Perkin Elmer; 7 mL). For the majority of the samples this was counted on a TriCarb 2900TR (Perkin Elmer) Liqud Scintillation Analyser. Here, the protocol was adjusted to achieve a maximal separation of α and β counts (no α/β discrimination). However due to circumstances beyond control, a small sample set was counted on a Quantulus 1220 (Wallac, Perkin-Elmer) LSC using α/β discrimination at PSA level of 80 (see section 2.7.1 for PSA discussion). The counts present in the α-region were used to determine $^{243}Am$ activity, and those in the β–region for $^{239}Np$. Then, 0.1 M + 0.05 M HF (6 x 1 mL)

was added to the column, and allowed to pass through to collect the $^{239}$Np fraction. An aliquot (2 µL) of the $^{239}$Np elutant was added to Ultima Gold™ scintillation cocktail (7 mL) and counted on the TriCarb 2900TR (Perkin Elmer) Liquid Scintillation Analyser to check the activity of $^{239}$Np.

For background correction, Ultima Gold™ scintillation cocktail was used as a blank (7 mL) in each LSC measurement. The activities of $^{239}$Np and $^{243}$Am were determined to monitor the successful separation of the two fractions, and to check for unexpected activity loss on the column for reasons of mass balance and waste activity estimation. The eluted $^{243}$Am fraction was heated to almost dryness again, and then re-dissolved in ~1 mL cHCl + HI (50:1 v/v) for a second purification step using a fresh AG®1-X8 ion exchange resin column (50–100 mesh) following the method discussed above. Samples from the first set were counted on the Quantulus 1220 (Wallac, Perkin-Elmer) LSC using α/β discrimination at PSA level of 28, with the majority of the samples counted on the TriCarb 2900TR (Perkin Elmer) Liquid Scintillation Analyser. The $^{237/239}$Np fraction was discarded. The purified $^{243}$Am fraction from column 2 was then used for columns 3 and 4.

### 2.9.2. Column 3 and 4: $^{239}$Np Milking

The purified $^{243}$Am fraction was left aside for 2–3 days prior to starting column 3 to allow the ingrowth of short-lived $^{239}$Np, and limit the undesirable ingrowth of $^{237}$Np. Thereafter, the $^{243}$Am stock solution (~7 mL) was evaporated to reduce its volume to ~1 mL. The separation of the Am fraction from the Np fraction, and the LSC analysis for column 3 were conducted as described for column 1 and 2 (see above). The $^{243}$Am fraction was stored for future applications. The $^{239}$Np fraction was taken to dryness after addition of a few drops of c$HNO_3$ to remove HF. Next, a few drops of cHCl were added, and the $^{239}$Np fraction was again evaporated to almost dryness. The remaining drop was then taken up in cHCl + HI (50:1 v/v) (~1 mL) and the solution was warmed up for 10 minutes to adjust the Np oxidation state to Np(IV). The $^{239}$Np solution was purified in column 4 and the fractions were collected and analysed with LSC following the procedure described for column 1. The $^{243}$Am fraction contained almost no $^{243}$Am. The $^{239}$Np fraction contained the activity of $^{239}$Np available as a spike for one set of

samples. A few drops of $cHNO_3$ were added to the $^{239}Np$ fraction and the solution was evaporated to dryness. This process was repeated twice. The final drop was taken up in 2 % $HNO_3$ (volume dependant on number of samples, 1 mL per sample, including one procedure blank and two reference samples for γ–spectroscopy).

### 2.9.3. Column 5: Removal of Sample Impurities

Ravenglass sediment samples (1.3 g) were ashed at 550 °C for 8 hours. Each sediment sample (1 g) was then leached with *aqua regia* (3:2 v/v cHCl:$cHNO_3$; 30 mL) at ~150 °C, and filtered (Whatman GF/A; 0.22 µm), and made up to a stock solution in 9 M HCl (30 mL). An aliquot (10 mL) of this stock solution was added to a 15 mL PFA vial, and spiked with 50–100 Bq of the freshly prepared $^{239}Np$ tracer (1 mL). This was taken to dryness, and the resulting residue suspended in cHCl (~2 mL). As the samples contained a lot of salts and minerals, each suspension was transferred to a 15 mL centrifuge tube and centrifuged (3 minutes at 4000 rpm; 1431 *g*). Each supernatant was transferred into a new 15 mL PFA vial. Each sample residue was rinsed three times with cHCl (3 x 1 mL), centrifuged and all rinse supernatants were added to the new sample vial. Next, HI (100 µL) was added to the solution (5 mL) in the new vial (forming conc. HCl + HI (50:1 v/v)). The cap was closed on each vial, and the solutions were warmed for 10 mins to reduce Np(V) to Np(IV). An AG®1-X8 resin column (Bio Rad laboratory; 100–200 mesh) was prepared in a 2 mL poly-prep column (Bio Rad laboratories) for each sample. Each one was preconditioned with de-ionised water (2 + 4 + 4 mL). Then, cHCl (2 + 2 mL) was passed through, followed by cHCl + HI (50:1 v/v) (2 + 2 + 2 mL). Next, the sample was loaded onto the column, and the vial rinsed twice with cHCl + HI (50:1 v/v) (2 x 1 mL). Each sample was transferred through the column by adding cHCl + HI (50:1 v/v) (2 + 4 + 4 mL). Any tetravalent Np and U remained on the resin, whilst trivalent Pu and any other impurities passed through the column. The Np fractions were then eluted with 0.1 M HCl + 0.05 M HF, with the majority of U assumed to be retained on the column (Zhao et al., 2014). Then, $cHNO_3$ (~1 mL) was added to each vial and the samples were slowly evaporated overnight.

### 2.9.4. Column 6: Removal of $^{238}U$

Nu Plasma High Resolution Multi-Collector Inductively Coupled Mass Spectrometry (HR MC ICP-MS) is able to tolerate low ppb levels of $^{238}U$. However, to prevent tailing of the $^{238}U$ peak into the peak of the analyte of interest ($^{237}Np$) an additional purification step was used to lower the amount of $^{238}U$ in each sample.

The sample residues were dissolved 2–3 times in 2 M $HNO_3$ (1 mL) and evaporated to dryness (to oxidise Np to Np(V)). During the final repeat, the solution was evaporated down to a small drop. This was taken up in 4 M $HNO_3$ (1 mL). A column bed of 0.2 mL UTEVA® resin (Eichrom Industries; 50–100 mesh ) was prepared in a disposable pipette plugged with a porous frit for each sample, and was preconditioned with 4 M $HNO_3$ (4 x 0.2 mL). A clean pre-weighed 15 mL PFA vial was placed under each column. The sample was then added to the column and the two vial rinses with 4 M $HNO_3$ (2 x 0.2 mL). The sample was eluted with 4 M $HNO_3$ (5 x 0.2 mL). Uranium was retained on the UTEVA® resin whilst was Np(V) passed through the column. The collected Np-containing effluent was evaporated, and the resulting residue was taken up in c$HNO_3$, and evaporated down to a small drop. This was then dissolved in 2 % $HNO_3$ (2 mL).

The samples were ready for analysis on the Nu Plasma HR Multi-Collector ICP-MS after ~2 weeks (6 half-lives) to allow the decay of short-lived $^{239}Np$. Prior to this, the $^{239}Np$ yield of each purified sample was determined *via* γ-spectroscopy (Canberra, Broad Energy Ge detector) using the γ-emission line at 277 keV. Two samples were prepared for each sample set as $^{239}Np$ reference samples. They represented 100 % yield and contained ~1 mL of the freshly prepared $^{239}Np$ spike and 1 mL of 2 % $HNO_3$. The $^{239}Np$ activity in the purified samples (after column 6) was measured by γ-spectroscopy, and compared with activities in the reference samples to determine the chemical yield during purification. Typically, Np recovery yields ranged between 20 to 90 %.

### 2.9.5. High Resolution Multi-Collector-Inductively Coupled Plasma-Mass Spectrometry (HR-MC-ICP-MS)

High Resolution Multi-Collector Inductively Coupled Plasma Mass Spectrometry (HR MC-IC-PMS) is able to combine the ionisation efficiency of an ICP ion

source with the detection capacity of a magnetic sector mass spectrometer. The technique is able to measure precise isotope ratios down to low ppt concentration. A Nu Plasma HR Multi-Collector ICP-MS instrument at the Glenn T. Seaborg Institute (Lawrence Livermore National Laboratory) was used in this project to quantify the $^{237}$Np activity in Ravenglass saltmarsh sediments (Figure 2.4).

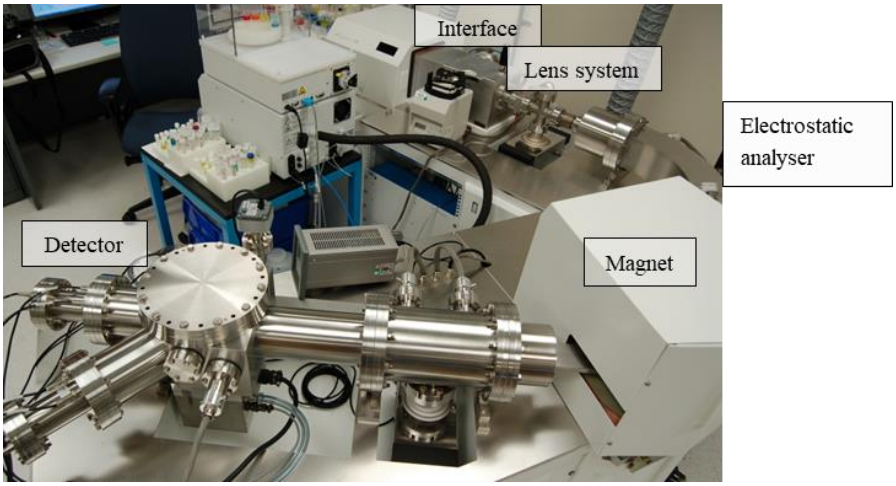


**Figure 2.4.** Key components of the NuPlasma High Resolution MC-ICPMS at the Glenn T Seaborg Institute, LLNL, USA.

Here, the sample was pumped into the heated Aridus II desolvating nebuliser, to dry the sample. Then small droplets of sample were delivered by a flow of plasma gas (Ar) and $N_2$ to the plasma torch ready for ionisation at temperatures reaching 10,000 K. These ions were accelerated across an electrical potential gradient. A range of slits focussed these particles into a beam. The ion beam passed through an energy filter generating a consistent energy spectrum. A magnetic sector field was used as a mass spectrometer able to separate and filter ions of different *m/z* to a high precision. Thus, lighter ions will be deflected more by the magnetic field than heavier ions, allowing for effective separation. The mass-resolved beams were directed to multiple collectors (9 Faraday collectors, and 4 electron multipliers (ion counters). The $^{237}$Np concentration was collected on the ion counter which detects ions for voltages < 10 mV. The data was collected during 20 second integration cycles. Standards (ranging between 0.01–10 ppt) were

made using in-house $^{237}$Np and NIST traceable SRM 4341 $^{237}$Np standard solutions, with 2 % $HNO_3$. These solutions were measured on the HR-MC-ICP-MS before and after the measurement of the Ravenglass samples. The error was determined by analysing a sub-set as duplicates, and these showed a 2σ error of 11.68 %.

### 2.10. Technetium Analysis ($^{99}$Tc)

The activity of $^{99}$Tc in a Ravenglass sediment core was determined using a procedure adapted from Keith-Roach et al. (2003). Sediment samples (1.5 g) were wet-ashed (as Tc is volatile and so cannot be ashed in the furnace) with *aqua regia* (3:2 v/v cHCl: c$HNO_3$). Solids were filtered (Whatman GF/A; 0.22 µm), and the filtrate evaporated to near-dryness, and then taken up in 8 M $HNO_3$ (20 mL). A $^{99m}$Tc master stock (140 MBq; 1 mL) was transported using a designated route in a lead lined Class A container from the Radiopharmacy Department of the Manchester Royal Infirmary to the Centre of Radiochemistry Research, and placed behind a lead castle at the back of the fumehood. Behind lead shielding, and using shielded pipettes, the master stock was diluted to 2.5 mL using 0.1 M $HNO_3$.

#### 2.10.1. Column 1: $^{99m}$Tc Cleaning

A TEVA® column (Eichrom; 2 mL, 100-150 mesh) was pre-conditioned with 0.1 M $HNO_3$ (10 mL). The dilute $^{99m}$Tc ($t_{1/2}$ = 6.02 hrs) master stock (2.5 mL) was then passed through the column to remove traces of NaCl, Ru, and Mo. The column was washed with 2 M $HNO_3$ (10 mL) to remove any impurities. Then, $^{99m}$Tc was eluted with 8 M $HNO_3$ (5 mL) into a HDPE Nalgene vial (30 mL) and this was the cleaned $^{99m}$Tc master-stock used in future work

#### 2.10.2. Column 2: $^{99}$Tc Extraction

$^{99m}$Tc yield monitor (20 kBq per sample; 183 µL) was added to the sample filtrates (20 mL) (from section 2.10.1). In addition, 3 x 20 kBq $^{99m}$Tc reference samples were made to 5 mL 2% $HNO_3$ in HDPE Nalgene (30 mL) plastic vials, The samples and references were counted three times on the Canberra HP(Ge) DSPEC-50 γ-spectrometer (as $^{99m}$Tc has a γ-emission at 141 keV with a $t_{1/2}$ of 6.01 hours), and this was regarded as T=0.

Saturated NaOH (~ 7 mL) was added to precipitate $Mg(OH)_2$ (to remove any components likely to precipitate). This solution was centrifuged (5 minutes at 2500 rpm; 559 *g*), and then filtered (Whatman GF/A; 0.22 µm). The resulting filtrate was then acidified to pH 6 (using a few drops of 0.1–1M $HNO_3$) to prevent any further precipitation, and centrifuged (5 minutes at 2500 rpm; 559 *g*). A TEVA® spec column (Eichrom; 2 mL, 100–150 mesh) was pre-conditioned with 2 M $HNO_3$ (15 mL), followed by the sample supernatant. The column was further washed with 2 M $HNO_3$ (40 mL), to remove any traces of Ru and Mo. The effluent was collected, sealed, and decay stored. Next $^{99}$Tc was eluted in 8 M $HNO_3$ (10 mL) into HDPE Nalgene (30 mL) vial. This was transferred to the Canberra HP(Ge) DSPEC-50 γ-spectrometer. The 3 x 20 kBq reference samples were made up to 10 mL with 8 M $HNO_3$, and counted on the Canberra HP(Ge) DSPEC-50 γ-spectrometer to determine the recovery of the $^{99m}$Tc. The samples were then transferred to PYREX glass beakers (100 mL), and evaporated down to near dryness using a heat-lamp. Each sample was made to 2.5 mL using 100 µL of 1 M $NH_3OH$ (to ensure complete dissolution of the sample), and balanced with 2 % $HNO_3$. The sample was left to stand for a minimum of 28 half-lives, to lower the activity (< 0.4 Bq/ mL) for $^{99}$Tc analysis on the Agilent 7500cx ICP-MS. A range of in house standards were made using a $^{99}$Tc stock solution (10 kBq/mL), and ranged between 0–300 ppt $^{99}$Tc standards, which were counted between each run on the ICP-MS.

### 2.11. Sequential Extraction ($^{241}$Am, $^{137}$Cs, Fe, and Mn)

In this project, sequential extraction experiments were used to study the binding interaction of $^{241}$Am, $^{137}$Cs and $^{239,240}$Pu with solid phases at the Irish Sea mud-patch and Ravenglass saltmarsh. This technique is based on an established extraction procedure (Tessier et al., 1979), amended for radionuclide analysis (Begg et al., 2011). Here, four fractions (exchangeable, reducible, oxidisable and residual) were targeted using reagents of increasing strength to determine the phases that were dominantly hosting $^{241}$Am, $^{137}$Cs and $^{239,240}$Pu. In addition, Fe and Mn association with these environmental phases was also investigated.

#### 2.11.1. Exchangeable Fraction

The exchangeable fraction includes metals that are adsorbed on solid surfaces by weak electrostatic interactions. Metals released *via* ion-exchange processes are most readily available, and are targeted in this fraction. To extract the exchangeable fraction from the sediment system sediment (1.0 g) was placed into a centrifuge tube (50 mL) and 1 M $MgCl_2$ (pH 7, 15 mL) was added. The samples were then shaken at room temperature on the orbital shaker for 2 hours. Next, they were centrifuged (10 minutes at 4500 rpm; 1186 *g*), and the supernatant divided for γ-analysis (10 mL), and ICP-AES analysis (2 mL), and the final few mL discarded. The sediment samples were then rinsed with de-ionised water (18.2 MΩ; 8 mL), and centrifuged (10 minutes at 4500 rpm; 1186 *g*). The supernatant was discarded, and the sediment residue transferred to the next step.

### 2.11.2. Reducible Fraction

The reducible fraction focuses on radionuclides that are associated with Fe and Mn oxides. This step also liberates any metals re-adsorbed during the exchangeable fraction (as a result of the low pH), and extracted radionuclides by targeting the dissolution of Fe and Mn oxides *via* a photo-electrochemical reduction process. In this project, 0.1 M $(NH_4)_2C_2O_4$ (pH 3, 15 ml) was added to the residue from the exchangeable fraction. This was allowed to shake at room temperature on the orbital shaker (17 hours), and the samples centrifuged thereafter (10 minutes at 4500 rpm; 1186 *g*). The supernatant was then divided for γ-analysis (10 mL), and ICP-AES analysis (2 mL), with the final few mL discarded. The sediment samples were then rinsed with de-ionised water (18.2 MΩ; 8 mL) by centrifugation (10 minutes at 4500 rpm; 1186 *g*). The supernatant was discarded, and the sediment residue transferred to the next step.

### 2.11.3. Oxidisable Fraction

The oxidisable fraction includes the radionuclides bound to organic matter, including coatings on mineral particles and detritus. The onset of oxidising conditions, can cause organic matter to degrade and release soluble trace metals (Tessier et al., 1979). Treatment with $H_2O_2$ results in the oxidation of sulfides and organic material *via* a radical-chain mechanism. The lixivant 30 % $H_2O_2$ (pH 3, 10 mL) was added to the residue from section 2.11.2 and heated (80 °C) until complete dryness in a sand bath (24 hours). The dried sediment was then leached

with 1 M $CH_3CO_2NH_4$ (6 % v/v $HNO_3$ (pH 2, 15 mL) at room temperature on the orbital shaker (6 hours). This step aims to isolate all the metals liberated during oxidation, as the metals liberated by $H_2O_2$ treatment have a tendency to re-absorb onto Fe and Mn (oxy)hydroxides. The samples were then removed from the orbital shaker and centrifuged (10 minutes at 4500 rpm; 1186 *g*). The supernatant was again divided for γ-analysis (10 mL), and ICP-AES analysis (2 mL), with the final few mL discarded. The sediment samples were then rinsed with deionised water (18.2 MΩ; 8 mL), and centrifuged (10 minutes at 4500 rpm; 1186 *g*). The supernatant was discarded, and the sediment residue transferred to the next step.

### 2.11.4. Residual Fraction

The residual fraction partially digests the sediment, and extracts any remaining metals or elements into solution. This is the most aggressive lixivant used in the sequential extraction procedure, and attacks any primary and secondary minerals (Tessier et al., 1979) that may have radionuclides completely associated with the crystalline lattice of sediment grains. The residue from section 2.11.3 was transferred to a glass beaker (25 mL) and leached in *aqua regia* (3:2 v/v cHCl: $cHNO_3$) for 3 hours in a sand bath (80 °C). The solution was then transferred into a new beaker (50 mL) and evaporated down to incipient dryness. The solutions were then taken up in 3 M $HNO_3$ (15 mL). The supernatant was then divided for γ-analysis (10 mL), and ICP-AES analysis (2 mL), with the final few mL discarded. The sediment residue was also discarded.

The γ-leachate from each extraction step (10 mL) was counted on the Canberra HP(Ge) DSPEC-50 γ-spectrometer for 24hrs, and the activity of $^{241}Am$ and $^{137}Cs$ determined from the characteristic γ-ray emission at 59.5 keV and 661.6 keV, respectively. The detector efficiency was calibrated using matrix-matched standards (of the same geometry) spiked with certified standard solutions of $^{241}Am$ (100 Bq) and $^{137}Cs$ (100 Bq) (Amersham International). The resulting spectra were also corrected for background noise. Triplicate data carried out showed a variance of ~20 % at 1 standard deviation for $^{137}Cs$ and ~ 12 % at 1 standard deviation for $^{241}Am$.

## 2.12. Sequential Extraction ($^{239,240}$Pu)

The procedure highlighted in section 2.11 was modified for $^{239,240}$Pu analysis. Here, the supernatant from each extraction step was taken to dryness in a PYREX glass beaker (100 mL), and boiled with *aqua regia* (3:2 v/v cHCl:c$HNO_3$) for 2 hrs to eliminate any traces of residual lixivant. This was then filtered (Whatman GF/A; 0.22 µm), and the filtrate evaporated to near-dryness. This was taken up in 3M $HNO_3$ (5 mL), and spiked with $^{242}$Pu tracer (0.075 Bq/100 µL), and evaporated to dryness. This was then taken up in 3 M $HNO_3$ (15 mL), and analysed by TEVA resin, electrodeposition, and α-spectroscopy (see section 2.6 for further detail).

## 2.13. Mathematical Model

A FORTRAN transport model utilised by Marsden et al. (2006) was used here to predict the distrubution profile for $^{239,240}$Pu at the Irish Sea mud-patch and Ravenglass saltmarsh. The predicted profile was compared with recent experimental $^{239.240}$Pu measurements from the mud-patch and saltmarsh sites. The $^{239,240}$Pu activities obtained for the Irish Sea mud-patch and Ravenglass saltmarsh were used here, alongside $^{239,240}$Pu activities for a longer gravity core (up to 1.5 m) for the the same Irish Sea mud-patch site (see Ray et al., 2018; Chapter 3).

The model is described fully in Marsden et al. (2006) but in summary, it is based on the assumption that a simple diffusion process can be used to simulate the effects of bioturbation within the Irish Sea mud-patch. The Sellafield discharge history for $^{239,240}$Pu acts as the input to the model. The Sellafield authorised discharge data is published as the total activity for a range of radionuclides per year, and this was interpolated for each model time step (10 per year). The model considers a 1-dimensional column of 150 cells, each with a thickness of 1 cm, which represents the upper 1.5 m of the mud-patch. At the start of the simulation (representing the first year that discharge data is available, 1952), the column is free of contamination. At each time step, the discharged activity enters the top of the column and diffusion occurs between all adjacent model cells, according to Fick's law of diffusion. This results in a net migration of radioactivity down the column with time. To represent bioturbation, the diffusion coefficient was constant for the top 10 cm, followed by a linear decrease to 0 at 150 cm. It is

important to note that this may be an over simplification of the model as the trend highlighted above has been developed based on the behaviour and feeding modes of *Maximuelleria lankestri*, which have been suggested to have the most dominant effect on the Irish-Sea mud-patch [insert Kershaw ref]. However, there may also be other benthic fauna which the behave in a dissimilar manner to the *Maximuelleria lankestri*.

In this work, the model was run to simulate the evolving mud-patch profile between 1952 and 2014 (the date of the most recent core sample), in order to make comparisons with latest experimental data. It should be noted that the model considers an 'average' location within the mud-patch and does not account for any lateral variability in observed activity profiles. Additionally, it is scalar or relative in nature, since it is not possible to calculate the fraction of the discharged activity that would be deposited on a particular section of the mud-patch. It does not account for any radioactive decay or in-growth. The model is also used to make predictions about the accumulation of resuspended activity deposited through tidal inundations at the Ravenglass saltmarsh. This was achieved by averaging the predicted activity in the top several cm of the mud-patch and assuming that this sediment is subject to continuous resuspension and subsequent deposition at the saltmarsh. However, the model does not explicitly simulate this resuspension and the material is not removed from the simulated column of sediment. Rather, the predicted profile of the Ravenglass saltmarsh is a reflection of the top several cm of the mud-patch column with time. It is important to note that the model assumes that sediment input is solely from the mud-patch, however in reality there will also be direct, continuous longshore transport from the Sellafield pipeline.

There are two uncertain parameters associated with the model: (i) diffusion coefficient ($D_z$); and (ii) resuspension depth (d). For this work two diffusion coeffcients ($9.5 \times 10^{-8}$ $cm^2/s$) used by Marsden et al. (2006), and $9.5 \times 10^{-7} cm^2/s$ were used to simulate the magnitude of bioturbation taking place at the Irish Sea mud-patch. A resupension depth of 5 cm was used for this work, as this was shown by Marsden et al. (2006) to be an optimum value. Thus, the top 5 cm of

mud-patch surface material was used to calculate the activity that would be transported to the Ravenglass saltmarsh for accumulation.

### 2.14. Thesis Analytical Strategy

Chapter 1 sets the scene for the thesis; the analytical methods utilised in this work focus on characterising the radionuclide and biogeochemical baseline for both the Irish Sea mud-patch and Ravenglass saltmarsh. A range of techniques utilised by previous authors e.g. Morris et al. (2000) and Marsden et al. (2006) for similar characterisations were used. Specifically, $^{241}$Am and $^{137}$Cs were quantified using gamma-spectroscopy as this requires minimal sample preparation with minimal data-processing. The alpha-emitters $^{238}$Pu and $^{239,240}$Pu were extracted using a TEVA resin based on the method by Nygren et al. (2003). This was followed by electrodeposition and alpha-spectroscopy as per in-house methods. The biogeochemical baseline in this chapter was determined using standard in-house XRF and ICP techniques. Novel microbial community for both sites was investigated using Ion Torrent methods. A simple, mathematical model was also used to build on the work of Marsden et al. (2006).

Chapter 2 builds on the results of chapter 1. Further, the radionuclides of interest in this chapter are $^{99}$Tc, $^{237}$Np and $^{236}$U and these are quantified at the Ravenglass saltmarsh site only (due to the difficult nature of the techniques utilised). Here, $^{99}$Tc was determined using the method by Keith Roach et al (2001) as it is a major contaminat in nuclear sites and also due to its high mobility as pertechnetate. The transuranics: $^{237}$Np and $^{236}$U are present in contaminated environmental systems in a trace levels and thus more difficult laboratory techniques are required for their detection. Neptunium-237 was extracted using the method of Zhao et al. 2014 and detected *via* HR-MC-ICPMS at Lawrence Livermore National Laboratory. Trace level $^{236}$U was quantified based on a method by Marsden et al. (2000) coupled with Kieth Fifield's expertise on Accelerator Mass Spectroscopy.

Chapter 3 investigates the geochemical association of $^{241}$Am, $^{137}$Cs, $^{239,240}$Pu, and Fe and Mn using the method of Tessier et al. (1979) and this was amended as per Begg et al. (2011). Here, the scheme identifies four types of radionuclide binding site, with a series of reagents exchanging/extracting the radionuclides from progressively stronger binding sites.

## References


Al-Qasmi, H., Law, G. T. W., Fifield, L. K., Livens, F. R., 2016. Origin of artificial radionuclides in soil and sediment from North Wales. J. Environ. Radioactiv. 151, 244–249.

Begg, J. D., Burke, I. T., Lloyd, J. R., Boothman, C., Shaw, S., Charnock, J. M., Morris, K. 2011. Bioreduction behavior of U(VI) sorbed to sediments. Geomicrobiol. J. 28, 160–171.

Biorad, 2000 AG ®1, AG MP-1 and AG 2 strong anion exchange resin. Instruction manual. Hercules. CA, USA

Broekaert, J. A. C. 2014. Inductively coupled plasma spectrometry: in Handbook of spectroscopy. Weinheim, Germany. 583–646.

Caporaso, J. G., Kuczynski, J., Stombaugh, J., Bittinger, K., Bushman, F. D., Costello, E. K., Fierer, N., Gonzalez Peña, A., Goodrich, J. K., Gordon, J. I., Huttley, G. A., Kelley, S. T., Knights, D., Koenig, J. E., Ley, R. E., Lozupone, C. A., 2010. QIIME allows analysis of high-throughput community sequencing data. Nat. Methods. 7(510), 335–336.

Clarke, K. R., Gorley, R., 2009. PRIMER: Getting started with v6. Plymouth Marine Laboratory

Day, J., Cross, J., 1981, $^{241}$Am from the decay of $^{241}$Pu in the Irish Sea. Nature, 292, 43–45.

Dean, J. R. 2005. Practical inductively coupled plasma spectroscopy. West Sussex. John Wiley and Sons. New Jersey, USA.

Eichrom Technologies, 2005. Uranium in soil (2 g sample). Analytical Procedures. ACS07. Rev. 1.5.

Fielder, H., Tench, O., 1971. Germanium (Li): Gamma spectrometer systems. Canberra Industries Inc.

Fifield, L. K., Allan, G., Stone, J. O., Ophel, T., 1994. The ANU AMS system and research program. Nucl. Instrum. Meth. B. 92. 85–88.

Fifield, L. K. 2008. Accelerator mass spectrometry of the actinides. Quat. Geochronol. 3, 276–290.

Fifield, L. K., Tims, S. G., Stone, J. O., Argento, D. C., De Cesare, M., 2013. Ultra-sensitive measurements of $^{36}$Cl and $^{236}$U at the Australian National University. Nucl. Instrum. Meth. B. 294, 126–131.

Gilmore, G. R. (2008) Practical Gamma-ray Spectrometry. 2nd edition. John Wiley & Sons. New Jersey, USA.

Hill, S. J. 2007. Inductively coupled plasma spectrometry and its applications. Blackwell publishing. Oxford, UK.

Horrocks, D. L. 1974. Applications of liquid ccintillation counting. Academic

Press. New York, USA.

Horwitz, D. 1996. Extraction chromatography of selected fission products: principles and achievement of selectivity: in International workshop application of extraction chromatography radionuclide measurement (HP199). 1–11.

Horwitz, E. P., Dietz, M. L., Chiarizia, R., Diamond, H., Maxwell, S. L., Nelson, M. R., 1995. Separation and preconcentration of actinides by extraction chromatography using a supported liquid anion exchanger: application to the characterization of high-level nuclear waste solutions. Anal. Chim. Acta. 310(1), 63–78.

Janssens, K. 2014. X-ray fluorescence analysis: in Handbook of spectroscopy. Weinheim, Germany. 449–506.

Keith-Roach, M. J., Morris, K., Dahlgaard, H., 2003. An investigation into technetium binding in sediments. Mar. Chem. 81, 149–162.

Kershaw, P.J., Pentreath, R.J., Woodhead, D.S., Hunt, G.J., 1992. A review of radioactivity in the Irish Sea, in: Aquatic Environmental Monitoring Report. Lowestoft, UK, MAFF Directorate of Fisheries Research. 32, 1–66.

De Laeter, J. 2001. Applications of inorganic mass spectrometry. John Wiley & Sons Inc. 467–479.

Lehto, J., Hou, X., 2010. Chemistry and analysis of radionuclides: laboratory techniques and methodology. Wiley-Vch.

MacKenzie, A., Scott, R., Allan, R. L., Ben Shaban, Y. A., Cook, G., Pulford, I. D., 1994. Sediment radionuclide profiles: implications for mechanisms of Sellafield waste dispersal in the Irish Sea. J. Environ. Radioactiv. 23, 39–69.

Marsden, O. J., Abrahamsen, L., Bryan, N. D., Day, P. J., Fifield, L. K, Gent, C., Goodall, P. S., Morris, K., Livens, F. R., 2006. Transport and accumulation of actinide elements in the near-shore environment: field and modelling studies. Sedimentology. 53(1), 237–248.

Marsden, O. J., Livens, F. R., Day, J. P., Fifield, L. K., Goodall, P. S., 2001. Determination of $^{236}U$ in sediment samples by accelerator mass spectrometry. Analyst, 126(5), 633–636.

National Diagnostics, 2004. Principles and applications of liquid scintillation counting: a primer for orientation. National Diagnostics. USA:

Nygren, U., Rodushkin, I., Nilsson, C., Baxter, D. C., 2003. Separation of plutonium from soil and sediment prior to determination by inductively coupled plasma mass spectrometry. J. Anal. Atom. Spectrom. 18(12), 1426–1434.

Passo, C., Cook, G., 1994. Handbook of environmental liquid scintillation spectrometry.Packard. Meriden, Conneticut, USA.

Quast, C., Pruesse, E., Yilmaz, P., Gerken, J., Schweer, T., Yarza, P., Peplies, J., Glöckner, F. O., 2012. The SILVA ribosomal RNA gene database project:

improved data processing and web-based tools. Nucleic. Acids. Res. 41, 591–596.

Rittersdorf, I. (2007) Gamma Ray Spectroscopy. Nuclear Engineering and Radiological Sciences. University of Michigan. USA.

Smith, H. A., Lucas, M., 1991. Gamma-ray detectors :in passive nondestructive assay of nuclear materials. US NRC. 43–64.

Sneddon, J., Vincent, M. D., 2008. ICP-OES and ICP-MS for the determination of metals: application to oysters. Anal. Let. 41(8), 1291–1303.

Tessier, A., Campbell, P. G. C., Bisson, M., 1979. Sequential extraction procedure for the speciation of particulate trace metals. Anal. Chem. 51(7), 844–851.

Tuniz, C., Bird, J. R., Fink, D., Herzog, G. F., 1998. Accelerator mass spectrometry: ultrasensitive analysis for global science. CRC Press. Florida, USA:

Zhao, P., Tinnacher, R. M., Zavarin, M., and Kersting,A B., 2014. Analysis of trace neptunium in the vicinity of underground nuclear tests at the Nevada National Security Site. J. Environ. Radioactiv. 137, 163–172.

# Chapter 3: Controls on Anthropogenic Radionuclide Distribution in the Sellafield-Impacted Eastern Irish Sea

This chapter is a manuscript submitted to the *Journal of Environmental Radioactivity*. Supporting Information is presented at the end of the manuscript.

# 3. Controls on Anthropogenic Radionuclide Distribution in the Sellafield-Impacted Eastern Irish Sea

Daisy Ray[1/2], Francis R. Livens[1/2], Peter Leary[3], Katherine Morris[2], Neil Gray[3], Liam Abrahamsen-Mills[4], Graham K. P. Muir[5], Kathleen A. Law[1], Adam J. Fuller[1], Nick D. Bryan[4], John A. Howe[6], Gordon T. Cook[5], Gareth T. W. Law[1/2*]

1. Centre for Radiochemistry Research, School of Chemistry, The University of Manchester, Manchester, M13 9PL, UK.

2. Research Centre for Radwaste and Decommissioning and Williamson Research Centre, School of Earth and Environmental Sciences, The University of Manchester, Manchester, M13 9PL, UK.

3. School of Natural and Environmental Sciences, Newcastle University, Newcastle, NE1 7RU, UK.

4. National Nuclear Laboratory, Chadwick House, Birchwood, Warrington, WA3 6AE, UK.

5. Scottish Universities Environmental Research Centre, Scottish Enterprise Technology Park, East Kilbride, G75 0QF, UK.

6. Scottish Association for Marine Science, Dunstaffnage Marine Laboratories, Oban, Argyll, PA37 1QA, UK.

*Corresponding author. Email: gareth.law@manchester.ac.uk; Tel: +44 (0)161 306 0514

## 3.1. Abstract

Understanding radionuclide biogeochemistry and mobility in natural environments is key to improving the management of legacy nuclear sites, and in building a robust safety case for radioactive waste geological disposal. Here, Sellafield-derived radionuclides and trace elements in Irish Sea sediment and porewater were studied to investigate the relative importance of sediment biogeochemistry vs. physical transport on radionuclide distribution in the marine environment. Actinide (Am, Pu) and fission product (Cs) distributions were determined at two locations, one which is hypothesised to act as a long-term secondary source of Sellafield-derived radionuclides (the Irish Sea mud-patch), and the other, a possible sink for Sellafield-derived radionuclides (the Ravenglass saltmarsh). Major element distributions and microbial community analysis at the sites suggest Pu distribution is largely independent of the ambient redox-related processes. Instead, Pu, along with Cs and Am distribution in Irish Sea sediments appears to be controlled by physical mixing and transport processes.

**Keywords:** Plutonium, Americium, Caesium, Irish Sea, Ravenglass, Sellafield.

## 3.2. Introduction

The authorised discharge of low-level aqueous waste from the Sellafield site (Cumbria, UK) to the Eastern Irish Sea has taken place since 1952 (Kershaw et al., 1992; Gray et al., 1995). Liquors from spent fuel reprocessing and purge waters from fuel storage ponds are the major contributors to this waste stream and contain a range of actinides and fission products (e.g. Am, Cs, Np, Pu, and U) (Kershaw et al., 1992). Once released into the Eastern Irish Sea, these radionuclides can accumulate in local coastal areas (Kershaw et al., 1990; MacKenzie and Scott, 1993) or are transported further afield (Kershaw and Baxter, 1995). As a result of the Sellafield discharges, the Irish Sea sediments present a unique natural laboratory in which to study the long-term biogeochemistry of anthropogenic radionuclides in the natural environment.

The discharge of low-level waste from the Sellafield site to the Eastern Irish Sea has varied since 1952, reflecting changes in industrial practice on-site (Kershaw et al., 1992; Gray et al., 1995). Discharged activities steadily increased

throughout the 1960s due to increased waste throughput and processing on-site. They then peaked in the mid-1970s as a result of increased storage times for Magnox fuels (Kershaw et al., 1992). Thereafter, discharged activities decreased significantly as effluent treatment technologies (the Enhanced Actinide Removal Plant (EARP) and the Site Ion Exchange Effluent Plant (SIXEP)) were commissioned (Kershaw et al., 1992). Contemporary discharges (for most radionuclides) are now three orders of magnitude lower than historical maxima, and are well below authorised discharge limits (Sellafield Ltd, 2017).

The Irish Sea is a macro-tidal, semi-enclosed marine system, with water entering from the Atlantic through St George's Channel in the south, and leaving *via* the North Channel (Carr and Blackley, 1986). Sellafield effluents are are then discharged into the shallow, Eastern Irish Sea *via* a pipeline extending 2.1 km seaward from the low water mark (Kershaw et al., 1992). Plutonium is primarily present in effluent as $^{238}$Pu, $^{239}$Pu, $^{240}$Pu, and $^{241}$Pu ($t_{1/2}$ = 87.7; 24,100; 6550; 14.4 years, respectively) and has access to four oxidation states under standard seawater Eh and pH: III, IV, V, VI (Morse and Choppin, 1991). Plutonium (III/IV) species readily undergo hydrolysis and, in marine systems are thought to be scavenged by suspended particulate matter, resulting in their removal from solution (Nelson and Lovett, 1978). It has been suggested that over 90 % of the Sellafield Pu discharge inventory has become associated with Irish Sea sediments as particle reactive Pu(IV) (Mackenzie and Scott, 1993). In contrast, Pu(V/VI) species form dioxo-cations (i.e. $PuO_2^+$ and $PuO_2^{2+}$) and in the Irish Sea, this minor Pu fraction (10 %) is mainly thought to have remained in seawater (MacKenzie et al., 1999). Laboratory studies have shown that the Fe(III)-reducing bacteria *G. metallireducens* and *S. oneidensis* can influence Pu speciation, reducing Pu(V)/Pu(VI) to monocrystalline Pu(IV) (Icopini et al., 2009; Renshaw et al., 2009). In addition, Pu has been shown to have a high affinity for Fe and Mn oxides, (Sanchez et al., 1985; Keeney-Kennicutt and Morse, 1985; Morgenstern and Choppin, 2002; Shaughnessy et al., 2003; Fjeld et al., 2003; Powell et al., 2005). However, it is less clear that these biogeochemical controls extend to the field. Sellafield-derived $^{241}$Am ($t_{1/2}$ = 432.2 years) exists predominantly as Am(III) (Aston and Stanners, 1981), and the majority of the discharged Am inventory is thought to have become associated with fine grained sediments (MacKenzie et

al., 1999). The $\beta^-$-decay of discharged $^{241}$Pu ($t_{1/2}$ = 14.4 years) also contributes to the ingrowth of $^{241}$Am in the Irish Sea, resulting in an increasing inventory of $^{241}$Am with time (Day and Cross, 1981). The affinity of $^{241}$Am and $^{239,240}$Pu for solid surfaces is highlighted by their high distribution coefficient ($K_d$ = (Bq/kg) particulate/(Bq/kg) seawater) in the Eastern Irish Sea, which is reported to be approximately $10^6$ for both radionuclides (Kershaw et al., 1999). The fission product $^{137}$Cs ($t_{1/2}$ = 30.2 years) exists as the highly mobile $Cs^+$ species in seawater and is considered to be a 'conservative' radionuclide, so would be quickly transported out of the Irish Sea (Baxter et al., 1979; Al-Qasmi et al., 2017). However, a fraction of Sellafield-derived Cs (~ 10 %) is thought to have been removed from local seawater *via* reaction with clay minerals, which are present in higher quantities in finer grained sediments e.g. inner mud-flat/saltmarsh environments (Jones et al., 1999).

A proportion of the Sellafield discharges have, over time, become associated with a belt of fine-grained sediments located ~ 10 km from the pipeline (known as the Irish Sea mud-patch, ~ 15 km long x 3 km wide). The mud-patch has then been suggested to act as a transient sink for particle reactive Sellafield-derived radionuclides (McCartney et al., 1994; Kershaw et al., 1999; Marsden et al., 2006). Once deposited in mud-patch sediments, macrobenthic organisms are then suggested to remobilise a portion of the sediment-associated radionuclides throughout the depth profile of the mud-patch *via* sediment mixing, with subsequent release back into the water column (Kershaw et al., 1983; Kershaw, 1984). The role of biogeochemistry in controlling radionuclide retention/release (with particular relevance to redox sensitive Pu) in the Irish Sea mud-patch is unclear. Regardless, once remobilised, the radionuclides can then be transported elsewhere in the Irish Sea by currents (Kershaw et al., 1983), and historically, this has been used to explain wide spread presence of radionuclides in UK and Irish marine sediments (Aston and Stanners, 1981; McCartney et al., 1994; Keogh et al., 2007). Recently published data from Welsh and Scottish coastal areas (Al-Qasmi et al., 2016, 2017) also indicate that the mud-patch remains a contemporary source of historically discharged radionuclides to UK coastal areas.

Sediments deposited in coastal areas in close proximity to Sellafield also have relatively high concentrations of anthropogenic radionuclides. For example, the

Ravenglass saltmarsh near Seascale in Cumbria is a low energy, intertidal region that accumulates Sellafield-derived radionuclides (Hamilton and Clarke, 1984). This site has been studied in the past (Aston and Stanners, 1981; Morris et al., 2000; Lucey et al., 2004; Marsden et al., 2006; Lindahl et al., 2011; Oh et al., 2009; Caborn et al., 2016), and the re-suspension of Irish Sea mud-patch sediment followed by transport to and deposition in the saltmarsh has been invoked as the key mechanism controlling radionuclide desorption in this area. Understanding of the biogeochemical controls on long-term radionuclide distribution and retention at the site is limited. Further, little is known about microbial communities present in these sediments or their potential effects on radionuclides.

Reflecting the above, here we examine the contemporary distribution of Sellafield-derived caesium, americium, and plutonium ($^{137}$Cs, $^{241}$Am, $^{238}$Pu, $^{239,240}$Pu, and $^{241}$Pu) in sediments sampled from the Irish Sea mud-patch and the Ravenglass saltmarsh (from herein referred to as mud-patch and Ravenglass, respectively). We compare the radionuclide distribution at both sites to historical Sellafield discharge records, sediment/porewater stable element geochemistry, and microbial ecology, and re-visit a mathematical model used by Marsden et al. (2006). In doing so, we seek to understand the relative importance of biogeochemical vs. physical controls on radionuclide distribution at both sites.

## 3.3. Methods and Materials

### 3.3.1. Sample Collection and Preparation

Sediment cores were collected from a belt of fine-grained sediment in the north-east Irish Sea mud-patch, (54’26.80 N, 03’42.89 W) in June 2014 and from Ravenglass (54’20.24 N, 03’24.06 W, respectively) in September 2014 (Figure 1). Sediment cores (depth ~35 cm, diameter 10 cm) were retrieved from the mud-patch using extruded acrylic core tubes and a hydraulic mega corer (Law et al., 2009). A further sediment core (~2.5 m) was taken using a gravity corer. Care was taken during coring to leave the sediment water interface as undisturbed as possible. Cores from Ravenglass (depth ~35 cm) were collected by manual insertion of core tubes, with an airtight bung placed over the top of the core prior to extraction. Two cores from each of the study sites (separated by ~20 cm) were

used for analyses. One core from each site was sectioned within 1 hour of collection in an $O_2$ free, $N_2$ filled atmosbag. The second core was sampled under a normal atmosphere. The cores were sectioned at 1 cm resolution from the sediment interface until a depth of 10 cm, and at 2 cm resolution thereafter. Porewater from each section in the first core was collected by centrifugation (10 minutes at 4500 rpm; 1811 *g*) followed by filtration (PTFE membrane syringe filter; 0.22 µm). The filtered solutions were then fixed *via* addition of 200 µl Aristar grade c$HNO_3$. The gravity core collected from the mud-patch was frozen soon after collection, and on return to the home laboratory logged, defrosted, sectioned (under a normal laboratory atmosphere) freeze-dried, and homogenised.


**Figure 3.1**. Map of the British Isles with inset showing the Sellafield site and the two study sites (Irish Sea mud-patch and Ravenglass saltmarsh).

### 3.3.2. Total Organic Matter

Sequential Loss on Ignition (LOI) was used to determine the total organic matter present in the sediment samples. Here, homogenised sediment (~5.5 g) from each sample was oven dried at 105 °C for 24 hours, then heated at 375 °C for 19 hours using a ramp rate of 1 °C/min, and finally ashed at 950 °C for 10 hours using a

ramp rate of 10 °C/min. These heating stages were used to eliminate water and organic matter (Rowell, 1994).

### 3.3.3. Elemental Analysis of Sediment and Porewater

The concentration of Al, Fe, K, Mg, Mn, and P in the bulk sediment was measured using a Panalytical Axios sequential XRF Spectrometer. Ground sediment (12 g) was added to powdered wax binder (3 g) and homogenised (7 minutes at 350 rpm; $g = 10.9$), and then pressed into pellets under pressure (7–10 tonnes). The pellets were analysed, and the resulting data oxide normalised and corrected for C content.

Acidified porewater (200 µL) samples were diluted in 2 % $HNO_3$ (4.8 mL) and analysed for Fe and Mn on a Perkin Elmer Optima 5300 Dual View ICP-AES. A range of matrix-matched certified standards (NIST standard1643e) were used for analyses ($R^2$ for both elements = 0.999).

### 3.3.4. Microbial Community Analysis

DNA was extracted using a FastDNA Spin Kit for Soil (MP Biomedicals) as per the manufacturer's instructions. DNA underwent PCR, using universal primer pair F515 and R926 (positions 515 to 926 in the V4–V5 region; *Escherichia coli* numbering), which target both Bacteria and Archaea. Forward primers used 'golay_12' barcodes and Torrent adaptor A for identification. Initial denaturation was at 95 °C for 5 minutes; 30 cycles of 95 °C for 1 minute, 55 °C for 1 minute, 72 °C for 1 minute; and a final elongation step of 72 °C for 10 minutes. PCRs were performed on a Techne 512 thermocycler, and in triplicate to reduce bias. Amplicons were cleaned using Agencourt AMPure XP (Beckman Coulter), quantified *via* Qubit 3.0 fluorometer (Life Technologies) and pooled.

Sequencing was performed on an Ion Torrent Personal Genome Machine (Thermo Fisher Scientific) on a 316 chip. Sequencing produced reads with a modal length of 481 bases. The average number of reads in individual binned closed-reference libraries after filtering and operational taxonomic unit (OTU) phylogenetic assignment filtering was 14836.41 for the mud-patch, ranging from 5808 to 23402, and 13271.68 for Ravenglass, ranging from 6922 to 21972. Libraries were rarefied to 5800 sequences for the mud-patch core, and 6900

sequences for the Ravenglass core to allow for comparative analysis of sequences. Sequences for both sediment cores were deposited in the NCBI's Sequence Read Archive (SRA), and are available under BioProject. Pipeline analysis was performed using QIIME 1.9.1, (Caporaso et al., 2010) with OTU matching performed at 99 % similarity against the SILVA128 closed-reference database (Quast et al., 2012). OTU tables were standardised by total for each sample depth, and square root transformed, in PRIMER 6 (Clarke and Gorley, 2009). Bray Curtis similarity and non-metric-Multidimensional Scaling analysis was then performed. Taxonomy summary bar charts are used to represent trends in community change as a function of depth (based on assignments of OTUs to the genus level where possible). Dominant taxa and their abundance change with depth were related to other geochemical parameters based on geochemical functions inferred from the conserved phenotypic characteristics of close relatives. It is important to highlight that Ion Torrent does not delineate live vs dead, or active vs inactive bacteria.

### 3.3.5. Measurement of $^{137}$Cs and $^{241}$Am

The activity of $^{241}$Am and $^{137}$Cs was measured by counting the pressed disc sample (12 g) from XRF analysis (see section 2.3) on a Canberra GC1019 hyper-pure germanium (HPGe) detector housed in a 11 cm thick lead shield (20–1800 keV) γ-detector for 24 hours. The detector was calibrated for efficiency using matrix-matched standards of the same geometry spiked with certified standard solutions of $^{241}$Am and $^{137}$Cs (Amersham International). Gamma spectra were also corrected for background.

### 3.3.6. Measurement of Pu isotopes ($^{238}$Pu, $^{239,240}$Pu, and $^{241}$Pu)

Plutonium ($^{238}$Pu, $^{239,240}$Pu) alpha activity was measured using a Canberra 7401 α-spectrometer and $^{241}$Pu activity was measured using a 1220 Quantulus Ultra low level liquid scintillation spectrometer. The Pu separation was based on that of Nygren et al. (2003) using Eichrom TEVA® resin. In brief, sediment samples (~1 g) were ashed (to remove the majority of the organic component) using a furnace for 7 hours at 500 °C. *Aqua regia* (3:2 v/v cHCl: c$HNO_3$) was then used for the partial dissolution of the sediment, followed by filtration to remove solids (Whatman GF/A; 0.22 µm). This was taken up in 3 M $HNO_3$ (15 mL), and spiked

with certified $^{242}$Pu tracer (NPL, Teddington; 100 µL, 0.75 Bq/mL), for yield recovery. Thereafter, $NaNO_{2(s)}$ was added to the sample to a concentration of 0.2 M, and warmed to 90 °C (to convert Pu to the tetravalent state). The sample was cooled, and passed through a pre-conditioned (3 M $HNO_3$; 5 mL) Eichrom TEVA® column (4.0 cm x 0.5 cm, 100–150 mesh). This binds Pu(IV) to the resin, and a series of 3 M $HNO_3$ washes (4 x 5 mL) elutes co-contaminants e.g. U(VI), Am(III), Np(V). 9 M HCI (5 mL) was then added to remove Th(IV). Plutonium was eluted with 9 M HCl and 0.1 M $NH_4I$ (15 mL) as Pu(III). 3 M $HNO_3$ (3 mL) was added to the eluted Pu fraction and taken to near dryness, followed by 30 % $H_2O_2$ (1 mL), and evaporated to near-dryness, and lastly cHCl (3 mL) and dryness. The residue was taken up in electrolyte solution (4 % $C_2H_8N_2O_4$ in 0.3 M HCl; 15 mL) and electroplated onto a stainless steel 25 mm planchette at 0.5 A, 20 V for 3 hours. The planchette was counted for 24 hours (Canberra 7401 α-spectrometer), and the resulting data was background corrected. The activity of $^{239,240}$Pu in select sediment samples from the mud-patch gravity core was analysed using a similar method. However, here an Ortec Octete α-spectrometer was used for $^{239,240}$Pu detection.

For $^{241}$Pu quantification, the eluted Pu fraction was evaporated to near-dryness using a heat lamp, and 2 % HCl (2 mL) added to the residue. This was transferred to a plastic scintillation vial (15 mL) and Optiphase Hi-safe 3 scintillation cocktail (5 mL) was added. Samples were counted for 4 hrs on the 1220 Quantulus after 24 hr stabilisation in darkness. Once counted, the samples were spiked with an internal $^{241}$Pu standard (10 Bq/100 µl), dark adapted again, and recounted. For radiometric measurements all errors are presented as 1 standard deviation based on counting statistics. All radionuclide activities presented have been decay corrected to the date of collection.

### 3.3.7. Mathematical Model

A mathematical model was used by Marsden et al. (2006) to rationalise radionuclide distribution at the mud-patch and Ravenglass sites using the Sellafield discharge history (Table S3). The model was re-visted here, using the parameters determined by Marsden et al. (2006). However, in this work we compare the model output with $^{239,240}$Pu field data taken from the mud-patch and

Ravenglass sediment cores in the same year (whereas Marsden et al. (2006) used Ravenglass core data that was taken 17 years after that from the mud-patch), as we feel this will better calibrate the model, and investigate its validity. In addition, $^{239,240}$Pu mud-patch data down to 1.5 m is used in this work, and the model output compared to this. The model is described fully in Marsden et al. (2006) and a summary is also provided in the SI (Text S1). For this work two values for the pseudo-diffusion coefficient; $9.5 \times 10^{-8}$ $cm^2/s$ (used by Marsden et al. (2006)), and $9.5 \times 10^{-7}$ $cm^2/s$, were used to represent bioturbation in the mud-patch, and hence to predict the resulting Ravenglass sediment profile.

### 3.4. Results and Discussion

#### 3.4.1. Sediment Biogeochemistry

The total organic matter content of the mud-patch was relatively constant with depth at ~1 wt % (Table S1), suggesting that organic matter input and turnover at this site is low. At Ravenglass, the total organic matter content ranged from, ~ 7 wt % at the sediment surface to ~4 wt % at depth (Table S2), possibly reflecting microbially mediated oxidation of organic matter (Froelich et al., 1979). Silicon concentrations were around 25 wt % at both sites, which is typical for marine sediments (Calvert and Pedersen, 1993). Porewater analysis of $NO_3^-$ was attempted at both sites using IC but low volumes of porewater were recovered from the sediment and analyte concentrations were below the limit of detection (0.05 mg/L).

At the mud-patch Eh was shown to decrease from 300–500mV to 50–250 mV between the overlying water and 5–10 cm depth, with the pH ~7.6 in this region (Malcolm et al., 1990).Whilst Eh was not measured, previous measurements at Ravenglass show a decrease in Eh with depth (+45 mV at 1 cm to -350mV at 24 cm) and a pH between 7.3 at 1 cm to 6.7 at 15 cm) (Lucey et al., 2004). Salinity values at Ravenglass vary from an upper limit of 31‰ at high tide (Hamilton and Clarke, 1984), to a lower limit of 0.2 ‰ (Carr and Blackley, 1986) during low water inundation, highlighting the dynamic nature of the estuary. Sediments at the mud-patch appeared to transition from a light grey to a slightly darker grey colour with depth, whilst at Ravenglass, the sediment colour changed slightly with depth from red/brown to brown/grey.

The concentration of the lithogenic elements (Al, Mg, K), and those with additional biogenic input (Si, P) in the sediments at the mud-patch and Ravenglass (Table S1 and S2, respectively) varied little with increasing depth. Aluminium at the mud-patch ranged from ~3–8 wt % throughout the core, and ~7–9 wt % in the saltmarsh sediments, with no trend evident at both sites. The distribution of Mg at the mud-patch ranged between 0.93–1.95 wt % with no discernible trend, and a near constant concentration (~1.8 wt %) was found at Ravenglass. There was a similar spatial distribution of K at the mud-patch, with concentrations ranging between 1.16–2.83 wt %, and between 2.62–2.93 wt % at Ravenglass. Silicon at the mud-patch varied between 24.9–26.9 wt %, and similarly at Ravenglass, however lower concentrations (~23 wt %) were observed in the mud-patch surface sediments. The concentration of P at the mud-patch ranged between 0.04–0.1 wt %, with little trend. In some marine sediment systems higher P concentrations are observed in surface sediments reflecting an input of labile organic matter. The low concentration of P and total organic matter observed at this site during sampling (which took place during the British Summer, when marine productivity is at its highest) indicates that this sediment system probably remains organic-poor year round. In contrast, higher concentrations of P were present in Ravenglass sediments (0.12–0.16 wt %), with the upper concentration observed between 9–21 cm. This subsurface enrichment may be due to a lithogenic input, caused by the degradation of P-containing phases.

Figures 3.2A and 3.2C show the distribution of solid phase Mn (expressed as a Mn/Al ratio to remove variance from the detrital (non-reactive) fraction; Calvert and Pedersen, 1993) in the mud-patch and Ravenglass cores, respectively. There was an enrichment of Mn close to the surface at both sites, however this was more marked at the mud-patch. The Mn enrichment is likely due to the input of Mn-oxyhydroxides as grain coatings or *via* inputs from rivers (Calvert and Pedersen, 1993). At the mud-patch, the Mn/Al ratio decreased from the surface to 5 cm in depth, consistent with microbially-mediated reduction of Mn(IV) (Froelich, 1979). In turn, Mn porewater concentrations at the mud-patch were enhanced (248–345 μM) between 0–4 cm (Figure 3.2E). They then decreased to 17 μM at 35 cm, likely reflecting gradual Mn sorption to the sediment; however,

the sediment Mn/Al ratio remained relatively constant below 4.5 cm (Figure 3.2A). At Ravenglass, the Mn/Al ratio decreased between 0–5 cm (Figure 3.2C) commensurate with a subsurface peak in porewater Mn (Figure 3.2G), with Mn concentrations reaching a maximum (104 μM) at 1 cm and decreasing to 4.1 μM by 6 cm. This porewater subsurface maximum and decrease in the Mn/Al ratio between 0–6 cm suggests that some microbially-mediated Mn(IV) reduction does occur at this site. However, whilst the porewater Mn concentrations at Ravenglass remained below 5.0 μM after a depth of 6 cm, the Mn/Al ratio did show a sub-surface maximum between 14–22 cm. The origin of this maximum is unclear.

The sediment Fe/Al ratios at the mud-patch and Ravenglass sites (Figure 3.2B and 3.2D) showed a similar trend with enhanced, near-constant ratios in the upper sections of each core. At both sites the Fe/Al ratios remained near constant to a depth of 12 cm; there was then a steady decrease in the Fe/Al ratio to 18 cm depth at the mud-patch, and 24 cm at Ravenglass, likely reflecting microbially-mediated reduction of Fe(III) (Froelich, 1979). Near constant Fe/Al ratios were then found to the bottom of the cores. Porewater Fe concentrations at the mud-patch were variable between 0–5 cm (Figure 3.2F), showing a sub-surface peak (226 μM) at 2 cm and near zero concentrations at the sediment surface and between 3–5 cm. Below 5 cm the porewater Fe concentrations then increased to 166 μM at 6.5 cm and gradually decreased to 39 μM by 35 cm, likely reflecting Fe(II) sorption to the deeper sediments or possibly precipitation of authigenic Fe(II) bearing phases (Calvert and Pedersen, 1993). At the Ravenglass site porewater Fe concentrations were similar to the mud-patch highlighting a variable trend between 0–5 cm, with a subsurface peak (152 μM) at 2.5 cm, and low Fe concentrations (18 μM) at 1 cm (Figure 3.2H). Thereafter, there was an increase to 100 μM at 6.5 cm, followed by a gradual decrease in concentration, likely for similar reasons as suggested for the mud-patch. Overall, the trends in sediment and porewater Fe likely reflect the input of Fe(III)-oxy(hydr)oxides to the surface sediments of both sites followed by microbially mediated Fe bio-cycling (Burdige, 1993). Sulfate/chloride ratios in Ravenglass porewater decrease with depth, indicative of robust sulfate reduction taking place at deeper anoxic sections of the core. At the mud-patch these ratios remain constant with depth suggesting limited sulfate reduction is taking place.

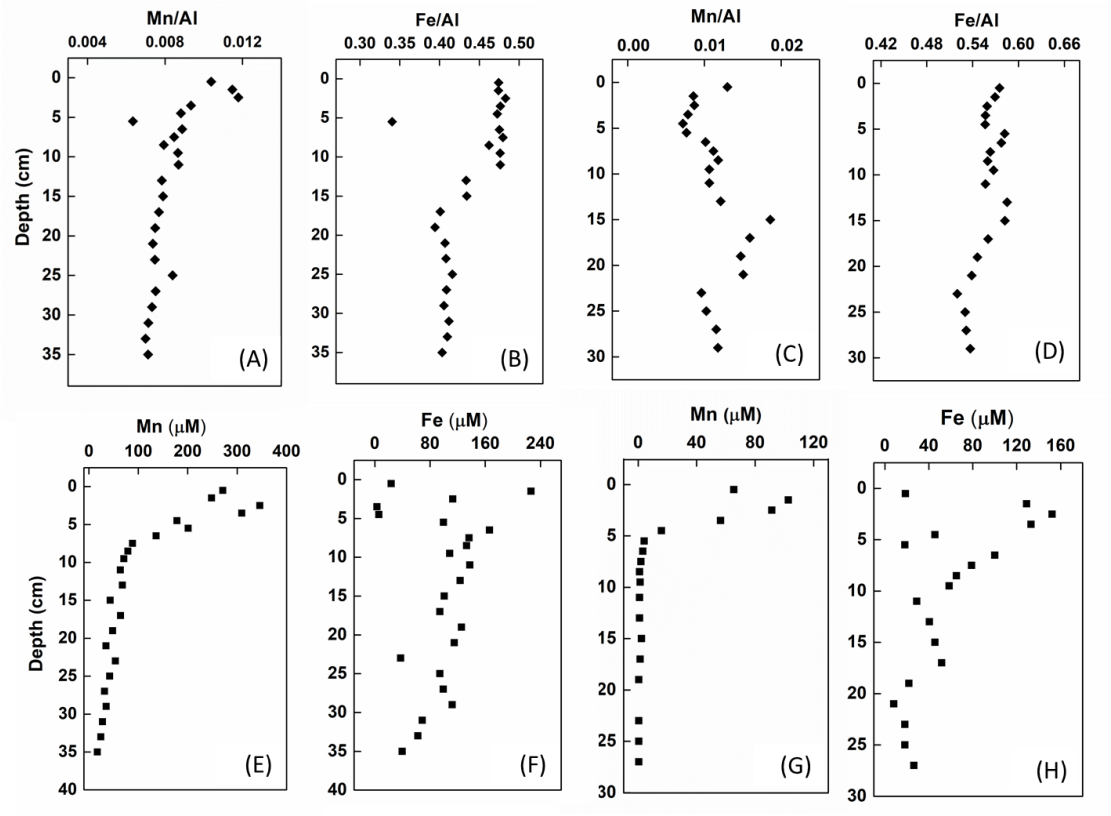


**Figure 3.2**. Sediment Mn/Al and Fe/Al ratios in the Irish Sea mud-patch (A and B) and Ravenglass saltmarsh (C and D), and porewater Fe and Mn concentrations in the Irish Sea mud-patch (E and F) and Ravenglass saltmarsh (G and H). Note each *x-axis* varies to best highlight trends in the data.

### 3.4.2. Characterisation of the Microbial Community

Typically, in a vertical soil or sediment profile, a thermodynamically controlled respiratory redox stratification of microbial metabolism can be observed, which proceeds from aerobic through to anaerobic and fermentative respiration (Thauer et al., 1977; Froelich et al., 1979) We aimed to better predict the dominant redox processes at the mud-patch and Ravenglass sites *via* the identification, presence and abundance of certain functionally indicative microbial taxa. This is based on the assumption of typical persistence of DNA within a sedimentary system of <2 years (Nielsen et al., 2007). The identification of key functional microbial taxa *via* DNA gives a time averaged picture of the dominant sediment biogeochemistry at the time of sampling.

The microbial community assemblages of both mud-patch and Ravenglass sedimentary systems do not appear to show the typical respiratory succession aforementioned. Instead, the microbial communities within both sites are highly diverse, and show a mix of aerobic and anaerobic respiratory groups, indicating that microenvironments of both oxidising and more reducing conditions persist, sometimes even at the same depth.

The microbial community at the mud-patch was reasonably homogenous with depth (Figure 3.3A). However, there were four exceptions in discrete horizons characterised by dominance of specific microbial taxa. At a depth of 0–1 cm the aerobes *Psychrobacter* spp. (41 %) and *Lutimonas* spp. (22 %) dominated (Figure 3.3D and 3.3C) (Romanenko et al., 2009; Teixeira and Merquior, 2014). Then, between 3–5 cm, 16–18 cm, and 20–22 cm the aerobic/facultative anaerobic family *Planococcaceae* (Figure S1) dominate, ranging from 49–69 % (Figure 3.3F and S2) (Shivaji et al., 2014), with the presence of the *Planococcaceae* genera, *Jeotgalibacillus* sp (21 %) (Figure S1), in the deeper region of the core. These instances of community dominance may be indicative of physical mixing by indigenous macrofauna. Past work close to the mud-patch sampling site refers to the presence of a large echiuran (*Maxmulleria lankesteri)* known to burrow to a depth of ~1.5 m (Kershaw et al., 1984). This onset of physical mixing may result in aerobes being localised along burrow walls and being mixed downwards, and conversely resulting in the upwards distribution of anerobic bacteria. The remainder of the mud-patch samples shared a similar, highly diverse, microbial community assemblage, showing a mix of strict aerobes, and facultative and strict anaerobes (Figure 3.3A). Aerobic taxa include the family *Planctomyceteaceae* (6.3 % ± 0.6 %) (Figure S2), and the ammonia oxidising phylum *Thaumarchaeota* (1.3 % ± 0.2 %) (Figure S2). Anaerobic taxa include the sulfate-reducing genus *Desulfobulbus* (4.9 % ± 0.4 %) (Figure 3.3B and S1) (Kuever, 2014a), and the syntrophic sulfate reducing family *Syntrophobacteraceae* (2.9 % ± 1.5 %) (Figure S2; Kuever, 2014b). This heterogeneity in respiratory function and homogeneity in microbial community structure is potentially indicative of low microbial function, impeded by low levels of organic carbon. Between the physical mixing and the limited supply of organic matter, respiratory redox succession is expected to be limited at the mud-patch site.

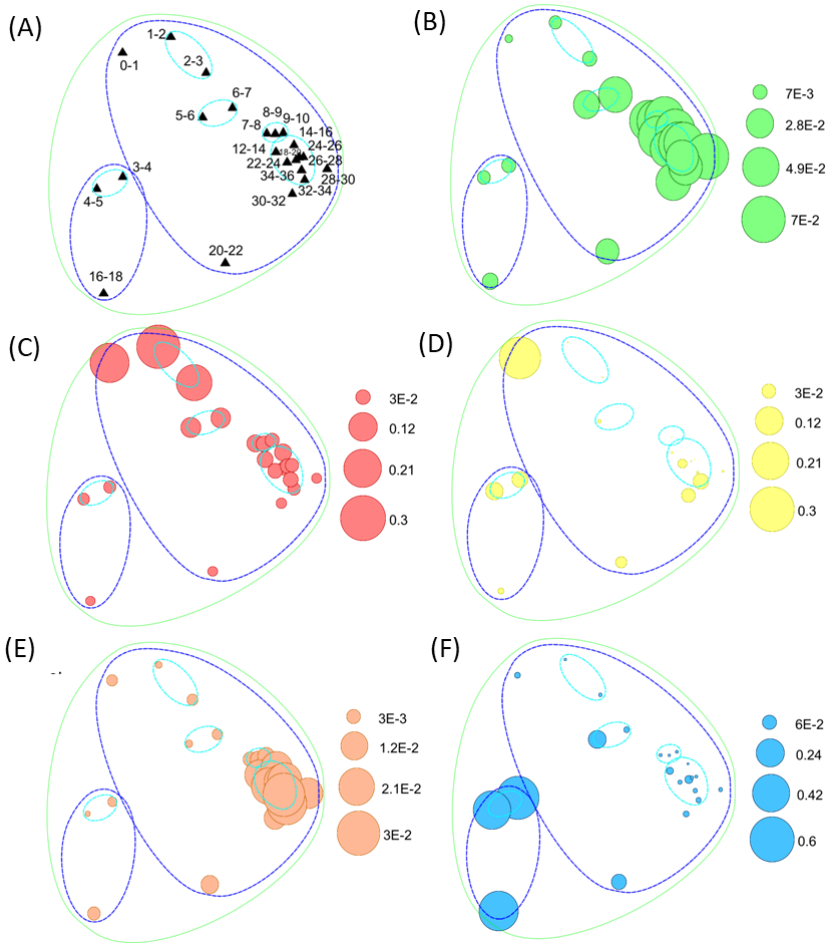


**Figure 3.3**. (A) Non-metric multidimensional scaling (nMDS) ordination based on Bray Curtis similarity resemblance matrix of OTUs derived from 16S rRNA gene sequencing for the Irish Sea mud-patch. 2D stress = 0.05. Labels represent sample depth in cm. Circles show similarity of 40 % (green), 60 % (blue), and 80 % (light blue). 2D Bubble nMDS of Bray Curtis similarity resemblance showing relative abundance of microbial families. Larger bubble size corresponds to higher relative abundances. (B) *Desulfobulbus*; (C) *Lutimonas*; (D) *Psychrobacter*; (E) *Thaumarchaeota* C3 group; (F) *Planococcus*. The fractional relative abundance of the respective family/genus at each given depth increment is shown in the key.

The microbial community within the Ravenglass sediment core showed a transition in community assemblage between two halves of the core, separated *via* Bray-Curtis analysis around the 7–8 cm horizon (Figure 3.4A). Similar to the mud-patch, the 0–4 cm zone contained both aerobic and anaerobic taxa. *Bacteriodetes* families, including *Flavobacteriaceae* (11.8 % ± 2.9 %) and *Draconibacteriaceae* (3.3 % ± 0.8 %) (Figure 3.4F and S3) (McBride, 2014; Mcllroy and Nielsen, 2014), and also the anaerobic families *Anaerolineaceae* (3.4 % ± 0.5 %) and anaerobic sulfate-reducing *Desulfobulbaceae* (6.1 % ± 0.7 %; Figure S3) (Yamada et al., 2006; Kuever, 2014a) were observed here. The 5–16 cm zone encapsulates the change in microbial community structure measured by Bray-Curtis nMDS (Figure 3.4A). *Flavobacteriaceae* and *Desulfobulbaceae* amongst others, declined in abundance.

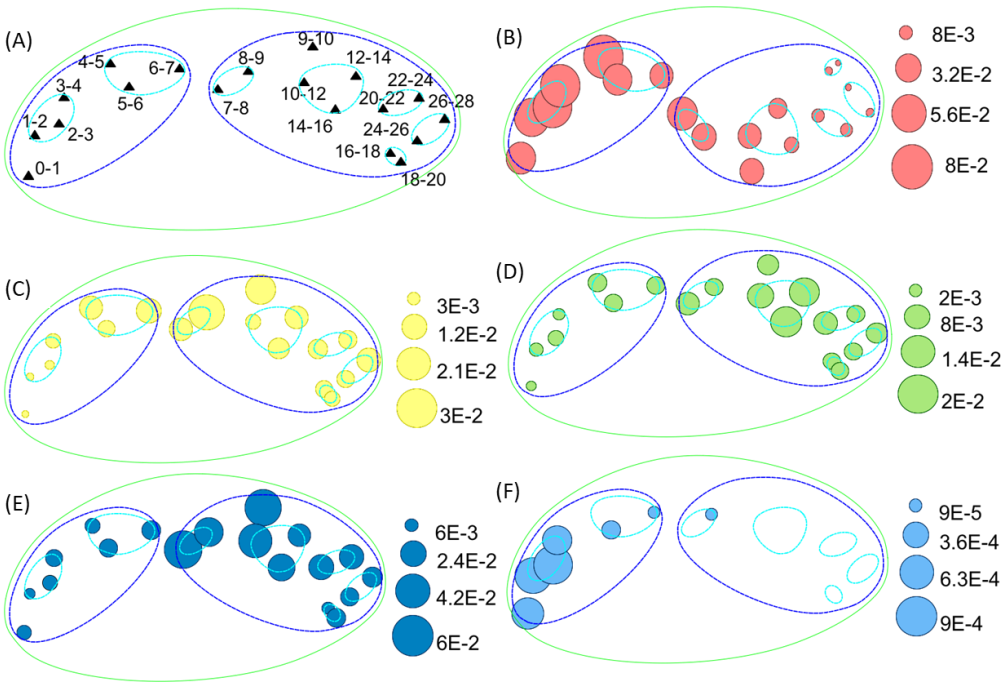


**Figure 3.4.** (A) Non-metric multidimensional scaling (nMDS) ordination based on Bray Curtis similarity resemblance matrix of OTUs derived from 16S rRNA gene sequencing for the Ravenglass saltmarsh. 2D stress = 0.02. Labels (top left) represent sample depth in cm. Circles show similarity of 40 % (green), 60 % (blue), and 80 % (light blue). 2D Bubble nMDS of Bray Curtis similarity resemblance showing relative abundance of microbial families. Larger bubble size corresponds to higher relative abundances. (B) *Desulfobulbus*; (C) *Thaumarchaeota*; (D) *Bathyarchaeota*; (E) SEEP SRB-1; (F)

*Draconibacterium*. The fractional relative abundance of the respective family/genus at each given depth increment is shown in the key.

This coincides with the emergence of the sulfate-reducing *Desulfobacteraceae* (4 % ± 0.6 %) (Figure S3) (Kuever, 2014a), and the micro-aerobic, nitrogen-fixing *Rhodospirallaceae* (4.4 % ± 0.3 %; Baldani et al., 2014). The ammonia oxidising *Thaumarchaeota* (1.7 ± 0.2 %) (Figure 3.4C and S3; Swan et al., 2014) and the methane cycling *Bathyarchaeota* (1.1 % ± 0.1 %) (Figure 3.4D and S3; Evans et al., 2015) further highlight the complex assemblage and nature of this sediment core. The decrease in this zone of the *Desulfobulbaceae* and increase of *Desulfobacteraceae* (Figure S3), two closely-related families of sulfate-reducers, suggests the core maintains anaerobic conditions at depth.

The microbial community within the 18–28 cm zone was 60 % similar, reflected in their clustering on the Bray Curtis nMDS (Figure 3.4A). Aerobic families, such as the *Phyllobacteriaceae* (1 % ± 0.3 %) (Willems, 2014) and the anaerobic *Desulfobacteraceae* (2.1 % ± 0.3 %) and *Anaerolineaceae* (4.3 % ± 1 %) (Figure S3) appear to show that the dominant redox conditions are heterogeneous, likely comprised of relatively high Eh anaerobic (denitrification, manganese, and iron reduction) processes. The presence of sulfate-reducers implies there is some degree of sulfate-reduction occurring. A lack of methanogenic taxa, such as the *Euryarchaeota*, signals a lack of this function.

The microbial community data from the Ravenglass saltmarsh suggests there is a transition in community assemblage between the two halves of the core, with maintenance of the complex heterogeneous mix of oxidising and reducing redox functions. This heterogeneous redox mixing is not reflected in the bulk geochemistry, which shows consistent sub-oxic conditions throughout most of the core, reflected by solid phase Fe and Mn reduction. The presence of the *Hyphomicrobiaceae* (0.9 % ± 0.1 %) (Figure S3) is indicative of a low carbon, high Eh environment (Oren and Xu, 2014), and LOI results subsequently showed an average of ~5 % total organic matter in the core. This suggests that the labile organic reservoir (i.e. excluding the highly refractory component) may be very

small. The absence of bioturbating fauna at the Ravenglass saltmarsh may be surprising as LOI results highlight the potential food supply, including evidence of substantial downcore organic matter decay. Moreover, the tide-driven "vertical percolation" that is recognised to take place at saltmarsh (Carr and Blackley, 1986) will likely bring with it water of varying (unknown) oxygen concentration. Thus, the presence of multiple bacterial functional groups at any given (averaged) depth horizon may be justified.

### 3.4.3. Radionuclide Distribution at the Irish Sea Mud-patch

The $^{137}$Cs distribution varied between 120–220 Bq/kg without trend in the mud-patch core (Figure 3.5A). The relatively uniform distribution down the core is consistent with bioturbation as described above. The presence of $^{137}$Cs at the near-surface suggests re-working of higher activity material from depth, as there would be near-zero $^{137}$Cs activity at the surface, based only on contemporary Sellafield discharges (Sellafield Ltd, 2017). The depth distribution of $^{241}$Am in the mud-patch was also broadly uniform (ranging between 193–504 Bq/kg), increasing slightly with depth (Figure 3.5B). There was also detectable $^{241}$Am at the surface (~200 Bq/kg) and as for $^{137}$Cs, the scattered distribution is likely consistent with physical mixing of older sediments towards the surface. The activities of $^{238}$Pu and $^{239,240}$Pu at the mud-patch increased from 26 and 140 Bq/kg at the surface to 48 and 296 Bq/kg at a depth of 9.5 cm (Figures 3.5C and 3.5D, respectively). Thereafter, there was a near constant activity concentration (between 30–350 Bq/kg) with depth, again suggesting physical mixing is a dominant control on radionuclide distribution at this site. The apparent enrichment of $^{238}$Pu and $^{239,240}$Pu at a depth of 25 cm may reflect recycling of older, higher activity material from the 1970s. Additionally, select samples at a range of depths (to 150 cm) were measured for $^{239,240}$ Pu from a longer gravity core, and showed a maximum activity of 624 Bq/kg at a depth of 50–52 cm (see Figure 3.7A). This may suggest that the maximum radionuclide concentration is buried in deeper sections of the sediment core, and supports the proposition that bioturbation at the site is returning activity to shallower regions of the mud-patch. Plutonium-241 activity concentrations were also measured at the mud-patch and these were low at the surface of the core (<1000 Bq/kg), and then increased to and varied between 2000–4000 Bq/kg from 2.5 cm to the bottom of the core

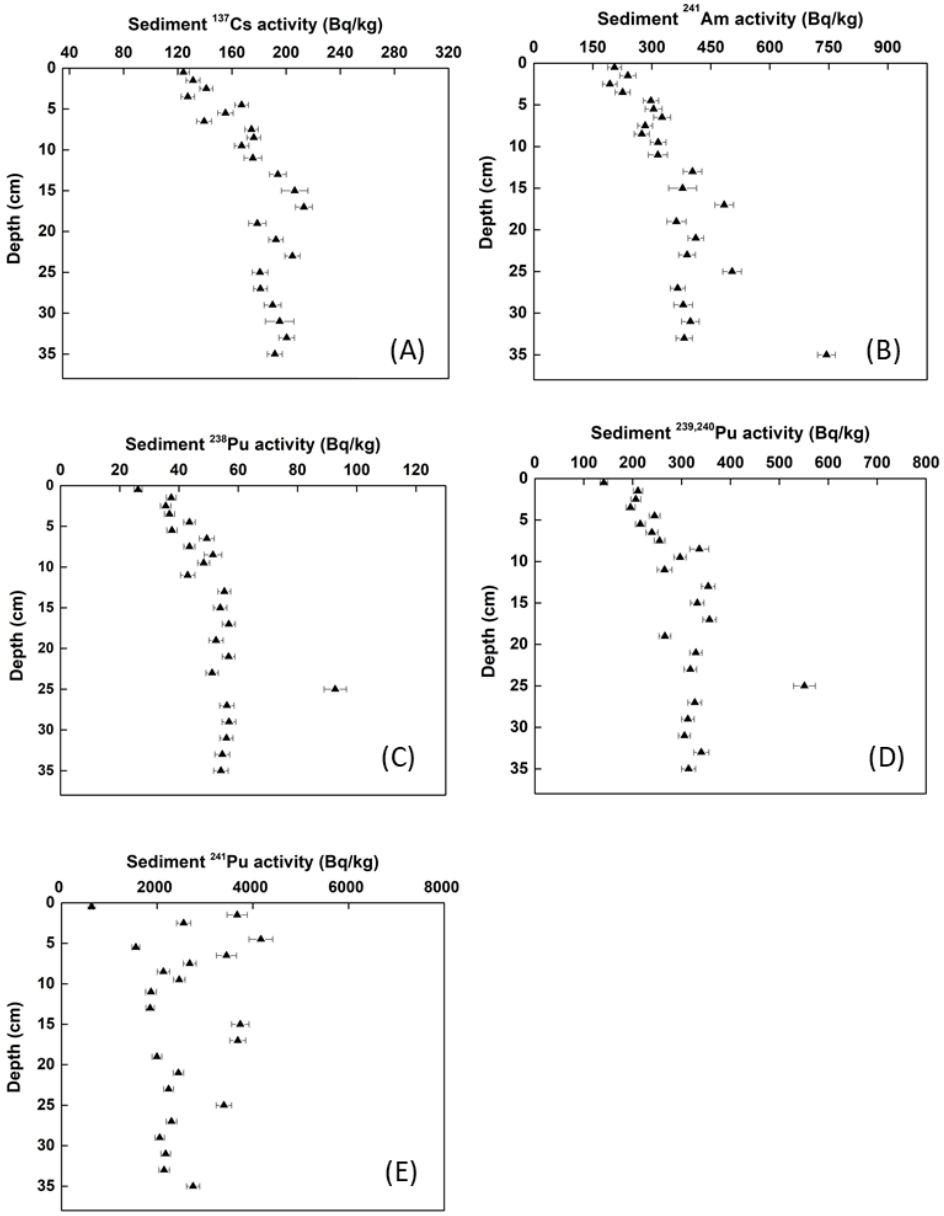


**Figure 3.5.** Activity concentrations of (A) $^{137}$Cs; (B) $^{241}$Am; (C) $^{238}$Pu; (D) $^{239,240}$Pu, and (E) $^{241}$Pu in the Irish Sea mud-patch sediment core in Bq/kg (error bars are 1σ based on counting errors).

(Figure 3.5E). Again, this is consistent with physical mixing, but incomplete homogenisation, of sediments at this site. Whilst laboratory experiments in the last four decades have shown that Pu has a high affinity for Fe and Mn oxides, (Sanchez et al., 1985; Keeney-Kennicutt and Morse, 1985; Morgenstern and Choppin, 2002; Shaughnessy et al., 2003; Fjeld et al., 2003; Powell et al., 2005)

the Pu distribution profiles for the mud-patch provide no evidence to suggest a correlation is present between Sellafield-derived Pu (Figure 3.5C–E) and the Fe(III) and Mn(IV/III) reducing zones (Figure 3.2A, 3.2B, 3.2E, 3.2F). In addition, it would be difficult to investigate biogeochemical control on the radionuclide distribution at the mud-patch as it has not reached a steady-state. Instead, contemporary radionuclide distribution here is being controlled by mixing and vertical migration of higher activity at depth, likely followed by re-dissolution or physical re-distribution of historically derived Sellafield radionuclides away from the sediment. Evidence for this is shown by the near-constant radionuclide ratios ($^{137}Cs/^{241}Am$, $^{241}Am/^{239,240}Pu$, and $^{238}Pu/^{239,240}Pu$) with depth at the mud-patch, in comparison to the dynamic trend in the ratios of the radionuclides released from the Sellafield pipeline (Table S4). This suggests that input is not due purely due to discharge only, as radionuclide activities would decrease much more sharply to the surface whereas they remain (relatively) high overall, as a result of mixing.

### 3.4.4. Radionuclide Distribution at the Ravenglass Saltmarsh

Although $^{210}Pb$ is commonly used to date sediments, it cannot be used here due to the input of anthropogenic $^{210}Pb$ to the Irish Sea (McCartney et al., 1990; Kershaw et al., 1992). Instead, as in Morris et al. (2000) and Marsden et al. (2006) the Sellafield discharge record was used to date the Ravenglass sediment core discussed in this study, as the site receives a steady input of sediment with limited physical mixing. A mean sedimentation rate was calculated for Ravenglass, by matching the maximum Pu and Am signals in the sediment core to the maximum signal in the Sellafield discharge record, extrapolating linearly to the sampling date (September 2014) and allowing for a 2 year lag-time (Table 3.1) (Aston and Stanners, 1982; Kershaw et al., 1990). Americium and plutonium were used to derive the sedimentation rate, as Am(III) and Pu(IV) are predominantly thought to associate with Irish Sea sediments (Nelson and Lovett, 1978). A sedimentation rate of 6.8 mm/yr was calculated, similar to those reported in earlier studies: 5.2 mm/yr and 6.9 mm/yr respectively (Morris et al. 2000; Marsden et al. 2006). The average sedimentation rate calculated from the radionuclide data was then used to calculate a chronology for the Ravenglass sediment core.

| Radionuclide | Sedimentation rate (cm/yr) |
|---|---|
| $^{241}$Am | 0.66 |
| $^{239,240}$Pu (1978) | 0.74 |
| $^{239,240}$Pu (1973) | 0.64 |
| $^{238}$Pu (1978) | 0.74 |
| $^{238}$Pu (1973) | 0.64 |
| **Average** | **0.68 ± 0.05 (1σ)** |

**Table 3.1.** Estimated sedimentation rates for the Ravenglass saltmarsh sediment core using maximum releases from the Sellafield authorised discharge record. An average of the particle reactive radionuclides (Am and Pu) has been used. Caesium-137 has been omitted from the calculation as it is highly mobile in the marine environment. As $^{238}$Pu and $^{239,240}$Pu show two peaks in the discharge history, these have both been used here to determine the sedimentation rate (similar to the approach taken by Morris et al., 2000).

The $^{137}$Cs distribution at Ravenglass showed a steady increase in activity for the upper 13 cm of the sediment core with a $^{137}$Cs activity between 700–1800 Bq/kg. Thereafter, there was a sharp increase in activity with depth reaching a maximum activity of ~7200 Bq/kg at a depth of 23 cm (Figure 3.6A). The sharp maximum in the Sellafield discharge record can be seen as a broader feature in the Ravenglass core. The broadening may reflect the relatively low $K_d$ of Cs, with a more important solution input to the sediment profile. Caesium dissolution from bio-mixed mud-patch sediment and gradual transport of solution Cs to Ravenglass may also contribute. The significance of solution transport for $^{137}$Cs has been recognised previously due to its low $K_d$ in environmental systems (Ridgway and Shimmield, 2002) and indeed, the majority (~90 %) of Sellafield derived Cs has probably been transported out of the Irish Sea. However, ~10 % of the discharged Cs is thought to have become associated with the fine-grained mud-patch, and given that Cs tends to associate with sediments by cation exchange in clay interlayers (particularly in illite and vermiculite (Hird et al., 1996; Bradbury and Baeyens, 2000) it can be suggested that bio-mixing of this material followed by physical transport controls Cs deposition at Ravenglass. The

presence of $^{137}$Cs at Ravenglass pre-1970 (at a depth of ~ 30 cm), may suggest diffusive transport of the solution component from areas of higher activity to regions of low activity. The $^{137}$Cs activities observed here agree with Lucey et al. (2004) and Marsden et al. (2006), and are lower than measured by Morris et al. (2000).

The $^{241}$Am distribution at Ravenglass showed a steady increase in activity for the upper 13 cm of the sediment core with $^{241}$Am activity ranging between 1200–1300 Bq/kg (Figure 3.6B). Thereafter, a sharp increase in activity was observed with depth reaching a maximum activity of 12 kBq/kg at 25 cm, and this was at a similar depth to the maximum $^{137}$Cs signal (Figure 3.6B). The gradual input of activity from the mud-patch to Ravenglass is again highlighted by the broad peak observed in the sediment core from 1970 to the early 1990s, in comparison to the well-resolved Sellafield $^{241}$Am discharge signal. Effluent discharge data for $^{241}$Am is available only from 1964 but, based on the accumulation rate for $^{241}$Am, the saltmarsh probably received a $^{241}$Am input from 1966 onwards. This highlights that Sellafield-derived Am is poorly soluble in seawater, and readily associates with the sediment component (Hetherington et al., 1976; Livingston and Bowen, 1977), being transported to Ravenglass *via* sediment surfaces. Our results show $^{241}$Am activity concentrations of a similar magnitude to that of Marsden et al. (2006) and Lucey et al (2004), which may highlight the decreasing importance of $^{241}$Pu decay to the Am concentration (as this would increase with time if $^{241}$Pu was contributing significantly to the $^{241}$Am inventory). The ingrowth of $^{241}$Am from $^{241}$Pu at Ravenglass is discussed in the SI (Text S2 and Figure S4).

The distribution of $^{238}$Pu, and $^{239,240}$Pu at Ravenglass showed a steady increase in activity for the top 11 cm of the sediment core with $^{238}$Pu activity ranging between 140–400 Bq/kg (Figure 3.6C), and $^{239,240}$Pu activity between 800–2000 Bq/kg (Figure 3.6D). Thereafter, a sharp increase in activity was observed with depth, reaching a maximum of 1300 Bq/kg at 21 cm, and $^{239,240}$Pu at 25 cm (7300 Bq/kg). The discharge histories for $^{238}$Pu and $^{239,240}$Pu exhibit two maxima in the 1970s, corresponding to 1973 and 1978 (Gray et al., 1995). There is a broad single peak observed in the $^{238}$Pu and $^{239,240}$Pu Ravenglass profiles, and this may be explained as the time-averaged deposition of the well-resolved Pu discharge signals *via* the mud-patch (as discussed by MacKenzie et al., 1994).

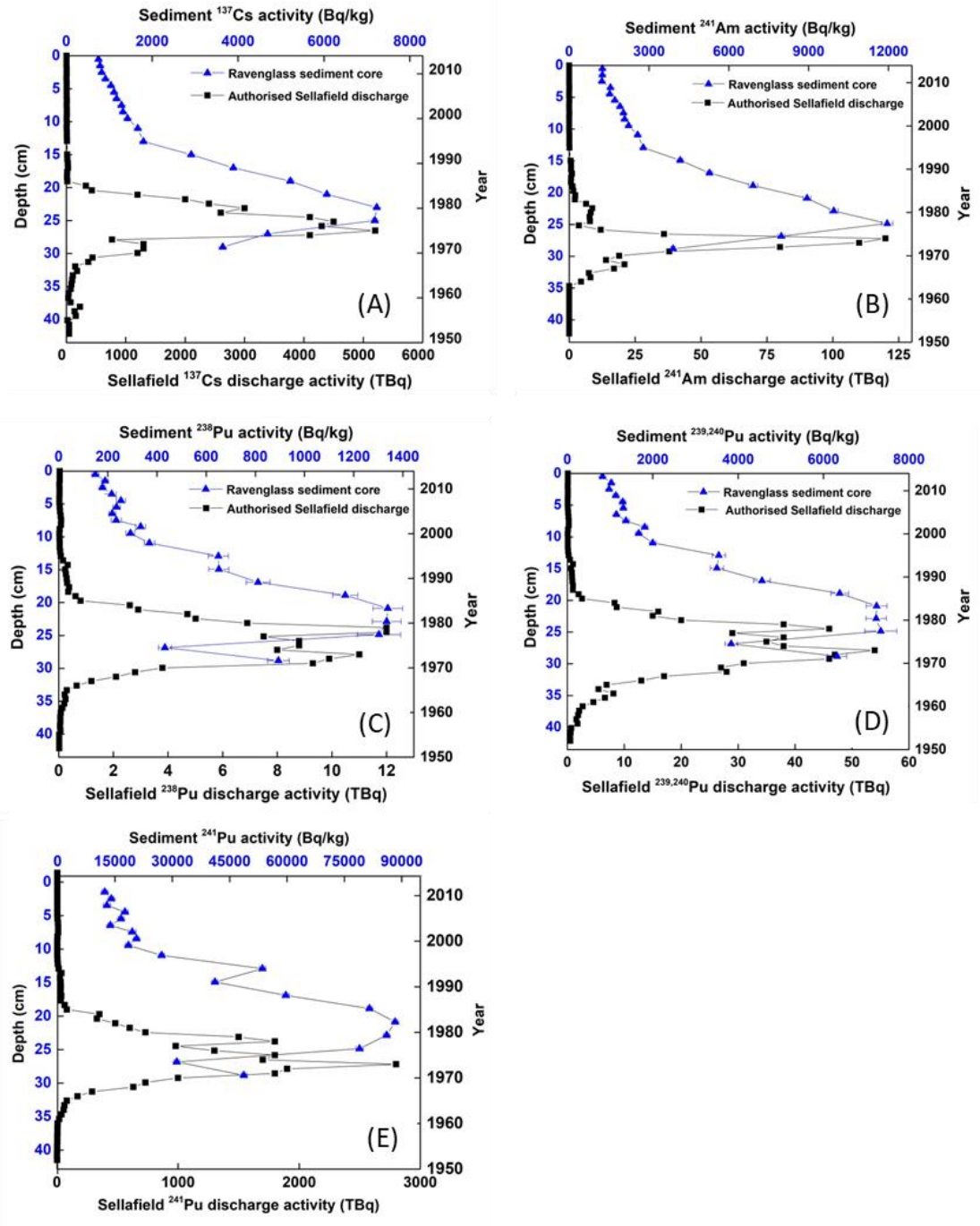


**Figure 3.6.** Activity of (A) $^{137}$Cs; (B) $^{241}$Am; (C) $^{238}$Pu; (D) $^{239,240}$Pu, and (E) $^{241}$Pu in the Ravenglass saltmarsh sediment core (black) dated using the Sellafield discharge history (blue) (error bars are 1σ based on counting errors, and may be smaller than markers).

The resolution of the sediment core here may prevent fine details from the Sellafield record being observed, as each section represents ~2-3 years of effluent

discharges (Morris et al., 2000). Maximum $^{239,240}$Pu values observed at Ravenglass agree with recent studies at the site (Lucey et al., 2004; Lindahl et al., 2011) and are lower than earlier work (Morris et al., 2000; Marsden et al., 2006). In addition, $^{239,240}$Pu activity at the top of the core also agrees well with surface samples taken at Ravenglass (Caborn et al., 2016), where the Pu activity was shown to decrease over period of 25 years, likely as a result of the decline in Sellafield discharges.

The activity of $^{241}$Pu at Ravenglass showed a broadly similar distribution to the other Pu isotopes. There was a steady increase in activity for the top 9 cm of the sediment core with $^{241}$Pu activity ranging between 12–20 kBq/kg (Figure 3.6E). Thereafter, a sharp increase in activity was observed with depth, reaching a maximum activity of ~86 kBq/kg at 23 cm (Figure 3.6E). Here, the authorised Sellafield discharge record showed a single peak due to the elevated release from the Sellafield site in 1973. This peak in discharge seems to be well preserved in the Ravenglass sediment core, with a broader peak than the discharges being observed. Interestingly, the average sedimentation rate used here (from Table 3.1) suggests that the maximum discharge signal arrived at Ravenglass in 1983, and this would imply that $^{241}$Pu has taken ~10 years to be transported from the Sellafield pipeline to the saltmarsh. The time-period observed for other Pu isotopes ($^{238}$Pu and $^{239,240}$Pu) was between 1–3 years (Figure 3.6C and 3.6D). As isotopes of any element will all be travelling at the same rate, it can be confidently suggested that the $^{241}$Pu signal is not due to post-depositional remobilisation (as this is not observed for the other Pu isotopes). Instead, the older/deeper edge of the $^{241}$Pu peak at 27 cm aligns with the same peak in the $^{238}$Pu and $^{239,240}$Pu (Figure 3.6C and 3.6D), and this may suggest that the decay of $^{241}$Pu once deposited at Ravenglass is causing discrepancies in the maximum $^{241}$Pu signal.

### 3.4.5. Pu Association with Fe/Mn at Ravenglass

Plutonium may exist in as many as four oxidation states in the environment: (III), (IV), (V), (VI) (Morse and Choppin, 1991). Here, the fate of Pu depends on the chemical form at the source location, and the geochemistry of the site (Kersting et al., 2013), as this can affect the oxidation state of the species. As Pu released in

the sea tank discharges from Sellafield was mainly present as Fe oxide flocs (Kershaw et al., 1992), there may be co-association of Pu present in the effluent with Fe surfaces (Malcolm et al., 1990). As both Fe/Mn are redox active, their cycling in the environment may result in scavenging (by adsorption or co-precipitation) of contaminants like Pu, or their release upon microbially-mediated metal reduction (Malcolm et al., 1990).

The major $^{239,240}$Pu sub-surface peaks observed at depth (~25 cm) at Ravenglass (Figure 6D), are not located in zones of active Mn/Fe cycling, or in regions with the highest concentrations of reactive Mn/Fe (see Figure 2). This may suggest that Mn/Fe cycling here has little control on Pu distribution in the sediment, similar to previous work (Malcolm et al., 1990). Previous studies have shown Pu to associate with Fe and Mn oxides at the Nevada Test Site (Francis and Dodge, 2015), and with Fe-oxide colloids at Mayak (Novikov et al., 2006). In addition, it has been suggested that Pu in marine sediments should associate with Fe and Mn oxide/hydroxide colloids (Aston and Stanners, 1981). However based on measurements presented here, there is little evidence to suggest such controls are important in Irish Sea estuarine sediments, similar to the observation of Malcolm et al. (1990).

### 3.4.6. Activity Ratios ($^{241}$Am:$^{239,240}$Pu and $^{238}$Pu:$^{239,240}$Pu)

Comparison of the radionuclide activity ratios at Ravenglass with the Sellafield discharge record can provide information on the behaviour of radionuclides. Thus, if a simple mechanism of accumulation of sediment is taking place at Ravenglass (based on the calculated sedimentation rate), in proportion to effluent releases, then activity ratios in the sediment core at depth should match those of the Sellafield discharge history (MacKenzie et al., 1994). Any variance may suggest the vertical mixing of waste of different ages either prior to deposition, or post-depositional mixing. The activity ratio of $^{241}$Am:$^{239,240}$Pu at Ravenglass was ~1–2 throughout the core, reaching 0.5 at the bottom of the core. This was similar to the $^{241}$Am:$^{239,240}$Pu ratio in the Sellafield discharge history (~ 0.1–3.0; 1964–2014) (Table S4), and this may highlight the limited remobilisation of these radionuclides at Ravenglass. Caesium ratios at Ravenglass were not compared

with the Sellafield history as Cs is highly soluble, and as such the majority of the discharged inventory has been transported out of the Irish Sea area.

The $^{238}$Pu:$^{239,240}$Pu activity ratios can provide information on the source of Pu. The $^{238}$Pu:$^{239,240}$Pu activity ratios for samples in the mud-patch core were between 0.15–0.21 (Figure S5A). This suggests that the origin of Pu is not from legacy UK weapons program (as this would have an activity ratio of <0.03), and instead originates from Sellafield discharges (Kershaw et al., 1995). The $^{238}$Pu:$^{239,240}$Pu activity ratios for Ravenglass range between 0.11–0.20 (Figure S5B), and this was slightly lower than $^{238}$Pu:$^{239,240}$Pu activity ratios in the Sellafield discharge history which have been ~ 0.33 since 1979 (Table S4). This ratio highlights that the source of Pu deposited at Ravenglass arises from civil nuclear operations, with no indication of the presence of lower burn-up material. In addition, lower ratios (0.1–0.14) observed at the bottom of the Ravenglass core may reflect some Pu remobilisation in older, deeper sections (~ 26–30 cm) of the core. The examination of a deeper core at the site would be required to determine whether $^{238}$Pu:$^{239,240}$Pu activity ratios continue to decline.

### 3.4.7. Mathematical model

The distribution profiles of measured $^{239,240}$Pu activities for the mud-patch were compared to modelled outputs (Figure 3.7). The model was shown to provide a better fit to the experimental data when a higher diffusion coefficient ($9.5 \times 10^{-7}$ cm$^2$/s; Figure 3.7A) was used compared to that used previously by Marsden et al. (2006) ($9.5 \times 10^{-8}$ cm$^2$/s; Figure 3.7B). Using the value employed by Marsden and co-workers resulted in a predicted $^{239,240}$Pu maximum that was 30 cm shallower (Figure 3.7B) than the $^{239,240}$Pu maxima obtained when using the higher diffusion coefficient (Figure 3.7A). The higher diffusion coefficient (Figure 3.7A) provided a better match to experimental data in the upper 20 cm of the sediment core and also more accurately predicted the depth of the $^{239,240}$Pu maxima.

There was however an overestimation in $^{239,240}$Pu activity at depth (58–110 cm). The model outputs from this study suggest that bioturbation may have been underpresented by Marsden and colleagues who used historical mud-patch data to calibrate the model. These results may suggest that biortubation at the mud-patch is more dynamic in nature (the magnitude decreases and increases). In addition,

this work may suggest that the use of a pseudo diffusion coefficient, solely, to model the physical mixing at the mud-patch is limited. Storms and tidal resuspension processes are also likely to be very important as they disturb the upper layers of the mud-patch sediment, leading to redistribution of sediment to the coast and elsewhere in the Irish Sea. The output of the model run shown in Figure 3.7A was used to predict the Ravenglass saltmarsh $^{239,240}$Pu profile (Figure 3.7C). This showed a good qualitative fit with the broad $^{239,240}$Pu peak observed experimentally at depth (20–26 cm), again indicating that the deposition of Sellafield derived Pu, and by inference $^{137}$Cs and $^{241}$Am, at the mud-patch is then followed by resuspension, transport, and deposition at Ravenglass (i.e. there does not appear to be any biogeochemical control on Pu deposition). It is important to note that the resulting Ravenglass profile (Figure 3.7) assumes Pu-contaminated sediment input solely from the mud-patch, however in reality there will also be direct, continuous longshore transport from the Sellafield pipeline.

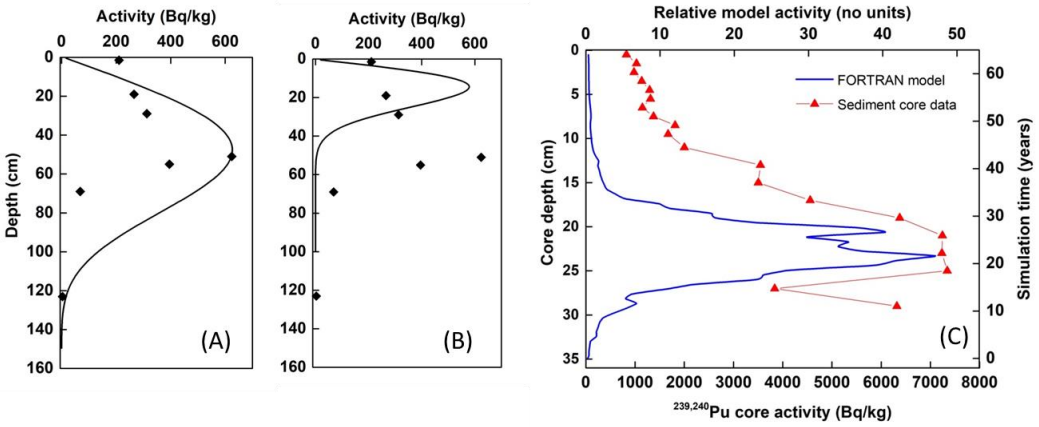


**Figure 3.7**. The distribution of $^{239,240}$Pu at the Irish Sea mud-patch using a diffusion coefficient of: (A) 9.5 x $10^{-7}$ $cm^2/s$; (B) 9.5 x $10^{-8}$ $cm^2/s$ (a scaling factor of 154 was applied to these model outputs to obtain the best fit i.e. a qualitative comparison was provided, rather than absolute activity); (C) mathematical model vs. sediment core $^{239,240}$Pu distribution for the Ravenglass saltmarsh (model activity (blue) vs. simulation time (red)).

### 3.5. Conclusions and Implications

Caesium, Pu, and $^{241}$Am containing low-level aqueous effluent is discharged under permit from the Sellafield site into the Eastern Irish Sea. Prior to improvements in effluent treatment at the Sellafield site (1980s), discharged activities were much higher. Regardless, at the point of discharge, Pu, $^{241}$Am, and some $^{137}$Cs associates with offshore fine-grained sediments at the Irish Sea mud-patch. Plutonium distribution at this site appears to be independent of Mn and Fe bio-cycling; instead Pu (and $^{137}$Cs and $^{241}$Am) distribution is controlled by bio-mixing at the site. This in turn re-suspends radiolabelled sediments, which are then transported elsewhere in the Irish Sea. The nearby Ravenglass saltmarsh has received and still appears to receive a supply of radiolabelled sediment from the mud-patch. At this site, Pu distribution again appears to be independent of Mn and Fe bio-cycling. As such, the commonly observed association and reaction of Pu with these ubiquitous environmental phases in constrained laboratory experiments are not manifest at these natural laboratory sites. Instead, Pu distribution at Ravenglass appears to be largely controlled by physical processes (sedimentation at the mud-patch followed by later bio-mixing, re-suspension, sediment transport, and eventual re-deposition). The same processes appear to control $^{137}$Cs and $^{241}$Am distribution at Ravenglass and after sedimentation there appears to be limited radionuclide remobilisation, and instead the radionuclide activity depth profiles mimic the time-integrated Sellafield discharge records. These findings for the Ravenglass saltmarsh are consistent with those of past workers (Morris et al., 2000; Lucey et al., 2004; Marsden et al., 2006; Lindahl et al., 2011) and as such, the $^{137}$Cs, $^{241}$Am, and Pu activity maxima should be further buried with time. However, a key observation from this work is the presence of $^{137}$Cs, $^{241}$Am, and Pu in the surface sediments of the Irish Sea mud-patch, in contrast to the low contemporary activity release from the Sellafield site. This suggests that bioturbation at this site will continue to act as a source of anthropogenic radioactivity to the UK Coastal Environment. Further, this finding is pertinent at present as construction of the proposed Moorside Nuclear Power Plant near Sellafield may disturb areas of the local seabed during site investigation/construction.

## References


Al-Qasmi, H., Law, G.T.W., Fifield, L.K., Livens, F.R., 2016. Origin of artificial radionuclides in soil and sediment from North Wales. J. Environ. Radioactiv. 151, 244–249.

Al-Qasmi, H., Law, G.T.W., Fifield, L.K., Howe, J., Brand, T., Cowie, G.L., Law, K.A., Livens, F.R., 2017. Deposition of artificial radionuclides in sediments of Loch Etive, Scotland. J. Environ. Radioactiv. (In press).

Aston, S.R., Stanners, D.A., 1981. Americium in intertidal sediments from the coastal environs of Windscale. Mar. Pollut. Bull. 12, 149–153.

Aston, S.R., Stanners, D.A., 1981. Plutonium transport to and deposition and immobility in Irish Sea intertidal sediments. Nature. 289, 581–582.

Aston, S.R., Stanners, D.A., 1982. The transport to and deposition of americium in intertidal sediments of the Ravenglass estuary and its relationship to plutonium. Environ. Pollut. Ser. B. 3, 1–9.

Baldani, J.I., Videira, S.S., dos Santos Teixeira, K.R., Reis, V.M., Martinez de Oliveria, A.L., Schwab, S., de Souza E.M., Pedraza, R.O., Baldani, V.L.D., Hartmann, A., 2014. The family *Rhodospirillaceae*, in: The Prokaryotes. 4th ed, Springer, 553–618.

Baxter, M.S., McKinley, I., MacKenzie, A., Jack, W., 1979. Windscale radiocaesium in the Clyde Sea area. Mar. Pollut. Bull. 10, 116–120.

Bradbury, M.H., Baeyens, B., 2000. A generalised sorption model for the concentration dependent uptake of caesium by argillaceous rocks. J. Contam. Hydrol. 42, 141–163.

Burdige, D.J., 1993. The biogeochemistry of manganese and iron reduction in marine sediments. Earth. Science. Rev. 35, 249–284.

Caborn, J.A., Howard, B.J., Blowers, P., Wright, S.M., 2016. Spatial trends on an ungrazed West Cumbrian saltmarsh of surface contamination by selected radionuclides over a 25 year period. J. Environ. Radioactiv. 151, 94–104.

Calvert, S., Pedersen, T., 1993. Geochemistry of recent oxic and anoxic marine sediments: implications for the geological record. Mar. Geol. 113, 67–88.

Caporaso, J.G., Kuczynski, J., Stombaugh, J., Bittinger, K., Bushman, F.D., Costello, E.K., Fierer, N., Gonzalez Peña, A., Goodrich, J.K., Gordon, J.I., Huttley, G.A., Kelley, S.T., Knights, D., Koenig, J.E., Ley, R.E., Lozupone, C.A., McDonald, D., Muegge, B.D., Pirrung, M., Reeder, J., Sevinsky, J.R., Turnbaugh, P.J., Walters, W.A., Widmann, J., Yatsunenko, T., Zaneveld, J., Knight, R., 2010. QIIME allows analysis of high-throughput community sequencing data. Nat. Methods. 7 (5), 335–336.

Carr, A., Blackley, M.W.L., 1986. Implications of sedimentological and hydrological processes on the distribution of radionuclides: the example of a saltmarsh near Ravenglass, Cumbria. Estuar. Coast. Shelf. S. 22, 529–543.

Clarke, K.R., Gorley, R., 2009. PRIMER: Getting started with v6. Plymouth marine laboratory, 1–10.

Cook, G.T., MacKenzie, A.B., McDonald, P., Jones, S.R., 1997. Remobilization of Sellafield-derived radionuclides and transport from the North-East Irish Sea. J. Environ. Radioactiv. 35, 227–241.

Day, J.P., Cross, J.E., 1981. $^{241}$Am from the decay of $^{241}$Pu in the Irish Sea. Nature. 292, 43–45.

Evans, P.N., Parks, D.H., Chadwick, G.L., Robbins, S.J., Orphan, V.J., Golding, S.D., Tyson, G.W., 2015. Methane metabolism in the archaeal phylum *Bathyarchaeota* revealed by genome-centric metagenomics. Science. 350 (6529), 434–438.

Fjeld, R.A., Serkiz, S.M., McGinnis, P.L., Elci, A., Kaplan, D.I., 2003. Evaluation of a conceptual model for the subsurface transport of plutonium involving surface mediated reduction of Pu(V) to Pu(IV). J. Contam. Hydrol. 67, 79–94.

Francis, A.J., Dodge, C.J., 2015. Microbial mobilization of plutonium and other actinides from contaminated soil. J. Environ. Radioactiv. 150, 277–285.

Froelich, P.N., Klinkhammer, G.P., Bender, M.L., Luedtke, N.A., Heath, G.R., Cullen, D., Dauphin, P., Hammond, D., Hartman, B., Maynard, V., 1979. Early oxidation of organic matter in pelagic sediments of the Eastern equatorial Atlantic: suboxic diagenesis. Geochim. Cosmochim. Ac. 43, 1075–1090.

Gray, J., Jones, S.R., Smith, A.D., 1995. Discharges to the environment from the Sellafield site, 1951–1992. J. Radiol. Prot. 15, 99–131.

Halcrow Ltd., 2013. Ravenglass estuary complex. Sefton Council.1–91.

Hamilton, E.I., Clarke, K.R., 1984. The recent sedimentation history of the Esk estuary, Cumbria, U.K: The application of radiochronology. Sci. Total. Environ. 35, 325–386.

Hetherington, J.A., Jefferies, D.F., Mitchell, N.T., Pentreath, R.J., Woodhead, D.S., 1976. Proceedings of the symposium on transuranium nuclides in the environment. IAEA. 139–153.

Hetherington, J.A., Harvey, B., 1978. Uptake of radioactivity by marine sediments and implications for monitoring metal pollutants. Mar. Pollut. Bull. 9, 102–106.

Hird, A.B., Rimmer, D.L., Livens, F.R., 1996. Factors affecting the sorption and fixation of caesium in acid organic soil. Eur. J. Soil. Sci. 47, 97–104.

Icopini, G.A., Lack, J.G., Hersman, L.E., Neu, M.P., Boukhalfa, H., 2009. Plutonium(V/VI) reduction by the metal-reducing bacteria *Geobacter metallireducens* GS-15 and *Shewanella oneidensis* MR-1. Appl. Environ. Microb. 75, 3641–3647.

Jones, D., Roberts, P., Strutt, M., Higgo, J., Davis, J., 1999. Distribution of Cs

and inventories of Pu, Am and Cs in Irish Sea intertidal sediments. J. Environ. Radioactiv. 44, 159–189.

Keeney-Kennicutt, W.L., Morse, J.W., 1985. The redox chemistry of $Pu(V)O_2^+$ interaction with common mineral surfaces in dilute solutions and seawater. Geochimica. Cosmochim. Ac. 49, 2577–2588.

Keogh, S.M., Aldahan, A., Possnert, G., Finegan, P., León Vintró, L., Mitchell, P.I., 2007. Trends in the spatial and temporal distribution of $^{129}I$ and $^{99}Tc$ in coastal waters surrounding Ireland using *Fucus vesiculosus* as a bio-indicator. J. Environ. Radioactiv. 95, 23–38.

Kershaw, P.J., Swift, D.J., Pentreath, R.J., Lovett, M.B., 1983. Plutonium redistribution by biological activity in Irish Sea sediments. Nature. 306, 774–775.

Kershaw, P.J., 1984. The incorporation of plutonium, americium and curium into the Irish Sea seabed by biological activity. Sci. Total. Environ. 40. 61–81.

Kershaw, P.J., Woodhead, D.S., Malcolm, S.J., Allington, D.J., Lovett, M.B., 1990. A sediment history of Sellafield discharges. J. Environ. Radioactiv. 12, 201–241.

Kershaw, P.J., Pentreath, R.J., Woodhead, D.S., Hunt, G.J., 1992. A review of radioactivity in the Irish Sea, in: Aquatic Environmental Monitoring Report. Lowestoft, UK, MAFF Directorate of Fisheries Research. 32, 1–66.

Kershaw, P.J., Baxter, A., 1995. The transfer of reprocessing wastes from North-West Europe to the Arctic. Deep-Sea. Res. Pt. II. 42 (6), 1413–1448.

Kershaw, P.J., Woodhead, D.S., Lovett, M.B., Leonard, K.S., 1995. Plutonium from European reprocessing operations–its behaviour in the marine environment. Appl. Radiat. Isotopes. 46, 1121–1134.

Kershaw, P.J., Denoon, D.C., Woodhead, D.S., 1999. Observations on the redistribution of plutonium and americium in the Irish Sea sediments, 1978 to 1996: concentrations and inventories. J. Environ. Radioactiv. 44, 191–221.

Kersting, A.B., 2013. Plutonium transport in the environment. Inorg. Chem. 52, 3533–3546.

Kuever, J., 2014a. The family *Desulfobacteraceae,* in: The Prokaryotes. 4th ed, Springer, 617–625.

Kuever, J., 2014b. The family *Syntrophobacteraceae*, in: The Prokaryoates. 4th ed, Springer, 289–299.

Law, G.T.W., Shimmield, T.M., Shimmield, G.B., Cowie, G.L., Breuer, E.R., Harvey, M.S., 2009. Manganese, iron, and sulphur cycling on the Pakistan margin. Deep-Sea. Res. Pt II. 56, 305–323.

Lindahl, P., Worsfold, P., Keith-Roach, M., Andersen, M. B., Kershaw, P., Leonard, K., Choi, M.-S., Boust, D., Lesueur, P., 2011. Temporal record of Pu isotopes in intertidal sediments from the North Eastern Irish Sea. Sci. Total. Environ. 409 (23), 5020–5025.

Livingston, H.D., Bowen, V.T., 1977. Windscale effluent in the waters and sediments of the Minch. Nature. 269, 586–588.

Lucey, J.A., Gouzy, A., Boust, D., Leon Vintro, L., Bowden, L., Finegan, P.P., Kershaw, P.J., Mitchell, P.I., 2004. Geochemical fractionation of plutonium in anoxic Irish Sea sediments using an optimised sequential extraction protocol. Appl. Radiat. Isotopes. 60, 379–385.

MacKenzie, A., Scott, R., Allan, R.L., Ben Shaban, Y.A., Cook, G.T., Pulford, I.D., 1994. Sediment radionuclide profiles: implications for mechanisms of Sellafield waste dispersal in the Irish Sea. J. Environ. Radioactiv. 23, 39–69.

MacKenzie, A.B., Scott, R.D., 1993. Sellafield waste radionuclides in Irish sea intertidal and salt marsh sediments. Environ. Geochem. Hlth. 15 (2/3),173–183.

MacKenzie, A.B., Cook, G.T., McDonald, P., 1999. Radionuclide distributions and particle size associations in Irish Sea surface sediments: implications for actinide dispersion. J. Environ. Radioactiv. 44, 275–296.

Malcolm, S.J., Kershaw, P.J., Cromar, N.J., Botham, L., 1990. Iron and manganese geochemistry and the distribution of $^{239,240}$Pu and $^{241}$Am in the sediments of the North- East Irish Sea. Sci. Total. Environ. 95, 69–87.

Malcolm, S.J., Kershaw, P.J., Lovett, M.B., Harvey, B.R., 1990. The interstitial water chemistry of $^{239,240}$Pu and $^{241}$Am in the sediments of the North-East Irish Sea. Geochim. Cosmochim. Ac. 54, 29–35.

Marsden, O.J., Abrahamsen, L., Bryan, N.D., Day, J. P., Fifield, K.L., Gent, C., Goodall, P.S., Morris, K., Livens, F.R., 2006. Transport and accumulation of actinide elements in the near-shore environment: field and modelling studies. Sedimentology. 53, 237–248.

McBride, M.J., 2014. The family *Flavobacteriaceae*, in: The Prokaryotes. 4$^{th}$ ed , Springer. 644–676.

McCartney, M., Kershaw, P.J., Allington, D.J., 1990. The behaviour of $^{210}$Pb and $^{226}$Ra in the Eastern Irish Sea. J. Environ. Radioactiv. 12, 243–265.

McCartney, M., Kershaw, P.J., Woodhead, D.S., Denoon, D.C., 1994. Artificial radionuclides in the surface sediments of the Irish Sea, 1968–1988. Sci. Total. Environ. 141, 103–138.

Mcllroy, S., Nielsen, P., 2014. The family *Saprospiraceae*, in: The Prokaryotes. 4$^{th}$ ed, Springer. 863–889.

Morgenstern, A., Choppin, G.R., 2002. Kinetics of the oxidation of Pu(IV) by manganese dioxide. Radiochim. Acta. 90, 69–74.

Morris, K., Butterworth, J.C., Livens, F.R., 2000. Evidence for the remobilization of Sellafield waste radionuclides in an intertidal salt marsh, West Cumbria, U.K. Estuar. Coast. Shelf S. 51, 613–625.

Morse, J.W., Choppin, G.R., 1991. The chemistry of transuranic elements in natural waters. Rev. Aquat. Sci. 4, 1–22.

Nelson, D.M., Lovett, M.B., 1978. Oxidation state of plutonium in the Irish Sea. Nature. 276, 599–601

Novikov, A., Kalmykov, S., Utsunomiya, S., Ewing, R., Horreard, F., Merkulov, A., Clark, S., Tkachev, V., Myasoedov, B., 2006. Colloid transport of plutonium in the far-field of the Mayak production association, Russia. Science. 314, 638–641.

Nygren, U., Rodushkin, I., Nilsson, C., Baxter, D.C., 2003. Separation of plutonium from soil and sediment prior to determination by inductively coupled plasma mass spectrometry. J. Anal. Atom. Spectrom. 18, 1426–1434.

Oh. J.-S., Warwick, P.E., Croudace, I.W., 2009. Spatial distribution of $^{241}$Am, $^{137}$Cs, $^{238}$Pu, $^{239,240}$Pu and $^{241}$Pu over 17 year periods in the Ravenglass saltmarsh, Cumbria, UK. Appl. Radiat. Isotopes. 67, 1484–1492.

Oren, A., Xu, X., 2014. The family *Hyphomicrobiaceae*, in: The Prokaryotes. Springer, 4th ed. 901–918.

Powell, B.A., Fjeld, R.A., Kaplan, D.I., Coates, J.T., Serkiz, S.M., 2005. $Pu(V)O_2$ adsorption and reduction by synthetic hematite and goethite. Environ. Sci. Technol. 39, 2107–2114.

Quast, C., Pruesse, E., Yilmaz, P., Gerken, J., Schweer, T., Yarza, P., Peplies, J., Glöckner, F.O., 2012. The SILVA ribosomal RNA gene database project: improved data processing and web-based tools. Nucleic. Acids. Res. 41, 591–596.

Renshaw, J.C., Law, N., Geissler, A., Livens, F.R., Lloyd, J.R., 2009. Impact of the Fe(III)-reducing bacteria *Geobacter sulfurreducens* and *Shewanella oneidensis* on the speciation of plutonium. Biogeochemistry. 94, 191–196.

Ridgway, J., Shimmield, G.B., 2002. Estuaries as repositories of historical contamination and their impact on shelf seas. Estuar. Coast. Shelf. S. 55, 903–928.

Romanenko, L.A., Tanaka, N., Frolova, G.M., Mikhailov, V. V., Lyudmila, C., Romanenko, A., 2009. *Psychrobacter fulvigenes* sp. nov., isolated from a marine crustacean from the Sea of Japan. Int. J. Syst. Evol. Microbiol. 59, 1480–1486.

Rowell, D.L., 1994. Soil Science: methods and applications, 1st ed. Pearson Education Limited.

Sanchez, A.L., Murray, J.W., Sibley, T.H., 1985. The adsorption of plutonium IV and V on goethite. Geochim. Cosmochim. Ac. 49, 2297–2307.

Sellafield Ltd, 2005–2015. Monitoring our environment: discharges and environmental monitoring.

Sellafield Ltd, 2017. Monitoring our environment: discharges and environmental monitoring.

Shaughnessy, D., Nitsche, H., Booth, C., Shuh, D., Waychuna, G., Wilson, R., Gill, H., Cantrell, K., Serne, R., 2003. Molecular interfacial reactions between Pu(VI) and manganese oxide minerals manganite and hausmannite. Environ. Sci.

Technol. 37, 3367–3374.

Shivaji, S., Srinivas, T.N.R., 2014. The family *Planococcaceae*, in: The Prokaryotes. 4th ed, Springer. 303–351.

Swan, B.K., Chaffin, M.D., Martinez-Garcia, M., Morrison, H.G., Field, E.K., Poulton, N.J., Dashiell, E., Masland, P., Harris, C.C., Sczyrba, A., Chain, P.S.G., Koren, S., Woyke, T., Stepanauskas, R., Randau, L., 2014. Genomic and metabolic diversity of marine Group I *Thaumarchaeota* in the mesopelagic of two subtropical gyres. PLOS. ONE. 9 (4), 1–9

Teixeira, L., Merquior, V., 2014. The family *Moraxellaceae*, in: The Prokaryotes. 4th ed, Springer. 442–476.

Thauer, R.K., Jungermann, K., Decker, K., 1977. Energy conservation in chemotrophic anaerobic bacteria. Bacteriol. Rev. 41, 100–180.

Willems, A., 2014. The family *Phyllobacteriaceae*, in: The Prokaryotes. 4th ed, Springer, 356–418.

Yamada, T., Sekiguchi, Y., Hanada, S., Imachi, H., Ohashi, A., Harada, H., Kamagata, Y., 2006. *Anaerolinea thermolimosa* sp. nov., *Levilinea saccharolytica* gen. nov., sp. nov. and *Leptolinea tardivitalis* gen. nov., sp. nov., novel filamentous anaerobes, and description of the new classes *Anaerolineae* classis nov. and *Caldilineae* classis nov. in the bacterial phylum *Chloroflexi*. Int. J. Syst. Evol. Microbiol. 56, 1331–1340.

# Supporting information for: Controls on Anthropogenic Radionuclide Distribution in the Sellafield-Impacted Eastern Irish Sea

Daisy Ray[1/2], Francis R. Livens[1/2], Peter Leary[3], Katherine Morris[2], Neil Gray[3], Liam Abrahamsen-Mills[4], Graham K. P. Muir[5], Kathleen A. Law[1], Adam J. Fuller[1], Nick D. Bryan[4], John A. Howe[6], Gordon T. Cook[5], Gareth T. W. Law[1/2*]

1. Centre for Radiochemistry Research, School of Chemistry, The University of Manchester, Manchester, M13 9PL, UK.

2. Research Centre for Radwaste and Decommissioning and Williamson Research Centre, School of Earth and Environmental Sciences, The University of Manchester, Manchester, M13 9PL, UK.

3. School of Natural and Environmental Sciences, Newcastle University, Newcastle, NE1 7RU, UK.

4. National Nuclear Laboratory, Chadwick House, Birchwood, Warrington, WA3 6AE, UK.

5. Scottish Universities Environmental Research Centre, Scottish Enterprise Technology Park, East Kilbride, G75 0QF, UK.

6. Scottish Association for Marine Science, Dunstaffnage Marine Laboratories, Oban, Argyll, PA37 1QA, UK.

*Corresponding author. Email: gareth.law@manchester.ac.uk; Tel: +44 (0)161 306 0514

**Text S1: Summary of FORTRAN mathematical model**

The FORTRAN model used in this work is based on the assumption that a simple diffusion process can be used to simulate the effects of bioturbation within the Irish Sea mud-patch. The Sellafield discharge history for $^{239,240}$Pu acts as the input to the model (Gray et al., 1995; Sellafield, 1993–2014) (Table S3). The Sellafield authorised discharge data is published as the total activity for a range of radionuclides per year, and this is interpolated for each model time step (10 per year). The model considers a 1-dimensional column of 150 cells, each with a thickness of 1 cm, which represents the upper 1.5 m of the mud-patch. At the start of the simulation (representing the first year that discharge data is available; 1952), the column is free of contamination. At each time step, the discharged activity enters the top of the column and diffusion occurs between all adjacent model cells, according to Fick's law of diffusion. This results in a net migration of radioactivity down the column with time. To represent bioturbation, the diffusion coefficient is constant in the top 10 cm, followed by a linear decrease to zero at 150 cm. In this work, the model has been run to simulate the evolving mud-patch profile between 1952 and 2014 (date of the core sample collection), in order to make comparisons with the latest experimental data. It should be noted that the model considers an 'average' location within the mud-patch and does not account for any lateral variability in observed activity profiles. Additionally, it is scalar or relative in nature, since it is not possible to calculate the fraction of the discharged activity that would be deposited on a particular section of the mud-patch. It does not account for any radioactive decay or in-growth.

The model is also used to make predictions about the accumulation of re-suspended activity deposited through tidal inundations at the Ravenglass saltmarsh. This is achieved by averaging the predicted activity in the top 5 cm of the mud-patch and assuming that this sediment is subject to continuous re-suspension and subsequent deposition at the saltmarsh. However, the model does not explicitly simulate this re-suspension and the material is not removed from the simulated column of sediment. Rather, the predicted profile of the Ravenglass saltmarsh is a reflection of the top 5 cm of the mud-patch column with time.

There are two uncertain parameters associated with the model: (i) diffusion coefficient ($D_z$) and (ii) resuspension depth (d). For this work two diffusion coefficients ($9.5 \times 10^{-8}$ $cm^2/s$) used by Marsden et al. (2006), and $9.5 \times 10^{-7}$ $cm^2/s$ were used to simulate the magnitude of bioturbation taking place at the Irish Sea mud-patch. A re-supension depth of 5 cm was used for this work, as this was shown by Marsden et al. (2006) to be an optimum value. Thus, the top 5 cm of the mud-patch surface material was used to calculate the activity that would be transported to the Ravenglass saltmarsh for accumulation.

| Depth (cm) | Total Organic Matter | Si | Al | K | P | Mg |
|---|---|---|---|---|---|---|
| 0.5 | 0.67 | 26.93 | 5.85 | 2.51 | 0.09 | 1.46 |
| 1-2 | 1.33 | 26.07 | 6.25 | 2.60 | 0.10 | 1.57 |
| 2-3 | 1.33 | 24.93 | 6.72 | 2.63 | 0.10 | 1.70 |
| 3-4 | 0.67 | 26.08 | 6.45 | 2.58 | 0.09 | 1.64 |
| 4-5 | 0.67 | 25.95 | 6.75 | 2.72 | 0.10 | 1.62 |
| 5-6 | 1.33 | 25.86 | 3.73 | 1.16 | 0.04 | 0.93 |
| 6-7 | 1.33 | 25.32 | 6.81 | 2.75 | 0.10 | 1.70 |
| 7-8 | 0.67 | 26.28 | 6.78 | 2.69 | 0.09 | 1.61 |
| 8-9 | 0.67 | 25.83 | 7.23 | 2.77 | 0.09 | 1.72 |
| 9-10 | 0.67 | 25.64 | 6.99 | 2.76 | 0.09 | 1.72 |
| 10-12 | 0.00 | 26.25 | 7.14 | 2.80 | 0.09 | 1.70 |
| 12-14 | 0.00 | 26.33 | 7.73 | 2.83 | 0.09 | 1.78 |
| 14-16 | 0.67 | 25.79 | 8.05 | 2.71 | 0.09 | 1.95 |
| 16-18 | 0.00 | 26.82 | 7.04 | 2.48 | 0.08 | 1.70 |
| 18-20 | 0.67 | 26.30 | 7.37 | 2.62 | 0.08 | 1.78 |
| 20-22 | 0.00 | 25.94 | 7.34 | 2.58 | 0.08 | 1.81 |
| 22-24 | 0.67 | 26.21 | 7.63 | 2.66 | 0.08 | 1.83 |
| 24-26 | 1.33 | 26.36 | 7.32 | 2.64 | 0.08 | 1.77 |
| 26-28 | 0.67 | 26.52 | 7.25 | 2.60 | 0.09 | 1.74 |
| 28-30 | 0.67 | 27.15 | 7.10 | 2.54 | 0.08 | 1.71 |
| 30-32 | 0.66 | 26.16 | 7.44 | 2.69 | 0.08 | 1.77 |
| 32-34 | 0.67 | 26.70 | 7.08 | 2.55 | 0.07 | 1.73 |
| 34-36 | 0.67 | 26.38 | 7.35 | 2.65 | 0.08 | 1.76 |

**Table S1**. Concentration of Total Organic Matter and stable elements (Si, Al, K, P, Mg in wt %) for the Irish Sea mud-patch sediment core.

| Depth (cm) | Total Organic Matter | Si | Al | K | P | Mg |
|---|---|---|---|---|---|---|
| 0-1 | 7.14 | 22.23 | 7.15 | 2.62 | 0.12 | 1.88 |
| 1-2 | 6.36 | 23.35 | 7.63 | 2.77 | 0.13 | 1.89 |
| 2-3 | 6.18 | 23.86 | 7.96 | 2.78 | 0.13 | 1.90 |
| 3-4 | 6.18 | 24.20 | 8.06 | 2.77 | 0.13 | 1.88 |
| 4-5 | 6.18 | 24.47 | 8.21 | 2.90 | 0.14 | 1.85 |
| 5-6 | 5.94 | 24.25 | 8.15 | 2.82 | 0.13 | 1.84 |
| 6-7 | 5.45 | 24.78 | 8.35 | 2.93 | 0.14 | 1.87 |
| 7-8 | 4.91 | 24.96 | 8.41 | 2.87 | 0.13 | 1.87 |
| 8-9 | 4.91 | 24.92 | 8.43 | 2.92 | 0.14 | 1.88 |
| 9-10 | 4.73 | 24.66 | 8.38 | 2.90 | 0.15 | 1.87 |
| 10-12 | 4.68 | 25.20 | 8.62 | 2.93 | 0.15 | 1.91 |
| 12-14 | 3.82 | 25.08 | 8.59 | 2.93 | 0.16 | 1.92 |
| 14-16 | 4.12 | 25.41 | 8.60 | 2.95 | 0.16 | 1.87 |
| 16-18 | 4.36 | 25.48 | 8.51 | 2.91 | 0.15 | 1.87 |
| 18-20 | 3.97 | 25.67 | 8.56 | 2.88 | 0.15 | 1.85 |
| 20-22 | 4.36 | 25.71 | 8.57 | 2.87 | 0.15 | 1.86 |
| 22-24 | 3.99 | 25.74 | 8.64 | 2.90 | 0.13 | 1.86 |
| 24-26 | 3.83 | 25.90 | 8.65 | 2.90 | 0.14 | 1.87 |
| 26-28 | 4.18 | 25.92 | 8.47 | 2.86 | 0.14 | 1.81 |
| 28-30 | 3.27 | 25.95 | 8.43 | 2.86 | 0.14 | 1.81 |

**Table S2**. Concentration of Total Organic Matter and stable elements (Si, Al, K, P, Mg in wt %) for the Ravenglass saltmarsh sediment core.

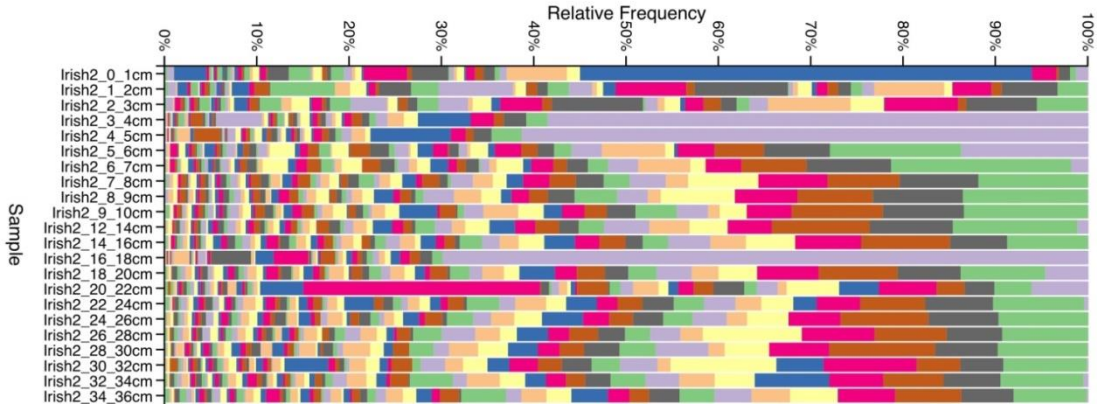
Relative Frequency
0%
10%
20%
30%
40%
50%
60%
70%
80%
90%
100%
Sample
Irish2_0_1cm
Irish2_1_2cm
Irish2_2_3cm
Irish2_3_4cm
Irish2_4_5cm
Irish2_5_6cm
Irish2_6_7cm
Irish2_7_8cm
Irish2_8_9cm
Irish2_9_10cm
Irish2_12_14cm
Irish2_14_16cm
Irish2_16_18cm
Irish2_18_20cm
Irish2_20_22cm
Irish2_22_24cm
Irish2_24_26cm
Irish2_26_28cm
Irish2_28_30cm
Irish2_30_32cm
Irish2_32_34cm
Irish2_34_36cm

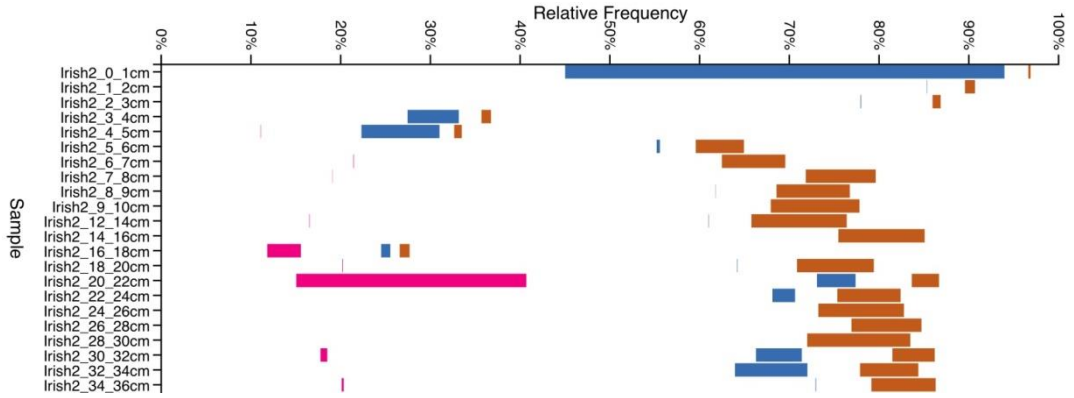
Relative Frequency
0%
10%
20%
30%
40%
50%
60%
70%
80%
90%
100%
Sample
Irish2_0_1cm
Irish2_1_2cm
Irish2_2_3cm
Irish2_3_4cm
Irish2_4_5cm
Irish2_5_6cm
Irish2_6_7cm
Irish2_7_8cm
Irish2_8_9cm
Irish2_9_10cm
Irish2_12_14cm
Irish2_14_16cm
Irish2_16_18cm
Irish2_18_20cm
Irish2_20_22cm
Irish2_22_24cm
Irish2_24_26cm
Irish2_26_28cm
Irish2_28_30cm
Irish2_30_32cm
Irish2_32_34cm
Irish2_34_36cm

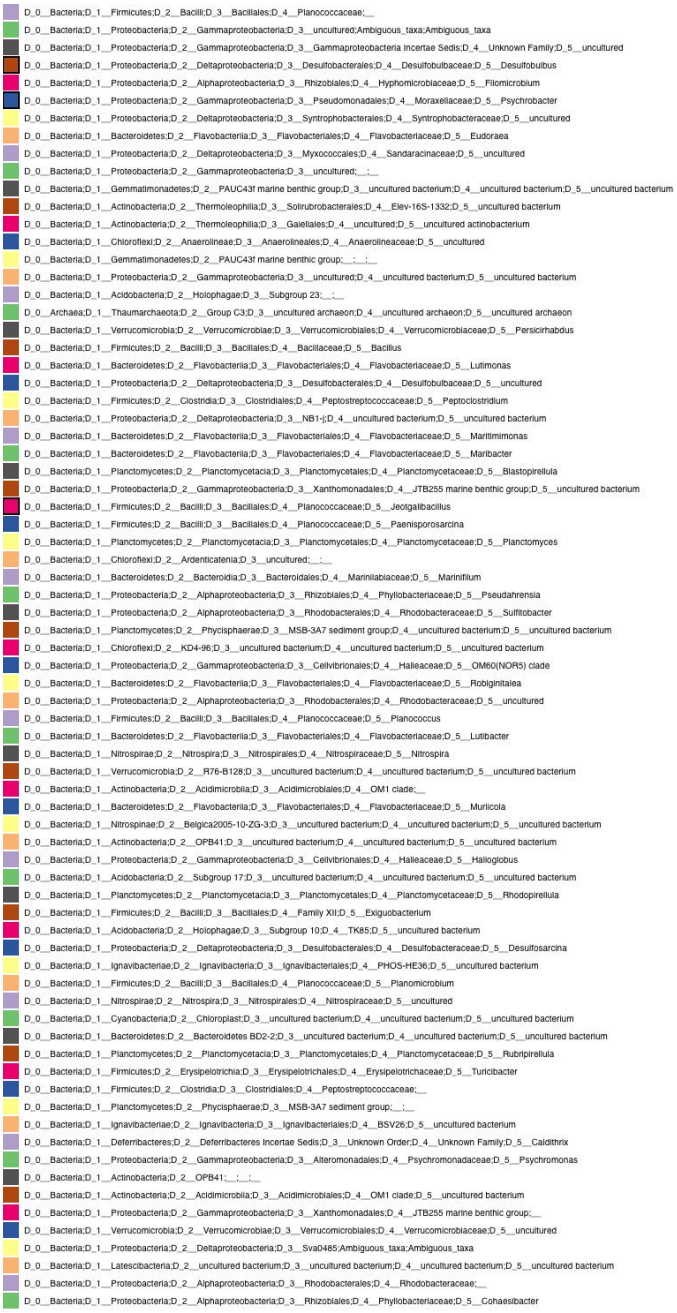


**Figure S1:** 100 % stacked bar chart of relative abundance of Irish Sea mud-patch core OTUs at genus level. OTU table was filtered to remove OTUs with total counts of <100. Each row represents one depth sample, and each colour represents one microbial genus. The width of the colour represents the percentage abundance of that family within a depth sample. The bottom bar chart shows microbial genera mentioned in the main text, and from right to left shows: *Desulfobulbus* (brown); *Psychrobacter* (blue); *Jeotgalibacillus* (fuschia). The legend is from right to left.

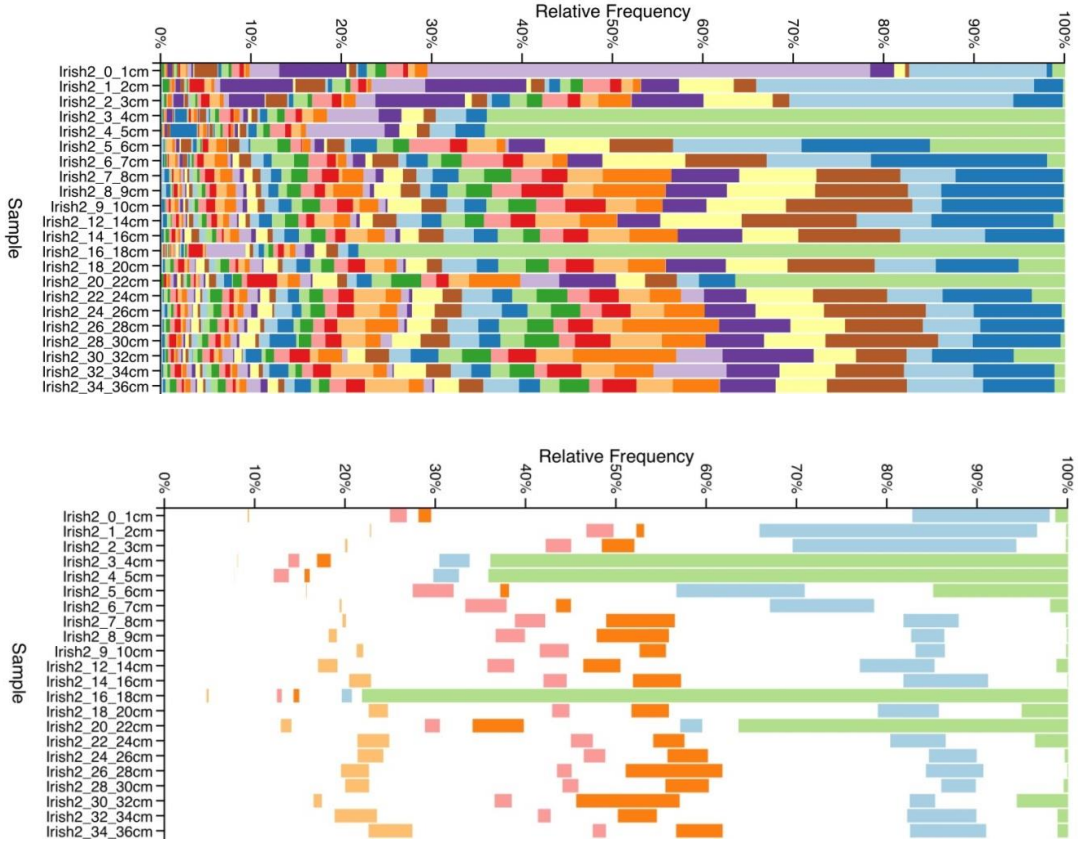
Relative Frequency
0%
10%
20%
30%
40%
50%
60%
70%
80%
90%
100%
Sample
Irish2_0_1cm
Irish2_1_2cm
Irish2_2_3cm
Irish2_3_4cm
Irish2_4_5cm
Irish2_5_6cm
Irish2_6_7cm
Irish2_7_8cm
Irish2_8_9cm
Irish2_9_10cm
Irish2_12_14cm
Irish2_14_16cm
Irish2_16_18cm
Irish2_18_20cm
Irish2_20_22cm
Irish2_22_24cm
Irish2_24_26cm
Irish2_26_28cm
Irish2_28_30cm
Irish2_30_32cm
Irish2_32_34cm
Irish2_34_36cm


Relative Frequency
0%
10%
20%
30%
40%
50%
60%
70%
80%
90%
100%
Sample
Irish2_0_1cm
Irish2_1_2cm
Irish2_2_3cm
Irish2_3_4cm
Irish2_4_5cm
Irish2_5_6cm
Irish2_6_7cm
Irish2_7_8cm
Irish2_8_9cm
Irish2_9_10cm
Irish2_12_14cm
Irish2_14_16cm
Irish2_16_18cm
Irish2_18_20cm
Irish2_20_22cm
Irish2_22_24cm
Irish2_24_26cm
Irish2_26_28cm
Irish2_28_30cm
Irish2_30_32cm
Irish2_32_34cm
Irish2_34_36cm

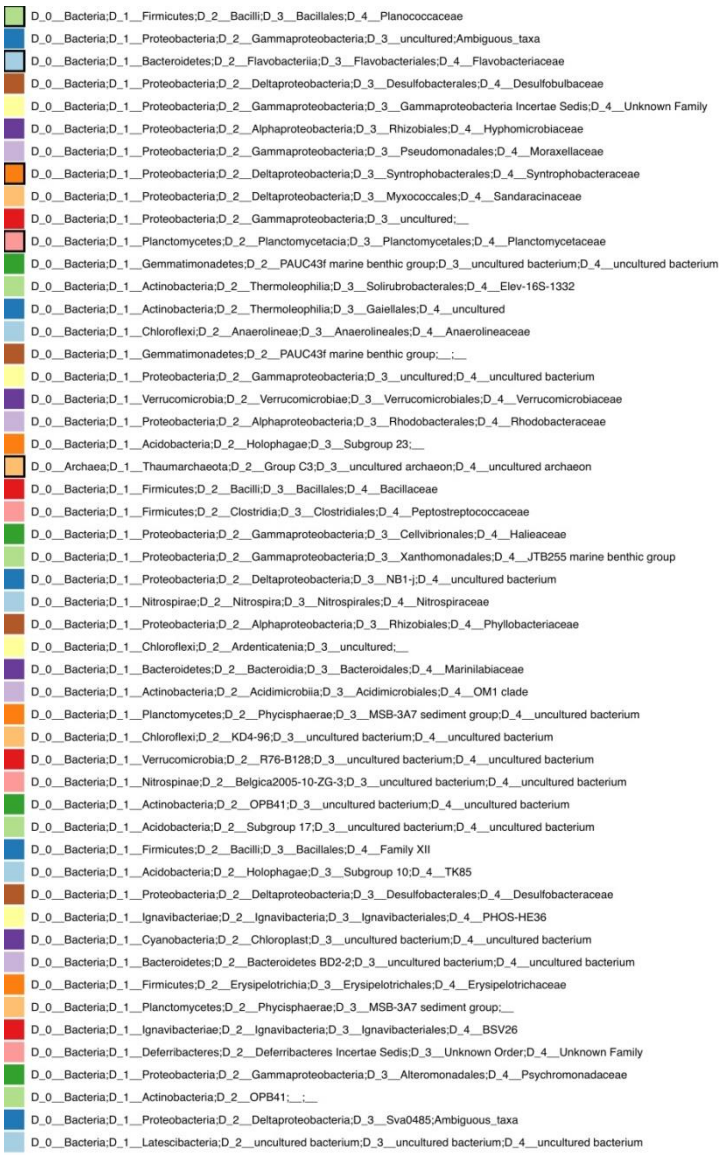


**Figure S2**. 100 % stacked bar chart of relative abundance of Irish Sea mud-patch core OTUs at family level. OTU table was filtered to remove OTUs with total counts of <100. Each row represents one depth sample, and each colour represents one microbial family. The width of the colour represents the percentage abundance of that family within a depth sample. The bottom bar chart shows microbial families mentioned in the main text, and from right to left shows: *Planococcaceae* (green); *Flavobacteriaceae* (blue); *Syntrophobacteraceae* (orange); *Planctomycetaceae* (pink); *Thaumarchaeota* (gold). The legend is from right to left

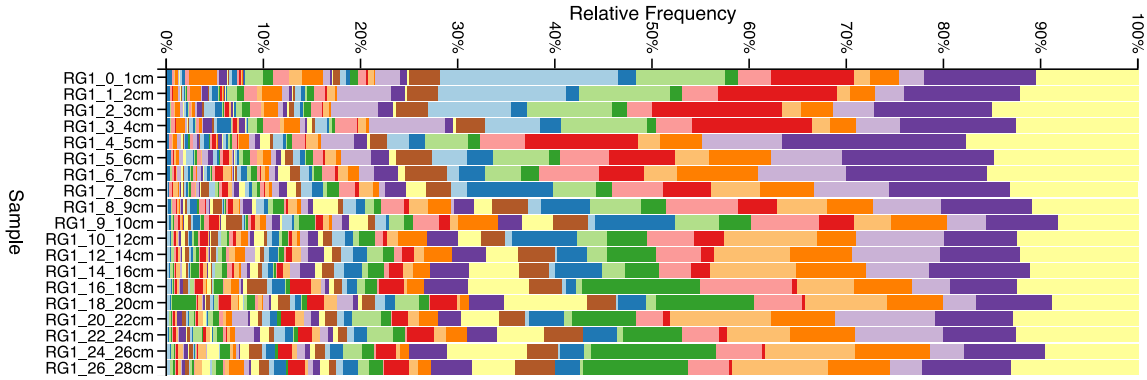
Relative Frequency
0%
10%
20%
30%
40%
50%
60%
70%
80%
90%
100%
Sample
RG1_0_1cm
RG1_1_2cm
RG1_2_3cm
RG1_3_4cm
RG1_4_5cm
RG1_5_6cm
RG1_6_7cm
RG1_7_8cm
RG1_8_9cm
RG1_9_10cm
RG1_10_12cm
RG1_12_14cm
RG1_14_16cm
RG1_16_18cm
RG1_18_20cm
RG1_20_22cm
RG1_22_24cm
RG1_24_26cm
RG1_26_28cm

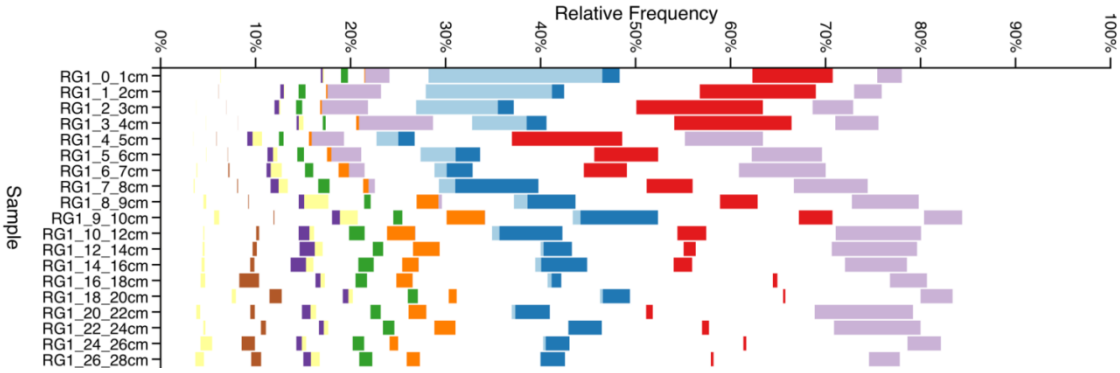
Relative Frequency
0%
10%
20%
30%
40%
50%
60%
70%
80%
90%
100%
Sample
RG1_0_1cm
RG1_1_2cm
RG1_2_3cm
RG1_3_4cm
RG1_4_5cm
RG1_5_6cm
RG1_6_7cm
RG1_7_8cm
RG1_8_9cm
RG1_9_10cm
RG1_10_12cm
RG1_12_14cm
RG1_14_16cm
RG1_16_18cm
RG1_18_20cm
RG1_20_22cm
RG1_22_24cm
RG1_24_26cm
RG1_26_28cm

.

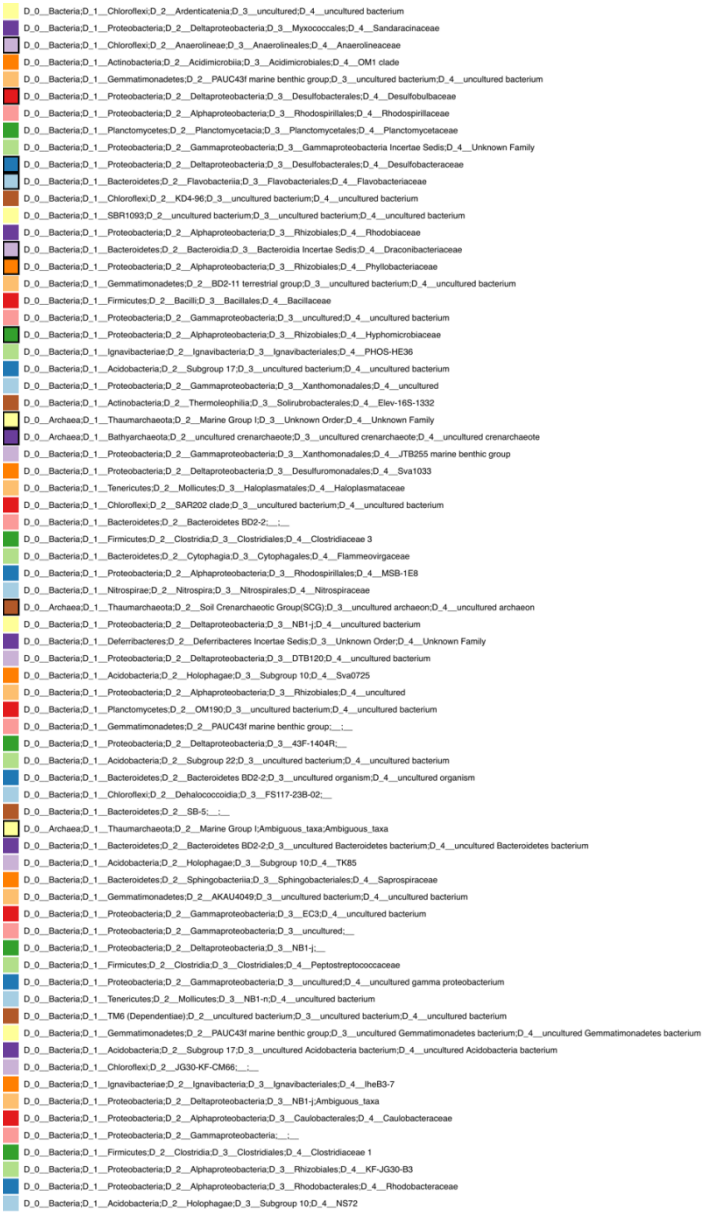


**Figure S3.** 100 % stacked bar chart of relative abundance of Ravenglass saltmarsh core OTUs at family level. OTU table was filtered to remove OTUs with total counts of <250. Each row represents one depth sample, and each colour represents one microbial family. The width of the colour represents the percentage abundance of that family within a depth sample. The bottom bar chart shows microbial families mentioned in the main text, and from right to left shows: *Anaerolineaceae* (purple)*; Desulfobulbaceae* (red); *Desulfobacteraceae* (dark blue); *Flavobacteriaceae* (light blue); *Draconibacteriaceae* (purple); *Phyllobacteraceae* (orange); *Hyphomicrobiaceae* (green); *Thaumarchaeota* (yellow); *Bathyarchaeota* (purple); *Thaumarchaeota* (brown, yellow). The legend is from right to left.

## Text S2: $^{241}$Am ingrowth from $^{241}$Pu

The decay of $^{241}$Pu ($t_{1/2}$ = 14.3 years) has been recognised to be the dominant contemporary contributor of $^{241}$Am in the Irish Sea. The percentage of $^{241}$Am ingrowth from $^{241}$Pu at the Ravenglass saltmarsh was determined by the model of Day and Cross, (1981) and the output of this is shown in Figure S4. This shows that the percentage of $^{241}$Am at the surface of the sediment core starts at ~40 % corresponding to the date of collection in 2014. This concentration of $^{241}$Am then steadily increases to 77 % at a depth of 11cm with the hypothesised date of this horizon being 1997. Thereafter, the concentration of $^{241}$Am exceeds 100 % with depth, and values reach ~ 300 % at the bottom of the core. The percentage is determined by the concentration of $^{241}$Am from $^{241}$Pu ingrowth divided by the total $^{241}$Am inventory (from γ-analysis data). Thus this calculation suggests that towards the bottom of the core (from 11 cm onwards) the concentration of $^{241}$Am is greater than the total $^{241}$Am inventory. This may be explained by the movement of a small proportion of young $^{241}$Pu leaking downwards from the middle of the core (which has received the high activity material from the 1970s). Thus, decay correction of young Pu assuming it is old will apply a big decay correction, and may explain the high percentages e.g. as the bottom horizon (hypothesised to be 1970) is not strictly accumulating material from the pipeline released in 1968, due to the potential leakage of $^{241}$Pu down the core. As this small proportion may represent a substantial activity compared to the activity that already resides in the older $^{241}$Pu, this may result in the over estimation of $^{241}$Am ingrowth from $^{241}$Pu decay.

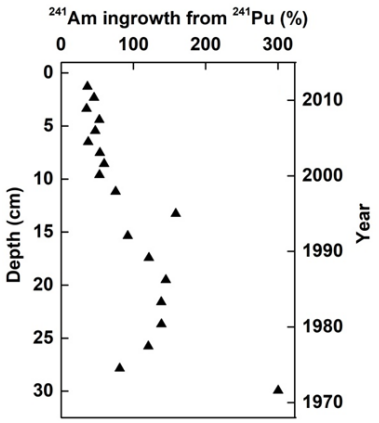


**Figure S4**. The fraction of $^{241}$Am in growth in the Ravenglass saltmarsh sediment core from $^{241}$Pu decay expressed as a percentage (%) of the total $^{241}$Am inventory determined by γ-spectroscopy. This was dated using the Sellafield discharge history (Table S3) and the average sedimentation rate (Table 1).

| Year | $^{137}$Cs | $^{241}$Am | $^{239,240}$Pu | $^{238}$Pu | $^{241}$Pu |
|---|---|---|---|---|---|
| **1952** | 46.0 | 0.00 | 0.54 | 0.02 | 2.0 |
| **1953** | 46.0 | 0.00 | 0.50 | 0.02 | 1.0 |
| **1954** | 46.0 | 0.00 | 0.60 | 0.02 | 2.3 |
| **1955** | 21.0 | 0.00 | 0.70 | 0.02 | 1.9 |
| **1956** | 160.0 | 0.00 | 1.80 | 0.06 | 3.7 |
| **1957** | 140.0 | 0.00 | 1.60 | 0.05 | 3.4 |
| **1958** | 230.0 | 0.00 | 1.90 | 0.06 | 3.9 |
| **1959** | 73.0 | 0.00 | 2.10 | 0.06 | 4.4 |
| **1960** | 34.0 | 0.00 | 2.70 | 0.08 | 6.2 |
| **1961** | 40.0 | 0.00 | 4.60 | 0.14 | 18.0 |
| **1962** | 74.0 | 0.00 | 6.60 | 0.20 | 37.0 |
| **1963** | 85.0 | 0.00 | 8.10 | 0.25 | 55.0 |
| **1964** | 100.0 | 4.50 | 5.50 | 0.22 | 62.0 |
| **1965** | 110.0 | 8.10 | 6.90 | 0.30 | 81.0 |
| **1966** | 180.0 | 7.50 | 13.00 | 0.66 | 170.0 |
| **1967** | 150.0 | 17.00 | 17.00 | 1.20 | 290.0 |
| **1968** | 370.0 | 21.00 | 28.00 | 2.10 | 630.0 |
| **1969** | 440.0 | 14.00 | 27.00 | 2.80 | 730.0 |
| **1970** | 1200.0 | 19.00 | 31.00 | 3.80 | 1000.0 |
| **1971** | 1300.0 | 38.00 | 46.00 | 9.30 | 1800.0 |
| **1972** | 1300.0 | 80.00 | 47.00 | 9.90 | 1900.0 |
| **1973** | 770.0 | 110.00 | 54.00 | 11.00 | 2800.0 |
| **1974** | 4100.0 | 120.00 | 38.00 | 8.00 | 1700.0 |

| | | | | | |
|---|---|---|---|---|---|
| **1975** | 5200.0 | 36.00 | 35.00 | 8.80 | 1800.0 |
| **1976** | 4300.0 | 12.00 | 38.00 | 8.80 | 1300.0 |
| **1977** | 4500.0 | 3.70 | 29.00 | 7.50 | 980.0 |
| **1978** | 4100.0 | 7.90 | 46.00 | 12.00 | 1800.0 |
| **1979** | 2600.0 | 7.80 | 38.00 | 12.00 | 1500.0 |
| **1980** | 3000.0 | 8.20 | 20.00 | 6.90 | 730.0 |
| **1981** | 2400.0 | 8.80 | 15.00 | 5.01 | 600.0 |
| **1982** | 2000.0 | 6.40 | 16.00 | 4.71 | 481.0 |
| **1983** | 1200.0 | 2.20 | 8.70 | 2.91 | 330.0 |
| **1984** | 430.0 | 2.30 | 8.30 | 2.60 | 350.0 |
| **1985** | 330.0 | 1.60 | 2.60 | 0.80 | 81.0 |
| **1986** | 18.0 | 1.30 | 2.00 | 0.62 | 63.0 |
| **1987** | 12.0 | 0.65 | 0.97 | 0.35 | 32.0 |
| **1988** | 13.0 | 0.75 | 1.00 | 0.38 | 36.0 |
| **1989** | 29.0 | 1.10 | 0.90 | 0.31 | 30.0 |
| **1990** | 23.5 | 0.75 | 0.84 | 0.29 | 31.6 |
| **1991** | 15.6 | 0.74 | 0.82 | 0.26 | 29.5 |
| **1992** | 15.3 | 0.54 | 0.69 | 0.24 | 25.3 |
| **1993** | 21.9 | 0.87 | 1.00 | 0.33 | 37.5 |
| **1994** | 13.8 | 0.38 | 0.50 | 0.16 | 14.4 |
| **1995** | 12.0 | 0.11 | 0.23 | 0.08 | 7.7 |
| **1996** | 10.0 | 0.07 | 0.16 | 0.05 | 4.4 |
| **1997** | 7.9 | 0.05 | 0.11 | 0.04 | 3.3 |
| **1998** | 7.5 | 0.05 | 0.11 | 0.03 | 3.5 |
| **1999** | 9.1 | 0.03 | 0.09 | 0.03 | 2.9 |
| **2000** | 6.9 | 0.03 | 0.08 | 0.03 | 3.2 |
| **2001** | 9.6 | 0.04 | 0.12 | 0.04 | 4.6 |
| **2002** | 7.7 | 0.04 | 0.26 | 0.08 | 10.0 |
| **2003** | 6.2 | 0.06 | 0.27 | 0.09 | 10.0 |
| **2004** | 9.7 | 0.04 | 0.22 | 0.07 | 8.1 |
| **2005** | 6.0 | 0.03 | 0.15 | 0.05 | 5.0 |
| **2006** | 6.0 | 0.05 | 0.11 | 0.04 | 3.6 |
| **2007** | 7.0 | 0.02 | 0.08 | 0.03 | 2.8 |
| **2008** | 5.1 | 0.03 | 0.08 | 0.03 | 2.4 |
| **2009** | 4.3 | 0.05 | 0.09 | 0.03 | 2.9 |
| **2010** | 4.8 | 0.03 | 0.09 | 0.03 | 3.2 |
| **2011** | 5.9 | 0.03 | 0.08 | 0.03 | 2.4 |
| **2012** | 3.6 | 0.02 | 0.11 | 0.03 | 3.0 |
| **2013** | 3.2 | 0.02 | 0.12 | 0.04 | 3.2 |
| **2014** | 2.6 | 0.02 | 0.11 | 0.04 | 2.9 |
| **2015** | 3.1 | 0.03 | 0.10 | 0.03 | 2.4 |

**Table S3.** Sellafield discharge record: (1952–2015) (Gray et al., 1992; BNFL 1993–2005; Sellafield Ltd, 2005–2017).

| Year | $^{238}Pu$: $^{239,240}Pu$ | $^{241}Am$: $^{239,240}Pu$ | $^{137}Cs$: $^{241}Am$ | $^{241}Am$: $^{239,240}Pu$ |
|---|---|---|---|---|
| **1952** | 0.04 | 0.00 | N/A | N/A |
| **1953** | 0.04 | 0.00 | N/A | N/A |
| **1954** | 0.03 | 0.00 | N/A | N/A |
| **1955** | 0.03 | 0.00 | N/A | N/A |
| **1956** | 0.03 | 0.00 | N/A | N/A |
| **1957** | 0.03 | 0.00 | N/A | N/A |
| **1958** | 0.03 | 0.00 | N/A | N/A |
| **1959** | 0.03 | 0.00 | N/A | N/A |
| **1960** | 0.03 | 0.00 | N/A | N/A |
| **1961** | 0.03 | 0.00 | N/A | N/A |
| **1962** | 0.03 | 0.00 | N/A | N/A |
| **1963** | 0.03 | 0.00 | N/A | N/A |
| **1964** | 0.04 | 0.82 | 22.2 | 0.82 |
| **1965** | 0.04 | 1.17 | 13.6 | 1.17 |
| **1966** | 0.05 | 0.58 | 24.0 | 0.58 |
| **1967** | 0.07 | 1.00 | 8.8 | 1.00 |
| **1968** | 0.08 | 0.75 | 17.6 | 0.75 |
| **1969** | 0.10 | 0.52 | 31.4 | 0.52 |
| **1970** | 0.12 | 0.61 | 63.2 | 0.61 |
| **1971** | 0.20 | 0.83 | 34.2 | 0.83 |
| **1972** | 0.21 | 1.70 | 16.3 | 1.70 |
| **1973** | 0.20 | 2.04 | 7.0 | 2.04 |
| **1974** | 0.21 | 3.16 | 34.2 | 3.16 |
| **1975** | 0.25 | 1.03 | 144.4 | 1.03 |
| **1976** | 0.23 | 0.32 | 358.3 | 0.32 |
| **1977** | 0.26 | 0.13 | 1216.2 | 0.13 |
| **1978** | 0.26 | 0.17 | 519.0 | 0.17 |
| **1979** | 0.32 | 0.21 | 333.3 | 0.21 |
| **1980** | 0.35 | 0.41 | 365.9 | 0.41 |
| **1981** | 0.33 | 0.59 | 272.7 | 0.59 |
| **1982** | 0.29 | 0.40 | 312.5 | 0.40 |
| **1983** | 0.33 | 0.25 | 545.5 | 0.25 |
| **1984** | 0.31 | 0.28 | 187.0 | 0.28 |
| **1985** | 0.31 | 0.62 | 206.3 | 0.62 |
| **1986** | 0.31 | 0.65 | 13.8 | 0.65 |
| **1987** | 0.36 | 0.67 | 18.5 | 0.67 |
| **1988** | 0.38 | 0.75 | 17.3 | 0.75 |
| **1989** | 0.34 | 1.22 | 26.4 | 1.22 |
| **1990** | 0.35 | 0.89 | 31.3 | 0.89 |
| **1991** | 0.32 | 0.90 | 21.1 | 0.90 |
| **1992** | 0.35 | 0.78 | 28.3 | 0.78 |
| **1993** | 0.33 | 0.87 | 25.2 | 0.87 |
| **1994** | 0.33 | 0.77 | 36.3 | 0.77 |
| **1995** | 0.33 | 0.47 | 109.1 | 0.47 |
| **1996** | 0.33 | 0.44 | 142.9 | 0.44 |

| | | | | |
|---|---|---|---|---|
| **1997** | 0.33 | 0.44 | 158.0 | 0.44 |
| **1998** | 0.33 | 0.48 | 150.0 | 0.48 |
| **1999** | 0.33 | 0.33 | 303.3 | 0.33 |
| **2000** | 0.33 | 0.36 | 230.0 | 0.36 |
| **2001** | 0.33 | 0.33 | 240.0 | 0.33 |
| **2002** | 0.33 | 0.16 | 192.5 | 0.16 |
| **2003** | 0.33 | 0.22 | 103.3 | 0.22 |
| **2004** | 0.33 | 0.18 | 242.5 | 0.18 |
| **2005** | 0.33 | 0.20 | 200.0 | 0.20 |
| **2006** | 0.33 | 0.45 | 120.0 | 0.45 |
| **2007** | 0.33 | 0.25 | 350.0 | 0.25 |
| **2008** | 0.33 | 0.37 | 170.0 | 0.37 |
| **2009** | 0.33 | 0.55 | 86.0 | 0.55 |
| **2010** | 0.33 | 0.32 | 160.0 | 0.32 |
| **2011** | 0.33 | 0.38 | 196.7 | 0.38 |
| **2012** | 0.33 | 0.19 | 180.0 | 0.19 |
| **2013** | 0.33 | 0.17 | 160.0 | 0.17 |
| **2014** | 0.33 | 0.18 | 130.0 | 0.18 |
| **2015** | 0.33 | 0.29 | 103.3 | 0.29 |

**Table S4.** Sellafield discharge record: Activity ratios (1952–2015).The $^{238}Pu/^{239,240}Pu$ activity ratio of 0.33 (based on average of 1982–1993 values) was used to estimate $^{238}Pu$ and $^{239,240}Pu$ values from 1993 onwards.

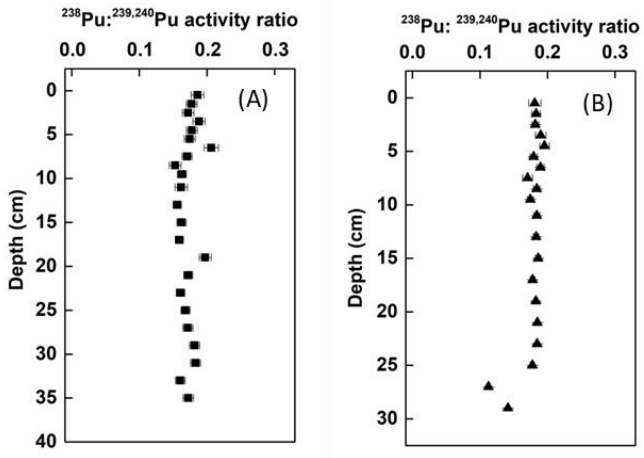


**Figure S5**. The $^{238}Pu/^{239+240}Pu$ activity ratios for the (A) Irish Sea mud-patch and, (B) Ravenglass saltmarsh sediment cores. Errors are based on 1σ counting errors of the individual radionuclides

BNFL, 1993–2005 Annual report on radioactive discharges and monitoring of the environment. Bristish Nuclear Fuels plc. Risley.

Day, J.P., Cross, J.E., 1981. $^{241}$Am from the decay of $^{241}$Pu in the Irish Sea. Nature. 292, 43–45.

Gray, J., Jones, S.R., Smith, A.D., 1995. Discharges to the environment from the Sellafield site, 1951–1992. J. Radiol. Prot. 15, 99–131.

Marsden, O.J., Abrahamsen, L., Bryan, N.D., Day, J. P., Fifield, K.L., Gent, C., Goodall, P.S., Morris, K., Livens, F.R., 2006. Transport and accumulation of actinide elements in the near-shore environment: field and modelling studies. Sedimentology. 53, 237–248.

Sellafield Ltd, 2005–2017. Monitoring our environment: discharges and environmental monitoring.

# Chapter 4: Sellafield-Derived Technetium, Uranium, and Neptunium Distribution in the Ravenglass Saltmarsh, UK

This chapter is a manuscript prepared for submission to the *Journal of Environmental Radioactivity*. Supporting Information is presented at the end of the manuscript.

# 4. Sellafield-Derived Technetium, Uranium, and Neptunium Distribution in the Ravenglass Saltmarsh, UK

Daisy Ray[1/2], Claudia Joseph[3], Adam Fuller[1], Katherine Morris[2], Francis R. Livens[1/2], James D. C. Begg[3], Annie Kersting[3], L. Keith Fifield[4], Pihong Zhao[3], Mavrik Zavarin[3], Heather Williams[5], Bev Ellis[5], Kathleen A. Law[1], Gareth T. W. Law[1/2*]

1. Centre for Radiochemistry Research, School of Chemistry, The University of Manchester, Manchester, M13 9PL, UK;

2. Research Centre for Radwaste and Decommissioning and Williamson Research Centre, School of Earth and Environmental Sciences, The University of Manchester, Manchester, M13 9PL, UK;

3. Glenn T. Seaborg Institute, Lawrence Livermore National Laboratory, 7000 East Ave, Livermore, CA, 94550, USA;

4. Department of Nuclear Physics, Research School of Physics and Engineering, The Australian National University, Acton, ACT 2601, Australia.

5. Nuclear Medicine Centre, Manchester Royal Infirmary, Manchester, M13 9WL, UK.

*Corresponding author: Tel: +44 (0) 161 306 0514; Email: gareth.law@manchester.ac.uk

## 4.1 Abstract

The Sellafield nuclear reprocessing facility in West Cumbria has discharged, under authorisation, low-level aqueous effluent into the Eastern Irish Sea since 1952. This effluent contains $^{99}$Tc, $^{237}$Np, and U isotopes and over time these radionuclides have accumulated in sediments on the Cumbrian coast, including at the Ravenglass saltmarsh. As all three radionuclides are redox-active, their mobility and eventual fate may be influenced by ambient sediment biogeochemistry. Here we examine the vertical distribution of $^{99}$Tc, $^{236}$U, and $^{237}$Np, in Ravenglass saltmarsh sediments relative to the site geochemistry and the discharge records of these radionuclides from Sellafield. The $^{99}$Tc activity in the sediment ranged between 150–230 Bq/kg and the distribution did not resemble the Sellafield $^{99}$Tc discharge history. Instead, the variable redox conditions present at Ravenglass and Tc coupling to Fe biocycling likely explain the contemporary $^{99}$Tc distribution at the site. Sediment $^{236}$U:$^{238}$U ratios ranged between $1.5 \times 10^{-6}$ and $7.4 \times 10^{-6}$ (~ 8 orders of magnitude higher than the natural baseline) and did not match the discharge history. Similar to Tc this may imply that the region of active metal cycling may influence $^{236}$U distribution. $^{237}$Np distribution ranged between 0.6–6.3 Bq/kg, and showed a better match with the discharge history in upper regions of the core. However, some degree of $^{237}$Np cycling was apparent in the zone of microbially mediated metal cycling.

**Keywords**: Technetium, Uranium, Neptunium, Sellafield, Ravenglass, Remobilisation.

## 4.2. Introduction

The discharge of aqueous low-level effluent has been taking place from the Sellafield site to the Eastern Irish Sea since 1952 (Kershaw et al., 1992; Gray et al., 1995). Legacy spent fuel reprocessing and storage pond waters are the major contributors of this effluent, and contain a range of actinides and fission products (e.g. Am, Cs, Pu, Tc, Np, and U) (Kershaw et al., 1992). Whilst modern day releases are much lower than authorised limits (Sellafield Ltd, 2017) historical discharges have resulted in the radioactive contamination of local coastal areas (Aston et al., 1985; Assinder et al., 1991; MacKenzie et al., 1994; McCartney et al., 1994; Kuwabara et al., 1996; Morris et al., 2000; Marsden et al., 2001) and

further afield (MacKenzie and Scott, 1982; Keith-Roach and Roos, 2004; McCubbin et al., 2006; Keogh et al., 2007; Jenkinson et al., 2014; Al-Qasmi et al., 2016, 2017). In addition, a proportion of the Sellafield-derived effluent has associated with an offshore belt of finely grained sediment (known as the Irish Sea mud-patch; ~15 km long x ~ 3 km wide), located ~10 km west from the discharge pipeline). Bio-mixing at the mud-patch is then suggested to redistribute some of the Sellafield radionuclides back into overlying waters (Kershaw et al., 1983). Thereafter, these radionuclides can be transported to intertidal sediments along the Cumbrian coastline and elsewhere (McCartney et al., 1994; Kershaw et al., 1999; Lucey et al., 2004; Lindahl et al., 2011; Al-Qasmi et al., 2016, 2017; Caborn et al., 2016). The Ravenglass saltmarsh is a low energy, depositional site located ~10 km south of Sellafield that has received a substantial input of Sellafield-derived radionuclides over time (Lucey et al., 2004; Oh et al., 2009; Morris et al., 2000; Marsden et al., 2006; Ray et al., 2018; Chapter 3) including $^{99}$Tc, $^{237}$Np, and U isotopes.

The fission product $^{99}$Tc is a β-emitter, and is of environmental importance due to its high solubility and long half-life ($t_{1/2}$ = 2.1 x $10^5$ years). Under oxidising conditions, the highly soluble pertechnetate dominates: $TcO_4^-$ (11 mol/ L) (Boyd, 1978) weakly sorbing to environmental geomedia (e.g. Burke et al., 2005; Liu and Fan, 2005; Lear et al., 2010). As a result pertechnetate is one of the most mobile radionuclide species in the environment (Bondietti and Francis, 1979; Lloyd et al., 2000) and indeed Sellafield-derived $^{99}$Tc has been measured in Scandinavian sediments and waters (Dahlgaard, 1995; Keith-Roach et al., 2003; Keith-Roach and Roos, 2004).

The addition of an electron donor to $^{99}$Tc contaminated sediments and groundwater to promote microbially-mediated metal-reducing conditions has been shown to effectively reduce $TcO_4^-$ to sparingly soluble Tc(IV), concurrent with Fe(III) reduction (Lloyd et al., 2000; McBeth et al., 2007; Law et al., 2010; Prakash et al., 2013; Newsome et al., 2014, 2017; Thorpe et al., 2016). The direct reduction of soluble $Tc(VII)_{(aq)}$ to $Tc(IV)_{(s)}$ has been shown to occur biotically *via* the interaction of hydrogenase enzymes on certain Fe(III) and sulphate-reducing bacteria (Lloyd et al., 2000; Wildung et al., 2000; Marshall et al., 2008). However, at environmental concentrations of Tc(VII) and Fe, the indirect,

abiotically-mediated reduction of Tc(VII) with biogenic Fe(II)-bearing minerals and sorbed Fe(II) is suggested to be the dominant reduction pathway (Lloyd et al., 2000; Begg et al., 2007; Zachara et al., 2007; Marshall et al., 2008; Plymale et al., 2011; Brookshaw et al., 2016) forming hydrous $TcO_2$-like chains (e.g. Fredrickson et al., 2004; Wildung et al., 2004; Burke et al., 2005; McBeth et al., 2007; Morris et al., 2008; Masters-Waage et al., 2017). However, below the solubility of this phase (~ $10^{-9}$ mol/L; Bondietti and Francis, 1979) it has been suggested that Tc(IV) will instead sorb to mineral surfaces (Burke et al., 2010; Lear et al., 2010). The biogenic production of iron sulphides can also lead to co-precipitation of Tc(IV)-S phases (Lee et al., 2014). It is now well established that Tc is cycled between the solution and solid phase under sub-oxic conditions, however little is known of whether Tc behaves in a similar way in the field, where it will be present at lower concentrations than those used in laboratory experiments. Meanwhile, real world sediment systems are more complex and heterogeneous (with regards to both composition and biogeochemistry).

In the Irish Sea, the discharge of $^{99}$Tc from Sellafield, like other radionuclides, reached a peak in the mid-to late-1970s (a maximum of 178 TBq). This was significantly reduced when effluent treatment facilities and stricter discharge limits were introduced, keeping activities fairly low (2–7 TBq) throughout the 1980s and early 1990s. Thereafter, the commissioning of the Enhanced Actinide Removal Plant (EARP) in March 1994 saw $^{99}$Tc activities reach ~ 190 TBq in 1995, similar to those seen in the late 1970s (Kershaw et al., 1992). This was because the plant was used to process current and legacy Medium-Activity Concentrate (MAC) effluent, and this was effective in reducing Pu discharges by half in 1994. However, as the treatment was not effective in the removal of Tc, this resulted in elevated $^{99}$Tc concentrations being discharged (Kershaw et al., 1999).

As Tc exists as the highly soluble, conservative $TcO_4^-$ in open oxygenated waters, the majority of studies have focused on determining $^{99}$Tc concentrations in seawater and its accumulation in biota to ascertain the impact of modern post-EARP discharges. (Leonard et al., 1997, 2004, 2008; McDonald et al., 1998; Kershaw et al., 1999; Smith et al., 2001; McCubbin et al., 2002; Lindahl et al., 2003). Other authors have examined Tc accumulation in Irish Sea sub-tidal

(McCubbin et al., 2006; Finegan et al., 2009; Jenkinson et al., 2014) and coastal sediments (Morris et al., 2000; Keith-Roach et al., 2003; Lucy et al., 2004; Finegan et al., 2009). The most recent work concerning $^{99}$Tc at the Ravenglass saltmarsh used sediments collected in 2002 (Lucey et al., 2004; Finegan et al., 2009) and showed a sub-surface enrichment of $^{99}$Tc, similar to Morris et al. (2000).

Uranium can be found naturally in the Earth's crust, predominantly as: $^{238}$U (~99.3 %), $^{235}$U (~0.72 %), and $^{234}$U (0.005 %). Uranium-236 ($t_{1/2}$ = 2.4 x $10^7$years) also exists in nature, but at low concentrations ($^{236}$U:$^{238}$U ratio of ~$10^{-14}$) (Marsden et al., 2001). The widespread nature of U in the environment means that any anthropogenic U signature is diluted with the background U. However, the constant neutron capture of $^{235}$U in a civil nuclear reactor generates $^{236}$U, increasing its concentration above the natural baseline, and as a result $^{236}$U can be used as a tracer to determine the environmental behaviour of anthropogenic U (e.g. Marsden et al., 2001; De Cesare et al., 2013; Al-Qasmi et al., 2016; Tims et al., 2016).

Under oxic conditions U is predominantly present as U(VI), forming the soluble uranyl species ($UO_2^{2+}$) (Waite et al., 1994; Gorman-Lewis et al., 2008). At circumneutral pH (in carbonate free conditions) hydroxyl complexes ($UO_2$-OH) will tend to exist (Choppin et al., 2002), however at the same pH in the presence of carbonate, U(VI)–carbonato-complexes ($UO_2(CO_3)_3^{4-}$) dominate (Clark et al., 1995). Oxidised U(VI) species have been recognised to sorb to organic matter and mineral surfaces, including clays and Fe oxy(hydr)oxides (Ortiz-bernad et al., 2004; Scott et al., 2005; Kaplan et al., 2016). These interactions are often reversible at pH >7 (Cumberland et al., 2016) and thus U may be available in a natural system.

The biotic reduction of U(VI) to crystalline $UO_2$ at circumneutral pH was shown in early work to be mediated by Fe(III)-reducing bacteria (Lovley et al., 1991). More recent studies have shown that the bioreduction of U(VI) can produce alternative U(IV) products, termed non-crystalline or monomeric U(IV) (Bernier-Latmani et al., 2010; Campbell et al., 2011; Wang et al., 2013). The abiotic reduction of U(VI) to U(IV) has also been shown to take place *via* redox reaction

with Fe(II)-bearing minerals (Latta et al., 2012; Brookshaw et al., 2015) with the simultaneous enzymatic reduction of Fe(III) and U(VI) also being observed (Behrends and Cappellen, 2005). There is also evidence of U incorporation into the lattice of Fe oxy(hydr)oxides (Duff et al., 2002; Marshall et al., 2014; Roberts et al., 2017).

The discharge of U from the Sellafield site to the Irish Sea was monitored from 1978 (Kershaw et al., 1992) and reached a maximum in the mid-1970s. The contemporary U discharge is now three orders of magnitude lower than historical values (Sellafield Ltd, 2017). The tracer $^{236}U$, has been used to determine Sellafield-derived U input to Ravenglass and other UK coastal sediments (Marsden et al., 2001; Al Qasmi et al., 2017). Here, Marsden et al. (2001) showed $^{236}U$:$^{238}U$ activity ratios at the Ravenglass saltmarsh that were well above the natural baseline, highlighting a distinct enrichment of $^{236}U$ in the middle of the sediment core (~18 cm).

The α-emitter $^{237}Np$ is formed as a by-product of nuclear fission and is present in spent fuel due to $^{241}Am$ decay. It is also of environmental importance due to its long half-life ($t_{1/2}$ = 2.1 x $10^6$ years) and high toxicity. Under oxidising conditions, Np is stable in solution as Np(V) (Hursthouse et al., 1991a; Choppin, 2006), existing mainly as the soluble neptunyl cation ($NpO_2^+$) (Keeney-Kennicutt and Morse, 1984; Yamamoto et al., 1991; Kaszuba and Runde, 1999) at pH <10 (Schmeide and Bernhard, 2010), with a solubility of up to $10^{-4}$ mol/L (Choppin, 2007). However, when carbonate concentrations are high, soluble Np–carbonato complexes will likely dominate (e.g. $NpO_2CO_3$) (Schmeide and Bernhard, 2010).

Laboratory studies have investigated the sorption of Np(V) to Fe oxy(hydr)oxides. Combes et al. (1992) have shown that the effective sorption of Np(V) to goethite (α–FeOOH) has led to ~95 % uptake onto the surface of the mineral. In addition, Np in sediments from the Ob River, Siberia was shown to predominantly associate with Mn and Fe oxides (Kenna, 2009). The desorption of Np(V) from Mn(hydr)oxides (Zhao et al., 2005) and Fe oxy(hydr)oxides (Keeney-Kennicutt and Morse, 1984; Nakata et al., 2000; Tinnacher et al., 2011) has been recognised, and this may suggest that Np may become re-mobilised after a period of adsorption. The reduction of Np(V) can occur *via* biotic and abiotic

pathways. The direct, enzymatic reduction of Np(V) and Np(V) citrate by bacteria has been observed, however this immobilisation of Np(IV) was dependent on the ligands present in solution (Icopini et al., 2007). The indirect reduction of Np(V) to Np(IV) in sterile Fe(II)-bearing sediment systems was shown to proceed *via* the abiotic electron transfer from reactive Fe(II) minerals to Np(V) (Law et al., 2010). The reduction of Np(V) has also been highlighted to take place on reactive Fe(II) surfaces e.g. mackinawite (FeS) (Moyes et al., 2002), green rust (an Fe(II)/Fe(III) layered double hydroxide) (Christiansen et al., 2011), and on phyllosilicates (Brookshaw et al., 2015) with the latter two studies observing the precipitation of nanoparticulate Np(IV) phases. The removal of Np during microbially-mediated Mn reduction in sediment microcosms was shown by Thorpe et al. (2015) and here X-ray Absorption Spectroscopy confirmed the reductive immobilisation of Np(V) to Np(IV).

Our understanding of Np biogeochemistry predominantly comes from laboratory experiments conducted at relatively high concentrations (micromolar and above) in simple systems. Furthermore, there is interest in examining the behaviour of Np in the environment as its long half–life and high solubility means it will be the most hazardous material in HLW over geological repository timescales (Thompson, 1982). The discharge record for $^{237}$Np releases are available from 1978, and show a maximum activity (0.59 TBq) for that year (Kuwabara et al., 1996) with current discharges approximately on order of magnitude lower (0.03 TBq) (Sellafield Ltd, 2017). Early measurements of $^{237}$Np focused on seawater, biota, and sediments in the Eastern Irish Sea, with $^{237}$Np activity shown to be 1.6 Bq/kg at the Irish Sea mud-patch (Pentreath and Harvey, 1981) with the activity of $^{237}$Np also measured in a single Ravenglass sample (6.5 mBq/g; Byrne, 1986). Thereafter, studies at the Esk estuary used varying analytical techniques to examine $^{237}$Np in surface sediment samples (Pentreath and Harvey, 1981; Assinder et al., 1991; Hursthouse et al., 1991b; Yamamoto et al., 1991; Kuwabara et al., 1996; Assinder, 1999). The most recent study of $^{237}$Np distribution at Ravenglass showed an activity of 0.6–13 Bq/kg between 0–20 cm in depth with an enhanced concentration at the near-surface of the sediment core (Morris et al., 2000) and this was considered to be due to post-depositional effects.

The distribution of Sellafield-derived $^{137}$Cs, $^{241}$Am, and Pu isotopes in the Eastern Irish Sea sediments has been reported previously (e.g. Aston and Stanners, 1981; Aston et al., 1985; Malcolm et al., 1990; MacKenzie and Scott, 1993; McCartney et al., 1994; Livens et al., 1994; Cook et al., 1997; Morris et al., 2000; McDonald et al., 2001; Marsden et al., 2006; Ray et al., 2018; Chapter 3). In contrast, however the distribution and behaviour of Sellafield-derived $^{99}$Tc, $^{236}$U, and $^{237}$Np, in Irish Sea coastal sediments is poorly documented and understood, due primarily to the difficulty in the analysis of these radionuclides when present at trace concentration. In addition, a wealth of laboratory work with constrained environmental systems has highlighted the importance of redox cycling processes (both abiotic and enzymatic reduction, and subsequent oxidation) in controlling Tc, U, and Np removal from solution onto sediments. It is not well known if these observations can be translated into the real environment systems, especially over decadal timescales and beyond, particularly when these radionuclides are present at low concentration. This can only be addressed in well-understood natural laboratory sites labelled with anthropogenic radionuclides. Accordingly, in this work we present a contemporary account of the distribution of $^{99}$Tc, $^{236}$U, and $^{237}$Np in Sellafield-impacted Ravenglass saltmarsh sediments, with an aim to understand the relative importance of site biogeochemistry (specifically Mn, and Fe reduction) vs. physical controls on long-term radionuclide distribution.

## 4.3. Methods

### 4.3.1. Sample Collection and Preparation

The Ravenglass saltmarsh is part of the Esk estuary situated 15 km south from the Sellafield nuclear reprocessing facility (Carr and Blackley, 1986). It is located in an area of high convergence, at the crossing-point of the rivers Esk, Mite, and Irt. The estuary is heterogeneous in nature, with the bulk of the sediment comprised of sands and gravels, separated by areas of saltmarsh-covered silt and clay (Carr and Blackley, 1986)

Sediment cores (~ 30 cm) were collected from the Ravenglass saltmarsh (54’20.24 N, 03’24.06 W) (Figure 4.1) during low-tide in September 2014. These cores were taken from a stable region of the saltmarsh (at least 30 m away from any edge features, or creeks), by manual insertion of core tubes, with an airtight

bung placed over the top of the core prior to extraction. Core 1 was sectioned under normal atmosphere at 1 cm resolution from the top of the core, until a depth of 10 cm, followed by 2 cm resolution thereafter. Radionuclide and solid Mn and Fe analysis (*via* XRF) were carried out on this sediment core (as per Ray et al., 2018; Chapter 3). Core 2 was sampled under an $O_2$ free, $N_2$ filled, Aldrich Atmosbag to retain the redox chemistry. This core was sampled at the same resolution as core 1.


**Figure 4.1.** Map of the UK highlighting the study area. Inset showing the location of the study site.

Porewater was collected from each section in core 2 by centrifugation (10 minutes at 4500 rpm; 1811 *g*) of the sediment followed by filtration (PTFE membrane syringe filter; 0.22 µm). The filtered solutions were then fixed *via* addition of Aristar grade c$HNO_3$ (200 µL). In this paper we present solid and porewater Mn and Fe results (discussed fully in Ray et al., 2018; Chapter 3) that were analysed using ICP-AES (Perkin Elmer Optima 5300 Dual View). The concentration of Fe, and Mn in the bulk sediment was measured using a Panalytical Axios sequential XRF Spectrometer. Here, ground sediment (12 g) was added to powdered wax binder (3 g) and homogenised (7 minutes at 350 rpm; $g = 10.9$), and then pressed into pellets under pressure (7–10 tonnes). The pellets were analysed, and the resulting data oxide normalised and corrected for C content. Porewater analysis of $NO_3$ was attempted using Ion Chromotography but was below the limit of detection (0.05 mg/L), suggesting

that there was no robust denitrification taking place at the Ravenglass saltmarsh. Further, sulfate/chloride ratios in porewater were shown to decrease with depth, indicative of sulfate reduction taking place in deeper horizons of the sediment core.

### 4.3.2. Measurement of $^{99}$Tc

The vertical distribution of $^{99}$Tc in the Ravenglass sediment core was based on a previously published separation procedure (Keith-Roach et al., 2003) with amendments made for analysis of sediment samples. In brief, sediment samples (1.5 g) were wet-ashed (as Tc is volatile and so cannot be dry-ashed at high temperature >150 °C) with *aqua regia* (3:2 v/v; cHCl:c$HNO_3$). A yield tracer, $^{99m}$Tc (~140 MBq in 1 mL NaCl; $7 \times 10^{-12}$ mol) was obtained from the Manchester Royal Infirmary Nuclear Medicine Centre, and diluted to 2.5 mL with 0.1 M $HNO_3$. A pre-filled TEVA® resin column (Eichrom, 2 mL, 100–150 mesh) was preconditioned with 0.1 M $HNO_3$ (10 mL) to remove any impurities from the stock solution (Na, Cl, Ru, Mo). Then, 2 M $HNO_3$ (10 mL) was added to the column and passed through, to further clean the stock solution, and then $^{99m}$Tc was eluted with 8 M $HNO_3$ (5 mL).

An aliquot (5 µL) of this cleaned master stock solution was made up to 5 mL with 0.1 M $HNO_3$ in a plastic vial (HDPE Nalgene; 30 mL) and counted 3 times in standard geometry on the DSPEC 50 γ–spectrometer for 5 minutes to verify the activity of $^{99m}$Tc. The cleaned master stock was then sub-sampled to create a sub-stock in 0.1 M $HNO_3$ (430 kBq; 1 mL). This sub-stock was used for all further work. Three 40 kBq samples (in 2 % $HNO_3$) were created from this sub-stock, and these samples were sealed and used for decay correction during subsequent column work. An aliquot of $^{99m}$Tc yield monitor (40 kBq) was then added to each of the Ravenglass sample supernatants. Once added, the yield monitor was left to equilibrate for 30 mins with occasional agitation. Saturated NaOH (5–8 mL) was added to the sample to precipitate any impurities in the sample. Next, the supernatant was centrifuged (5 minutes at 4500 rpm; 1181 *g*) and the resulting supernatant filtered (Whatman GF/A; 0.22 µm). The filtrate was acidified to pH 6 (using a range of $HNO_3$ molarities (0.01–8 M $HNO_3$) to prevent further precipitation, and centrifuged (5 minutes at 4500 rpm; 1181 *g*) to remove any

solids, and filtered (Whatman GF/A; 0.22 µm). Then, TEVA® resin (Eichrom; 2 mL; 100–150 mesh) was pre-conditioned with 2 M $HNO_3$ (15 mL), and the filtrates passed through. The columns were washed with 2 M $HNO_3$ (40 mL) to remove Ru and Mo. The Tc bearing fraction was then eluted from the column with 8 M $HNO_3$ (10 mL) into a vial (HDPE Nalgene; 30 mL), and this was counted on the DSPEC γ–spectrometer for 5 minutes, at the $^{99}$Tc γ-emission line (140 keV) to allow recovery calculations of the $^{99m}$Tc tracer. The sample supernatants were then transferred to PYREX beakers (100 mL) and slowly evaporated to near dryness using a heat lamp. Samples were made up to 2.5 mL standard volume with 2 % $HNO_3$ and 1 M $NH_3OH$ (100 µl). The samples were then transferred to centrifuge tubes (15 mL) and rinsed with another 2 % $HNO_3$ (2.5 mL). Finally the samples were left to decay store for 14 half-lives (84 hours) to ensure the activity of $^{99m}$Tc was less than 0.4 Bq/mL after dilution (5 mL). The samples were counted on an Agilent 7500cx ICP-MS using standards that ranged in concentration from 0–300 ppt. The recovery of $^{99m}$Tc ranged between 40–68 % and the limit of detection for the analysis on the ICP–MS was ~ 50 pg/L.

### 4.3.3. Measurement of $^{236}$U

The activity of ultra-trace $^{236}$U was determined *via* extraction chromatography (Eichrom Technologies, 2005), similar to the method utilised by Al-Qasmi et al. (2016). Ravenglass saltmarsh sediment (2.0 g) was ashed at 500 °C for 5 hours and spiked with $^{233}$U yield tracer (300 µl; 4.8 mBq/mL). The sample was then boiled with *aqua regia*, (3:2 v/v, cHCl:c$HNO_3$) for 2 hours, and the resulting solution filtered (Whatman GF/A; 0.22 µm). The sediment residue was then rinsed with deionised water, and the filtrate evaporated to near-dryness. The dried residue was dissolved in 3 M $HNO_3$ (30 mL). Then, UTEVA® resin (Eichrom; 2 mL; 100–150 mesh) was preconditioned with 3 M $HNO_3$ (5 mL), and the sample (30 mL) passed through the column. The sample was washed through with 3 M $HNO_3$ (5 mL), 9 M HCl (20 mL), and 5 M HCl/0.05 M oxalic acid (20 mL). All these eluates were discarded, and thereafter U was eluted with 1 M HCl (15 mL) to a beaker containing carrier solution (10 % w/v $KHSO_4$; 1 mL).

The U samples were prepared for Accelerator Mass Spectrometry (AMS) based on the methods by Marsden et al. (2001) and Al-Qasmi et al. (2006). The U

fraction (15 mL) was reduced to (~3 mL), and Fe(III) nitrate nonahydrate in 0.1 M HCl (1 mL; 5 mg Fe/mL) added. This was evaporated to dryness, and the residue was dissolved in 1 M $HNO_3$ (15 ml) to remove any residual chlorides. This was evaporated to dryness and baked for ~1 hour at ~250 °C to convert the iron nitrate into iron oxide. The oxide residue was then placed in a Carbolite 201 furnace (450 °C for 8 hours) to ensure the conversion to Fe oxide. The U oxide (0.1 g) was mixed with Al powder (1 mg) and the mixture pressed into the small pit of an Al sample holder. The samples were then loaded onto the 32-sample wheel, inserted into the ion source of the AMS, and sequentially sputtered and analysed. The $^{236}U$:$^{238}U$ ratio was determined using a 14UD pelletron accelerator at the Australian National University. The detection system is based on a combined high-resolution velocity measurement by time-of-flight and energy measurements (see Fifield, 2008; Fifield et al., 2013). In addition, $^{236}U$:$^{234}U$ and $^{234}U$:$^{238}U$ ratios were measured using AMS, and calibrated for yield errors from the $^{233}U$ peak. Recoveries of the $^{233}U$ tracer were up to 20 %.

### 4.3.4. Measurement of $^{237}Np$

The activity of $^{237}Np$ in Ravenglass saltmarsh sediments was determined using column chromatography and HR-MC-ICP-MS (Zhao et al., 2014). Full details on the method used can be found in the SI (Section S1). In brief, $^{239}Np$ was used as the yield tracer, and was milked from the $^{243}Am$ parent stock solution. This was purified using two cycles of AGX®18 ion exchange resin (Bio-Rad laboratory; 2 mL; 50–100 mesh) to limit the ingrowth of $^{241}Am$ (as it decays to form the analyte of interest, $^{237}Np$). The purified $^{243}Am$ fraction was then passed through two further cycles of AGX®18 resin (Bio-Rad laboratory; 2 mL; 50–100 mesh) to milk the $^{239}Np$ daughter. The activity of the tracer obtained was monitored using liquid scintillation counting (TriCarb 2900TR, Perkin Elmer and Quantulus 1220, Wallac Perkin Elmer).

Ravenglass sediment samples (1.3 g) were ashed in a furnace (8 hours, 500 °C) to remove any organics and then boiled with *aqua regia* (3:2 v/v, cHCl:c$HNO_3$) for 2 hours. The resulting solution was spiked with clean $^{239}Np$ tracer (50–100 Bq). This solution was then passed through a further AGX®18 (Bio-Rad laboratory; 2 mL; 100–200 mesh) column to reduce any impurities arising from the sample. It

is generally considered that slow exchange rates can occur when large ions are absorbed onto higher cross-linked resins (Durham and Mills, 1953), and as such a greater mesh size, with a lower cross linkage was used for this step. Lastly, the purified sample was passed through UTEVA® resin (Eichrom; 2 mL; 50–100 mesh,) to reduce the amount of $^{238}$U, and prevent the tailing of the $^{238}$U peak with $^{237}$Np during NuPlasma HR-MC-ICP-MS analysis at the Glenn T. Seaborg Institute, Lawrence Livermore National Laboratory. Samples were analysed on the NuPlasma ICP-MS after ~2 weeks to allow th the decay of short-lived $^{239}$Np. The $^{239}$Np yield recovery was determined *via* γ-spectroscopy (Broad energy Ge detector, Canberra) and the γ-emission line at 277 keV was monitored. The $^{239}$Np activity in the purified samples was measured by γ-spectroscopy and compared to activities in the reference samples to determine the chemical yield during purification. Typically, Np recovery yields ranged between 20–90 %.

### 4.4. Results and Discussion

The Sellafield discharge histories for $^{99}$Tc, $^{237}$Np, and total U are available from 1978 (Gray et al., 1995; BNFL, 1993–2005; Sellafield Ltd, 2005–2017). It may be reasonable to assume that these radionuclides followed a similar trend to the releases of $^{241}$Am, $^{137}$Cs, and the Pu isotopes prior to offical records being kept, refecting changes in the operational history on-site (maximum discharge activity in mid-1970s). The exception to this is the discharge of $^{99}$Tc which also increased in the early 1990s due to the commissioning of EARP. The discharge histories for each of the radionuclides was used to date the sediment profiles discussed in this study, using an accumulation rate of 0.68 cm/yr (see Ray et al., 2018; Chapter 2), which was similar to previous authors (Morris et al., 2000; Marsden et al., 2006). It has now been widely accepted that the radionuclides discussed here take ~2 years to arrive to Ravenglass after disposal from the Sellafield pipeline (Aston and Stanners, 1982; Kershaw et al., 1990), and as such this lag-time was considered when matching the discharge histories to the Ravenglass sediment core radionculide profiles. As the analysis of trace concentrations of $^{99}$Tc, $^{236}$U, and $^{237}$Np require diffcult experimental techniques (short-lived, high activity tracers etc.), only select samples were analysed in this work.

### 4.4.1. Technetium ($^{99}$Tc) Distribution

The distribution of $^{99}$Tc with depth in Ravenglass sediments is shown in Figure 4.2A. The activity at the surface of the Ravenglass core was ~ 150 Bq/kg, highlighting possible contemporary deposition of $^{99}$Tc at the site, which is known to be a stable, active area of sedimentation (Aston and Stanners, 1998; Morris et al., 2000). Thereafter, the $^{99}$Tc activity increased with depth, reaching a maximum activity of 226 Bq/kg at 11 cm; this was followed by a marginal decrease in activity to a depth of 15 cm (162 Bq/kg). Subsequently, a further increase in activity (210 Bq/kg) was observed until 21 cm depth, and this activity remained fairly constant until the bottom of the sediment core (197 Bq/kg at 29 cm; Figure 4.2A). This $^{99}$Tc distribution is markedly different to previously published data from the site. For example, the next most recent $^{99}$Tc study at Ravenglass used sediment cores collected in 2002, and whilst the measured $^{99}$Tc activities (~ 50–225 Bq/kg; Lucey et al., 2004) are similar to those presented here, their $^{99}$Tc distribution showed marked enrichment at the sediment near surface (~ 6 cm). The authors suggested that this reflected preservation of elevated $^{99}$Tc input to the Irish Sea (post-EARP) and Ravenglass (Lucey et al., 2004). Earlier work from Ravenglass (using sediment cores collected in 1996 and showing lower $^{99}$Tc activities: 11–60 Bq/kg) also observed a distinct $^{99}$Tc maxima close to the sediment surface (6.5 cm; Morris et al., 2000); however, here the presence of $^{99}$Tc in deeper parts of the sediment (~ 8–20 cm) was suggested to reflect possible post-depositional remobilisation/migration of Tc. Beyond this suggestion, neither of the studies discussed the influence that the site biogeochemistry may have on $^{99}$Tc distribution.

We also note that the contemporary distribution of $^{99}$Tc at Ravenglass does not match the Sellafield $^{99}$Tc discharge history (also shown in Figure 4.2A). Here, discharged $^{99}$Tc peaked (190 TBq) during the mid-1990s due to EARP and in the late 1970's (180 TBq) (corresponding to ~ 12 and 24 cm respectively in the sediment core) and was otherwise much lower, including at present day (1.7 TBq). However, $^{99}$Tc is present at elevated activities throughout our core and this contrasts with the distribution profiles of other Sellafield-derived radionuclides at Ravenglass, namely $^{137}$Cs, $^{241}$Am, and $^{239,240}$Pu. These radionuclides are likely transported to the Ravenglass saltmarsh after prior reaction with sediments in the

Irish Sea mud-patch. Then, once deposited in the saltmarsh, they show limited to no post-depositional remobilisation, and preserve a record of the time-integrated Sellafield discharge record with depth (MacKenzie et al., 1994; Morris et al., 2000; Lucey et al., 2004; Lindahl et al., 2011; Ray et al., 2018; Chapter 3). This is clearly not the case with $^{99}$Tc; indeed, our contemporary $^{99}$Tc data (Figure 4.2A) appears to support Morris' assertion that post-depositional processes influence $^{99}$Tc distribution at Ravenglass.

A wealth of work on Tc biogeochemistry in laboratory systems has shown that Tc readily responds to changes in redox conditions. In particular, microbially-mediated Fe(III)-reducing conditions have been shown to favour Tc(VII) removal from solution, either as discrete $TcO_2$ phases or as Tc(IV) sorbed to solids (e.g. Frederickson et al., 2004; Burke et al., 2010; Lear et al., 2010). Thereafter, if redox conditions change and oxidising conditions prevail (e.g. $O_2$ or $NO_3^-$ are introduced to the sediment system), Tc(IV) can be partially oxidised and remobilised into solution (Law et al., 2010; Masters-Waage et al., 2017), and the presence of mixed Tc(VII)/Tc(IV) phases have previously been documented in Humber Estuary sediments (Burke et al., 2006).

At Ravenglass, the sediment system has been shown to be suboxic in the shallow subsurface (Ray et al., 2018; Chapter 3), with active Mn and Fe oxy(hydr)oxide cycling evident from porewater and sediment profiles (Figure 4.3; Ray et al., 2018; Chapter 3). Microbial community data (see Ray et al., 2018; Chapter 3) also supports this observation but additionally highlights that the sediment biogeochemistry is complex, with biomarkers for oxidising and reducing microbial communities often present in the same sediment horizons.

The Ravenglass saltmarsh also experiences percolation of water up through the sediments during tidal inundation (Carr and Blackley, 1986). Reflecting this, we suggest that the contemporary $^{99}$Tc distribution with depth in the Ravenglass sediments likely reflects some form of Tc response to the sites variable but dominantly suboxic chemistry. Here, $^{99}$Tc may arrive to the site already associated with sediments that are transported from the Irish Sea mud-patch (as per $^{137}$Cs, $^{241}$Am, and Pu; Ray et al., 2018; Chapter 3), and/or be transported to the site as $Tc(VII)_{(aq)}$ in seawater and then fixed in the sediment *via* diffusion and

reduction of $Tc(VII)_{(aq)}$ to $Tc(IV)_{(s)}$. Thereafter, the ephemeral redox conditions at the site "smear" $^{99}Tc$ throughout the sediments through repeated changes in solubility, masking any discharge trends for $^{99}Tc$ and redistributing Tc previously documented at the site (Morris et al., 2000; Lucey et al., 2004).

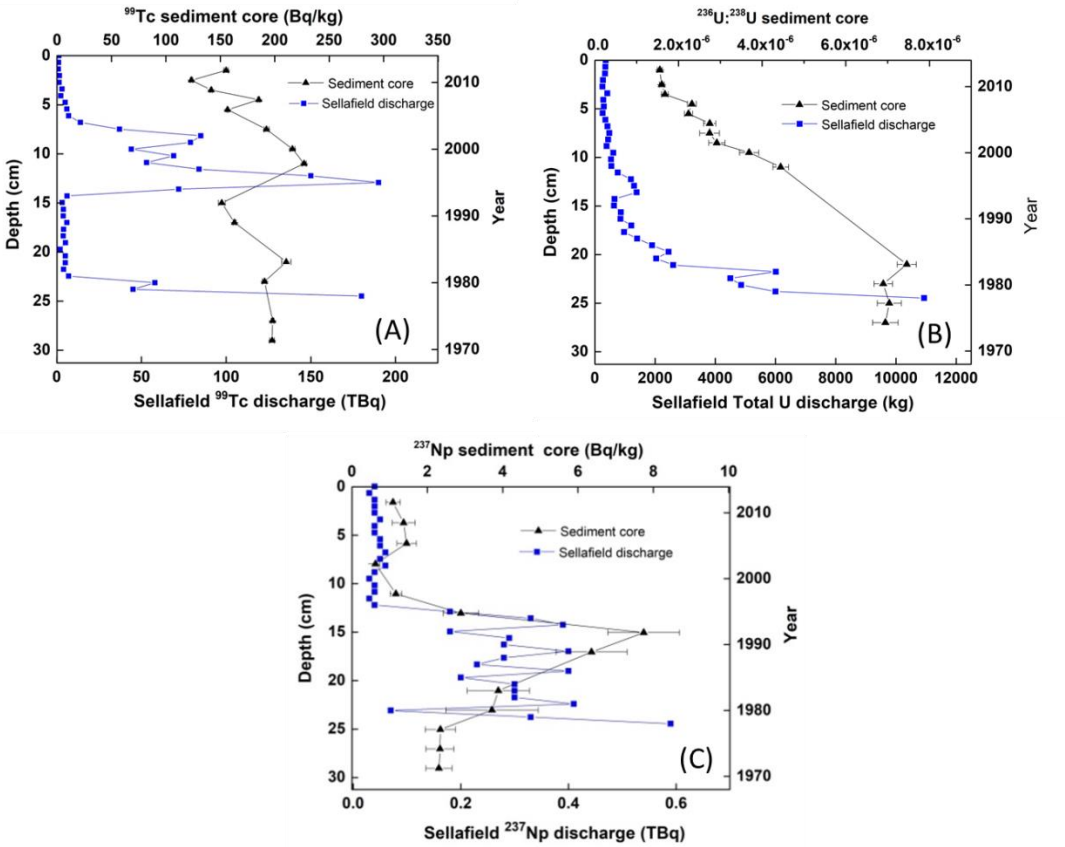


**Figure 4.2.** (A) Spatial distribution of $^{99}Tc$ in the Ravenglass sediment core vs. $^{99}Tc$ Sellafield discharges between 1978–2014; (B) spatial distribution of $^{236}U$:$^{238}U$ in the Ravenglass sediment core vs. total U Sellafield discharges between 1978–2014; (C) spatial distribution of $^{237}Np$ in the Ravenglass sediment core vs. $^{237}Np$ Sellafield discharges between 1978–2014. The sediment core was dated using an accumulation rate of 0.68 cm/yr obtained from particle reactive $^{241}Am$, $^{238}Pu$, and $^{239,240}Pu$ data (see Ray et al., 2018; Chapter 3).

Recent work in $^{99}$Tc amended sediment microcosm systems undergoing redox cycling has shown that Tc remains dynamic and can cycle between the sediment and solution phases over long timescales (> 1.5 years) (Masters-Waage et al., 2017). Further, the study showed that Tc was found to associate with Fe oxy(hydr)oxides phases in the sediment and solution (specifically Fe colloids). We thus suggest that the variable redox conditions manifest at the Ravenglass saltmarsh, and specifically Tc coupling to Fe biocycling, may explain the contemporary Tc distribution at this site (Figure 4.2A). Further, we note, that the sequential extraction work of Keith Roach et al. (2003) has previously recognised a predominant association of Tc with metal oxy(hydr)oxides in Ravenglass sediments.

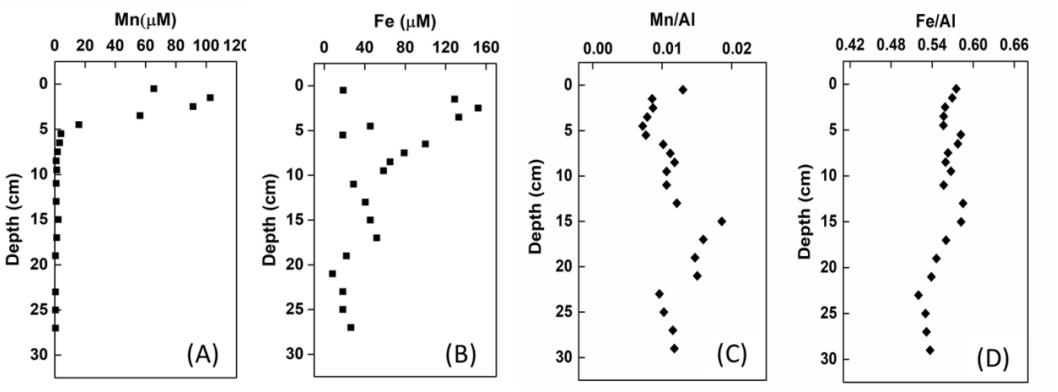


**Figure 4.3**. Porewater Mn and Fe concentrations (A and B) and solid Mn/Al and Fe/Al ratios (C and D) in the Ravenglass sediment core. Note each *x-axis* varies to best highlight trends in the data.

### 4.4.2. Uranium ($^{236}$U) Distribution

The distribution of $^{236}$U (expressed as a $^{236}$U:$^{238}$U ratio) with depth in Ravenglass saltmarsh sediments is shown in Figure 4.2B. The lowest $^{236}$U activity was observed at the surface of the core ($1.5 \times 10^{-6}$), and this steadily increased with depth until 20 cm, where a maximum $^{236}$U activity of $7.5 \times 10^{-6}$ was attained. This marginally decreased to $6.9 \times 10^{-6}$ by 23 cm, and remained near-constant to the bottom of the core (Figure 4.2B). This profile highlights the presence of elevated $^{236}$U:$^{238}$U in the order of $10^{-6}$ throughout the core (~8 orders of magnitiude higher than the natural $^{236}$U:$^{238}$U baseline ($10^{-14}$; Zhao et al., 1997). This is also similar

to other studies conducted with Irish Sea materials (Marsden et al., 2001; Povinec et al., 2002; Lee et al., 2008; Srncik et al., 2011; Eigl et al., 2013) that have highlighed the presence of Sellafield derived U.

The most recent study of $^{236}U$ distribution in Ravenglass saltmarsh sediments used materials collected in 2000 (Marsden et al., 2001), and presented a profile which contrasts significantly to that shown in Figure 4.2B. Marsden et al. (2001) showed a distinct $^{236}U$:$^{238}U$ peak centred at 18 cm depth ($2.7 \times 10^{-5}$) in their core, with the $^{236}U$:$^{238}U$ ratio decreasing to $6.4 \times 10^{-6}$ and $9.6 \times 10^{-6}$ at 0.6 and 29 cm, respectively. If this feature where to be buried with no depositional remobilisation, this sub-surface peak would now be centred at ~27.5 cm (using a sed rate of 0.68 cm/yr; Ray et al., 2018; Chapter 3), and this is clearly not the case (Figure 4.2B). Marsden and co-workers suggested that the sub-surface peak likely reflected the preservation of the Sellafield U discharge history (Figure 2B) in the Ravenglass sediment, after physical transport of U-bearing sediment particles to from the Irish Sea mud-patch. They also suggested that the width of the $^{236}U$ peak may reflect some degree of post-depositional remobilisation of $^{236}U$ from the sediment during burial.

The contemporary distribution of $^{236}U$ at Ravenglass is compared to the Sellafield total U discharge history in Figure 4.2B. Of note, the U discharged from the Sellafield pipeline contains a range of U isotopes, including $^{235}U$, $^{236}U$, and $^{238}U$; however, only the mass of total U discharged has been recorded. Sellafield U discharges peaked in the late 1970s (~10000 kg/yr), and subsequently decreased throughout the 1980s, reaching consistenly low values by 1992 (~60 kg/yr) that continue to this day. Whilst there is some commonality between the comtemporary $^{236}U$ distribution in the Ravenglass sediments and the discharge record (i.e. reflecting some preservation of the discharge history), there is a slight offset between the decrease in U discharge starting in the mid-1980s and the U distribution preserved in the sediment core. Specifically, the $^{236}U$ activity remains reasonably high in shallow sediment horizons (irrespective of any potential lag effect in the transport of U to Ravenglass; Aston and Stanners; 1982; Kershaw et al., 1990) relative to a significant decrease in U discharges. However, a lack of fidelty in our data between 11 and 21 cm precludes full evaluation of this offset. Regardless, U does not appear to behave as per $^{137}Cs$, $^{241}Am$, and Pu (see Ray et

al., 2018; Chapter 3) which show strong preservation controls. Instead, at least some of the Sellafield-derived U may respond to post-depositional redox controls as previously discussed for $^{99}$Tc and as suggested by Marsden et al. (2001).

The behaviour of U in suboxic to anoxic sediment systems is well understood (see the review of Newsome et al., 2014) with changes in redox conditions shown to influence its solubility and hence mobility. In particular, microbially mediated Fe(III)-reducing conditions have been shown to encourage $U(VI)_{(aq)}$ removal from solution, either as crystalline $UO_{2(s)}$ (e.g. Lovley et al., 1991) or non-crystalline, monomeric $U(IV)_{(s)}$ phases (e.g. Bernier-Latmani et al., 2010; Campbell et al., 2011). Thereafter, any fluctuations in the redox conditions may cause partial remobilisation of U back into solution, either *via* oxidation of $U(IV)_{(s)}$ to $U(VI)_{(aq)}$ with $O_2$, $NO_3^-$, Fe(III) minerals and Mn(IV) oxides (Finneran et al., 2002; Senko et al., 2002, 2005; Sani et al., 2005; Begg et al., 2011; Law et al., 2011; Wang et al., 2013). Given the dynamic biogeochemistry of the Ravenglass site (see section 4.4.1), it is likely that some $^{236}$U cycles in the Ravenglass sediment, as per Tc. Here, U likely arrives to the saltmarsh associated with Irish Sea mud-patch sediments, or is transported to the site as U(VI) in seawater, followed by reductive precipitation in the sediments under Fe(III)-reducing conditions. Therafter, as U is buried in the sediment, a proportion is remobilised under the ephemeral redox conditions, and this labile U moves to shallower and/or deeper sediment horizons, where it is either removed again to the sedments (e.g. *via* sorption of U(VI) to mineral phases, or *via* reductive precipitation), or is potentially lost to overlying waters.

### 4.4.3. Neptunium ($^{237}$Np) Distribution

The distribution of $^{237}$Np with depth in Ravenglass sediments is shown in Figure 4.2C. The activity of $^{237}$Np observed between 0–11 cm at Ravenglass is low (0.6–1.45 Bq/kg). Thereafter, a sharp increase in $^{237}$Np activity is observed, and this reaches a maximum activity (7.7 Bq/kg) at a depth of 15 cm. This $^{237}$Np peak is followed by a subsequent decrease in $^{237}$Np activity (2.3 Bq/kg) to a depth of 25 cm, with this activity remaining reasonably constant to the bottom of the core (Figure 4.2C). The presence of a distinct $^{237}$Np peak in the Ravenglass core differs to previously published data from the site. The next most recent study

found similar $^{237}$Np activities in Ravenglass sediments (0.7–13.0 Bq/kg; Morris et al., 2000) but here, the $^{237}$Np distribution profile showed a slight enrichment in activity at the sediment surface (depth of 0.6 cm), with no subsurface peak observed. Further, as this profile did not show any pronounced peaks with depth (corresponding to the elevated 1978 discharges), and did not reflect the $^{237}$Np discharge history, the authors suggested that Np had possibly migrated through the sediment after deposition (Morris and Livens, 1996). Of note, earlier work at Ravenglass also examined $^{237}$Np concentrations in surface samples, and these studies showed similar $^{237}$Np activities to those presented here (4.4 Bq/kg; Assinder et al., 1991; 3.6 Bq/kg; Yamamoto et al., 1991). Pentreath and Harvey (1981) highlighted that the $^{237}$Np activity at the Irish Sea mud-patch was ~1.6 Bq/kg.

We also observe that the contemporary distribution of $^{237}$Np at Ravenglass does not match the Sellafield $^{237}$Np discharge history (Figure 4.2C). Sellafield discharged $^{237}$Np peaked in 1978 (corresponding to ~24 cm in our sediment core) and showed noticeable fluctuations in activity (but remained high) until 1996 (11 cm in our core); thereafter a much lower $^{237}$Np activity was discharged and this is maintained to present day. The $^{237}$Np activity peak in our core is centred in a sediment horizon dated to the early 1990s. As discussed for $^{99}$Tc and $^{236}$U, this contrasts with the distribution of Sellafield-derived Cs, Am, and Pu in Ravenglass sediments (see Ray et al., 2018; Chapter 3), which preserve the Sellafield discharge record. Thus the $^{237}$Np profile presented here may agree with Morris' proposal that post-depositional remobilisation of $^{237}$Np may influence its distribution; assuming that Np is transported to the site adhered to sediment grains remobilised from the Irish Sea mud-patch (Pentreath and Harvey, 1981). However, it is also important to note that Np can be transported, and deposited to the site in solution.

Compared to Tc and U, Np biogeochemistry is poorly defined. However, there is evidence to suggest that Np(V) can sorb to Fe(III) and Mn(IV) oxy(hydroxides) (Combes et al., 1992; Wilk et al., 2005; Kenna, 2009). Accordingly, Np may sorb to sediments in the Irish Sea mud-patch *via* this mechanism and then be transported to Ravenglass, and/or aqueous Np may be transported to Ravenglass, followed by sorption to Fe- and Mn-bearing sediment present at this site.

Alternatively, Np(V) can be reduced to solid Np(IV) phases under microbially mediated Mn and Fe(III) reducing conditions (e.g. Moyes et al., 2002; Law et al., 2010; Brookshaw et al., 2015; Thorpe et al., 2015). This reaction pathway may have encouraged $Np_{(aq)}$ removal to sediments either at the mud-patch (with subsequent transport to Ravenglass), or directly at Ravenglass. Regardless, once deposited at Ravenglass, fluctuating redox conditions at the site could have encouraged Np to migrate to a depth where $Np(IV)_{(s)}$ phases are most stable. Neptunium redox cycling has been documented in sediment systems, albeit under constrained laboratory conditions (Law et al., 2010; Thorpe et al., 2015). Here, Np(IV) was partially remobilised as Np(V) when the sediment system was exposed to dissolved $O_2$, whilst some of the Np(IV) was resistant to oxidation and remained associated with the sediments. At Ravenglass, we note that the contemporary Np maximum (Figure 4.2C) is situated in the zone of active Fe(III) reduction (Figure 4.3), where one would expect $Np(V)_{(aq)}$ to be reduced to, and stabilised, as Np(IV). However, given the ephemeral redox conditions at the site, this pool of Np(IV) cannot be completely buried with depth as some of the Np in the sediment is likely remobilised by upwards moving oxic water, brought into the sediment system by rising tides. In turn, there is a degree of preservation and burial of the time-integrated $^{237}Np$ discharge signal, but also recycling of a proportion of the Np in the region of Fe-cycling, possibly explaining the subsurface horizon.

### 4.5. Conclusions

Low-level aqueous waste containing $^{99}Tc$, $^{237}Np$, and U is legally discharged from the Sellafield site into the Eastern Irish Sea. An enhanced discharge of total U and $^{237}Np$ occurred in 1978, whereas $^{99}Tc$ discharges increased in 1978 and 1994, the latter as a result of the commissioning of EARP. Regardless, at the point of discharge, $^{99}Tc$, $^{237}Np$, and U likely associate with finely grained sediments in the Irish Sea, where radionuclide-associated particulates are bio-mixed, and remobilised, and subsequently transported to coastal locations in Cumbria. Previous work from the same sampling campaign (Ray et al., 2018; Chapter 3) has highlighted that the distribution of Sellafield-derived $^{137}Cs$, $^{241}Am$, and Pu in Ravenglass sediments shows a good agreement to their discharge histories, thereby inferring that there is likely deposition and burial of these

radionuclides, with little post-depositional remobilisation. In contrast, the sediment profiles of $^{99}$Tc, $^{236}$U, and $^{237}$Np in Ravenglass sediments do not provide a good match to their Sellafield discharge histories. Instead, as previously observed in laboratory experiments, it seems likely that there is some cycling of $^{99}$Tc, $^{236}$U, and $^{237}$Np between the solution and sediment phase favoured by the prevailing suboxic conditions at the Ravenglass saltmarsh. Thus, this results in the post-depositional remobilisation of all three radionuclides in the order: Tc > U > Np. A key finding of this work is that redox-active cycling of these radionuclides may occur in the field over many decades, an observation that has previously been largely restricted to the laboratory. In addition, $^{99}$Tc, $^{237}$Np, and U were all detected in surface sediments of Ravenglass, in contrast to low modern releases from the Sellafield pipeline. This suggests that the offshore Irish Sea sediments will continue to supply radionuclide-associated silt to coastal locations in the UK. As the UK government (e.g. the Environment Agency and Food Standards Agency) does not monitor $^{99}$Tc, $^{237}$Np, and U in the Eastern Irish Sea area (due to the difficulty in analysis), this work provides a unique, contemporary insight into the behaviour of these radionuclides in the marine environment > 65 years after they were first discharged into the marine environment.

## References


Al-Qasmi, H., Law, G.T.W., Bryan, N.D., Livens, F.R., 2015. Transport and accumulation of stable metals and radonuclides in Dulas Bay, North Wales. Environmental Radiochemical Analysis V. 50–60.

Al-Qasmi, H., Law, G.T.W., Fifield, K.L., Livens, F.R., 2016. Origin of artificial radionuclides in soil and sediment from North Wales. J. Environ. Radioactiv. 151, 244–249.

Al-Qasmi, H., Law, G.T.W., Fifield, K.L., Howe, J., Brand, T., Cowie, G.L., Law, K.A., Livens, F.R., 2017. Deposition of artificial radionuclides in sediments of Loch Etive, Scotland. J. Environ. Radioactiv (In press).

Assinder, D.J., Yamamoto, M., Kim, C.K., Seki, C.R., Takaku, Y., Yamauchi, Y., Komura, K., Ueno, K., Bourne, G.S., 1991. Neptunium in intertidal coastal and estuarine sediments in the Irish Sea. J. Environ. Radioactiv. 14, 135–145.

Assinder, D.J. 1999. A review of the occurrence and behaviour of neptunium in the Irish Sea. J. Environ. Radioactiv. 44 (2–3), 335–347.

Aston, S.R., Stanners, D.A., 1981. Americium in intertidal sediments from the coastal environs of Windscale. Mar. Pollut. Bull. 12 (5), 149–153.

Aston, S.R., Stanners, D.A., 1981. Plutonium transport to and deposition and immobility in Irish Sea intertidal sediments. Nature. 289 (5798), 581–582.

Aston, S.R., Stanners, D.A., 1982. The transport to and deposition of americium in intertidal sediments of the Ravenglass estuary and its relationship to plutonium. Environ. Pollut. B. 3 (1), 1–9.

Aston, S.R., Assinder, D.J., Kelly, M., 1985. Plutonium in intertidal coastal and estuarine sediments in the Northern Irish Sea. Estuar. Coast. Shelf. S. 20(6), 761–771.

Begg, J.D.C., Burke, I.T., Morris, K., 2007. The behaviour of technetium during microbial reduction in amended soils from Dounreay, UK. Sci. Total. Environ. 373, 297–304.

Begg, J.D.C., Burke, I.T., Lloyd, J.R., Boothman, C., Shaw, S., Charnock, J.M., Morris, K., 2011. Bioreduction behavior of U(VI) sorbed to sediments. Geomicrobiol. J. 28, 160–171.

Behrends, T., Cappellen, P. Van., 2005. Competition between enzymatic and abiotic reduction of uranium(VI) under iron reducing conditions. Chem. Geol. 220, 315–327.

Bernier-Latmani, R., Veeramani, H., Vecchia, A., Junier, P., Lezama-Pacheco, J., Suvorova, E., Sharp, J., Wigginton, N., Bargar, J., 2010. Non-uraninite products of microbial U(VI) reduction. Environ. Sci. Technol. 44 (24), 9456–9462.

BNFL, 1993–2005. Annual report on radioactive discharges and monitoring of the environment. Bristish Nuclear Fuels plc. Risley.

Bondietti, E., Francis, C., 1979. Geologic migration potentials of technetium-99 and neptunium-237. Science. 203 (1), 1337–1340.

Boyd, G., 1978. Osmotic and activity coefficients of aqueous $NaTcO_4$ and $NaReO_4$ solutions at 25 $^oC$. J. Solution. Chem. 7, 229–238.

Brookshaw, D.R., Pattrick, R.A.D., Bots, P., Law, G.T.W., Lloyd, J.R., Mosselmans F.J.W., Vaughan, D.J., Dardenne, K., Morris, K., 2015. Redox interactions of Tc(VII), U(VI), and Np(V) with microbially reduced biotite and chlorite. Environ. Sci. Technol. 49, 13139–13148.

Brookshaw, D.R., Lloyd, J.R., Vaughan, D.J., Pattrick, R.A.D., 2016. Effects of microbial Fe(III) reduction on the sorption of Cs and Sr on biotite and chlorite. Geomicrobiol. J. 33 (3–4), 206–215.

Burke, I., Boothman, C., Lloyd, J.R., Livens, F.R., Charnock, J.M., McBeth, J., Mortimer, J., Morris, K., 2006. Reoxidation behavior of technetium, iron, and sulfur in estuarine sediments. Environ. Sci. Technol. 40, 3529–3535.

Burke, I.T., Boothman, C., Lloyd, J.R., Mortimer, R.J.G., Livens, F.R., Morris, K., 2005. Effects of progressive anoxia on the solubility of technetium in sediments. Environ. Sci. Technol. 39 (11), 4109–4116.

Burke, I.T., Boothman, C., Lloyd, J.R., Livens, F.R, Charnock, J.M., McBeth, J. M., Mortimer, R.J.G., Morris, K., 2006. Reoxidation behavior of technetium, iron, and sulfur in estuarine sediments. Environ. Sci. Technol. 40, 3529–3535.

Burke, I. T., Livens, F.R., Lloyd, J.R., Brown, A.P., Law, G.T.W., McBeth, J.M., Ellis, B.L., Lawson, R.S., Morris, K., 2010. The fate of technetium in reduced estuarine sediments: combining direct and indirect analyses. Appl. Geochem. 25, 233–241.

Byrne, A. R., 1986. Determination of $^{237}Np$ in cumbrian (UK) sediments by neutron activation analysis: preliminary results. J. Environ. Radioactiv. 4, 133–144.

Caborn, J.A., Howard, B.J., Blowers, P., Wright, S.M., 2016. Spatial trends on an ungrazed west cumbrian saltmarsh of surface contamination by selected radionuclides over a 25 year period. J. Environ. Radioactiv. 151, 94–104.

Campbell, K.M., Davis, J.A., Bargar, J., Giammar, D., Bernier-Latmani, R., Kukkadapu, R., Williams, K.H., Veramani, H., Ulrich, K.-U., Stubbs, J., Yabusaki, S., Figueroa, L., Lesher, E., Wilkins, M. J., Peacock, A., Long, P.E., 2011. Composition, stability, and measurement of reduced uranium phases for groundwater bioremediation at Old Rifle, CO. Appl. Geochem. 26, 167–169.

De Cesare, M., Fifield, L.K., Sabbarese, C., Tims, S.G., De Cesare, N., D'onofrio, A., D'arco, A., Esposito, A.M., Petraglia, A., Roca, V., Terrasi, F., 2013. Actinides AMS at CIRCE and $^{236}U$ and Pu measurements of structural and environmental samples from in and around a mothballed nuclear power plant. Nucl. Instrum. Meth. B. 294, 152–159.

Choppin, G.R., Liljenzin, J., Rydberg, J., 2002. Radiochemistry and Nuclear

Chemistry. Oxford. Heinemann and Butterworth.

Choppin, G.R. 2006. Environmental behavior of actinides. Czech. J. Phys. 56, 13–21.

Choppin, G.R. 2007. Actinide speciation in the environment. J. Radioanal. Nucl. Chem. 273 (3), 695–703.

Christiansen, B.C., Geckeis, H., Marquardt, C.M., Bauer, A., Römer, J., Wiss, T., Schild, D. and Stipp, S.L.S., 2011. Neptunyl ($NpO_2^+$) interaction with green rust, $GR_{Na,SO_4}$. Geochim. Cosmochim. Ac. 75, 1216–1226.

Fifield, L.K., Tims, S.G., Stone, J.O., Argento, D.C., De Cesare, M., 2013. Ultra-sensitive measurements of $^{36}Cl$ and $^{236}U$ at the Australian National University. Nucl. Instrum. Meth. B. 294, 126–131.

Clark, D.L., Hobart, D.E., Neu, M.P., 1995. Actinide carbonate complexes and their importance in actinide environmental chemistry. Chem. Rev. 95, 25–48.

Combes, J.-M., Chisholm-Brause, C.J., Brown, G.E., Parks, G.A., Conradson, S. D., Eller, P.G., Trlay, I.R., Hobart, D.E., Meljer, A., 1992. EXAFS spectroscopic study of neptunium(V) sorption at the $\alpha$-FeOOH/water interface. Environ. Sci. Technol. 26, 376–382.

Cook, G.T., MacKenzie, A.B., McDonald, P., Jones, S.R., 1997. Remobilization of Sellafield-derived radionuclides and transport from the north-east Irish Sea. J. Environ. Radioactiv. 35 (3), 227–241.

Cumberland, S.A., Douglas, G., Grice, K., Moreau, J.W., 2016. Uranium mobility in organic matter-rich sediments: a review of geological and geochemical processes. Earth. Sci. Rev. 159, 160–185.

Dahlgaard, H., 1995. Transfer of european coastal pollution to the Arctic: radioactive Tracers, Mar. Pollut. Bull. 31, 3–7.

Duff, M.C., Coughlin, J.U., Hunter, D.B., 2002. Uranium co-precipitation with iron oxide minerals. Geochim. Cosmochim. Ac. 66 (20), 3533–3547.

Durham, R.W., Mills, R., 1953. The absorption of plutonium by anion resins. Atomic Energy of Canada. Ontario (CEI-62).

Eichrom Technologies. 2005. Uranium in soil (2 gram sample). Analytical Procedures, ACS07, Rev. 1.5.

Eigl, R., Srncik, M., Steier, P., Wallner, G., 2013. $^{236}U/^{238}U$ and $^{240}Pu/^{239}Pu$ isotopic ratios in small (2 L) sea and river water samples. J. Environ. Radioactiv. 116, 54–58.

Fifield, L.K. 2008. Accelerator mass spectrometry of the actinides. Quat. Geochronol. 3, 276–290.

Finegan, P., León Vintró, L., Mitchell, P.I., Boust, D., Gouzy, A., Kershaw, P.J., Lucey, J.A. 2009. Accumulation, solid partitioning and remobilisation of $^{99}Tc$ in subtidal and intertidal sediments in the Irish Sea. Cont. Shelf. Res. 29, 1995–

2010.

Finneran, K.T., Housewright, M.E., Lovley, D.R., 2002. Multiple influences of nitrate on uranium solubility during bioremediation of uranium-contaminated subsurface sediments. Environ. Microbiol. 4(9), 510–516.

Fredrickson, J.K., Zachara, J.M., Kennedy, D.W., Kukkadapu, R.K., McKinley, J. P., 2004. Reduction of $TcO_4^-$ by sediment-associated biogenic Fe(II) reduction of $TcO_4^-$ by sediment-associated biogenic Fe(II). Geochim. Cosmochim. Ac. 68 (15), 3171–3187.

Froehlich, M.B., Chan, W.Y., Tims, S.G., Fallon, S.J., Fifield, L.K., 2016. Time-resolved record of $^{236}U$ and $^{239,240}Pu$ isotopes from a coral growing during the nuclear testing program at Enewetak Atoll (Marshall Islands). J. Environ. Radioactiv. 165, 197–205.

Gorman-Lewis, D., Fein, J.B., Burns, P.C., Szymanowski, J.E.S., Converse, J., 2008. Solubility measurements of the uranyl oxide hydrate phases metaschoepite, compreignacite, Na–compreignacite, becquerelite, and clarkeite. J. Chem. Thermodyn. 40, 980–990.

Gray, J., Jones, S.R., Smith, A.D., 1995. Discharges to the environment from the Sellafield Site, 1951–1992. J. Radiol. Prot. 15 (2), 99–131.

Hursthouse, A.S., Baxter, M.S., Livens, F.R., Duncan, H.J., 1991a. Transfer of Sellafield-derived $^{237}Np$ to and within the terrestrial environment. J. Environ. Radioactiv. 14, 147–174.

Icopini, G.A., Boukhalfa, H., Neu, M.P., 2007. Biological reduction of Np(V) and Np(V) citrate by metal-reducing bacteria. Environ. Sci. Technol. 41, 2764–2769.

Jenkinson, S., McCubbin, D., Kennedy, P.H., Dewar, A., Bonfield, R., Leonard, K., 2014. An estimate of the inventory of $^{99}Tc$ in the sub-tidal sediments of the Irish Sea. J. Environ. Radioactiv. 133, 40–47.

Kaplan, D.I., Kukkadapu, R., Seaman, J.C., Arey, B.W., Dohnalkova, A.C., Buettner, S., Li, D., Varga, T., Scheckel, K.G., Jaffé, P. R., 2016. Iron mineralogy and uranium-binding environment in the rhizosphere of a wetland soil. Sci Total. Environ. 569–570, 53–64.

Kaszuba, J.P., Runde, W.H., 1999. The aqueous geochemistry of neptunium: dynamic control of soluble concentrations with applications to nuclear waste disposal. Environ. Sci. Technol. 33, 4427–4433.

Keeney-Kennicutt, W.L., Morse, J.W., 1984. The interaction of $Np(V)O_2^+$ with common mineral surfaces in dilute aqueous solutions and seawater. Mar. Chem. 15 (2), 133–150.

Keith-Roach, M.J., Morris, K., and Dahlgaard, H., 2003. An investigation into technetium binding in sediments. Mar. Chem. 81, 149–162.

Keith-Roach, M.J., Roos, P., 2004. Redox-dependent behaviour of technetium-99 entering a permanently stratified anoxic fjord (Framvaren fjord, Norway). Estuar. Coastal. Shelf. S. 60, 151–161.

Kenna, T.C. 2009. Using sequential extraction techniques to assess the partitioning of plutonium and neptunium-237 from multiple sources in sediments from the Ob River (Siberia). J. Environ. Radioactiv. 100, 547–557.

Keogh, S.M., Aldahan, A., Possnert, G., Finegan, P., León Vintró, L., Mitchell, P. I., 2007. Trends in the spatial and temporal distribution of $^{129}$I and $^{99}$Tc in coastal waters surrounding Ireland using *Fucus vesiculosus* as a bio-indicator. J. Environ. Radioactiv. 95 (1), 23–38.

Kershaw, P.J., Swift, D.J., Pentreath, R.J., Lovett, M.B., 1983. Plutonium redistribution by biological activity in Irish Sea sediments. Nature. 306 (5945), 774–775.

Kershaw, P.J., Woodhead, D.S., Malcolm, S.J., Allington, D.J., Lovett, M.B., 1990. A sediment history of Sellafield discharges. J. Environ. Radioactiv, 12, 201–241.

Kershaw, P.J., Pentreath, R.J., Woodhead, D.S., Hunt, G.J., 1992. A review of radioactivity in the Irish Sea, in: Aquatic Environmental Monitoring Report. Lowestoft, UK. Ministry of Agriculture Fisheries and Food. 32, 1–66.

Kershaw, P., McCubbin, D., Leonard, K., 1999. Continuing contamination of north Atlantic and Arctic waters by Sellafield radionuclides. Sci. Total. Environ. 237/238, 119–132.

Kuwabara, J., Yamamoto, M., Assinder, D.J., Komura, K., Ueno, K., 1996. Sediment profile of Np-237 in the Irish Sea: estimation of the total amount of Np-237 discharged from Sellafield. Radiochim. Acta. 73 (2), 73–81.

Latta, D.E., Boyanov, M.I., Kemner, K.M., O'loughlin, E.J., Scherer, M.M., 2012. Abiotic reduction of uranium by Fe(II) in soil. Appl. Geochem. 27, 1512–1524.

Law, G.T.W., Geissler, A., Boothman, C., Burke, I.T., Livens, F., Lloyd, J.R., Morris, K., 2010. Role of nitrate in conditioning aquifer sediments for technetium bioreduction. Environ. Sci. Technol. 44, 150–155.

Law, G.T.W., Geissler, A., Lloyd, J.R., Livens, F.R., Boothman, C., Begg, J.D. C., Denecke, M.A., Rothe, J., Dardenne, K., Burke, I.T., Charnock, J.M., Morris, K., 2010. Geomicrobiological redox cycling of the transuranic element neptunium. Environ. Sci. Technol. 44, 8924–8929.

Law, G.T.W., Geissler, A., Burke, I.T., Livens, F.R., Lloyd, J.R., McBeth, J.M., Morris, K., 2011. Uranium redox cycling in sediment and biomineral systems. Geomicrobiol. J. 28, 497–506.

Lear, G., McBeth, J.M., Boothman, C., Gunning, D.J., Ellis, B.L., Lawson, R.S., Morris, K., Burke, I.T., Bryan, N. D., Brown, A.P., Livens, F.R., Lloyd, J.R., 2010. Probing the biogeochemical behavior of technetium using a novel nuclear imaging approach. Environ. Sci. Technol. 44 (1), 156–162.

Lee, J.-H., Zachara, J.M., Fredrickson, J.K., Heald, S.M., McKinley, J.P., Plymale, A.E., Resch, C.T., Moore, D.A., 2014. Fe(II)- and sulfide-facilitated

reduction of $^{99}Tc(VII)O_4^-$ in microbially reduced hyporheic zone sediments, Geochim. Cosmochim. Ac. 136, 247–264.

Lee, S.H., Povinec, P.P., Wyse, E., Hotchkis, M.A.C., 2008. Ultra-low-level determination of $^{236}U$ in IAEA marine reference materials by ICPMS and AMS. Appl. Radiat. Isotopes. 66, 823–828.

Leonard, K.S., McCubbin, D., Brown, J., Bonfield, R., Brooks, T., 1997. Distribution of Technetium-99 in UK coastal waters. Mar. Pollut. Bull. 34 (8), 628–636.

Leonard, K.S., McCubbin, D., McDonald, P., Service, M., Bonfield, R., Conney, S., 2004. Accumulation of technetium-99 in the Irish Sea?. Sci. Total. Environ. 322, 255–270.

Leonard, K., McCubbin, D., Jenkinson, S., Bonfield, R., McMeekan, I., 2008. An assessment of the availability of Tc-99 to marine foodstuffs from contaminated sediments. CEFAS. Lowestoft (RL 09/08).

Lindahl, P., Ellmark, C., Gäfvert, T., Mattsson, S., Roos, P., Holm, E., Erlandsson, B., 2003. Long-term study of $^{99}Tc$ in the marine environment on the Swedish west coast. J. Environ. Radioactiv. 67, 145–156.

Lindahl, P., Worsfold, P., Keith-Roach, M., Andersen, M. B., Kershaw, P., Leonard, K., Choi, M.-S., Boust, D., Lesueur, P., 2011. Temporal record of Pu isotopes in inter-tidal sediments from the northeastern Irish Sea. Sci. Total. Environ. 409 (23), 5020–5025.

Liu, D.J., Fan, X.H., 2005. Adsorption behavior of $^{99}Tc$ on Fe, $Fe_2O_3$ and $Fe_3O_4$. J. Radioanal. Nucl. Chem. 264 (3), 691–698.

Livens, F.R., Horrill, A.D., Singleton, D., 1994. Plutonium in estuarine sediments and the associated interstitial waters. Estuar. Coastal. Shelf. S. 38, 479–489.

Lloyd, J.R., Sole, V.A., Van Praagh, C.V., Lovley, D.R., 2000. Direct and Fe(II)-mediated reduction of technetium by Fe(III)-reducing bacteria. Appl. Environ. Microb. 66 (9), 3743–3749.

Lovley, D.R., Phillips, E.J., Gorby, Y.A., Landa, E.R., 1991. Microbial reduction of uranium. Nature. 350, 413–416.

Lucey, J.A., Gouzy, A., Boust, D., Leon Vintro, L., Kershaw, P.J., Mitchell, P.I., 2004. Geochemical fractionation of plutonium in anoxic Irish Sea sediments using an optimised sequential extraction protocol. Appl. Radiat. Isotopes. 60, 379–385.

MacKenzie, A.B., Scott, R.D., 1982. Radiocaesium and plutonium in intertidal sediments from southern Scotland. Nature. 299, 613–616.

MacKenzie, A.B., Scott, R.D., 1993. Sellafield waste radionuclides in lrish Sea intertidal and salt marsh sediments, Environ. Geochem. Hlth. 15(2/3), 173–184.

MacKenzie, A., Scott, R., Allan, R.L., Ben Shaban, Y.A., Cook, G., Pulford, I. D., 1994. Sediment radionuclide profiles: implications for mechanisms of

Sellafield waste dispersal in the Irish Sea. J. Environ. Radioactiv. 23, 39–69.

Malcolm, S.J., Kershaw, P.J., Lovett, M.B., Harvey, B.R., 1990. The interstitial water chemistry of $^{239,240}$Pu and $^{241}$Am in the sediments of the north-east Irish Sea. Geochim. Cosmochim. Ac. 54, 29–35.

Marsden, O.J., Livens, F.R., Day, J.P., Fifield, L.K., Goodall, P.S., 2001. Determination of U-236 in sediment samples by accelerator mass spectrometry. Analyst. 126 (5), 633–636.

Marsden, O.J., Abrahamsen, L., Bryan, N.D., Day, P.J., Fifield, L.K., Gent, C., Goodall, P.S., Morris, K., Livens, F.R., 2006. Transport and accumulation of actinide elements in the near-shore environment: field and modelling studies. Sedimentology. 53 (1), 237–248.

Marshall, M.J., Plymale, A., Kennedy, D.W., Shi, L., Wang, Z., 2008. Hydrogenase- and outer membrane c-type cytochrome-facilitated reduction of technetium(VII) by *Shewanella oneidensis* MR-1. Environ. Microbiol. 10 (1), 125–136.

Marshall, T.A., Morris, K., Law, G.T.W., Livens, F.R., Mosselmans, F.J.W., Bots, P., Shaw, S., 2014. Incorporation of uranium into hematite during crystallization from ferrihydrite. Environ. Sci. Technol. 48, 3724–3731.

Masters-Waage, N.K., Morris, K., Lloyd, J.R., Shaw, S., Mosselmans, F.J.W., Boothman, C., Bots, P., Rizoulis, A., Livens, F.R., Law, G.T.W., 2017. Impacts of repeated redox cycling on technetium mobility in the environment. Environ. Sci. Technol. 51, 14301–14310.

McBeth, J.M., Lear, G., Lloyd, J.R., Livens, F.R., Morris, K., Burke, I.T., 2007. Technetium reduction and reoxidation in aquifer sediments. Geomicrobiol. J. 24, 189–197.

McBeth, J.M., Lloyd, J.R., Law, G.T.W., Livens, F.R., Burke, I.T., Morris, K. 2011. Redox interactions of technetium with iron-bearing minerals. Min. Mag. 75 (4), 2419–2430.

McCartney, M., Kershaw, P.J., Woodhead, D.S., Denoon, D.C., 1994. Artificial radionuclides in the surface sediments of the Irish Sea, 1968–1988. Sci. Total. Environ. 141 (1–3), 103–138.

McCubbin, D., Leonard, K.S., Brown, J., Kershaw, P.J., Bonfield, R., Peak, T., 2002. Further studies of the distribution of technetium-99 and caesium-137 in UK and European coastal waters. Cont. Shelf. Res. 22, 1417–1445.

McCubbin, D., Leonard, K.S., McDonald, P., Bonfield, R., Boust, D., 2006. Distribution of technetium-99 in sub-tidal sediments of the Irish Sea. Cont. Shelf. Res. 26 (4), 458–473.

McDonald, P., Busby, R., McCartney, M., 1998. Temporal and spatial responses of the bioindicator *fucus* to discharges of $^{99}$Tc in the eastern Irish Sea. In international symposium on marine pollution. Monaco, 25–30.

McDonald, P., Vives I Batlle, J., Bousher, A., Whittall, A., Chambers, N., 2001.

The availability of plutonium and americium in Irish Sea sediments for re-dissolution. Sci. Total. Environ. 267, 109–123.

Morris, K., Livens, F.R., 1996. The distribution of transuranic elements in sediment profiles from an intertidal area in west cumbria, UK. Radiochim. Acta. 74, 195–198.

Morris, K., Butterworth, J.C., Livens, F.R., 2000. Evidence for the remobilization of Sellafield waste radionuclides in an intertidal saltmarsh, west Cumbria, UK. Estuar. Coastal. Shelf. S. 51 (5), 613–625.

Morris, K., Livens, F.R., Charnock, J.M., Burke, I.T., McBeth, J.M., Begg, J.D. C., Boothman, C., Lloyd, J.R., 2008. An X-ray absorption study of the fate of technetium in reduced and reoxidised sediments and mineral phases. Appl. Geochem. 23, 603–617.

Moyes, L.N., Jones, M.J., Pattrick, R. A.D., 2002. An X-ray absorption spectroscopy study of neptunium(V) reactions with mackinawite (FeS). Environ. Sci. Technol. 36 (2), 179–183.

Nakata, K., Nagasaki, S., Tanaka, S., Sakamoto, Y., Tanaka, T., Ogawa, H., 2000. Sorption and desorption kinetics of Np(V) on magnetite and hematite. Radiochim. Acta. 88, 453–457.

Newsome, L., Morris, K., Lloyd, J.R., 2014. The biogeochemistry and bioremediation of uranium and other priority radionuclides. Chem. Geol. 51, 1595–1604.

Newsome, L., Cleary, A., Morris, K., Lloyd, J. R., 2017. Long-term immobilization of technetium via bioremediation with slow-release substrates. Environ. Sci. Technol. 51, 1595–1604.

Oh, J.-S., Warwick, P.E., Croudace, I. W., 2009. Spatial distribution of $^{241}$Am, $^{137}$Cs, $^{238}$Pu, $^{239,240}$Pu and $^{241}$Pu over 17 year periods in the Ravenglass saltmarsh, Cumbria, UK. Appl. Radiat. Isotopes. 67, 1484–1492.

Ortiz-bernad, I., Anderson, R.T., Vrionis, H.A., Lovley, D.R., 2004. Resistance of solid-phase U(VI) to microbial reduction during in-situ bioremediation of uranium-contaminated groundwater. Appl. Environ. Microb. 70(12), 7558–7560.

Pentreath, R.J., Harvey, B.R., 1981. The presence of $^{237}$Np in the Irish Sea. Mar. Ecol. Prog. Ser. 6, 243–247.

Plymale, A.E., Frederickson, J.K., Zachara, J.M., Dohnalkova, A.C., Heald, S. M., Moore, D.A., Kennedy, D.W., Marshall, M.J., Wang, C., Resch, C.T., Ponnusamy, N., 2011. Competitive reduction of pertechnetate ($^{99}TcO_4^-$) by dissimilatory metal reducing bacteria and biogenic Fe(II). Environ. Sci. Technol. 45, 951–957.

Povinec, P.P., Badie, C., Baeza, A., Barci-Funel, G., Bergan, T.D., Bojanowski, R., Burnett, W., Eikenberg, J., Fifield, L.K., Serradell, V., Gastaud, J., Goroncy, I., Herrmann, J., Hotchkis, M.A.C., Ikaheimonen, T.K., Jakobson, E., 2002. Certified reference material for radionuclides in seawater IAEA-381 (Irish

seawater). J. Radioanal. Nucl. 251 (3), 369–374.

Prakash, D., Gabani, P., Chandel, A.K., Ronen, Z., Singh, O.V., 2013. Bioremediation: a genuine technology to remediate radionuclides from the environment. Microb. Biotechnol, 6 (4), 349–360.

Ray, D., Livens, F.R., Leary, P., Gray, N., Abrahamsen-Mills, L., Muir, G.K.P., Law., K.A., Fuller, A.J., Bryan, N.D., Howe, J., Cook, G.T., Law, G.T.W., 2018. Controls on anthropogenic radionucldie distribution in the Sellafield-impacted eastern Irish Sea, UK. J. Environ. Radioactiv (Submitted).

Roberts, H., Morris, K., Law, G.T.W., Mosselmans, J.F.W., Bots, P., Kvashina, K., Shaw, S., 2017. Uranium(V) incorporation mechanisms and stability in Fe(II)/Fe(III) (oxyhydr)oxides. Environ. Sci. Tech. Let. 4, 421–426.

Sani, R.K., Peyton, B., Dohnalkova, A., Amonette, J., 2005. Reoxidation of reduced uranium with iron(III) (hydr)oxides under sulfate-reducing conditions. Environ. Sci. Technol, 39, 2059–2066.

Schmeide, K., Bernhard, G., 2010. Sorption of Np(V) and Np(IV) onto kaolinite: effects of pH, ionic strength, carbonate and humic acid. Appl. Geochem. 25(8), 1238–1247.

Scott, T.B., Allen, G.C., Heard, P.J., Randell, M.G., 2005. Reduction of U(VI) to U(IV) on the surface of magnetite. Geochim. Cosmochim. Ac. 69, 5639–5646.

Sellafield Ltd, 2017. Monitoring our environment: discharges and environmental monitoring. Annual Report 2016.

Sellafield Ltd, 2005–2017. Monitoring our environment: discharges and environmental monitoring.

Senko, J., Istok, J.D., Suflita, J., Krumholz, L., 2002. In-situ evidence for uranium immobilization and remobilization. Environ. Sci. Technol. 36, 1491–1496.

Senko, J.M., Mohammed, Y., Dewers, T.A., Krumholz, L.R., 2005. Role for Fe(III) minerals in nitrate-dependent microbial U(IV) oxidation. Environ. Sci. Technol. 39, 2529–2536.

Sherman, D.M., Peacock, C.L., Hubbard, C.G., 2008. Surface complexation of U(VI ) on goethite ($\alpha$ -FeOOH ). Geochim. Cosmochim. Ac. 72, 298–310.

Smith, V., Fegan, M., Pollard, D., Long, S., Hayden, E., Ryan, T.P., 2001. Technetium-99 in the Irish marine environment. J. Environ. Radioactiv. 56, 269–284.

Srncik, M., Hrnecek, E., Steier, P., Wallner, G., 2011. Determination of U, Pu and Am isotopes in Irish Sea sediment by a combination of AMS and radiometric methods. J. Environ. Radioactiv. 102, 331–335.

Thompson, R.C. 1982. Neptunium: the neglected actinide: a review of the biological and environmental literature. Radiat. Res. 90 (1), 1–32.

Thorpe, C.L., Lloyd, J.R., Law, G.T.W., Williams, H.A., Atherton, N., Cruickshank, J.H., Morris, K., 2016. Retention of $^{99m}$Tc at ultra-trace levels in flowing column experiments–insights into bioreduction and biomineralization for remediation at nuclear facilities. Geomicrobiol. J. 33 (3–4), 199–205.

Thorpe, C.L., Morris, K., Lloyd, J.R., Denecke, M.A., Law, K.A., Dardenne, K., Boothman, C., Bots, P., Law, G.T.W., 2015. Neptunium and manganese biocycling in nuclear legacy sediment systems. Appl. Geochem. 63, 303–309.

Tims, S.G., Froehlich, M.B., Fifield, L.K., Wallner, A., De Cesare, M., 2016. $^{236}$U and $^{239,240}$Pu ratios from soils around an Australian nuclear weapons test site. J. Environ. Radioactiv. 151, 563–567.

Tinnacher, R.M., Zavarin, M., Powell, B.A., Kersting, A.B., 2011. Kinetics of neptunium(V) sorption and desorption on goethite: an experimental and modeling study. Geochim. Cosmochim. Ac. 75, 6584–6599.

Waite, T.D., Davis, J.A., Payne, T.E., Waychunas, G.A., Xi, N., 1994. Uranium(VI) adsorption to ferrihydrite: application of a surface complexation. Geochim. Cosmochim. Ac. 58(24), 5465–5478.

Wang, Z., Sung-Woo, L., Kapoor, P., Tebo, B., Giammar, D., 2013. Uraninite oxidation and dissolution induced by manganese oxide: a redox reaction between two insoluble minerals. Geochim. Cosmochim. Ac. 100, 24–40.

Wildung, R.E., Gorby, Y.A., Krupka, K.M., Hess, N.J., Li, S.W., Plymale, A.E., McKinley, J.P., Fredrickson, J.K., 2000. Effect of electron donor and solution chemistry on products of dissimilatory reduction of technetium by *Shewanella putrefaciens*. Appl. Environ. Microb. 66 (6), 2451–2460.

Wildung, R.E., Li, S.W., Murray, C.J., Krupka, K.M., Xie, Y., Hess, N.J., Roden, E.E., 2004. Technetium reduction in sediments of a shallow aquifer exhibiting dissimilatory iron reduction potential. FEMS. Microbiol. Ecol. 49 (1), 151–162.

Wilk, P., Shaughnessy, D., Wilson, R., Nitsche, H., 2005. Interfacial interactions between Np(V) and manganese oxide minerals manganite and hausmannite. Environ. Sci. Technol. 39, 2608–2615.

Yamamoto, M., Yamauchi, Y., Komura, K., Ueno, K., Assinder, D.J., 1991. Chemical leaching behaviour of $^{237}$Np from intertidal coastal sediment in the Irish sea. J. Radioan. Nucl. Ch. Le. 154 (5), 299–307.

Yamamura, T., Kitamura, A., Fukui, A., Nishikawa, S., Yamamoto, T., Moriyama, H., 1998. Solubility of U(VI) in highly basic solutions. Radiochim. Acta. 83, 139–146.

Zachara, J.M., Heald, S.M., Jeon, B.-H., Kukkadapu, R.K., Liu, C., McKinley, J. P., Dohnalkova, A.C., Moore, D.A. 2007. Reduction of pertechnetate [Tc(VII)] by aqueous Fe(II) and the nature of solid phase redox products. Geochim. Cosmochim. Ac. 71, 2137–2157.

Zavarin, M., Powell, B.A., Bourbin, M., Zhao, P., Kersting, A.B., 2012. Np(V) and Pu(V) ion exchange and surface-mediated reduction mechanisms on

montmorillonite. Environ. Sci. Technol. 46, 2692–2698.

Zhao, P., Johnson, M.R., Roberts, S.K., Zavarin, M., 2005. Np and Pu sorption to manganese oxide minerals. Lawrence Livermore National Laboratory (UCRL-TR-214984).

Zhao, P., Tinnacher, R.M., Zavarin, M., Kersting, A.B., 2014. Analysis of trace neptunium in the vicinity of underground nuclear tests at the Nevada National Security Site. J. Environ. Radioactiv. 137, 163–172.

Zhao, X.-L., Kilius, L.R., Litherland, A.E., Beasley, T., 1997. AMS measurement of environmental U-236: preliminary results and perspectives. Nucl. Instrum. Meth. B. 126, 297–300.

# Supporting Information for: Sellafield-Derived Technetium, Uranium, and Neptunium Distribution in the Ravenglass Saltmarsh, UK

Daisy Ray[1/2], Claudia Joseph[3], Adam Fuller[1], Katherine Morris[2], Francis R. Livens[1/2], James D. C. Begg[3], Annie Kersting[3], L. Keith Fifield[4], Pihong Zhao[3], Mavrik Zavarin[3], Heather Williams[5], Bev Ellis[5], Kathleen A. Law[1], Gareth T. W. Law[1/2*]

1. Centre for Radiochemistry Research, School of Chemistry, The University of Manchester, Manchester, M13 9PL, UK;

2. Research Centre for Radwaste and Decommissioning and Williamson Research Centre, School of Earth and Environmental Sciences, The University of Manchester, Manchester, M13 9PL, UK;

3. Glenn T. Seaborg Institute, Lawrence Livermore National Laboratory, 7000 East Ave, Livermore, CA, 94550, USA;

4. Department of Nuclear Physics, Research School of Physics and Engineering, The Australian National University, Acton, ACT 2601, Australia.

5. Nuclear Medicine Centre, Manchester Royal Infirmary, Manchester, M13 9WL, UK.

*Corresponding author: Tel: +44 (0) 161 306 0514; Email: gareth.law@manchester.ac.uk

## S1: Summary of $^{237}$Np extraction method

### Neptunium analysis ($^{237}$Np)

The experimental procedure developed by Zhao et al. (2014) was adapted used in this project to determine the activity of $^{237}$Np in Ravenglass saltmarsh sediments. This was carried out at the Glenn T. Seaborg institute at the Lawrence Livermore National Laboratory. Perfluoroalkoxy (PFA) jars (Savillex) were thoroughly cleaned with boiling 5% $HNO_3$ and18.2 MΩ DI.

A $^{239}$Np ($t_{1/2}$ = 2.36 days; 50–100 Bq/mL) yield tracer solution was used to monitor the loss of $^{237}$Np during the experimental procedure. The $^{243}$Am ($t_{1/2}$ = 7370 yrs) stock solution used in this method was produced from the transformation of five successive neutron captures of $^{238}$U during the irradiation of nuclear fuel (Zhao et al., 2014), and the α-decay of $^{243}$Am generates the desirable $^{239}$Np tracer. Additionally, the stock solution contains $^{241}$Am as a contaminant, the decay of which produces $^{237}$Np, the analyte of interest. The long half-life of $^{237}$Np ($t_{1/2}$ = 2.14 x $10^6$ years) results in its accumulation in the stock solution, whilst $^{239}$Np reaches a secular equilibrium with $^{243}$Am after two weeks. As a result the $^{237}$Np/$^{239}$Np ratio increases with time. The first stage of the experiment involved purifying the long-lived $^{243}$Am parent to limit the presence of $^{237}$Np in the $^{239}$Np tracer.

### Column 1 and 2:$^{243}$Am purification

The $^{243}$Am stock solution was purified by removing both Np isotopes using two cycles of AG®1-X8 ion exchange resin (Bio rad laboratory; 2 mL; 50-100 mesh). A few drops of c$HNO_3$ were added to the $^{243}$Am stock (20–30 kBq), this was then taken down to almost dryness and re-dissolved in cHCl + HI (50:1 v/v) (~1 mL). The solution was warmed in a closed jar on the hotplate for 10-20 minutes to adjust the Np oxidation state to Np(IV), and placed aside to cool. A column was made from a 1 mL disposable pipette plugged with a porous frit, and packed with AG®1-X8 ion exchange resin (50–100 mesh). This was preconditioned with deionised water 18.2 MΩ (1 mL) followed by cHCl + HI (50:1 v/v) (1 mL). The $^{243}$Am stock was loaded onto the column, as well as two rinses of the vial with cHCl + HI (50:1 v/v) (2 x 0.5 mL) to collect any residual $^{243}$Am stock solution. The Np(IV) was retained on the column whilst $^{243}$Am(III) was eluted from the

column with 5 x 1 mL of cHCl + HI (50:1 v/v) and 2 – 3 mL of cHCl and collected in a pre-weighed 15 mL PFA vial. An aliquot (2 µL) of the $^{243}$Am eluent was added to Ultima Gold™ scintillation cocktail (7 mL; Perkin Elmer). For the majority of the samples this was counted on a TriCarb 2900TR (Perkin Elmer) Liqud Scintillation Analyser. Here, the protocol was adjusted to achieve a maximal separation of α and β counts (no α/ β discrimination); $^{243}$Am = α = 300–600 keV and $^{239}$Np = β = 0–600 keV. Thus, the counts in the 0 – 300 keV window were used for $^{239}$Np and the counts in 300–600 keV window were calculated as a fraction as $^{243}$Am was also detected in this region. The counts in both the α and β regions were used to determine the $^{239}$Np activity (as it was assumed that there would be no $^{243}$Am here). However due to circumstances beyond control, a small sample set was counted on a Quantulus 1220 (Wallac, Perkin-Elmer) LSC using α/β discrimination at PSA level of 80. The counts present in the 500–900 keV α-region were used to determine $^{243}$Am activity, and the 100–1000 keV β–region for $^{239}$Np. Then, 0.1 M + 0.05 M HF (6 x 1 mL) was added to the column, and allowed to pass through to collect the $^{239}$Np fraction in another pre-weighed 15 mL PFA vial. An aliquot (2 µL) of the $^{239}$Np elutant was added to Ultima Gold™ scintillation cocktail (7 mL) and counted on the TriCarb 2900TR (Perkin Elmer) Liquid Scintillation Analyser to check the activity of $^{239}$Np.

For background correction, Ultima Gold™ scintillation cocktail was used as a blank (7 mL) in each LSC measurement. The activities of $^{239}$Np and $^{243}$Am were determined to monitor the successful separation of the two fractions, and to check for unexpected activity loss on the column for reasons of mass balance and waste activity estimation. The eluted $^{243}$Am fraction was heated to almost dryness again, and then re-dissolved in ~1 mL cHCl + HI (50: 1 v/v) for a second purification step using a fresh AG®1-X8 ion exchange resin column (Bio rad Laboratory; 2mL; 50–100 mesh) following the method discussed above. Samples from the first set were counted on the Quantulus 1220 (Wallac, Perkin-Elmer) LSC using α/β discrimination at PSA level of 28, with the majority of the samples counted on the TriCarb 2900TR (Perkin Elmer) Liquid Scintillation Analyser. The $^{237/239}$Np fraction was discarded. The purified $^{243}$Am fraction from column 2 was then used for columns 3 and 4.

**Column 3 and 4: $^{239}$Np milking**

The purified $^{243}$Am fraction was left aside for 2 – 3 days prior to starting column 3 to allow the ingrowth of short-lived $^{239}$Np, and limit the undesirable ingrowth of $^{237}$Np. Thereafter, the $^{243}$Am stock solution (~ 7 mL) was evaporated to reduce its volume to ~1 mL. The separation of the Am fraction from the Np fraction, and the LSC analysis for column 3 were conducted as described for column 1 and 2. The $^{243}$Am fraction was stored for future applications. The $^{239}$Np fraction was taken to dryness after addition of a few drops of c$HNO_3$ to remove HF. Next, a few drops of cHCl were added, and the $^{239}$Np fraction was again evaporated to almost dryness. The remaining drop was then taken up in cHCl + HI (50:1 v/v) (~1 mL) and the solution was warmed up for 10 minutes to adjust the Np oxidation state to Np(IV). The $^{239}$Np solution was purified in column 4 and the fractions were collected and analysed with LSC following the procedure described for column 1. The $^{243}$Am fraction contained almost no $^{243}$Am. The $^{239}$Np fraction contained the activity of $^{239}$Np available as a spike for one set of samples. A few drops of c$HNO_3$ were added to the $^{239}$Np fraction and the solution was evaporated to dryness. This process was repeated twice. The final drop was taken up in 2 % $HNO_3$ (volume dependant on number of samples, 1 mL per sample, including one procedure blank and two reference samples for $\gamma$ – spectroscopy).

**Column 5: Removal of sample impurities**

Ravenglass sediment samples (1.3 g) were ashed at 550 °C for 8 hrs. Each sediment sample (1 g) was then leached with *aqua regia* 3:2 cHCl : c$HNO_3$ (30 mL) at ~150 °C, and filtered (Whatman GF/A; 0.22 µM), and made up to a stock solution in 9 M HCl (30 mL). An aliquot (10 mL) of this stock solution was added to a 15 mL PFA vial, and spiked with 50 – 100 Bq of the freshly prepared $^{239}$Np tracer each (1 mL). The precise weights of each sample and added $^{239}$Np spike were recorded. This was taken to dryness, and the resulting residue suspended in cHCl (~ 2 mL). As the samples contained a lot of salts and minerals, each suspension was transferred to a 15 mL centrifuge tube and centrifuged (3 minutes at 4000 rpm; $g$ = 1431) Each supernatant was transferred into a new 15 mL PFA vial. Each sample residue was rinsed three times with cHCl (3 x 1 mL),

centrifuged and all rinse supernatants were added to the new sample vial. Next, HI (100 µL) was added to the solution (5 mL) in the new vial (forming conc. HCl + HI (50:1 v/v)). The cap was closed on each vial. The solutions were allowed to warm up for 10 mins to reduce Np to Np(IV). An AG®1-X8 resin column (chloride form, 100 – 200 mesh) was prepared in a 2 mL poly-prep column (Bio Rad laboratories) for each sample. Each one was preconditioned with MQW (2 + 4 + 4 mL). Then, cHCl (2 + 2 mL) was passed through, followed by cHCl + HI (50: 1 v/v) (2 + 2 + 2 mL). A new 15 mL PFA vial was placed under each column. Next, the sample was loaded onto the column, and two vial rinses with cHCl + HI (50:1 v/v) (2 x 1 mL). Each sample was transferred through the column by adding cHCl + HI (50:1 v/v) (2 + 4 + 4 mL). Any tetravalent Np and U remained on the resin, whilst trivalent Pu and any other impurities passed through the column. The PFA vials under each column were replaced by new ones. The Np fractions were then eluted with 0.1 M HCl + 0.05 M HF, with the majority of U assumed to be retained on the column (Zhao et al., 2014). Then, c$HNO_3$ (~ 1 mL) was added to each vial and the samples were slowly evaporated overnight.

**Column 6: Removal of $^{238}$U**

Nu Plasma High Resolution Multi-Collector Inductively Coupled Mass Spectrometry (HR MC ICP-MS is able to tolerate low ppb levels of $^{238}$U. However, to prevent tailing of the $^{238}$U peak into the peak of the analyte of interest ($^{237}$Np) an additional purification step was used to lower the amount of $^{238}$U in each sample.

The sample residues were dissolved 2 – 3 times in 2 M $HNO_3$ (1 mL) and evaporated to dryness (to oxidise Np to Np(V)). During the final repeat, the solution was evaporated down to a small drop. This was taken up in 4 M $HNO_3$ (1 mL). A column bed of 0.2 mL UTEVA® resin (Eichrom Industries) was prepared in a disposable pipette plugged with a porous frit for each sample, and was preconditioned with 4 M $HNO_3$ (4 x 0.2 mL). A clean pre-weighed 15 mL PFA vial was placed under each column. The sample was then added to the column and the two vial rinses with 4 M $HNO_3$ (2 x 0.2 mL). The sample was eluted with 4 M $HNO_3$ (5 x 0.2 mL). Uranium was retained on the UTEVA® resin

while Np(V) passed through the column. The collected Np-containing effluent was evaporated, and the resulting residue was taken up in c$HNO_3$, and evaporated down to a small drop. This was then dissolved in 2 % $HNO_3$ (2 mL). The PFA vials with the samples were weighed again.

The samples were ready for analysis on the Nu Plasma HR Multi-Collector ICP-MS after ~ 2 weeks (6 half-lives) to allow the decay of short-lived $^{239}$Np. Prior to this, the $^{239}$Np yield of each purified sample was determined *via* γ – spectroscopy (Canberra, Broad Energy Ge detector) using the γ-emission line at 277 keV. Two samples were prepared for each sample set as $^{239}$Np reference samples for γ-spectroscopy. They represented 100 % yield and contained ~1 mL of the freshly prepared $^{239}$Np spike and 1 mL of 2 % $HNO_3$. The $^{239}$Np activity in the purified samples (after column 6) was measured by γ – spectroscopy, and compared with activities in the reference samples to determine the chemical yield during purification. Typically, Np recovery yields ranged between 20 to 90 %.

Zhao, P., Tinnacher, R. M., Zavarin, M., Kersting,A B., 2014. Analysis of trace neptunium in the vicinity of underground nuclear tests at the Nevada National Security Site. J. Environ. Radioactiv. 137, 163–172.

# Chapter 5: Sequential Extraction of $^{241}$Am, $^{137}$Cs, and $^{239,240}$Pu from Ravenglass Saltmarsh Sediments

This chapter is a manuscript prepared for submission to the *Journal of Environmental Radioactivity*.

# 5. Sequential Extraction of $^{241}$Am, $^{137}$Cs, and $^{239,240}$Pu from Ravenglass Saltmarsh Sediments

Daisy Ray[1/2], Ellie Katsouris[1], Francis R. Livens[1/2], Adam J. Fuller[1], Katherine Morris[2], Kathleen A. Law[1], Gareth T.W. Law[1/2*]

1. Centre for Radiochemistry Research, School of Chemistry, The University of Manchester, Manchester, M13 9PL, UK;

2. Research Centre for Radwaste and Decommissioning and Williamson Research Centre, School of Earth and Environmental Sciences, The University of Manchester, Manchester, M13 9PL, UK;

*Corresponding author. Email: gareth.law@manchester.ac.uk; Tel: +44 (0)161 306 0514

## 5.1. Abstract

Authorised low-level aqueous effluent has been discharged from the Sellafield nuclear reprocessing facility to the Eastern Irish Sea. This effluent contains a range of radionuclides including $^{241}$Am, $^{137}$Cs, and $^{239,240}$Pu. Over time these radionuclides have associated with an offshore belt of finely-grained sediments close to the discharge pipeline, known as the Irish Sea mud-patch, which is hypothesised to act as a long-term source of radionuclides in the area. The Ravenglass saltmarsh is an intertidal site in West Cumbria, which has accumulated Sellafield-derived radionuclides. As the radionuclides were discharged over 65 years ago, it is important not only to monitor their distribution but also to understand their bioavailability in marine sediments. This can improve our understanding of radionuclide accessibility in this system, and may help strengthen future safety cases associated with the remediation of contaminated land, and nuclear accidents. We utilise a sequential extraction process to determine the dominant geochemical association of $^{241}$Am, $^{137}$Cs, $^{239,240}$Pu, and two reactive metals, Fe and Mn in sediment cores taken from the Irish Sea mud-patch, and Ravenglass saltmarsh. The results show that $^{241}$Am at both sites was predominantly bound to geochemical fractions suggested to be environmentally inaccessible, whereas $^{137}$Cs was present across all four of the fractions examined at both sites. In contrast, the reducible oxide fraction was the dominant host for $^{239,240}$Pu at both sites, and this may imply that Pu may be accessible under anoxic, reducing conditions.

**Keywords**: Americium, Caesium, Plutonium, Sellafield, Ravenglass, Bioavailability.

## 5.2. Introduction

The Sellafield nuclear reprocessing facility has discharged, under authorisation aqueous low-level effluent into the Eastern Irish Sea since 1952. This effluent contains several anthropogenic radionuclides, and has released approximately 41300 TBq of $^{137}$Cs, 540 TBq of $^{241}$Am, and 740 TBq of Pu(α) (Kershaw et al., 1992; Gray et al., 1995). The discharge of these radionuclides and others reached a maximum in the early to mid-1970s, as a result of the longer residence time of spent fuel in storage ponds. Thereafter, effluent activity decreased as enhanced

effluent treatment and stricter discharge limits were introduced (Kershaw et al., 1992; Gray et al., 1995). Contemporary releases are now two orders of magnitude lower than the 1970s, and are well below site discharge limits (Sellafield Ltd, 2017). The discharge of low-level effluent from the Sellafield pipeline over many decades has contaminated offshore Irish Sea sediments (McCartney et al., 1994; Kershaw et al., 1999; Ray et al., 2018) and local coastal areas (Kershaw et al., 1990; MacKenzie and Scott, 1993; Lucey et al., 2004; Lindahl et al., 2011; Ray et al., 2018). As the discharge has taken place over a period of ~65 years, this authorised release provides a unique opportunity to understand the long-term geochemical association of anthropogenic radionuclides in marine sediment systems. Once released into the Eastern Irish Sea, the Sellafield-derived radionuclides exhibit differing environmental behaviour, and their bioavailability, particularly in the Irish Sea offshore environment remains unclear.

The fission product $^{137}$Cs ($t_{1/2}$ = 30.2 years) is present as the (reasonably) conservative $Cs^+$ cation in seawater. The measured $K_d$ value for Cs is $10^3$–$10^4$ (Hunt and Kershaw, 1990), reflecting its high solubility in aqueous media. As a result, the concentration of Cs in seawater (and its mobility), is controlled by its association on the surface of soil minerals, commonly *via* cation exchange (Sawhney, 1972; Cornell, 1992). Caesium is not readily adsorbed onto Fe-oxide minerals (Wang et al., 2000) and is instead principally adsorbed to clay mineral surfaces, and can be incorporated into the clay structure (Chibowski and Zygmunt, 2002; Fuller et al., 2015). The majority of Sellafield-derived Cs has been transported out of the Irish Sea northwards along the western coast of Scotland and into the Atlantic Ocean, the North Sea, and further afield (Jefferies et al., 1973). However, a small proportion of the discharged Cs inventory (~ 10 %) has been suggested to be removed from solution, being retained on sediments close to the discharge pipeline *via* sorption to clay minerals (Jones et al., 1988). Following this removal, Cs has been suggested to be remobilised from surface sediments in the offshore Irish Sea area (Hunt and Kershaw, 1990; MacKenzie and Scott, 1993; McCartney et al., 1994) and as such it may be important to understand the interaction of Cs with the sediment system here.

The radionuclide $^{241}$Am ($t_{1/2}$ = 432.2 years) is commonly found in the environment as Am(III) (Lovett, 1978; Lehto and Hou, 2010; McDonald, 2011)

and is sparingly soluble ($K_d$ value = $10^6$; McDonald et al., 2001). The high charge density of Am(III) means it undergoes hydrolysis and precipitates as a solid or sorbs to geomedia (Lehto and Hou, 2010), and consequently Am is generally found associated with colloids, sediment, and humic materials. It has previously been suggested that $Am(CO)_3(OH)$ is the limiting species for the solubility of Am in sea water (MacKenzie et al., 1994). In the Eastern Irish Sea, the majority of Am discharged from the pipeline is suggested to have associated with fine grained sediment (MacKenzie et al., 1999). Here, the decay of discharged $^{241}Pu$ ($t_{1/2}$ = 13.5 years) to $^{241}Am$ has resulted in an increasing contemporary inventory of $^{241}Am$ (McDonald, 2011).

Redox-active Pu ($K_d = 10^4–10^6$) can exist as one of either four oxidation states (III, IV, V, VI) (Morse and Choppin, 1991) under natural conditions. In most waters Pu(IV) and Pu(V) are the dominant species, although Pu(III) and Pu(VI) can also exist (Kersting, 2013). Plutonium(IV) has been shown to be sparingly soluble under oxidising conditions at near-neutral pH (~ $10^{-14}$ mol/L; Neck et al., 2007) and is relatively immobile (Lovett, 1978). It can also exist as a free ion, however it tends to be hydrolysed in solution. In contrast, Pu(V) is more soluble than Pu(IV) (~ $10^{-8}$ mol/L; Neck et al., 2007), and as a result it is more mobile and does not form strong complexes, instead existing as the $Pu(V)O_2$ species. In the Eastern Irish Sea, the majority (90 %) of the discharged Pu inventory has likely become associated with sediments in the area as the particle-reactive Pu(IV) species (MacKenzie and Scott, 1993). Previous studies have shown that Pu(IV) can sorb to a range of mineral surfaces (e.g. iron and manganese oxy(hydr)oxides, clays, and quartz; Keeney-Kennicutt and Morse, 1985; Sanchez et al., 1985; Lu et al., 2003; Lujanienσ et al., 2007; Begg et al., 2013) and in some cases this association has driven the surface-mediated reduction of Pu(V) (Powell et al., 2004, 2005; Zavarin et al., 2012).

The behaviour of Pu has also been examined in several contaminated environmental systems, with Pu shown to migrate in groundwater and surface water *via* colloidal transport at the Nevada Test Site (Kersting et al., 1999) and the Rocky Flats Environmental Technology Site (Santschi and Roberts, 2002). At the Mayak site, Russia, Pu was shown to be bound to iron-oxide colloids (Novikov et al., 2006). The Irish Sea mud-patch and Ravenglass saltmarsh in

Cumbria are two field sites that have been contaminated by reactor-derived radionuclides with both sites recently shown to be contaminated by Pu (300 Bq/kg and 7 kBq/kg, respectively). In addition, the distribution of Pu at the Ravenglass saltmarsh was shown to be independent of the ambient biogeochemistry and was instead controlled by the time-integrated deposition of the Sellafield signal (see Ray et al., 2018; Chapter 3). Thus, these radio-labelled sediments provide a unique opportunity to investigate the geochemical association of Pu, and understand whether Pu is accessible for microbially mediated processes.

The bioavailability and migration of radionuclides in sediments is dependent on their chemical form, and their association with geomedia (e.g. mineral, clays, quartz). Sorption will likely be the dominant interaction taking place, however, it is important to note that co-precipitation and incorporation of the radionuclide with environmental substrates may also occur. Thus, the identification of the main binding sites and phase associations of these radionuclides in sediments can determine their potential for remobilisation. Sequential extractions can reveal the dominant radionuclide hosting phase and provide insight into their potential environmental availability. A limitation of using sequential extractions is the operationally defined nature of the technique (i.e. the reagents are non-specific to some degree). However, the method does provide an indication of the chemical association of the radionuclides of interest.

Previous sequential extraction work using Irish Sea mud-patch sediments (collected in 1998) have shown that Pu was predominantly associated with the strongly bound reducible oxide (44.%) and organic complex (44 %) fractions, whilst Am was extracted mainly in the organic complex fraction (40 %) (McDonald et al., 2001). At the Esk estuary, Lucey et al. (2004) collected sediment cores in 2002, and found Pu to be predominantly associated with carbonates (45 %), with a smaller fraction present in the easily accessible exchangeable fraction (29 %). More recent work by Kimber et al. (2015) at the same site focused on one sediment horizon (10–15 cm; collected in 2008), and showed that the majority of the $^{241}$Am inventory was associated with the reducible oxide (35 %) and organic fractions (59 %), whilst Pu was measured dominantly in the strongly bound residual fraction (95 %). This may suggest that

there are variable host phases of Pu in the estuarine environment, and provides further reinforcement to determine its geochemical association in the Eastern Irish Sea. In this paper we investigate the association of $^{137}Cs$, $^{241}Am$, and $^{239,240}Pu$ with four geochemical fractions (easily exchanged; bound to reducible oxides, including oxides of Fe and Mn; bound to sulphides and/or organic matter; incorporated with aluminosilicates and/or other refractory minerals). From here on in, the Irish Sea mud-patch is referred to as the 'mud-patch' and the Ravenglass saltmarsh as 'Ravenglass'.

## 5.3. Method

### 5.3.1. Sediment Collection and Preparation

The mud-patch is an offshore belt of finely-grained sediment (~ 15 km long x 3 km wide), located ~ 10 km from the pipeline, and has been suggested to act as long-term secondary source of Sellafield-derived radionuclides. The sediment composition of the mud-patch has been shown to be comprised of fine sand (46 %), silt (37 %) and clay (13 %) (McDonald et al., 1990). Early work at the site has shown the accumulation rate at the mud-patch to be low (maximum of 0.08 cm/yr) with the sediment being mixed to a depth of 1.5 m (Kershaw et al., 1983; Kershaw, 1984). The total organic matter content of the mud-patch has been shown to be relatively constant with depth a(~1 wt %), and this may suggest that organic matter input and turnover at this site is low (Ray et al., 2018; Chapter 3)

The Ravenglass saltmarsh is part of the Esk estuary situated 15 km south from the Sellafield nuclear reprocessing site (Carr and Blackley, 1986). It is also located in an area of high convergence; at the crossing-point of the rivers Esk, Mite, and Irt. The sediments of the estuary have been shown to be predominantly silt (~75 %; >2–63 µm) with lower quantities present as clay (~19%; <0.2 µm) and sand (7 %; >63 µm) (Morris et al., 2000). The majority of the clay in the estuary is illite (Kelly and Emptage, 1992). Previous work has highlighted that this site is an area of active accretion with sedimentation rates observed between 0.2–6.8 cm/yr (Aston and Stanners, 1981; Clifton and Hamilton, 1982; Morris et al., 2000; Marsden et al., 2006; Ray et al., 2018; Chapter 3). Total organic matter content at Ravenglass ranged from ~ 7 wt % at the sediment surface to ~4 wt % at depth,

possibly reflecting microbially mediated oxidation of organic matter with depth (see Ray et al., 2018; Chapter 3 for further discussion).

Sediment cores were collected from the mud-patch (54'27.96 N, 03'44.00 W), and Ravenglass (54'20.24 N, 03'24.06 W) in June and September 2014, respectively. A sediment core (depth ~35 cm; diameter 10 cm) was retrieved from the mud-patch using extruded acrylic core tubes and a hydraulic mega corer (Ray et al., 2018; Chapter 3). Care was taken during coring to leave the sediment water interface as undisturbed as possible. Cores from Ravenglass (depth ~30 cm; diameter 10 cm) were collected by manual insertion of core tubes, with an airtight bung placed over the top of the core prior to extraction. The cores were sectioned at 1 cm resolution from the sediment interface until a depth of 10 cm, and at 2 cm resolution thereafter, under normal atmosphere. Sectioned sediments were then sealed in PVC bags, frozen at -80 °C and returned to the laboratory. The sediment samples were then freeze dried, and homogenised using a Fritsch agate ball grinder ready for analysis. All sections of the sediment core extracted from the Irish Sea mud-patch and Ravenglass saltmarsh were analysed for $^{137}$Cs, $^{241}$Am, $^{239,240}$Pu, and Fe and Mn partioning using sequential extraction experiments.

### 5.3.2. Sequential Extraction

The geochemical association of $^{241}$Am, $^{137}$Cs, $^{239,240}$Pu, and Fe and Mn was investigated using the method of Tessier et al. (1979), amended as per Begg et al. (2011). Here, the scheme identifies four types of radionuclide binding site, with a series of reagents exchanging/extracting the radionuclides from progressively stronger binding sites. The reagents and volumes used for the extraction process are shown in Table 5.1. These fractions, which are arbitrarily defined (i.e. the reagents are non-specific to some degree), break down the radionuclide/metal bonds to investigate the availability of these species in the sediment system. Of note, $^{241}$Am, $^{137}$Cs, Fe, and Mn concentrations were determined from a single extraction, whilst $^{239,240}$Pu determination was carried out on a second, separate extraction. A select sample set which represented the depth distribution of the high and low Pu concentrations at the mud-patch and Ravenglass sediment cores (determined in Ray et al. 2018; Chapter 3) was investigated.

| Fraction name | Reagent | Time/temp | Geochemical phase |
|---|---|---|---|
| Exchangeable | Magnesium chloride, $MgCl_2$ (1 M, pH 7) | 2 hrs/room temp | Exchangeable/readily available metals |
| Reducible | Ammonium oxalate, $(NH_4)_2C_2O_4$ (0.1 M) adjusted to pH 2-3 with 0.1 M HCl | 17 hrs/room temp | Metals associated with reducible oxides |
| Oxidisable | Hydrogen peroxide, $H_2O_2$ (30 %) adjusted to pH 2-3 with $HNO_3$, heated to complete dryness, then leached with ammonium acetate (0.1 M) in 6 % (v/v) $HNO_3$ (pH 2) | 24 hrs/80 °C then 6 hrs/room temp | Metals bound to sulphides and organic matter |
| Residual | *Aqua regia* (3:2 v/v cHCl: $cHNO_3$) | 3 hrs/~80–110 °C | Metals bound to Alumnosilicates and other refractory minerals |

**Table 5.1.** Sequential extraction treatments, including the fraction targeted, the reagent used, reaction conditions, and the geochemical host phase targeted.

In brief, dried, homogenised sediment (1.0 g) was placed in a centrifuge tube (Corning; 50 mL) and 1 M $MgCl_2$ (pH 7; 15 mL) was added. This was shaken at room temperature on the orbital shaker (2 hours) and centrifuged (10 minutes; 1431 *g*). At pH 7 $Mg^{2+}$ will replace easily exchangeable structural cations from surfaces of clay minerals, and other surfaces bringing them into solution. The resulting supernatant was then split for gamma (10 mL), and ICP-AES analysis (2 mL). Then, the sediment residue was rinsed with 18 MΩ DI $H_2O$ (10 mL), followed by centrifugation (10 minutes; 1431 *g*) ready for the next lixivant. The resulting supernatant was discarded. Thereafter, 0.1 M $(NH_4)_2C_2O_4$ (pH 3; 15 ml) was added to the sediment residue, and shaken at room temperature on the orbital shaker (17 hours). As oxalate ($C_2O_4^{2-}$) is a reducing agent, this step targets any metals that are associated with reducible oxides, including Fe and Mn oxides. A similar centrifugation (10 minutes; 1431 *g*), sub-sampling and rinsing step was then carried out ready for the oxidisable extraction step. Here, hydrogen peroxide,

30 % $H_2O_2$ (pH 3; 10 mL) was added to the residue and heated (80 °C) until complete dryness in a sand bath (24 hours). As $H_2O_2$ is an oxidising agent, this treatment causes the oxidation of organic matter, and sulphides, releasing any bound metals into solution. No distinction is made between metals associated with these two fractions (Baeyens et al., 2003). Then, ammonium acetate (1 M $CH_3CO_2NH_4$ in 6 % v/v $HNO_3$; pH 2; 15 mL) was added to the sediment residue at room temperature on an orbital shaker (6 hours). This second step performed after the $H_2O_2$ treatment aims to isolate any metals liberated during the oxidative first step (Tessier et al., 1979) (to prevent the re-absorption of any metals onto Mn and Fe oxyhydroxides that have been liberated by $H_2O_2$ treatment). Centrifugation, sub-sampling and rinsing steps were then carried out ready for the final residual extraction step. The sediment residue was transferred to PYREX glass beakers (25 mL) and boiled in *aqua regia* (3:2 v/v; cHCl:c$HNO_3$; 15 mL) for 3 hours. The supernatant was then filtered (Whatman GF/A; 0.22 µm) and the filtrate was evaporated to incipient dryness. This was then taken up in 3 M $HNO_3$ (15 mL) and the supernatant split for gamma (10 mL) and ICP-AES analysis (2 mL). The sediment residue was then discarded.

### 5.3.3. Analysis of Extraction Leachates for Mn and Fe

The supernatant (2 mL) from each extraction was made up for ICP-AES analysis by diluting to 5 mL using 2 % $HNO_3$ (3 mL). The concentration of Mn and Fe was determined using the Perkin Elmer Optima 5300 Dual View ICP-AES. A range of certified standards (0.05–10 ppm) were used for both analytes, and produced a calibration line of $R_2$ = 0.999 (Fe) and $R_2$ =0.999 (Mn). The data (per extraction) is expressed as a percentage of the total Fe/Mn extracted across all four fractions for each specific depth horizon.

### 5.3.4. Analysis of Extraction Leachates for $^{137}$Cs and $^{241}$Am.

The $^{137}$Cs and $^{241}$Am leachate (10 mL) from each extraction step (section 5.3.2) was transferred to a container of fixed geometry (100 mL), and counted on a Canberra GC1019 hyper-pure germanium (HPGe) detector housed in a 11 cm thick lead shield (20–1800 keV) for 24 hrs. The characteristic γ-ray emission at 59.5 keV and 661.6 keV were examined to quantify for $^{137}$Cs and $^{241}$Am, respectively. The detector efficiency was calibrated using matrix-matched

standards. This was prepared by spiking 18 MΩ DI $H_2O$ (10 mL) with certified standard solutions of $^{241}Am$ (100 Bq) and $^{137}Cs$ (100 Bq) (Amersham International). The sample volume, geometry and location of the sample on the detector remained constant for each run. The resulting spectra were also corrected for background noise. The reported radionuclide ($^{241}Am$, $^{137}Cs$, and $^{239,240}Pu$ values (in cps) were converted to activity (Bq/kg), and this was expressed as a percentage of the total radionuclide activity extracted across all four fractions at a specific depth horizon.

### 5.3.5. Analysis of Extraction Leachate for $^{239,240}Pu$

Ion extraction chromatography was then used to extract Pu from the exchangeable, reducible, oxidisable, and residual fractions. In brief, the leachate from each extraction (10 mL) was evaporated to near-dryness and boiled with *aqua regia* (3:2 v/v, cHCl:c$HNO_3$) followed by filtration to remove the solids (Whatman GF/A; 0.22 µm;). This was taken up in 3 M $HNO_3$ (15 mL) and spiked with a certified $^{242}Pu$ tracer (NPL, Teddington; 100 µL; 0.75 Bq/mL) for yield recovery. Thereafter, $NaNO_{2(s)}$ was added to the sample to a concentration of 0.2 M, and warmed to 90 °C (to convert Pu to the tetravalent state). The sample was cooled, and passed through a pre-conditioned (3 M $HNO_3$; 5 mL) Eichrom TEVA® column (Eichrom; 2 mL; 100–150 mesh). This binds Pu(IV) to the resin, and a series of 3 M $HNO_3$ washes (4 x 5 mL) were added to elute any co-contaminants e.g. U(VI), Am(III), Np(V). Then, 9 M HCI (5 mL) was added to remove Th(IV). Plutonium was eluted with 9 M HCl and 0.1 M $NH_4I$ (15 mL) as Pu(III). Carrier solution (10 % $KHSO_4$; 1 mL) was added to prevent Pu from sticking to the glassware. This was followed by the addition of 3M $HNO_3$ (3 mL) and heated to near dryness, followed by the addition of 30 % $H_2O_2$ (1 mL), and then further heating to near-dryness. Lastly, cHCl (3 mL) was added and again the sample was heated to near-dryness. The residues were then taken up into electrolyte solution (4 % $C_2H_8N_2O_4$ in 0.3 M HCl; 15 mL) and electroplated onto stainless steel 25 mm planchettes at 0.5 A, 20 V for 3 hours. The planchettes were counted using a Canberra 7401 α-spectrometer for 24 hours and the resulting data was corrected for background noise.

## 5.4. Results and Discussion

### 5.4.1. Geochemical Association of Mn and Fe

Manganese and Fe are two common and reactive metals in sediment systems and are often used as redox indicators. We previously measured and reported the solid Mn/Al and Fe/Al distribution at the mud-patch and Ravenglass (Ray et al., 2018; Chapter 3). Here, we determine the association of Mn and Fe with key geochemical phases in to understand the partitioning of these metals. In sediments under oxidising conditions, Mn will be present as Mn(III) and Mn(IV), and these species can form insoluble hydrous oxides (e.g. $Mn(OH)_2$ and $MnO_2$) that can scavenge radionuclides. Under oxidising conditions Fe(III) can form insoluble hydrous oxides that can also sorb radionuclides. The variation in the bulk distribution of Mn/Al and Fe/Al at the mud-patch and Ravenglass (Figure 5.1B, 5.1D, 5.1F, and 5.1H) combined with porewater profiles that are shown in (Ray et al., 2018; Chapter 3), reflect the redox cycling of these two metals in the sediments of both sites.

The partitioning of Mn and Fe (% of total element extracted) across the four geochemical fractions examined (exchangeable, reducible, oxidisable, and residual) at both of these sites are shown in Figures 5.1A, 5.1C, 5.1E, 5.1G. At the mud-patch Mn was extracted predominantly in the reducible, oxidisable, and residual fractions. The partitioning of Mn across these fractions was generally consistent and showed little variation with depth (28–44 %; reducible fraction; 24–38 %, oxidisable fraction; 23–42 %, residual fraction; Figure 5.1A). This highlights that Mn has a relatively heterogeneous distribution across these fractions with depth, with a sizeable proportion of its inventory likely to accessible by bacteria and or capable of adsorbing radionuclides. At the mud-patch, Fe was predominantly extracted in the strongly bound residual fraction ranging between 81–90 %, of total Fe extracted (Figure 5.1B). This may imply that Fe at the mud-patch is bound/incorporated with silicates (e.g. feldspar, quartz, and clays), with only a small proportion accessible for microbial processes and/or capable of reacting with radionuclides.

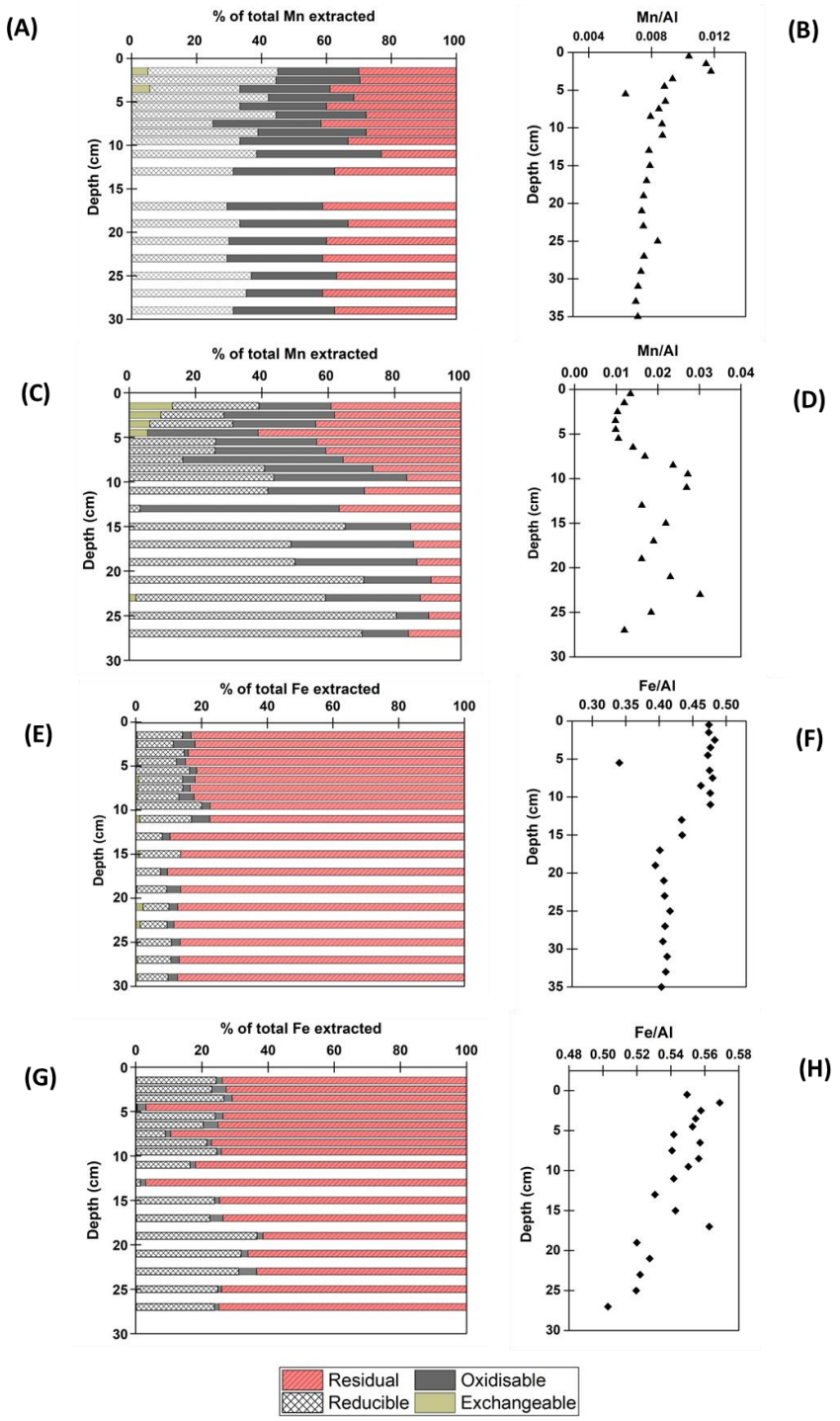


**Figure 5.1.** Association of Mn and Fe with operationally defined fractions (shown in key) in a sediment core taken from the Irish Sea mud-patch (A and E), and the Ravenglass saltmarsh (C and G). Results are from a single sequential extraction and are presented as a percentage of the total activity extracted from each sample of the sediment core. Bulk Mn/Al and Fe/Al are also shown for the Irish Sea mud-patch (B and F), and Ravenglass saltmarsh (D and H).

At Ravenglass, the top 11 cm encompasses the highest percentage of Mn associated with the oxidisable (22–40 %), and residual (16–61 %) fraction (Figure 5.1C). Thereafter, in deeper sediments, Mn is extracted predominantly in the reducible fraction (49–81 %). This increase in reducible Mn at depth is reflected with a decrease in Mn extracted in the oxidisable (10–37 %) and residual (10–15 %) fractions. There was less variance observed with the partioning of Fe at Ravenglass, which was predominantly extracted in the strongly bound residual fraction (92–98 %) throughout the sediment core (Figure 5.1D). Thus, the majority of the Fe inventory is present in the strongly bound residual fraction, and will unlikely be bioavailable/reactive.

### 5.4.2. Geochemical Association of $^{241}$Am

In sediments Am will exist as the particle reactive Am(III) under environmental conditions, being readily hydrolysed, with the resulting precipitate able to associate with various geomedia. A detailed discussion on the bulk $^{241}$Am distribution at the mud-patch and Ravenglass (Figure 5.2B and 5.2D), can be found in Ray et al. (2018) (Chapter 3). However, it can be seen that there is no change in the partioning of $^{241}$Am at Ravenglass (Figure 5.2C) in the region of high total $^{241}$Am (Figure 5.2D) and this may suggest that $^{241}$Am deposited at both sites is likely unreactive. The partitioning of $^{241}$Am (% of total element extracted) across four environmental fractions (exchangeable, reducible, oxidisable, and residual) at the mud-patch and Ravenglass are shown in Figure 5.2A and 5.2C, respectively. Triplicate data carried out showed a variance of ~ 12 % at 1 standard deviation.

At the mud-patch the majority of $^{241}$Am was extracted in the residual fraction (87–98 %), with a minor fraction extracted in the oxidisable fraction (1–12 %) (Figure 5.2A). Thus, the majority of Sellafield-derived $^{241}$Am is likely present as products of hydrolysis (e.g. $Am(OH)_3$), which are chemically stable. *Aqua regia* dissolves these phases releasing Am into solution. This reflects the recalcitrant nature of Am hydrolysis products and/or Am that becomes associated with organic matter. Whilst the mud-patch sediments will likely act as a source of Am to the Irish Sea for some time to come (Ray et al., 2018; Chapter 3), the sequential extraction data indicate that the Am will likely remain particle bound.

Similar to the mud-patch, $^{241}$Am at Ravenglass was partitioned dominantly between the oxidisable (14–77 %) and residual fractions (22–85 %) only (Figure 5.2C). The greater inventory of $^{241}$Am extracted in the oxidisable fraction at all depths may be due to the higher organic matter content at Ravenglass (4–7 % in contrast to the mud-patch; ~1 %) (see Ray et al., 2018; Chapter 3). This may suggest that in sediments of higher organic matter content, $^{241}$Am will preferentially associate with this fraction. In turn, as the organic matter is decomposed, this may release Am back into solution. It is also important to highlight that the organic matter will vary at both sites; at the mud-patch this will likely be of marine origin and in the form of sorptively protected organic matter bound to clay mineral surfaces. Conversely, organic matter at Ravenglass will originate from terrestrial sources , and may include more humic-rich organic matter, which may be present as discrete organic matter debris. With this in mind, the sequential extractions used here may be better at targeting one fraction over another, with no further knowledge known. Of note, previous work at the Esk estuary (on one sediment horizon) showed the dominant association of $^{241}$Am with the oxidisable organic fraction (59 %; Kimber et al., 2015). The favourable association of Am with humics has also been shown by Livens and Singleton, (1991), with the humic acid fraction highlighted to hold 75 % of the organically associated Am in Esk estuarine sediments. However, as Am was extracted predominantly in the residual fraction at Ravenglass, this suggests that it will not be bioavailable or easily remobilised from the site. This supports earlier work which highlighted that post depositional remobilisation of Am was limited at Ravenglass, with the sediment profile instead preserving the time-integrated Sellafield discharge signal (see Ray et al., 2018; Chapter 3).

### 5.4.3. Geochemical Association of $^{137}$Cs

The fission product $^{137}$Cs will exist in the Irish Sea as the highly soluble $Cs^+$ cation, with only a small fraction of its inventory being retained to sediments likely *via* association with clay minerals. The bulk $^{137}$Cs distribution at the mud-patch and Ravenglass is shown in Figures 5.2F and 5.2H, and is discussed further in Ray et al. (2018) (Chapter 3). The partitioning of $^{137}$Cs (% of total element extracted) across four environmental fractions (exchangeable, reducible, oxidisable, and residual) at the mud-patch and Ravenglass is shown in Figures

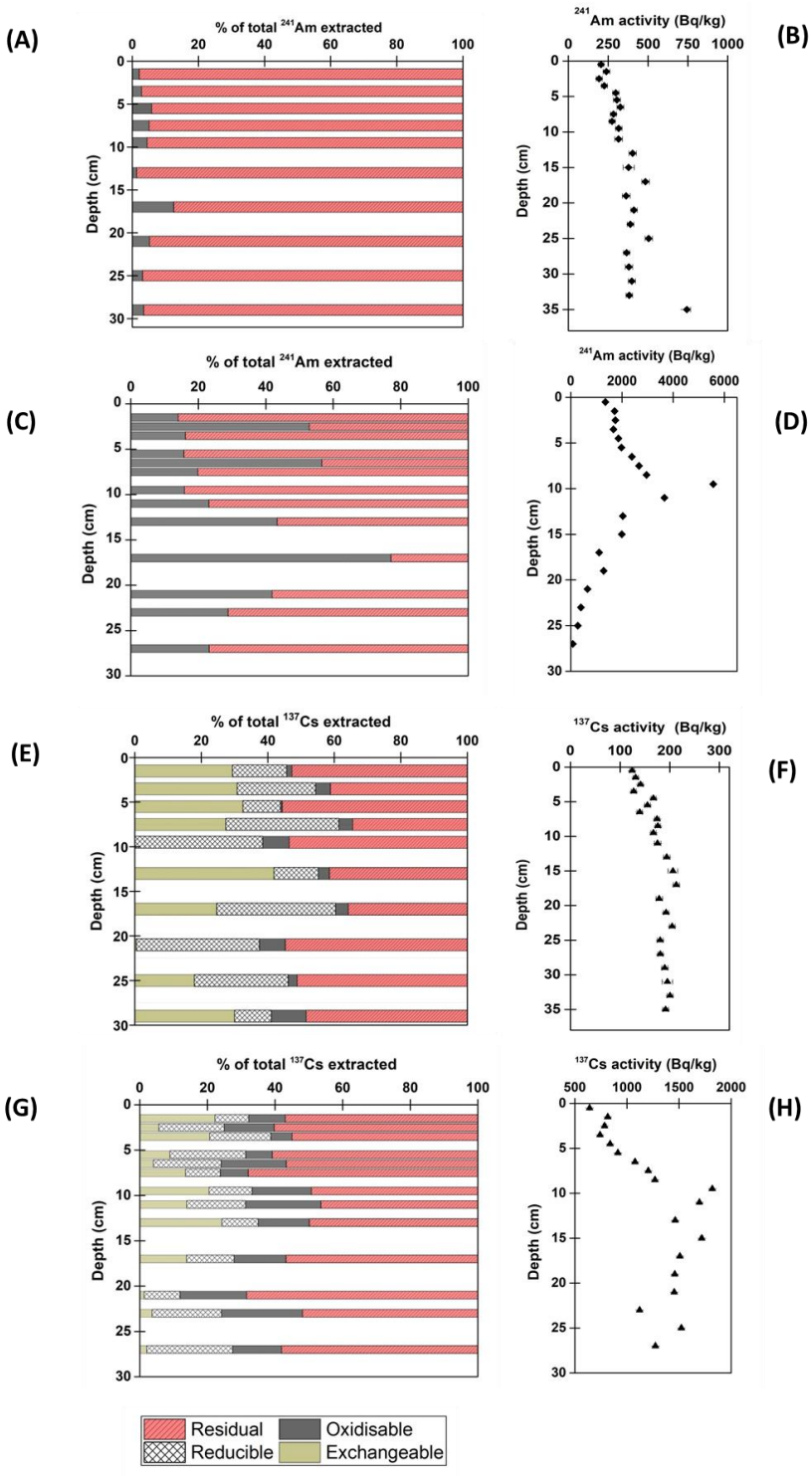


**Figure 5.2.** Association of $^{241}$Am and $^{137}$Cs with operationally defined fractions (shown in key) in a sediment core taken from the Irish Sea mud-patch (A and E), and the Ravenglass saltmarsh (C and G), respectively. Results are from a single sequential extraction and are presented as a percentage of the total activity extracted from each sample of the sediment core. Total $^{241}$Am and $^{137}$Cs are also shown for the Irish Sea mud-patch (B and F), and Ravenglass saltmarsh (D and H), respectively.

5.2E and 5.2G, respectively. There is also no observable trend between high total Cs at Ravenglass (Figure 5.2D) and the geochemical association of Cs (Figure 5.2C) in this region.

At the mud-patch, $^{137}$Cs was extracted in all four environmental fractions (Figure 5.2E), with no clear trend observed with depth down the sediment core. The majority of the extracted $^{137}$Cs was present in the residual fraction (34–75 %), followed by a significant, yet variable fraction present as easily exchangeable $^{137}$Cs (0–42 %). In addition, $^{137}$Cs was also extracted in the reducible fraction (11–38 %) with the smallest fraction extracted in the oxidisable fraction (1–14 %). At Ravenglass, $^{137}$Cs was also associated with all four environmental fractions (Figure 5.2G). The largest proportion of Cs was again associated with the residual fraction (50–68 %) throughout the sediment core. Thereafter, there was a generally equal distribution of $^{137}$Cs extracted in the remaining fractions (exchangeable; 1–22 %; reducible; 10–22 %; oxidisable; 6–22 %). Triplicate data carried out showed a variance of ~20 % at 1 standard deviation.

It is well known that Cs will preferentially associate with clay minerals in sediments (Sawhney, 1972; Hird et al., 1996; Jones et al., 1999; Fuller et al., 2014, 2015). The mud-patch sediments have been shown to have a clay fraction of ~13 % (McDonald et al., 1990), with a slightly higher fraction at Ravenglass (~19 %; Morris et al., 2000). Further, the majority of $^{137}$Cs at the mud-patch and Ravenglass was extracted in the residual fraction, followed by the exchangeable fraction. As a result it is likely that most of the $^{137}$Cs inventory is associated within clay interlayers at both sites, and released on extraction with *aqua regia*. However, as Cs was also extracted in the exchangeable fraction, particularly at the mud-patch, this may suggest that Cs is also binding to weakly bound surface sites on clays, most likely basal or in some cases edge sites. As Cs was extracted in the exchangeable fraction in the majority of the sediment horizons at both sites, this may imply that it may be bioavailable in these contaminated systems. It is interesting to note that when the Ravenglass sediment core is dated (using the Sellafield discharge history; see Ray et al., 2018; Chapter 3) that $^{137}$Cs activity is observed at depth, before maximum Sellafield discharges had taken place (see Ray et al.,2018; Chapter 3). The presence of this feature (which was not observed

with Pu or Am) may highlight the redissolution of Cs as it can be easily exchanged from clay surface sites, and this may cause its distribution to vary.

### 5.4.4. Geochemical Association of $^{239,240}$Pu

Plutonium predominantly exists as Pu(IV) and Pu(V) in marine systems, with Pu(IV) shown to be relatively immobile, existing as a free ion, and Pu(V) present as the more mobile $Pu(V)O_2$ complex. The majority (90 %) of the discharged Pu inventory has likely associated with Irish Sea sediments as the particle-reactive Pu(IV) species (MacKenzie and Scott, 1993).

The bulk $^{239,240}$Pu distribution at the mud-patch and Ravenglass is shown in Figure 5.3B and 5.3D (see Ray et al., 2018; Chapter 3 for further discussion). The partitioning of $^{239,240}$Pu (% of total element extracted) across four geochemical fractions (exchangeable, reducible, oxidisable, and residual) at the mud-patch and Ravenglass are shown in Figure 5.3A and 5.3C, respectively. For the shallow sediment sample at the mud-patch (3–4 cm) $^{239,240}$Pu was dominantly extracted in the reducible (39–48 %) and residual fractions (38–56 %), with a small proportion of the extracted Pu inventory present in the exchangeable (<5 %) and oxidisable fractions (4–8 %; Figure 5.3A). For the deeper sample (24–26 cm), the partitioning of Pu is similar to the shallow horizon, with Pu extracted dominantly in the reducible (32 %) and residual (47 %) fractions. The results obtained for the mud-patch agree with previous work which also showed the dominant association of Pu with reducible oxides (McDonald et al., 2001).

At Ravenglass, $^{239,240}$Pu was extracted predominantly in the reducible fraction (71–75 %) for the higher activity, mid-core sample (10–12 cm), followed by the residual (24–31 %) and oxidisable fractions (0–4 %; Figure 5.3C). There was a good reproducibility for the duplicate samples at both sites (shown in Figure 5.3A and 5.3C) providing validity for the results obtained. For the sample at 24–26 cm, $^{239,240}$Pu was also predominantly associated with the reducible fraction (69 %), with less Pu extracted in the oxidisable (14 %) and residual (16 %) fractions. This suggests that Pu associates most preferentially with the reducible oxide fraction at both sites, and this includes any Pu that may be associated with Fe and Mn oxides, consistent with traditionally held views (Keeney-Kennicutt and Morse, 1985; Sanchez et al., 1985; Powell et al., 2004, 2005). Further, it has previously

been shown that there is no extensive post-depositional remobilisation of Pu (in contrast to Tc, Np, U; Chapter 4) in Ravenglass sediments, and instead its distribution was largely controlled by the transport and preservation of the Sellafield-discharge signal (similar to Cs and Am; Ray et al., 2018; Chapter 3). This work builds on this finding and highlights that Pu could potentially be remobilised under anoxic, reducing conditions as well as during the degradation of organic matter. However, as there was little cycling of Pu observed previously (Ray et al., 2018; Chapter 3) this may be negligible.

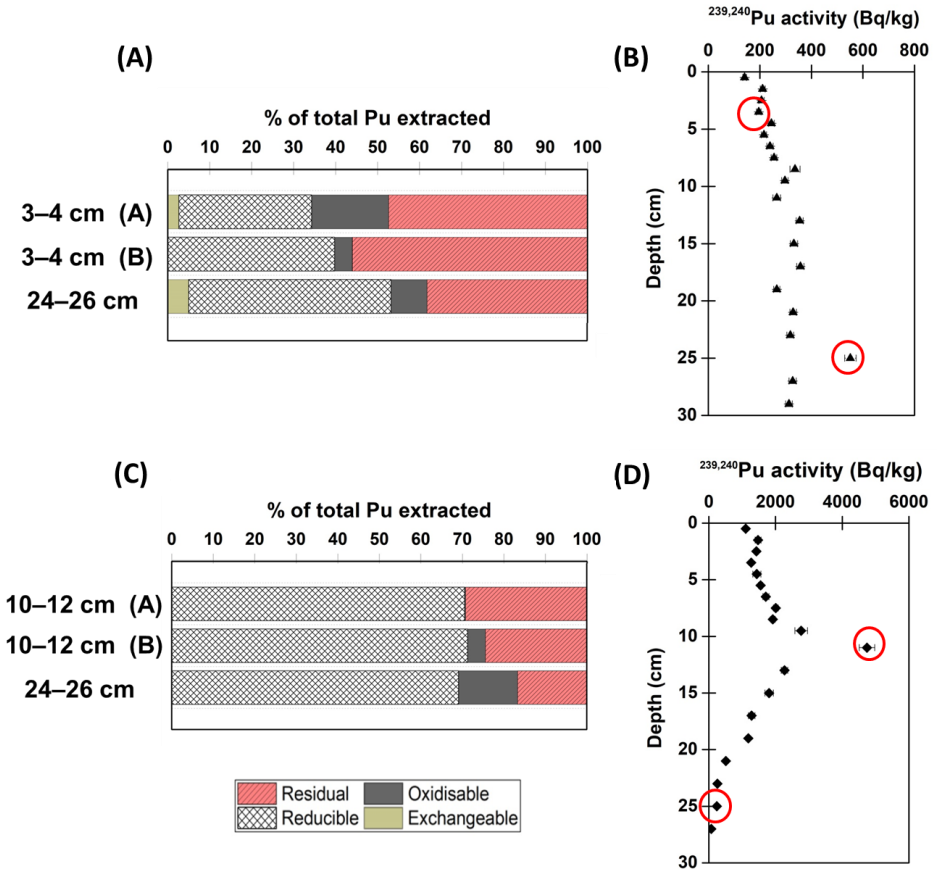


**Figure 5.3.** Association of $^{239,240}$Pu with operationally defined fractions (shown in key) in select samples from (A) the Irish Sea mud-patch and (C) Ravenglass saltmarsh. Results are from the same sequential extraction, and are presented as a percentage of the total activity extracted from each sample. Total $^{239,240}$Pu distributions are also shown for (B) the Irish Sea mud-patch and (D) Ravenglass saltmarsh.

Previous sequential extraction work at Ravenglass has shown the geochemical association of Pu to vary. For example, Pu was shown to dominantly associate with the residual fraction, followed by a smaller Pu fraction present in the reducible oxide fraction (Mudge et al., 1988; Kimber et al., 2015). In addition, more recent work by Lucey et al. (2004) found that the majority of Pu was bound to carbonate minerals, followed by the exchangeable/readily oxidisable fraction. Discrepancies between studies investigating the geochemical association of Pu, or Am and Cs may be caused by (a) the operationally defined nature of the procedure; (b) the varying reagents used (and thus the need for standardisation); (c) the slightly different locations of each study at the Esk estuary, which will be experiencing slightly different biogeochemical conditions.

### 5.5. Conclusions and Implications

This work provides a deeper insight into the environmental behaviour of Sellafield-derived $^{137}$Cs, $^{241}$Am, and Pu. Our earlier work showed that these radionuclides were largely unreactive in Ravenglass sediments, with their deposition likely controlled by their physical transport from the mud-patch, followed by burial of the time-integrated Sellafield signal, with no extensive post-depositional effects. Here, we have shown that that the majority of the $^{241}$Am and $^{137}$Cs inventory at both sites is present in the strongly bound refractory fraction, and therefore $^{241}$Am and $^{137}$Cs will not be largely remobilised from the sediments. In turn, these radionuclides are unlikely to be released in large amounts over a reasonable time frame. However, for both radionuclides the next largest fraction was with organic matter for $^{241}$Am (12–77 %), and exchangeable sites for $^{137}$Cs (0–42 %), suggesting that a minor fraction of the $^{241}$Am and $^{137}$Cs inventory may be remobilised over time. Plutonium was dominantly associated with the reduced oxide fraction at Ravenglass and this suggests that the Pu inventory may be bioavailable under anoxic, reducing conditions. However, a large proportion of the Pu inventory was also extracted in the residual fraction. We have previously shown that the distribution of Pu at Ravenglass is independent to Fe and Mn redox cycling, with no signs of post-depositional remobilisation. However, this work shows that Pu may be remobilised as it is dominantly present at this site in the reducible oxide fraction. There is a current drive to understand the oxidation state and coordination environment of Pu, on a molecular scale, using

synchrotron techniques. As the experiments used prior to synchrotron analysis can have a radiological impact (due to the high activity of Pu used to meet the detection limit of X-ray Absorption Spectroscopy), this work can provide important insight into the dominant geochemical association of Pu in the natural environment.

## References


Aston, S.R., Stanners, D.A., 1981. Plutonium transport to and deposition and immobility in Irish Sea intertidal sediments. Nature. 289 (5798), 581–582.

Baeyens, W., Monteny, F., Leermakers, M., Bouillon, S., 2003. Evaluation of sequential extractions on dry and wet sediments. Anal. Bioanal. Chem. 376, 890–901.

Begg, J.D.C., Burke, I.T., Lloyd, J.R., Boothman, C., Shaw, S., Charnock, J.M., Morris, K. 2011. Bioreduction behavior of U(VI) sorbed to sediments. Geomicrobiol. J. 28, 160–171.

Begg, J.D.C., Zavarin, M., Zhao, P., Tumey, S.J., Powell, B., Kersting, A.B., 2013. Pu(V) and Pu(IV) sorption to montmorillonite. Environ. Sci. Technol. 47, 5146–5153.

Chibowski, S., Zygmunt, J., 2002. The influence of the sorptive properties of organic soils on the migration rate of $^{137}$Cs. J. Environ. Radioactiv. 61, 213–223.

Choppin, G.R., Wong, P.J., 1998. The chemistry of actinide behavior in marine systems. Aquat. Geochem. 4, 77–101.

Cook, G.T., MacKenzie, A.B., McDonald, P., Jones, S.R., 1997. Remobilization of Sellafield-derived radionuclides and transport from the north-east Irish Sea. J. Environ. Radioactiv. 35 (3), 227–241.

Cornell, R.M., 1992. Adsorption behaviour of cesium in marl. Clay. Miner. 27, 363–371.

Fuller, A.J., Shaw, S., Peacock, C.L., Trivedi, D., Small, J.S., Abrahamsen, L.G., Burke, I.T., 2014. Ionic strength and pH dependent multi-site sorption of Cs onto a micaceous aquifer sediment. Appl. Geochem. 40, 32–42.

Fuller, A.J., Shaw, S., Ward, M.B., Haigh, S.J., Mosselmans, J.F.W., Peacock, C. L., Stackhouse, S., Dent, A.J., Trivedi, D., Burke, I.T., 2015. Caesium incorporation and retention in illite interlayers. App. Clay. Sci. 108, 128–134.

Gray, J., Jones, S.R., Smith, A.D., 1995. Discharges to the environment from the Sellafield site, 1951–1992. J. Radiol. Prot. 15 (2), 99–131.

Grütter, A., von Gunten, H.R., Kohler, M., Rössler, E. 1990. Sorption, desorption and exchange of cesium on glaciofluvial deposits. Radiochim. Acta. 50, 177–184.

Hird, A.B., Rimmer, D.L., Livens, F.R. 1996. Factors affecting the sorption and fixation of caesium in acid organic soil. Eur. J. Soil. Sci. 47(1), 97–104.

Hunt, G.J., Kershaw, P., 1990. Remobilisation of artificial radionuclides from the sediment of the Irish Sea. J. Radiol. Prot. 10 (2), 147–151.

Jefferies, D., Preston, A., Steele, A., 1973. Distribution of caesium-137 in british coastal waters. Mar. Pollut. Bull. 4, 118–122.

Jones, D.G., Roberts, P.D., Miller, J.M., 1988. The distribution of gamma-

emitting radionuclides in surface subtidal sediments near the Sellafield plant. Estuar. Coast. Shelf. S. 21, 143–161.

Jones, D., Roberts, P., Strutt, M., Higgo, J., Davis, J., 1999. Distribution of $^{137}Cs$ and inventories of $^{238}Pu$, $^{239,240}Pu$, $^{241}Am$ and $^{137}Cs$ in Irish Sea intertidal sediments. J. Environ. Radioactiv. 44, 159–189.

Keeney-Kennicutt, W.L., Morse, J.W., 1985. The redox chemistry of $Pu(V)O_2^+$ interaction with common mineral surfaces in dilute solutions and seawater. Geochim. Cosmochim. Ac. 49, 2577–2500.

Keith-Roach, M.J., Morris, K., Dahlgaard, H., 2003. An investigation into technetium binding in sediments. Mar. Chem. 81, 149–162.

Kershaw, P.J., Swift, D.J., Pentreath, R.J., Lovett, M.B., 1983. Plutonium redistribution by biological activity in Irish sea sediments. Nature. 306 (22/29), 774–775.

Kershaw, P.J., Swift, D.J., Pentreath, R.J., Lovett, M.B., 1984. The incorporation of plutonium, americium and curium into the Irish Sea seabed by biological activity. Sci. Total. Environ. 40, 61–81.

Kershaw, P.J., Pentreath, R.J., Woodhead, D.S., Hunt, G.J., 1992. A review of radioactivity in the Irish Sea, in: Aquatic Environmental Monitoring Report. Lowestoft, UK. Ministry of Agriculture Fisheries and Food. 32, 1–66.

Kershaw, P.J., Denoon, D.C., Woodhead, D.S., 1999. Observations on the redistribution of plutonium and americium in the Irish Sea sediments, 1978 to 1996: concentrations and inventories. J. Environ Radioactiv. 44 (2–3), 191–221.

Kershaw, P.J., Woodhead, D.S., Malcolm, S.J., Allington, D.J., Lovett, M.B. 1990. A sediment history of Sellafield discharges. J. Environ. Radioactiv. 12, 201–241.

Kersting, A., Efurd, D., Finnegan, D., Smith, D., Thompson, J., 1999. Migration of plutonium in ground water at the Nevada Test Site. Letters to Nature. 397, 56–59.

Kersting, A.B. 2013. Plutonium transport in the environment. Inorg. Chem. 52, 3533–3546.

Kimber, R.L., Corkhill, C.L., Amos, S., Livens, F.R., Lloyd, J.R., 2015. Geochemical association of Pu and Am in selected host-phases of contaminated soils from the UK and their susceptibility to chemical and microbiological leaching. J. Environ. Radioactiv. 142, 96–102.

Lehto, J., Hou, X., 2010. Chemistry and analysis of radionuclides: laboratory techniques and methodology. Wiley-Vch.

Leonard, K.S., McCubbin, D., Blowers, P., Taylor, B.R., 1999. Dissolved plutonium and americium in surface waters of the Irish sea, 1973–1996. J. Environ. Radioactiv. 44, 129–158.

Lindahl, P., Worsfold, P., Keith-Roach, M.J., Andersen, M.B., Kershaw, P., Leonard K., Choi, M.-S., Boust, D., Lesueur, P., 2011. Temporal record of Pu isotopes in inter-tidal sediments from the northeastern Irish sea. Sci. Total. Environ. 409 (23), 5020–5025.

Livens, F. R. 1985. Geochemistry of plutonium and other artificial radionuclides in cumbrian soils. University of Glasgow.

Livens, F.R., Singleton, D.L., 1991. Plutonium and americium in soil organic matter. J. Environ. Radioactiv. 13, 323–339.

Lovett, M.B., Nelson. D.M., 1978. Oxidation state of Pu in the Irish Sea. Nature. 276, 599–601.

Lu, N., Reimus, P.W., Parker, G.R., Conca, J.L., Triay, I.R., 2003. Sorption kinetics and impact of temperature, ionic strength and colloid concentration on the adsorption of plutonium-239 by inorganic colloids, Radiochim. Acta. 91, 713–720.

Lucey, J.A., Gouzy, A., Boust, D., Leon Vintro, L., Kershaw, P.J., Mitchell, P.I., 2004. Geochemical fractionation of plutonium in anoxic Irish Sea sediments using an optimised sequential extraction protocol. App. Radiat. Isotopes. 60, 379–385.

Lujanienơ, G., Motiejnjnas, S., Šapolaitơ, J., 2007. Sorption of Cs, Pu and Am on clay minerals. J. Radioanal. Nucl. Chem. 274 (2), 345–353.

MacKenzie, A., Scott, R., Allan, R.L., Ben Shaban, Y.A., Cook, G., Pulford, I. D., 1994. Sediment radionuclide profiles: implications for mechanisms of Sellafield waste dispersal in the Irish Sea. J. Environ. Radioactiv. 23, 39–69.

MacKenzie, A.B., Cook, G.T., McDonald, P., 1999. Radionuclide distributions and particle size associations in Irish sea surface sediments: implications for actinide dispersion. J. Environ. Radioactiv, 44, 275–296.

MacKenzie, A.B., Scott, R.D., 1993. Sellafield waste radionuclides in Irish Sea intertidal and salt marsh sediments. Environ. Geochem. Hlth. 15, 173-184.

Malcolm, S.J., Kershaw, P.J., Cromar, N.J., Botham, L., 1990. Iron and manganese geochemistry and the distribution of $^{239,240}$Pu and $^{241}$Am in the sediments of the north east Irish sea. Sci. Total. Environ. 95, 69–87.

McCartney, M., Kershaw, P.J., Woodhead, D.S., Denoon, D.C., 1994. Artificial radionuclides in the surface sediments of the Irish Sea, 1968–1988. Sci. Total Environ. 141 (1–3), 103–138.

McDonald, P., 2011. Radioactivity in the Irish Sea. Environmental radiochemical analysis IV. RSC publishing. 2, 87–94.

McDonald, P., Cook, G.T., Baxter, M.S., Thomson, J.C., 1990. Radionuclide transfer from Sellafield to south-west Scotland. J. Environ. Radioactiv. 12, 285–298.

McDonald, P., Vives I Batlle, J., Bousher, A., Whittall, A., Chambers, N., 2001.

The availability of plutonium and americium in Irish sea sediments for re-dissolution. Sci. Total. Environ. 267, 109–123.

Morris, K., Butterworth, J.C., Livens, F.R., 2000. Evidence for the remobilisation of Sellafield waste radionuclides in an intertidal salt marsh, west Cumbria, U.K. Estuar. Coast. Shelf. S. 51 (5), 613–625.

Morse J.W., Choppin G.R., 1991. The chemistry of transuranic elements in natural waters. Rev. Aquat. Sci. 4, 1–22.

Neck, V., Altmaier, M., Seibert, A., Yun, J.I., Marquardt, C.M., Fanghänel, T., 2007. Solubility and redox reactions of Pu(IV) hydrous oxide: evidence for the formation of $PuO_{2+x}$(s, hyd). Radiochim. Acta. 95, 193–207.

Novikov, A., Kalmykov, S., Utsunomiya, S., Ewing, R., Horreard, F., Merkulov, A., Clark, S., Tkachev, V., Myasoedov, B., 2006. Colloid transport of plutonium in the far-field of the Mayak Production Association, Russia. Science. 314 (5799), 638–641.

Powell, B.A., Fjeld, Robert, A., Kaplan, D,I., Coates, J.T., Serkiz, S.M., 2004. $Pu(V)O_2$ adsorption and reduction by synthetic magnetite ($Fe_3O_4$). Environ. Sci. Technol. 38, 6016–6024.

Powell, B.A., Fjeld, R.A., Kaplan, D.I., Coates, J.T., Serkiz, S.M., 2005. $Pu(V)O_2$ adsorption and reduction by synthetic hematite and goethite. Environ. Sci. Technol. 39, 2107–2114.

Ray, D., Livens, F.R., Leary, P., Gray, N., Abrahamsen-Mills, L., Muir, G.K.P., Law., K.A., Fuller, A.J., Bryan, N.D., Howe, J., Cook, G.T., Law, G.T.W., 2018. Controls on anthropogenic radionucldie distribution in the Sellafield-impacted eastern Irish Sea, UK. J. Environ. Radioactiv (submitted).

Robbins, J., Lyle, M., Heath, G.R., 1984. A sequential extraction procedure for partitioning elements among co-existing phases in marine sediments. Oregon State University.

Sanchez, A.L., Murray, J.W., Sibley, T.H. 1985. The adsorption of plutonium IV and V on goethite. Geochim. Cosmochim. Ac. 49, 2297–2307.

Santschi, P., Roberts, K.,. 2002. Actinide migration from contaminated soil to surface water at the Rocky Flats Environmental Technology Site. J. Nucl. Sci. Technol. 3, 485–488.

Sawhney, B., 1972. Selective sorption and fixation of cations by clay minerals: a review. Clays. Clay. Miner. 20, 93–100.

Sellafield Ltd., 2017. Monitoring our environment: discharges and environmental monitoring. Annual Report 2016.

Tessier, A., Campbell, P.G.C., Bisson, M., 1979. Sequential extraction procedure for the speciation of particulate trace metals. Anal. Chem. 51 (7), 844–851.

Wang, X., Dong, W., Li, Z., Du, J., Tao, Z., 2000. Sorption and desorption of radiocesium on red earth and its solid components: relative contribution and

hysteresis. App. Radiat. Isotopes, 52, 813–819.

Zavarin, M., Powell, B.A., Bourbin, M., Zhao, P., Kersting, A.B., 2012. Np(V) and Pu(V) ion exchange and surface-mediated reduction mechanisms on montmorillonite. Environ. Sci. Technol. 46, 2692–2698.

## Chapter 6: Conclusions and Implications

In this final chapter the hypotheses detailed in Chapter 1 are re-visited, and thesis conclusions are made, alongside the discussion of relevant future research.

.

# 6. Thesis Conclusions and Implications

## 6.1. Conclusions

This thesis has explored the fate and distribution of Sellafield-derived radionuclides, to further understand their behaviour in the marine environment. In Chapter 1, Hypothesis 1 stated that the *"Post-depositional remobilisation of Sellafield-derived $^{137}Cs$ and $^{241}Am$ at the Ravenglass saltmarsh will be negligible".* This hypothesis was proven to be true, as Chapter 3 highlighted that the distribution of $^{137}Cs$ and $^{241}Am$ in Ravenglass sediments showed a good agreement to their Sellafield discharge histories. Consequently, this suggests that $^{137}Cs$ and $^{241}Am$ are largely unreactive in Ravenglass sediments, with their deposition likely controlled by their physical transport from the mud-patch, followed by burial of the time-integrated Sellafield signal, with no extensive post-depositional effects. In addition, the broad sediment distribution for both of these radionuclides relative to the Sellafield discharge history implies that the vertically 'mixed' input from the Irish Sea mud-patch (or similar) is the dominant source of $^{137}Cs$ and $^{241}Am$ to Ravenglass. Further, Chapter 5 showed that $^{137}Cs$ and $^{241}Am$ in Ravenglass sediments were dominantly associated with the strongly-bound refractory fraction, and as such this will also limit remobilisation form the solid. However, $^{137}Cs$ was also extracted in the easily exchangeable fraction, and this may suggest that some of its inventory may be remobilised over time, and this could rationalise the presence of $^{137}Cs$ activity prior to maximum $^{137}Cs$ Sellafield discharges (as shown in Chapter 3).

Hypothesis 2 stated that *"Plutonium ($^{238}Pu$, $^{239,240}Pu$, and $^{241}Pu$) at the Ravenglass saltmarsh will be influenced by the ambient site biogeochemistry, leading to significant post-depositional remobilisation".* This hypothesis was also tested in Chapter 3, and was proven to be false, as the distribution of Pu ($^{238}Pu$, $^{239,240}Pu$, and $^{241}Pu$) at the Ravenglass saltmarsh was shown to behave independently to the ambient site biogeochemistry, and instead reflected its authorised discharge history (similar to $^{137}Cs$ and $^{241}Am$). The Ravenglass saltmarsh was shown to be suboxic, characterised by the cycling of reactive Fe and Mn between the solid and solution phase. Further, novel microbial ecology results supported this observation but additionally showed highlighted the

complex sediment system, as biomarkers for oxic and anoxic functions often persisted in the same sediment horizon. Thus, the Pu distribution observed at Ravenglass is surprising; as it would have been thought that the suboxic, dynamic conditions of the site would favour the redox-cycling, and mobility of Pu. As a result, this field observation contrasts with traditionally held views from laboratory experiments that have highlighted the association of Pu with Fe and Mn oxy(hydr)oxides, including the surface-mediated reduction of Pu(V) in some cases. Further, as Pu was dominantly extracted in the stable reducible oxide fraction, this may rationalise the negligible cycling observed, as the majority of the inventory is likely inaccessible by bacteria.

Hypothesis 3 stated that "*The activity of $^{137}$Cs, $^{241}$Am, and the Pu isotopes ($^{238}$Pu, $^{239,240}$Pu, and $^{241}$Pu) at the surface of the Irish Sea mud-patch will be negligible, due to low modern discharge rates from the Sellafield Ltd. site*". This hypothesis was tested in Chapter 3, and was proven to be false as there was a measured activity of $^{137}$Cs (~120 Bq/kg) $^{241}$Am (~170 Bq/kg), and $^{239,240}$Pu (~150 Bq/kg) at the surface of the Irish Sea mud-patch sediment core. As contemporary discharge for all these radionuclides are now well below discharge limits (in comparison to the mid-1970s), this suggests that bio-mixing of the seabed by macrobenthic organisms is ongoing, and this continues to physically mix, and remobilise radionuclide activity into the Eastern Irish Sea. Further, as the macrobenthic organisms can physically mix the Irish Sea mud-patch profile down to 1.5 m, the smeared $^{137}$Cs, $^{241}$Am, and Pu profiles observed likely represent the mixing of higher-activity radionuclides from depth (corresponding to the mid-1970s), with lower-activity in upper sections from more, modern lower discharges. In turn, as radionuclide activity is still being measured at the surface of the core approximately ~ 40 years after peak discharge; this strongly suggests that the Irish Sea mud-patch will continue to supply the UK coastal environment with Sellafield-derived contaminants.

Hypothesis 4 stated that "*The distribution of $^{99}$Tc and $^{236}$U in Ravenglass saltmarsh sediments will be influenced by the biogeochemistry of the site*". This hypothesis was proven true in Chapter 4, as the distribution of $^{99}$Tc and $^{236}$U did not reflect their discharge histories (in contrast to $^{137}$Cs, $^{241}$Am, and the Pu isotopes discussed in Chapter 3). Instead, the distribution of Tc was shown to be

smeared throughout the core, and did not resemble the Sellafield $^{99}$Tc discharge history. Uranium-236 distribution at the Ravenglass saltmarsh resembled aspects of its discharge history, highlighting the preservation of the discharge signal at the site. However, the decrease in Sellafield U discharges observed in the late 1970s was not matched by a decrease in the U distribution at Ravenglass, which instead remained high. Further, the biogeochemistry of the site was characterised in Chapter 1, and this was shown to have prevailing suboxic conditions, including a dynamic microbial community. Thus, it was proposed that these conditions were favourable for the cycling of $^{99}$Tc, and $^{236}$U between the solution and sediment phase in Ravenglass sediments, causing their post-depositional migration. Further, $^{237}$Np was also examined in Chapter 3, and similarly to $^{99}$Tc, and $^{236}$U, the distribution of $^{237}$Np in Ravenglass saltmarsh sediments did not entirely match its authorised discharge record. Thus, it was concluded that there was post-depositional effects on Np distribution at the site, likely caused by the solid-solution cycling of this radionuclide under favourable anoxic conditions.

Hypothesis 5 stated that *"Sellafield-derived plutonium ($^{239,240}$Pu) will be dominantly hosted in the reducible oxide fraction in Irish Sea mud-patch and Ravenglass sediments".* This hypothesis was proven to be true in Chapter 5 as $^{239.240}$Pu was shown to be dominantly extracted in the reducible oxide fraction in Irish Sea mud-patch and Ravenglass sediments At the Irish Sea mud-patch, Pu was predominantly extracted in the reducible oxide (39–48 %) and residual fraction (38–56 %) in the upper horizon of the sediment core (3–4 cm), with the partitioning remaining similar at depth (24–26 cm). At Ravenglass a greater proportion of Pu was extracted in the reducible fraction (71–75 %) for the higher activity, mid-core sample (10–12 cm), with a smaller proportion present in the reducible fraction (24–31 %). There was a similar partioning between these fractions for the lower-activity Pu sample at depth (24–26 cm). Further, the partitioning of $^{239,240}$Pu at Ravenglass is similar in both the high and low total $^{239,240}$Pu samples, and may suggest that it there is limited association between Pu and the site geochemistry. The presence of Pu in the reducible oxide fraction at both sites, suggests that it may be accessible under anoxic, reducing conditions.

Hypothesis 6 highlighted that *"Sellafield-derived $^{137}$Cs and $^{241}$Am will be dominantly hosted in the exchangeable and organic fractions respectively, in*

*Irish Sea mud-patch and Ravenglass sediments"* This hypothesis was proven to be false as $^{137}$Cs and $^{241}$Am were both hosted dominantly in the residual fraction at all examined sediment depths. The majority of the Cs inventory was extracted in the residual fraction at the Irish Sea mud-patch (34–75 %) and Ravenglass saltmarsh (50–68 %), and this was followed by Cs extracted in the exchangeable fraction (0–42 %; Irish Sea mud-patch; 1–22 %; Ravenglass saltmarsh). Thus, this shows that a greater inventory of Cs is likely associated within the clay interlayer, instead of with easily exchangeable basal sites on the clay surface. The partioning of $^{241}$Am at all depths was shown to be dominantly in the residual fraction at the Irish Sea mud-patch (87–98 %) and Ravenglass saltmarsh (22–85 %), and this was followed by Am extracted in the oxidisable fraction (1–12 %; Irish Sea mud-patch; 14–77 %; Ravenglass saltmarsh). Thus, it may be assumed that a large proportion of the $^{241}$Am inventory will not be bioavailable.

### 6.2. Implications.

This thesis has important implications for the assessment and long-term monitoring of radionuclides in the marine environment. It has revealed a number of observations regarding the biogeochemistry, and the long-term fate of several reactor-derived anthropogenic contaminants. In turn, this knowledge can aid our understanding of radionuclides in natural laboratories, and this may prove beneficial to the nuclear industry e.g. in response to future releases from nuclear sites, or unplanned release of stored effluent after a nuclear accident. Further, this examination into contaminated sediments is particularly pertinent at present as the construction of the proposed Moorside Nuclear Reactor near Sellafield may disturb or result in dredging of the local seabed during site investigation/construction. This thesis has shown that the offshore Irish Sea sediments are contaminated by legacy Sellafield-derived radionuclides. However, we have shown that $^{137}$Cs, $^{241}$Am, and $^{239,240}$Pu at the offshore mud-patch site are dominantly hosted in stable environmental fractions, and will not be released over long timescales. This observation may provide confidence to NuGEN, the nuclear company who are proposing to build Moorside in West Cumbria. In addition, predicted sea-level rise would make low lying coastal nuclear sites e.g. Sellafield and the Low- Level Waste repository (LLWR) vulnerable to tidal inundation with oxygenated seawater. This may be important, as this thesis has shown that Tc,

Np, and U undergo post-depositional remobilisation to some degree, under dynamic redox conditions.

The findings of this thesis also provide an important insight into the environmental behaviour of radionuclides that are most commonly studied in the laboratory (in concentrations that are often not representative of those found in the field). For example, the behaviour of Tc, U, Np, and Pu have been shown to be influenced by the redox-cycling of trace elements under constrained laboratory conditions, partitioning between solid and solution under microbially-mediated metal reducing conditions. This thesis has shown that Tc, Np, and U respond to these redox conditions in the field, to some degree, thus confirming findings from laboratory studies. Further, it has been highlighted that the post-depositional remobilisation of the radionuclides decreases in the order Tc > U > Np, and this is also similar to the expected mobility of these radionuclides. A key finding of this work is that redox-active cycling of radionuclides does occur in the field over many decades, and this may influence the mobility of radionuclides in suboxic sediment systems.

Further, it is interesting to note that Pu distribution was controlled by physical transport showing no significant post-depositional remobilisation at the Ravenglass saltmarsh. This is in contrast to published literature and may raise important discussion on field vs. laboratory behaviour of Pu. Further, this work has shown that Pu will likely remain associated with reducible oxide or residual fractions, with limited remobilisation if the Ravenglass site remains stable. At the Irish Sea mud-patch, it can be strongly assumed that vertical bio-mixing will continue for many decades, and this will remobilise Sellafield-derived radionuclides into the Eastern Irish Sea, and continue to supply areas of the UK coastal environment. However, as the radionuclides examined at the Irish Sea mud-patch have been shown to be stable, this may be an important finding for monitoring organisations (e.g. the Environment Agency and Food Standards Agency).

### 6.3. Further Work

This field study has presented the bulk distribution of a number of redox-active and in-active radionuclides, and the importance of redox-driven biogeochemistry

on their long-term fate. The findings have shown that ambient site conditions at the Ravenglass saltmarsh are favourable for the cycling of redox-active radionuclides, and this may lead to their remobilisation. An obvious next step may be to collect non-contaminated sediment from the Ravenglass saltmarsh, and off-shore Irish Sea sediments and label them with a suite of radionuclides (e.g. $^{99}$Tc, $^{237}$Np, and $^{239,240}$Pu). These systems could be aged to examine the development of long-term products, or redox cycling microcosm experiments could be designed whereby the system is held at different parts of the redox ladder *via* the stimulation of various TEAs (e.g. Fe, $SO_4^{2-}$).

The bioavailability of Cs, Am, and the Pu isotopes in this thesis was determined by sequential extractions, the findings of which supported the bulk distribution of these radionuclides. Thus, it may be interesting to examine the novel geochemical association of $^{99}$Tc, $^{237}$Np, and $^{236}$U in Ravenglass sediments using similar sequential extractions. This would determine whether these radionuclides are hosted in an environmentally accessible fraction; as would be expected from their bulk distribution profiles observed in Chapter 4. Further, $^{14}$C has been discharged from the Sellafield pipeline, and has been examined at the offshore Irish Sea mud-patch. However, there is little information on its distribution and long-term fate in coastal locations in Cumbria (e.g. Ravenglass saltmarsh). This may be of importance as $^{14}$C has a long half-life, high environmental mobility, and high bio-availability.

This thesis has focused on examining radionuclides that have been transported by the physical deposition of sediment-bearing phases or in solution. However, hot particles have been observed in samples of liquid effluent from the Sellafield nuclear reprocessing site (Kershaw et al., 1986), and been transported to the Esk estuary. Further, it has been suggested that a fraction of the radionuclide inventory may be buried at Ravenglass as ‘hot particles’ (1–20 μm in diameter) and these particles have been identified previously (Sajih and Livens, 2010). Preliminary investigations conducted during this project have found the presence of higher-activity particles at the Ravenglass saltmarsh, one of which is shown in Figure 6.1.

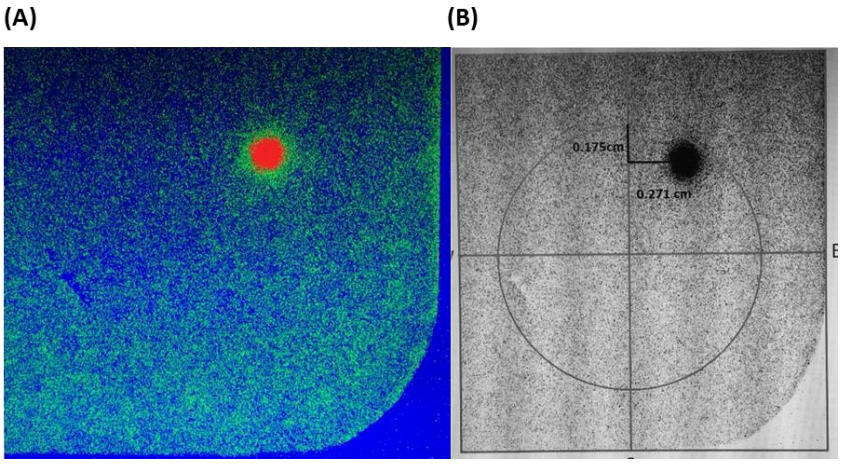


**Figure 6.1.** (A) Autoradiography image of the higher activity Ravenglass particle (red indicates a greater no. of radioactive emissions detected by the phosphor autoradiography screen; (B) black and white autoradiography image highlighting the location of the hot spot on the SEM stub

Further, attempts to characterise these particles using Scanning Electron Microscopy were time-consuming due to the heterogeneous sediment matrix. As a result, on-going work by fellow researchers has led to the finding of several ~ pure U particles (~ 12 µm in diameter), which have been processed for further analysis using a Focused Ion Beam. These small (10 x 5 x 2 µm) sub-sections will be taken to the Diamond Light source in February 2018 and characterised using nano-focussed EXAFS, XANES, and XRD. This synchrotron based technique will identify the coordination environment and oxidation state of the U species, and provide a better understanding of the particles found at Ravenglass. Isotopics will also be investigated using SIMS techniques at the University of Manchester. In turn, this is important for monitoring organisations like the Environment Agency who are committed to monitoring public coastlines and beaches in Cumbria for hot particles.

## References

Kershaw, P. J., Brealey, J. H., Woodhead, D. S., Lovett, M. B., 1986. Alpha-emitting, hot particles in the Irish Sea. Sci. Total. Environ. 53, 77–87.

Masters-Waage, N. K., Morris, K., Lloyd, J. R., Shaw, S., Mosselmans, J.F.W., Boothman, C., Bots, P., Rizoulis, A., Livens, F.R., Law, G. T. W., 2017. Impacts of repeated redox cycling on technetium mobility in the environment. Environ. Sci. Technol .51, 14301–14310.

Sajih, M., Livens, F. R., 2010. Identification and characterisation of radioactive particles in salt marsh sediments. IOP Conference Series: Mater. Sci. Eng. 9, 1–8.